Drug-Excipient Interaction Investigation using Calorimetry and Related Techniques

Tanya Sian Swaine

A thesis submitted in partial fulfilment of the requirements

for the degree of Doctor of Philosophy

The University of Huddersfield

in collaboration with

Biocompatibles UK Ltd

2018

Acknowledgements

I would like to take the opportunity to thank my main supervisor Dr Laura Waters, for initiating this project. I am grateful to my second supervisor Dr Gareth Parkes, for your time, support in discussing my work and for keeping my sprites up by making me laugh, I could not have enjoyed this journey without you.

I express thanks to Biocompatibles Ltd and to Prof Andrew Lewis, for funding and guidance throughout my PhD. Thank you also for the opportunity to attend conferences, to spend time in Camberley with such a great company and for recommending an Idle born girl to venture into London. I am most definitely in debt for the rest of my life to Dr Yiqing Tang, for your kindness and patience with my every question and to Dr Pedro Garcia, for your care and encouragement. I have thoroughly enjoyed this project and I am grateful to this team for the valuable detailed reviewing my work, and also for the counsel and mentoring I have received to make me the successful scientist that I am.

I appreciate all the University of Huddersfield staff but specifically Ibrahim George, Dr Richard Hughes and David Casson, for your advice and help in solving the many instrument issues. I would like to recognise Malvern Instruments Ltd especially Tony Gibson, Dr Irina Dorin and Dr Marina Dobreva, for answer my numerous questions on the ITC and Origin®, I sorely wish I had your details on day one.

A special thanks to my colleagues who created such a fun environment for me to work in, to my friends who have kept me going day to day, and to my family who had faith and believed in me all the way. In particular to my parents for the ethics and morals they instilled in me, without you I could not have made it this far. And finally, to Sooty for sitting with me whilst I wrote every word.

I dedicate this thesis to my grandparents Mary and Bernard Swaine, and parents Denise and Kevin Swaine, for your love, strength and encouragement, my life has truly been enriched by you all.

'The future is not set, there is no fate but what we make for ourselves.' Irish proverb

'Blessed are those who find wisdom, those who gain understanding, for she is more profitable than silver and yields better returns than gold. She is more precious than rubies; nothing you desire can compare with her. Long life is in her right hand; in her left hand are riches and honour. Her ways are pleasant ways, and all her paths are peace. She is a tree of life to those who take hold of her; those who hold her fast will be blessed.' Proverbs 3:13-18 NIV

Contents

Abbreviations

ABC transporter – Adenosine triphosphate binding cassette transporter

AMPS – 2-acrylamido-2-methylpropane sulfonate sodium salt

APC – 7-ethyl-10-[4-N-(5-aminopentanoic acid)-1-piperidino] carbonyloxycamptothecin

API – Active pharmaceutical ingredient

APS – Academy of Pharmaceutical Sciences

ATP – Adenosine triphosphate

AUC – Area under the curve

AVM – Arteriovenous malformation

BCHE – Butyrylcholinesterase

BCLC – Barcelona-Clinic Liver Cancer

c – Shape of the binding isotherm

CAB – Cellulose acetate butyrate

$CaCl_2$ – Calcium chloride

$CaCl_2.6H_2O$ – Calcium chloride hexahydrate

Ca^{2+} – Calcium ion

CES – Carboxylesterase

$(CH_2OH)_3CNH_2$ – Tris(hydroxymethlyl)aminomethane

$(CH_3)_2CO$ – Acetone

Cl^- – Chloride ion

C_{max} – Maximum concentration

CPP – Cell penetrating peptide

CRC – Colorectal cancer

CRS – Controlled Release Society

CT – Computed tomography

cTACE – Conventional transarterial chemoembolisation

cTn – Cardiac troponin

Cu^{2+} – Copper ion

CYP – Cytochrome P450

$C_6H_{12}O_2$ – Butyl acetate

DDES – Drug delivery embolisation system

DDLT – Deceased donor liver transplantation

DDS – Drug delivery system

DEB – Drug eluting bead

DEBDOX™ – Drug eluting bead loaded with Doxorubicin

DEBIRI™ – Drug eluting bead loaded with Irinotecan

DMSO – Dimethyl sulfoxide

DNA – Deoxyribonucleic acid

Dox – Doxorubicin

DP – Differential power

DSC – Differential scanning calorimetry

ECM – Extra cellular matrix

EDTA – Ethylenediaminetetraacetic acid

Epi – Epirubicin

EPR – Enhanced permeability and retention

EtOH – Ethanol

Fe^{2+} – Iron ion

f1 – Difference factor

f2 – Similarity factor

HBP – Human blood plasma

HBV – Hepatitis B virus

HCC – Hepatocellular carcinoma

HCl – Hydrochloric acid

HCO_{3-} – Bicarbonate ion

HCV – Hepatitis C virus

HDR – High-dynamic-range

HO^- – Hydrogen monoxide

HPO_4^{2-} – Hydrogen phosphate ion

HPLC – High performance liquid chromatography

HSM – Hot stage microscopy

HVT – Hypervascular tumour

H_2O – Water

Ida – Idarubicin

IDR – Intrinsic dissolution rate

IFP – Interstitial fluid pressure

Iri – Irinotecan

ITC – Isothermal titration calorimetry

IVIVC – In vitro: in vivo correlation

k – Rate constant

K – Binding constant

K-ATPase – Potassium adenosine triphosphatase

KCl – Potassium chloride

$K_2HPO_4 \cdot 3H_2O$ – Potassium phosphate dibasic trihydrate

$K_2S_2O_8$ – Potassium persulfate

K^+ – Potassium ion

L – Ligand

LDLT – Living donor liver transplantation

LOD – Limit of detection

M – Metabolite

mCRC – Malignant colorectal cancer

MDR – Multiple drug resistant

$M_{Drug\ Eluted}$ – Concentration of drug eluted

$M_{Drug\ Loaded}$ – Concentration of drug loaded

$MgCl_2 \cdot 6H_2O$ – Magnesium chloride hexahydrate

Mg^{2+} – Magnesium ion

Mit – Mitoxantrone

MLC2 – Myosin light chain

MM-CK – Muscular creatine kinase

MMP-2 – Matrix metalloproteinase-2

Mn^{2+} – Manganese ion

MRI – Magnetic resonance imaging

MT-CK – Mitochondrial creatine kinase

mtDNA – Mitochondrial deoxyribonucleic acid

M_{tot} – Total macromolecule concentration

n – Number of time points

n – Molar ratio

N – Reaction stoichiometry

Na – Sodium

NAAADA – N-acryloyl-aminoacetaldehyde dimethylacetal

NaCl – Sodium chloride/Saline

$NaHCO_3$ – Sodium bicarbonate

NaOH – Sodium hydroxide

Na_2SO_4 – Sodium sulfate

Na^+ – Sodium ion

NO – Nitric oxide

NPC – 7-ethyl-10-(4-amino-1-piperidino) carbonyloxycamptothecin

OH^- – Hydroxide

ONOO – Peroxynitrite

OS – Overall survival

PAA – Poly-acrylic acid

PBS – Phosphate buffered saline

PBSS – Phosphate buffered serology saline

PEG – Polyethylene glycol

PEGDA – Polyethylene glycol diacrylate

PEI – Percutaneous ethanol injection

PEO – Poly-ethylene oxide

PET – Positron emission tomography

PGR – Postgraduate Researcher

pHe – Extracellular pH

pHi – Intracellular pH

PMA – Polymethacrylate

pO_2 – Partial oxygen pressure

PST – Performance status

PVA – Polyvinyl alcohol

R – Receptor

R – Dissolution value of one sample

RF – Radiofrequency ablation

RGB – Red, green and blue

RMM – Relative molecular mass

RMS – Root mean squared

ROS – Reactive oxygen species

RPM – Revolutions per minute

RSC – Royal Society of Chemistry

SAA – Sodium acrylate alcohol

SBF – Simulated body fluid

SDI – Surface dissolution imaging

SEM – Scanning electron microscope

SIM – Single injection method

SN-38 – 7-Ethyl-10-hydroxy-camptothecin

SN-38G – 7-Ethyl-10-hydroxy-camptothecin glucuronide

SO_3 – Sulfur trioxide

SO_4^{2-} – Sulfate ion

SPA – 3-sulfopropyl acetate sodium salt

SPECT – Single photon emission computed tomography

t – Time

T – Dissolution value of a second sample

TACE – Transarterial chemoembolisation

TAT – Trans-activating transcriptional activator

TGA – Thermogravimetric analysis

t_{max} – Time at maximum concentration

TMEDA – Tetramethylethylenediamine

TNF-α – Tumour necrosis factors alpha

Top – Topotecan

TOPI – Topoisomerase I

TOPII – Topoisomerase II

Trans reg – Transcriptional regulatory

$t_{1/2}$ – Half-life

$t_{50\ \%}$ – Time taken for 50 % of the drug to be eluted

$T\Delta S$ – Temperature multiplied by change in entropy

UGT – Uridine diphosphate glucuronosyltransferase

UK – United Kingdom

UKICRS – UK and Ireland Controlled Release Society

USA – United States of America

USP – United States Pharmacopeia

UV – Ultraviolet

UV-Vis – Ultraviolet-Visible

Zn^{2+} – Zinc ion

β1ADR – Beta 1 adrenergic receptor

ΔH – Change in enthalpy

ΔS – Change in entropy

ΔG – Change in Gibbs free energy

λ_{max} – Maximum wavelength

3D – Three-dimensional

3DM – Three-dimensional microscope

3MT® – Three Minutes Thesis

Equations

Figures

Tables

Abstract

Beads loaded with drugs have been shown to be useful for drug delivery, yet only limited research has been undertaken on analysing drug-bead interactions and the behaviour of the resultant products. This study investigated specific drug-bead physicochemical parameters, such as factors affecting binding and subsequent drug release phenomena under conditions mimicking the clinic and the body.

Isothermal titration calorimetry (ITC) was initially used to investigate interactions between a drug, doxorubicin (Dox) and a drug eluting bead (DEB), DC Bead™. Dox was titrated into polymer beads at various temperatures, concentrations, volumes, and pH's of the drug and the polymer considered. Furthermore, washing the beads in acid prior to analysis displaced sodium ions which had previously interfered with the drug-bead interaction. Similar binding ratios were found with DC Bead™ to that of previously reported ultra-violet visible (UV-Vis) spectroscopic analysis of 0.90:1 bead binding sites to the drug. The technique was extended to evaluate a range of drugs with DC Bead™ such as Mitoxantrone (Mit), Irinotecan (Iri), Topotecan (Top), in addition to other types (DC Bead Lumi™, LifePearl™, Tandem™ and HepaSphere™) and sizes of beads (from 60 to 700 nm). The thermodynamic information collected suggests that interactions were significantly greater in DC Bead™ than the competitor product LifePearl™. Mit-DC Bead™ was the only drug which bound to two bead sites per drug molecule, consequently half the concentration of drug was required for bead saturation. Alternatively, Iri-DC Bead™ and Top-DC Bead™ involved two drug sites depending on the experimental pH, however this encompassed partial binding to each site resulting in ratios similar to that of Dox.

The open-loop flow-through elution method determined drug elution with different parameters such as packing material, flow rate, salt concentration, eluent type and bead volume. Rate of elution increased with a decrease in bead size, as a result of a larger surface area to volume ratio. DC Bead™ and DC Bead LUMI™ fully eluted Dox at a range of concentrations, however Tandem™ only eluted ~80 % of the drug, possibly due to drug permanently bound to the beads. Initially DC Bead™ had a higher concentration of drug released in comparison to the slower more sustained release of DC Bead LUMI™ and Tandem™, and Iri was found to elute much faster than Dox. The method achieved flow rates of 0.1 mL/min, close to that of an embolised vessel. At these slow flow rates LifePearl™ was found to have similar characteristics to DC Bead™, which correlated well with the acquired ITC data.

Three-dimensional microscopy (3DM) and hot stage microscopy (HSM) supported the view that bead swelling effects changed the elution profile. It was also evident that DC Bead™, DC Bead LUMI™ and Lifepearl™ homogenously loaded and completely eluted, whereas Tandem™ heterogeneously loaded did not fully elute. HepaSphere™ images indicated significant aggregation and fragmentation.

Investigation of the drug *in vitro* could be used to predict elution characteristics *in vivo*, with potential implications for product development and quality assurance. In summary, knowledge of the drug-bead interactions facilitated a deeper understanding of drug-bead binding to be attained using ITC and drug-bead release accomplished with a method of elution. These methods developed will undoubtedly assist in developing optimum treatment options.

Chapter 1 : Introduction

The term cancer is used to describe cellular modifications that result in uncontrolled cell growth. Trillions of cells make up the human body and it takes only one abnormal cell for oncogenesis to occur [1]. There is evidence to suggest that cancer has existed since 300 BC, despite this cancer treatments have been around for less than 100 years [2]. Traditionally cancer treatment was based upon location and cell type. However, no two cancers are identical, and it is now widely accepted that the cells associated with a tumour are diverse and perform different roles during evolution of the tumour. Traditional grouping and the accompanying therapies may not lead to effective results. The recent ability to identify genetic and biological changes has introduced the world to personalised medicine [1].

1.1. Cancer Prevention, Diagnosis and Therapeutics

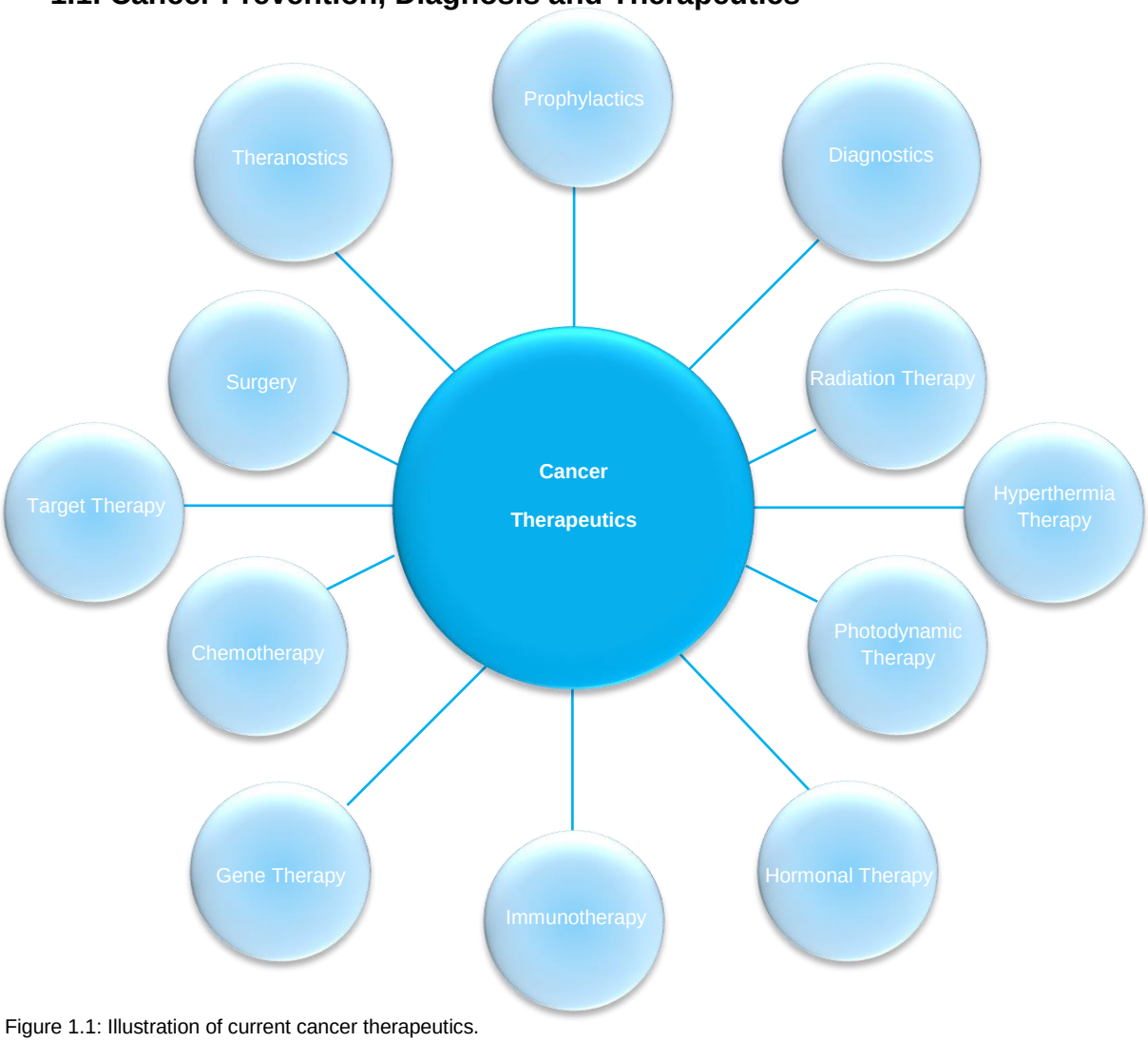

Figure 1.1: Illustration of current cancer therapeutics.

A decline in cancer death rates can be accredited to extensive efforts in the prevention, detection and improved therapeutic strategies associated with the categories of Figure 1.1 [3].

Current cancer therapies includes diagnostics; this may show the type, location and rate of cancer growth [4]. Early diagnosis allows immediate intervention to prevent the further development of cancer [5]. A biopsy may be required for an accurate diagnosis, wherein a surgeon may remove a portion of the suspicious tissue. A pathologist examines cells, tissues and organs for biomarkers, and then interprets the laboratory tests to help diagnose the disease and determine the treatment options [6]. An evaluation can also be done using imaging to visualise the cancer. Methods of imaging include computed tomography (CT), magnetic resonance imaging (MRI), positron emission tomography (PET), single photon emission computed tomography (SPECT), optical imaging, endoscopy, fluoroscopy, mammography and ultrasound. The main advantage of imaging is that it is a non-invasive technique, however the disadvantage is that it is common to have false negative results, where the image does not identify micrometastases and early stages of cancer [7,8].

Nanoparticles may encapsulate or conjugate to both imaging agents and therapeutic agents. This multifunctional product allows diagnosis of the cancer and delivery of the therapy simultaneously, alongside real-time monitoring of flow patterns, particle distribution and response to the therapy; this is known as a theranostic. More than one imaging particle may be joined to a delivery system, which means more than one imaging technique may be used to evaluate a cancer; this may give numerous amounts of information and is known as multimodal or multiplexed imaging [5]. It is important that the delivery system and imaging agent are isobuoyant, so that the device remains in an even suspension and does not sediment out during delivery [9]. Unfortunately, cancer is usually detected once it has reached a visible size or it begins to interfere with a patient's health. Diagnostics are not only used to identify cancer but also have the potential of staging the disease throughout treatment, determining the response to therapy and for identifying recurrence [5].

1.2. Hepatocellular Carcinoma (HCC) and Colorectal Cancer (CRC)

According to the International Agency for Research on Cancer, liver cancer is currently the sixth most lethal malignancy worldwide and accounts for 9.1 % of all cancer deaths. In 2012 an estimated 782,000 new cases were diagnosed and more than 746,000 deaths were reported. Prevalence figures in 2012 suggested 633,000 patients received diagnosis 5 years ago and to be either cured or still living with the disease. Hepatocellular carcinoma (HCC) or hepatoma is the primary form of liver cancer, mainly caused by the hepatitis B virus (HBV), hepatitis C virus (HCV) and cirrhosis. However, lifestyle factors are also related to the risk of developing a tumour. The highest occurrence of the disease is in Asia because of HBV and HCV infections. People infected with the virus have a higher risk of developing chronic hepatitis, which may lead to cirrhosis of the liver, liver damage, liver cancer, liver failure and ultimately fatality. Liver cancer is more likely to affect the elderly and males [10].

Colorectal cancer (CRC), also known as cholangiocarcinoma or bowel cancer, is the third most common cancer in the world with more than 1,361,000 new cases diagnosed and attributed to 694,000 fatalities in 2012. In 2012 there were 3,544,000 patients alive 5 years after their diagnosis. This cancer is also more likely to affect the elderly and the risk is slightly higher in males. In spite of advances in diagnosis and treatment in this area, incident rates are highest in Australia and New Zealand. Bowel cancer is predominantly associated with lifestyle influences, however some medical conditions and hereditary history are also connected to this disease [11].

Cancers can often spread from the original site and metastasise to lymph nodes, the most frequently observed site of extra-lymphatic involvement is the liver [12,13]. Secondary malignancies account for 95 % of all malignancies, which can lead to hepatic failure and subsequently death [13,14]. Despite extensive screening and preventative strategies 25 % of colon cancers and 50 – 70 % of rectum cancers will spread through the bowel wall, and 50 – 60 % will metastasise to lymph nodes [12,13].

Patients may be categorised into five groups, referred to as stages 0, A, B, C and D. Stage 0 patients are those that have been diagnosed very early and are likely to undergo curative treatment such as resection of the solid tumour or liver transplant [15]. For patients who have been diagnosed at this stage five year survival rates are 90 % [12,13]. Unfortunately, many patients are not suitable for curative treatments and as a result more than three quarters of these must partake in palliative treatment [16,17]. Patients categorised as stage A (early), B (intermediate) or C (advanced) are candidates for alternative palliative therapies. Patients with asymptomatic multinodular HCC stage B are suitable for transarterial

chemoembolisation (TACE), whereas stage D (terminal) patients are symptomatically treated [15]. Overall survival (OS) rates of five years drops to 64 % with progression of the disease [12]. The staging system can be linked to a treatment schedule created by hepatologist Jordi Bruix; known as the Barcelona-Clinic Liver Cancer (BCLC) treatment strategy delineated in Figure 1.2. This classification uses pre-established prognostic variables and allocates therapies according to treatment-related status from very early (stage 0) to terminal stage cancer (stage D). Prognosis is defined by tumour status, performance status and liver function using the Child-Pugh's score [18].

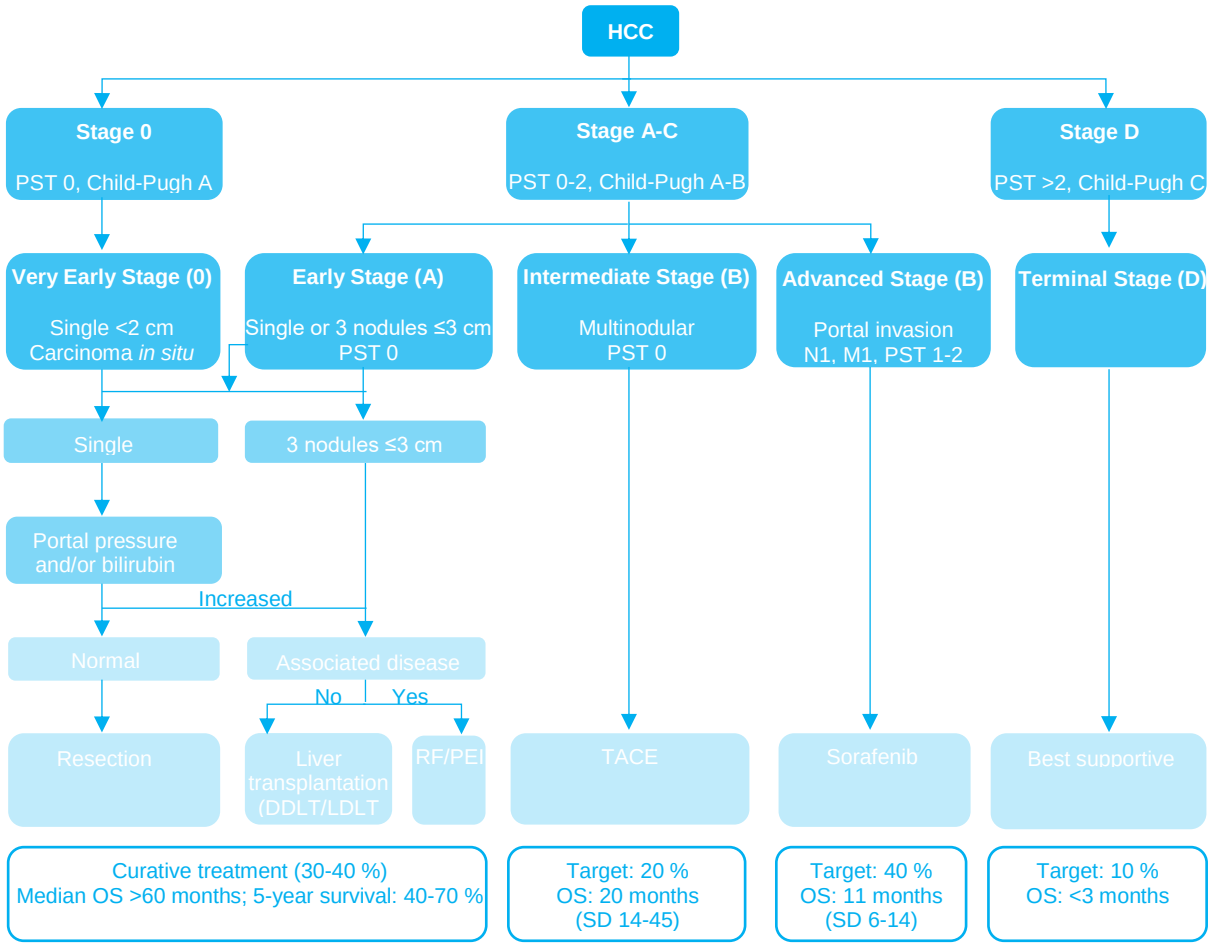

Figure 1.2: BCLC (Barcelona-Clinic Liver Cancer) algorithm (HCC – hepatocellular carcinoma, PST – performance status, DDLT – deceased donor liver transplantation, LDLT – living donor liver transplantation, RF – radiofrequency ablation, PEI – percutaneous ethanol injection, TACE – transarterial chemoembolisation, OS – overall survival. N1 and M1 refer to tumour size, number and vascular invasion) [18].

1.3. Drug Delivery Systems (DDS)

The first drug delivery system (DDS) was developed in 1952, which was the 12-hour delivery of dextroamphetamine (dexedrine) in an oral capsule formulation introduced by Smith Kline & French [19]. Since then there have been numerous advances in delivery with various formulations of implants, ingestible capsules, mucosal inserts and topical patches. Microscopic degradable polymer DDSs followed the significant developments in the field, which led to the nanoscopic era [20]. Naturally occurring and synthetic polymeric materials have played a significant role in the research and development of most controlled-release technologies over the last 25 years, shown by an increase in the number of publications and patents [21]. These DDSs are devices that enable the administration of a therapeutic substance into the body controlling elements of release rate, release time and site of drug release into the body [22]. Currently there are four classified controlled release mechanisms: diffusion-controlled (reservoir and matrix), chemically-controlled (pendent chain and biocrodible/biodegradable), solvent-activated (osmotic and swelling) and magnetically-controlled systems [21].

Biomaterials can be effective ways to deliver a variety of drugs to the body, and as much as the choice of drug varies so can the way in which it is delivered [23]. They can be made of a variety of materials such as inorganic nanoparticles, liposomes, polymers and viral carriers [24]. Effective carriers must be stable during delivery, yet still allow the drug to achieve therapeutic action and have minimal side effects [25]. DDSs may be used to deliver substances with difficult physicochemical properties, and so it is essential that the device can solubilise and carry hydrophobic drugs [23,25]. The design must also contain properties that offer protection to the drug, the carrier and the body. The carrier protects the drug from various defence mechanisms of the body as proteins can destabilise, inactivate or phagocytise the drug. The transporting material reduces cytotoxicity to normal organs, tissues or cells, and preventing interactions with cells provides the carrier with more time to circulate in the blood and increases the chances of reaching the tumour. It is necessary to maximise the probability of tumour accumulation by means of enhanced permeability and retention (EPR) [25].

The transportation device can also have additional mechanisms for environmental, cellular or molecular targets [25]. Smart biomaterials can respond to the body environment such as pH, temperature and the presence of salt, as well as selectively release a drug at a predetermined site of the body [23]. The high concentration of metalloproteinases distributed within the tumour has introduced carriers with regions cleavable by matrix metalloproteinase-2 (MMP-2) [26]. Most tumours have a low pH which

provides a means of stimulating trans-activating transcriptional activator (TAT), a cell penetrating peptide (CPP) that can facilitate uptake of the drug [27,28]. Carriers have been developed to contain molecular targets used to bind surface markers overexpressed in certain cancer lines [29]. The most recent advancement in targeted delivery of drugs is the use of nanotechnology. The practice of nanotechnology in this field has had its limitations, but microparticle DDSs have shown their capabilities to retain large quantities of drug and deliver these drugs to a targeted area in a controlled and sustained manner. Unlike the delivery of nano DDSs, the delivery of micro DDSs often requires surgery under general anaesthetic, however the TACE procedure provides a non-invasive means of administering drugs for chemotherapy and radiotherapy treatment under local anaesthetic [23].

The tumour environment often has low partial oxygen pressure (pO_2) because of its poorly formed vasculature [30]. Unfortunately, rather than stunting growth of the tumour through oxygen starvation it has been shown to promote metastasis [31,32]. Hypoxia also creates an environment where the cancer cells are capable of resisting both chemotherapy and radiation, this is because a DDS will have difficulties diffusing though the vasculature into the tumour region [32,33]. A lack of oxygen will reduce proliferation rates in cancer cells, which in turn will decrease the effect of drugs that target mitotic mechanisms of fast growing cells. Hypoxia may influence the production of cancer stem cells, possibly due to typical stem cells being activated to restore ischemia damaged tissue [31,32]. Furthermore, surviving cells of chemotherapy and radiation may even project the Darwin theory, whereby remaining cells are more aggressive and more resistant after each course of treatment; these are known as multiple drug resistant (MDR) cancers [34]. The points above are key issues which a DDS may need to address to provide effective interventional oncological treatment.

Tumours frequently have a lower extracellular pH (pHe) in comparison to their intracellular pH (pHi). This is caused by a build-up of waste products such as lactic acid from aerobic and anaerobic glycolysis, as a result of the dysfunctional vasculature and lymphatic system [33,35,36]. Therefore, a DDS which releases a therapeutic agent within a low pH could be beneficial. If a low pHe isn't present one can be artificially created by the addition of glucose to non-diabetic patients [37].

The rate of diffusion across openings between vascular endothelial cells; known as fenestrae, can be influenced by certain drug carrier characteristics such as concentration, hydrophilicity, shape, size and surface charge, along with properties associated with blood vessels such as the density, distribution and size of fenestrae [25]. Particles smaller than the distance between the collagen fibrils have

greater intratumoural distribution and can cross the extracellular matrix (ECM) [38]. However, the probability of intratumoural distribution decreases with particles that interact with ECM components and non-target cells [25]. Distribution may be enhanced by using penetrating peptides, by breaking down ECM components with enzymes or by increasing blood perfusion with drugs which increase the diameter of blood vessels, before administering the DDS [39–42].

Targeted delivery can be either active or passive. Active targeting is specific receptor binding, ligand binding or other protein interactions, and supports delivery to a specific target cell or molecule. Passive targeting is the design of particles that increase the probability of reaching the target. Whichever mechanism, the desired result is to increase the therapeutic effect and reduce any side effects. Yet the delivery of an arbitrary amount of drug to a designated target is not necessarily targeted drug delivery. Many targeted drug transporters hit other locations in addition to the specific target site [25]. The theory is to target delivery of the drug to terminate only cancer cells like a ‘magic bullet’ [43]. Thus far this is impossible with current technology, and the reality is that only the immune system comes close to achieving Paul Ehrlich’s concept of the magic bullet [44].

1.4. Transarterial Chemoembolisation (TACE)

Conventional TACE (cTACE) has been developed over three decades [45,46]. It is used for the treatment of inoperable hypervascular tumours (HVTs) and arteriovenous malformations (AVMs) [47]. The procedure, often delivered sequentially, can be performed with various chemotherapeutics and doses, and with or without iodised oil. Embolic materials can be biodegradable or permanent and vary in size, hence the procedural techniques are numerous and as a result leads to inconsistent outcomes caused by a lack of a standardised method for performing cTACE [16,47–64]. Embolic agents prevent blood flow through a vessel using biological or physical properties. Biological agents strip the vessel of the endothelial lining causing the structure to breakdown and collapse. Mechanical agents occlude the lumen of the vessel at either a proximal or distal level. Embolotherapies can be in the form of balloons, coils, polymer liquids, particulates and sponges [65]. The first particulate embolisation agent was available in 1949 and consisted of polyvinyl alcohol (PVA) foam particles [66]. This technology was later developed into irregular particles which could be assorted into size ranges by sieving particles through progressively smaller sized meshes stacked on top of one another. The irregular shape of the particles can cause blockages in the catheter and interlocking of the particles causes a more proximal aggregation, precluding more distal occlusion. The desire for a more controlled embolic agent led the development of tightly calibrated microspheres [9]. Microspheres achieve a more distal penetration, attributable to their flow-directed nature and more compressible features due to the materials containing a large amount of water; terming the formation as hydrogels [67]. In the 1970s it was suggested that embolic agents have the potential to be combined with chemotherapy in order to occlude vessels and deliver a drug in one procedure; this is known as TACE [68]. Whilst TACE had a beneficial approach for intervention radiologists there was no standardised procedure, which made clinical comparisons extremely difficult until the launch of a drug eluting bead (DEB) for TACE; known as DC Bead™ [9,69,70].

DEBs may be used to deliver chemotherapeutic agents to cancer cells [70]. Randomised control trials indicated that DEB-TACE provided an improved local response, an enhanced complete response, fewer recurrences and a longer time to progression compared with the traditional TACE procedure. Although in these studies there was no statistical difference in survival rate, DEB-TACE was better tolerated by patients, especially those with advanced HCC disease [71,72]. Figure 1.3 frameworks the key DEB-TACE benefits. It is possible that once patients are treated with DEB they may be down-staged and receive resection or transplantation [73]. DEB-TACE is currently being investigated for the treatment

of further malignancies such as gastroenteropancreatic endocrine tumours, intrahepatic cholangiocarcinoma and uveal melanoma metastases [74–77].

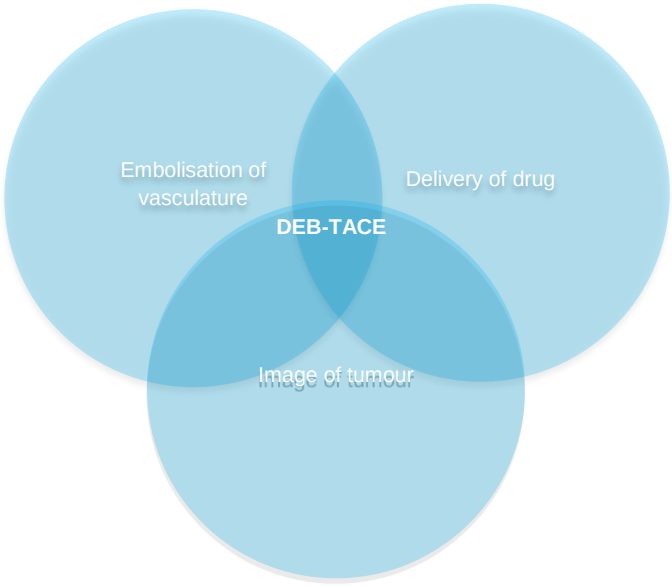

Figure 1.3: Outline of the DEB-TACE procedure benefits.

1.5. DC Bead™

DC Bead™ (known as LC Bead™ in the United States of America (USA) [13,49,68,70,78–81]) is a 510K FDA cleared and CE-Mark approved drug delivery embolisation system (DDES), which provides localised controlled sustained delivery of chemotherapeutic agents, as well as embolisation of the tumour feeding arteries [47,70,82–86]. The device is manufactured by Biocompatibles UK Ltd, which is a part of the BTG plc group companies. DC Bead™ was developed in 2002 for the advancement of interventional oncology, with a view to standardise the TACE procedure providing handling advantages and patient benefits.

Regulatory control places immense importance on a distinction between the drug and the device. If the device is introduced into the body for purposes other than administration of an active ingredient, such as a physical therapeutic effect or a drug to prevent complications from the device, then it is strictly regulated as a device rather than a DDS. However, when there is not a clear division of characteristics the allocation to either category is decided on a case by case basis [22]. DC Bead™ is both a device and a DDS, as the product can be administered with and without the drug to deliver the therapeutic agent and/or block tumour feeding vessels.

1.5.1. Composition

The beads consist of a biocompatible PVA hydrogel microsphere, that has been modified with hydrophilic 2-acrylamido-2-methylpropane sulfonate sodium salt (AMPS) and is tinted blue to allow visualisation of drug loading [47,70,87–89]. The basic preparation steps of DC Bead™ can be seen in Figure 1.4. The negatively charged sulfonate groups enable the bead to complex with positively charged drugs [14,47,69,88,90]. The beads are a non-degradable compressible polymer and are available in a range of sizes from 70-700 µm. These are supplied steam sterilised in a 10 mL colour coded glass vial sealed with a rubber stopper and aluminium cap, as demonstrated in Table 1.1. Each vial contains 2 mL of beads stored in 6 mL of phosphate buffered saline (PBS) and is intended for single patient use. The size of bead and the amount of drug is selected according to the pathology of the patient receiving treatment by a physician with appropriate interventional occlusion training.

PVA + HCl + NAAADA → AMPS + $K_2S_2O_8$ + CAB + $C_6H_{12}O_2$ → 333 K + TMEDA → H_2O, NaCl → Sieve + H_2O → $(CH_3)_2CO$ + 313 K

Figure 1.4: Preparation of DC Bead™.

(Monomers: PVA (polyvinyl alcohol) and AMPS (2-acrylamido-2-methylpropanesulfonate sodium salt), catalyst: HCl (hydrochloride acid) and NAAADA (N-acryloyl-aminoacetaldehyde dimethylacetal), initiators: $K_2S_2O_8$ (potassium persulfate) and TMEDA (tetramethylethylenediamine), stabilisers: CAB (cellulose acetate butyrate) and $C_6H_{12}O_2$ (butyl acetate), washing: H_2O (water), NaCl (saline), drying: $(CH_3)_2CO$ (acetone)) [91]

The first size range of DC Bead™ to be used in clinical practice was 500-700 µm, the size was based upon the predicate Gelfoam particles that were conventionally in use [92]. Gradually, as physicians became more confident in its use the preferred size of DEB decreased, as smaller beads are more favoured to achieve deeper tumour penetration and increase the delivery of drug as a result of a bead surface area to volume ratio [93]. This has led to the development of 70-150 µm beads, to meet the desire to deliver a large concentration of drug at a greater distal level [94].

Table 1.1: Available DC Bead™, their sizes and label colour [95].

Bead Reference	Bead Size (µm)	Label Colour	Product Image
M1	70-150	Black	
103	100-300	Yellow	
305	300-500	Blue	
507	500-700	Red	

1.5.2. Chemistry

The selected drug is taken up by the bead through an ion-exchange mechanism [47,88]. When mixed with certain chromatic drugs the beads change colour, which indicates the drug has been loaded. The beads have a high water content of >95 %, which enables the diffusion of molecules into and out of the polymer structure [82,96]. Elution rate and uptake of the drug is dependent upon bead size, as diffusion is inversely proportional to bead diameter, attributed to the increase in surface area to volume ratio [13,47]. However, it is worth noting that some compounds can have drug-drug interactions, which can affect how the drug binds and elutes from the delivery vehicle [89]. The beads initially increase in diameter as they are reconstituted in water, but then decrease as water is displaced from the bead and the drug is sequestered from the solution. As the diameter of the bead decreases the resistance to compression of

the bead increases, i.e. they become somewhat stiffer [13,47]. The ion-exchange mechanism is a reversible interaction, and upon contact with ions contained in blood the drug is released from the bead.

1.5.3. Treatment

Doxorubicin (Dox) and Irinotecan (Iri) are drugs used in the treatment of various cancers [14,97]. Dox is an anthracycline, whilst Iri is a semi-synthetic derivative of camptothecin. Both are highly hydrophobic and are subsequently formulated with hydrochloric acid (HCl), this increases the solubility for their use in the treatment of primary and secondary cancer [4,98,99]. DC Bead™ is CE-Mark approved for loading with either Dox or Iri, Figure 1.5 and 1.6 indicate the significant colour change upon drug loading.

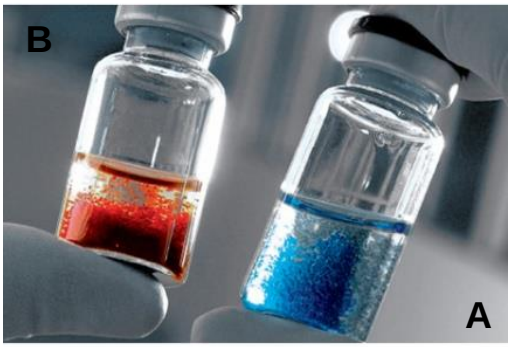

Figure 1.5: DC Bead™ unloaded (A) and DC Bead™ loaded with Dox illustrating the intense colour change from blue to red (B) [100].

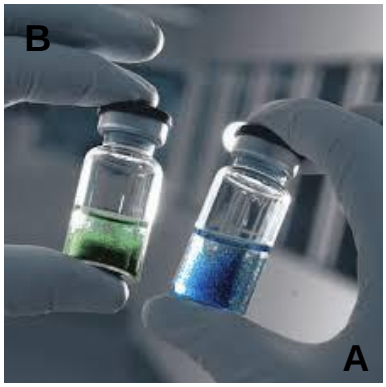

Figure 1.6: DC Bead™ unloaded (A) and DC Bead™ loaded with Iri illustrating the intense colour change from blue to turquois (B) [101].

Figures 1.7 and 1.8 show Dox and Iri loading into DC Bead™, and the subsequent elimination of water.

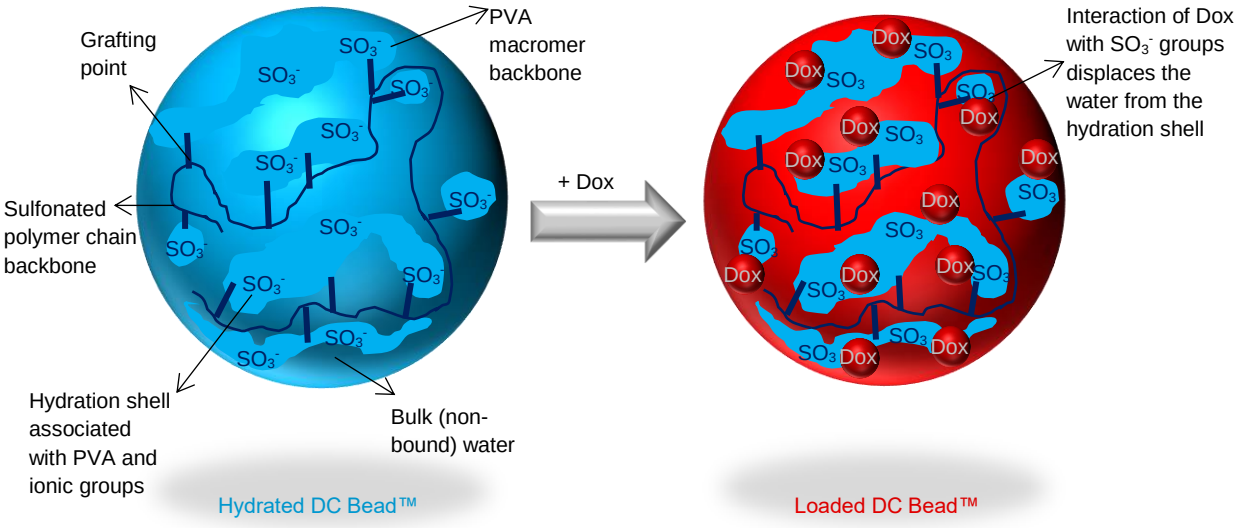

Figure 1.7: DC Bead™ mode of loading with Dox [102].

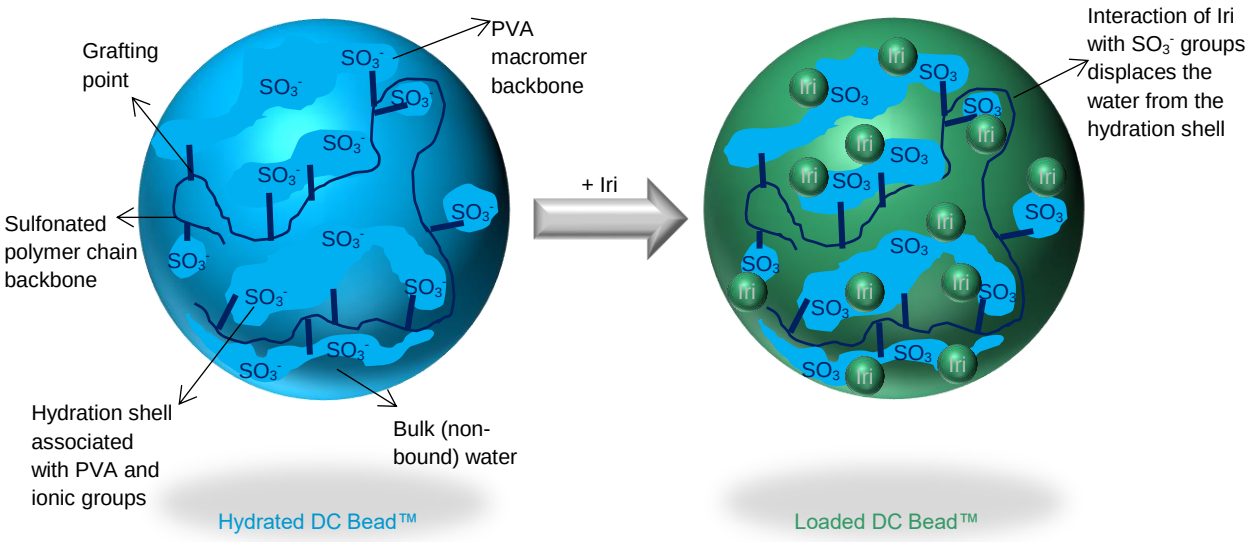

Figure 1.8: DC Bead™ mode of loading with Iri [103].

Figures 1.9 and 1.10 display the respective chemical structures of Dox and Iri binding to DC Bead™.

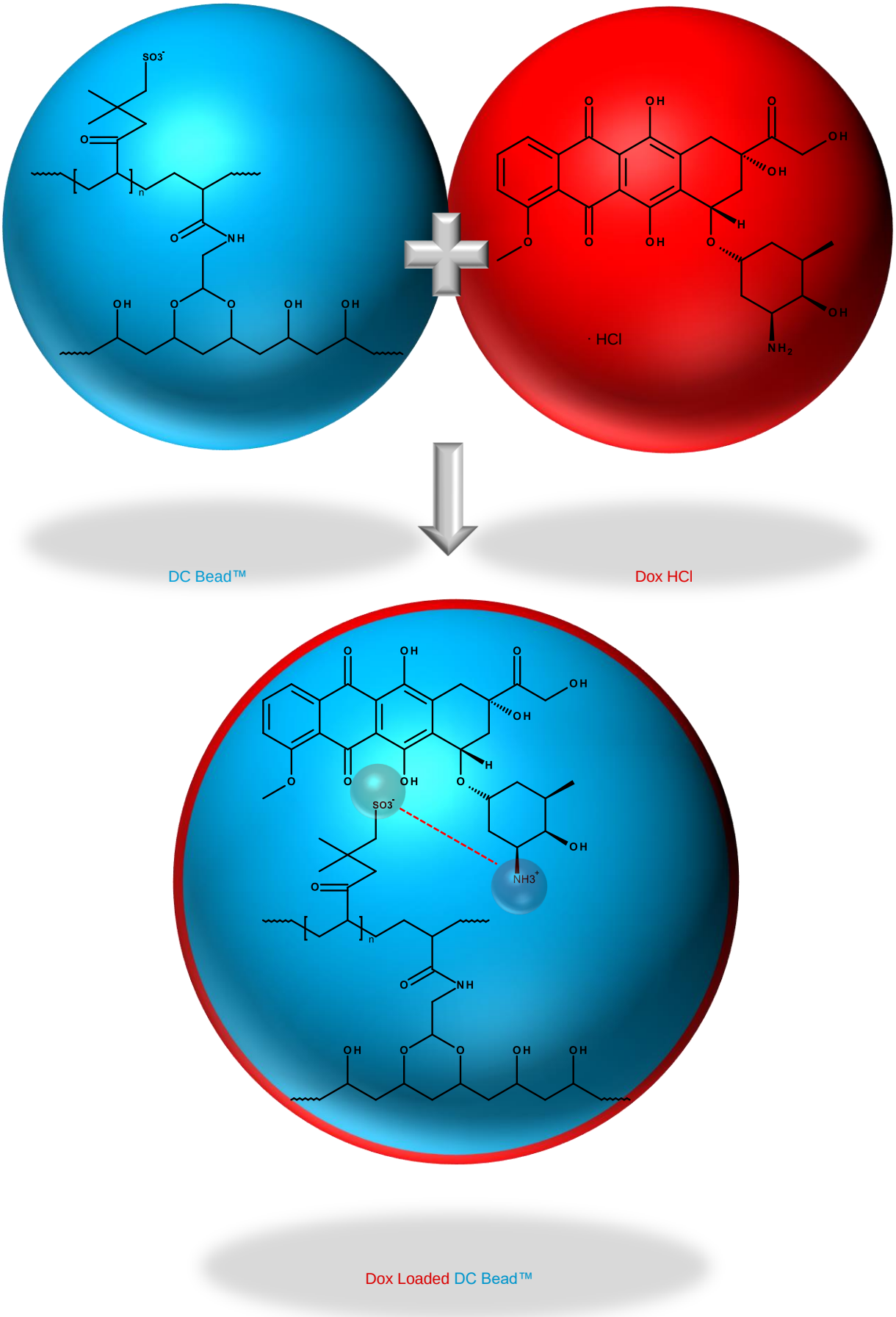

Figure 1.9: Structural formula of DC Bead™, Dox and the combined product.

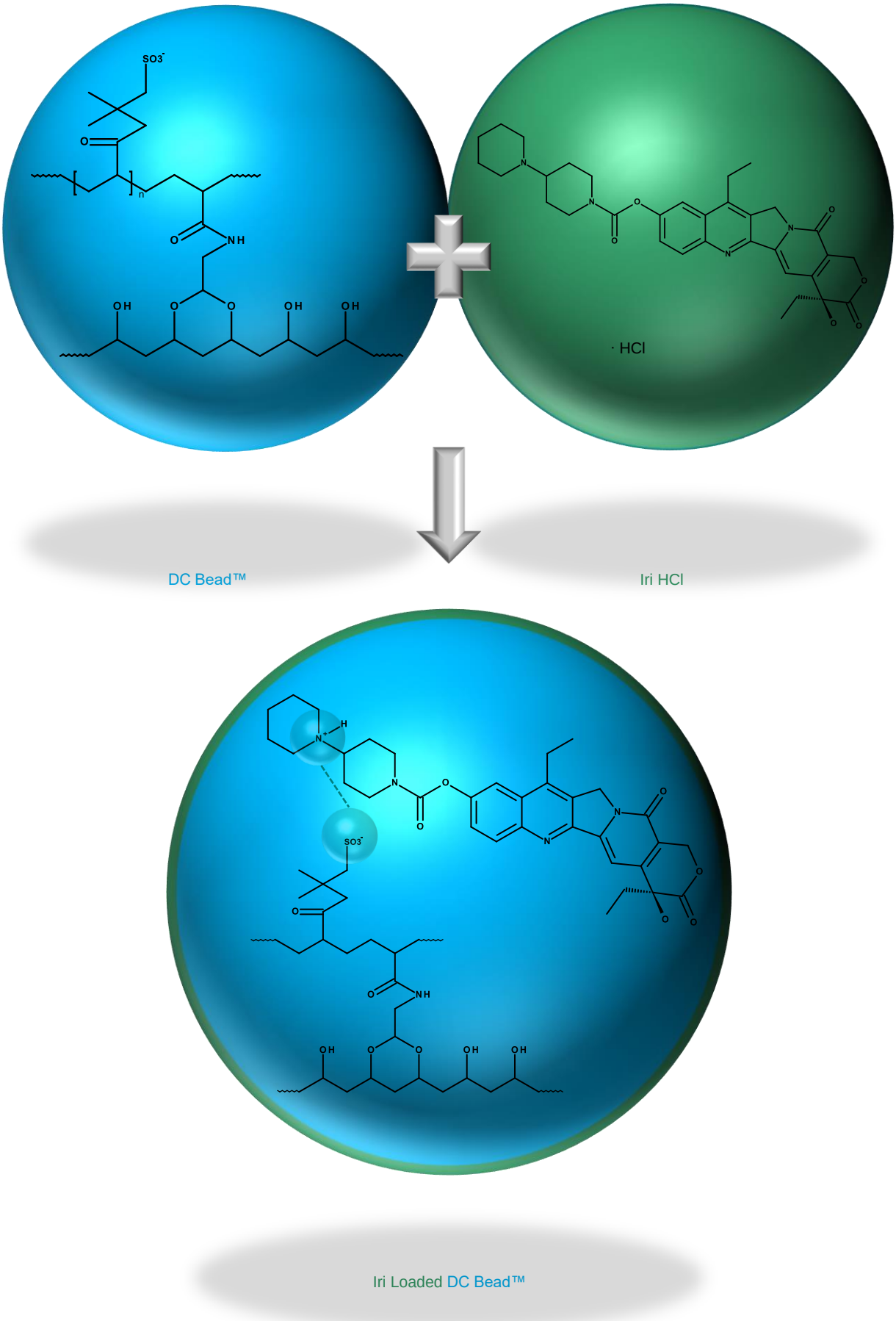

Figure 1.10: Structural formula of DC Bead™, Iri and the combined product.

Chemotherapy has a range of cardiomyocyte effects, this mechanism of chemotherapeutic effect is unclear, however it seems that the action through which Dox kills cancer cells or interrupts cell growth is derived from the inhibition of topoisomerase II (TOPII), signalling pathway activation, free radical generation, deoxyribonucleic acid (DNA) intercalation and binding, as shown in Figure 1.11. TOPII simultaneously cuts both strands of the DNA helix in order to manage DNA tangles and supercoils. Inhibition of these processes leads to apoptosis and consequently a reduction in tumour burden [104–106]. Dox penetrates cells, and the intercalation of DNA prevents DNA synthesis and inhibits TOPII. The generation of free radicals through interfering with both enzymatic and non-enzymatic pathways leads to the accumulation of iron and induced lipid peroxidation, which ultimately results in membrane damage [104,107–110]. Additionally, mitochondrial damage, increased concentration of calcium ions (Ca^{2+}), reduced level of K-ATPase (potassium-adenosine triphosphatase), decreased activity of sodium (Na), prevention of the sarcoplasmic reticulum function, down regulation of myocardial TNF-α (tumour necrosis factor-alpha) and Dox binding to bivalent cations of Ca^{2+}, copper (Cu^{2+}), magnesium (Mg^{2+}) and zinc (Zn^{2+}) have all been implicated in lethal Dox-induced cardiotoxicity [111–115].

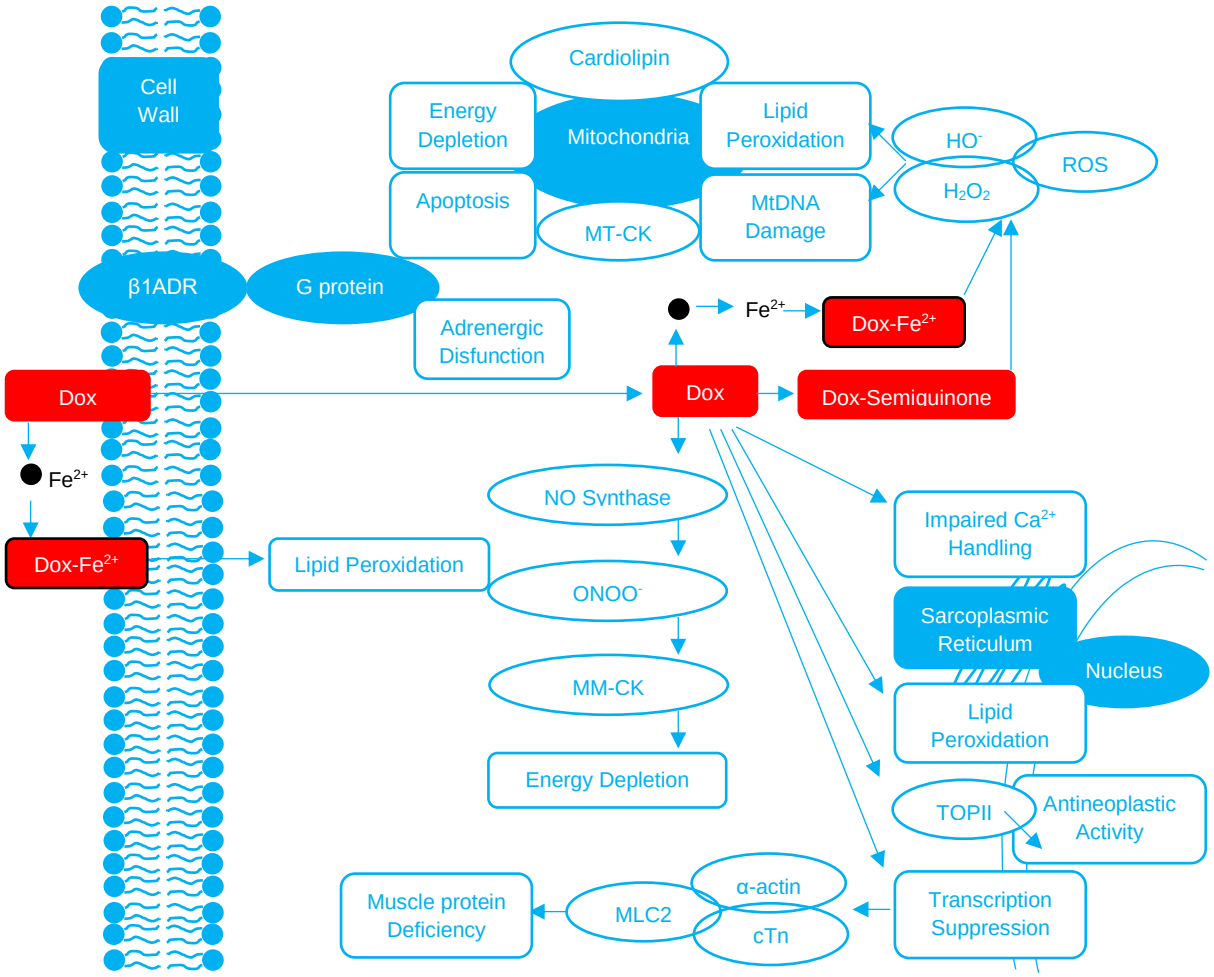

Figure 1.11: Dox mode of action (Dox – Doxorubicin, Fe^{2+} – Iron, β1ADR – β1 adrenergic receptor, mtDNA – Mitochondrial deoxyribonucleic acid, MT-CK – Mitochondrial creatine kinase, H_2O_2 – Hydrogen peroxide, ROS – Reactive oxygen species, HO- – Hydrogen monoxide, NO – Nitric oxide, ONOO – Peroxynitrite, MM-CK – Muscular creatine kinase, Ca^{2+} – Calcium, TOPII – Topoisomerase II, Trans reg – Transcriptional regulatory, MLC2 – Myosin light chain, cTn – Cardiac troponin) [116].

Iri belongs to a class of topoisomerase I (TOPI) inhibitors. TOPI is a DNA enzyme responsible for controlling and modifying DNA during replication and translation of genetic materials. In Figure 1.12 Iri undergoes hydrolysis by carboxylesterases (CES), which is then metabolised to form 7-ethyl-10-hydroxy-camptothecin (SN-38) in the liver by cytochrome P450 (CYP) isoforms. The pharmacologically active compound is transported across cell membranes by adenosine triphosphate (ATP)-binding cassette transporters (ABC transporters), SN-38 can then be inactivated through glucuronidation by uridine diphosphate glucuronosyltransferase (UGT). Iri and its active metabolite bind to the TOPI-DNA complex, preventing religation of the single-strand breaks in the DNA molecule [117,118].

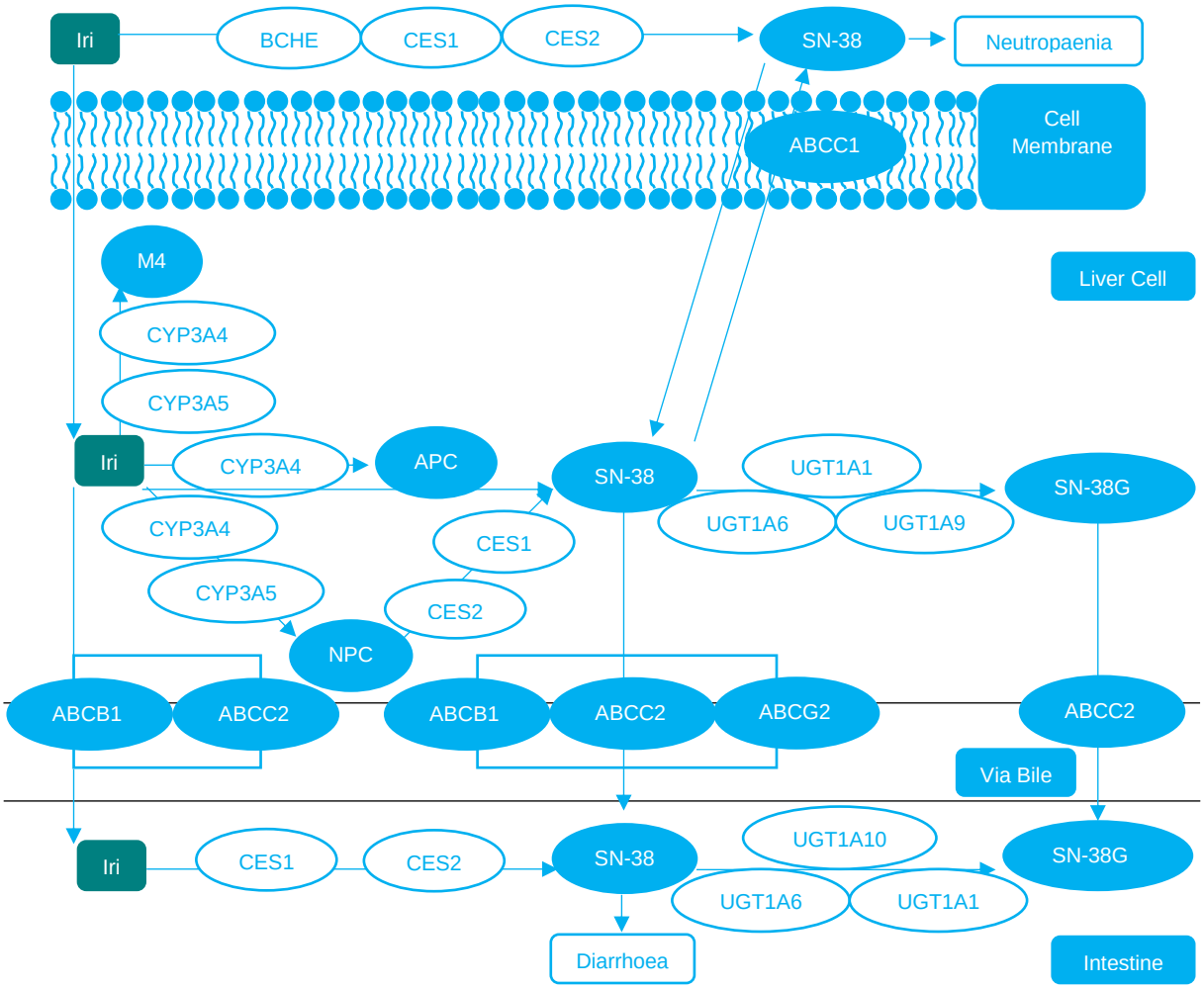

Figure 1.12: Iri mode of action. (Iri – Irinotecan. Metabolites (M) of Iri: SN-38 (active glucuronide metabolite), SN-38G (inactive glucuronide metabolite), APC (7-ethyl-10-[4-N-(5-aminopentanoic acid)-1-piperidino] carbonyloxycamptothecin) and NPC (7-ethyl-10-(4-amino-1-piperidino) carbonyloxycamptothecin). ABC (ATP (adenosine triphosphate) – binding cassette transporter family), BCHE (butyrylcholinesterase), CES (carboxylesterase), CYP (cytochrome P450 isoform), UGT (uridine diphosphate glucuronosyltransferase isoform)) [119].

DC Bead™ loaded with Dox (DEBDOX™) is intended for the treatment of malignant hypervascularised tumours such as HCC [120]. DC Bead™ can be loaded with a maximum of 37.5 mg Dox/mL of hydrated bead. Typically, 2 – 4 mL of beads is administered over a course of treatment with a maximum of 150 mg of Dox per patient according to systemic dose limits. DC Bead™ loaded with Iri (DEBIRI™) is indicated for the treatment of malignant CRC (mCRC) metastasised to the liver. Generally, mCRC tumours are diffuse and less vascular than HCC tumours, consequently Iri is the favoured drug for this implantation [74,121,122]. In this case 50 mg Iri/mL of beads with a recommended dose of up to 4 mL of beads is administered, equating to a maximum of 200 mg of Iri per treatment [89].

The DEB-TACE procedure is minimally invasive and intended to be performed by a physician such as an interventional radiologist. Figure 1.13 depicts where a small incision is made, usually in the

groin, typically under local anaesthetic and a guide wire is used to position an appropriately sized microcatheter into the hepatic branch of the main tumour feeding artery. The tumour is imaged with an angiography, the aim is to be as selective as possible and administer the agent deep within the arterial tree of the target organ [66]. The saline packing solution of the DEBs must be removed before the mixture of chemotherapeutic agent (in this case either Dox or Iri) is saturated in the beads along with non-ionic contrast media [56,83]. The beads are left to sequester the drug, and drug loading time is dependent upon bead size and drug concentration [16]. Once the beads with medium are in the correct location, this is simultaneously administered intravenously into the femoral artery, which is then carried into the tumour and surrounding tissue with blood flow [56]. The beads compressible nature allows them to traverse the arterial network. Eventually the non-degradable beads occlude the vessels, slowing blood flow to the target tissue, consequently reducing oxygen and nutrients supplied to the site [123]. The use of a biomaterial to deliver a drug as well as an imaging agent makes this a theranostic system [124–129]. The presence of imaging agent allows identification and quantification of a delivery vehicle to a target site [4].

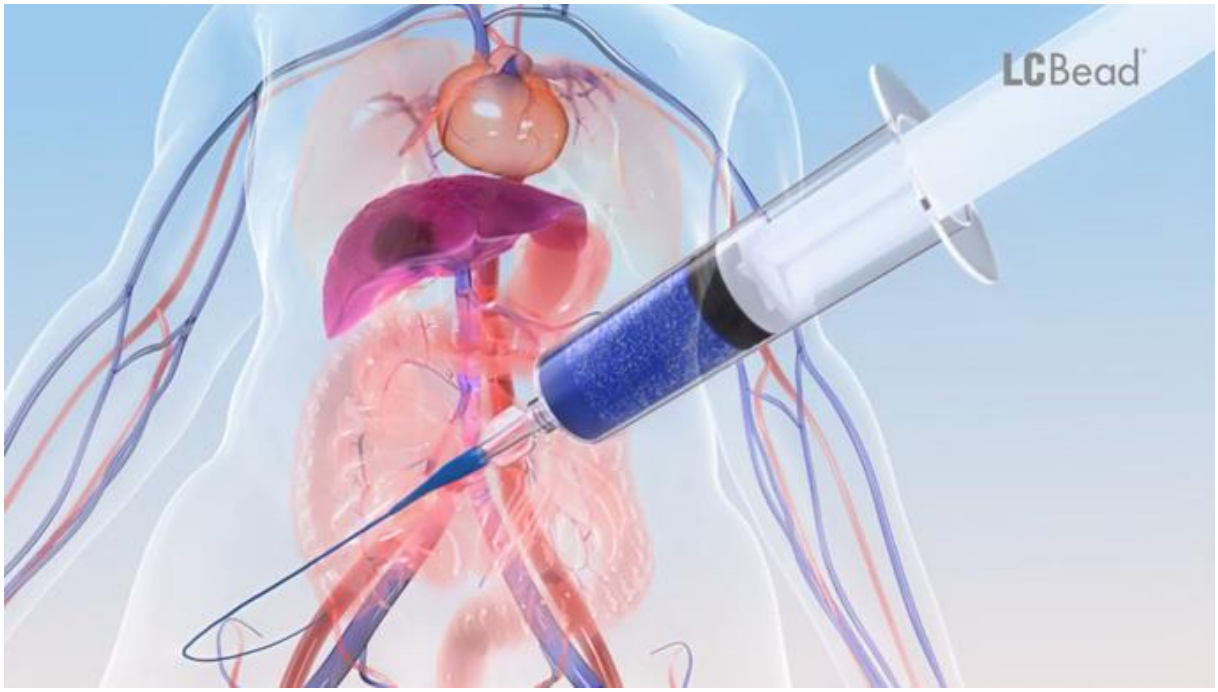

Figure 1.13: Administration of DC Bead™ [130].

Hypoxia occurs because cancer cells can grow at a rate that cannot be matched with neovascularisation, resulting in insufficient oxygen and nutrients transported to the tumour [1]. Hypoxia also triggers the

release of growth factors that causes angiogenesis in order to deliver required nutrition and oxygen to the tumour [131]. When angiogenesis transpires nascent vessels do not mature properly as a result of being developed too quickly. These vessels are leaky, which increases the transport of drug carriers into the tumour by Brownian motion through endothelial fenestrae, rather than by convective flow [25,132]. A dysfunctional vasculature and lymphatic system, and compressive stress from excessive cell growth leads to high interstitial fluid pressure (IFP). These forces lead to a high net inwards pressure which aids the transport of the DDS [133]. Defective vasculogenesis also provides a way of diagnosing progression of the disease [131]. The lymphatics would usually carry the macromolecule away with tissue fluid, however retention in the tumour is enhanced because the tumour compresses and damages lymphatics as it grows. Embolisation of vessels reduces the wash-out of the chemo-emulsion allowing drug release into the plasma over a prolonged period of time, simultaneously inducing ischemia and necrosis, resulting in an antineoplastic effect on the cancer cells [16,47,56,134].

1.5.4. Benefits

The benefits of DEB-TACE are: 1. A reduction in adverse reactions by delivering the active agent directly to the target site [70,88]. 2. Direct delivery as this increases the duration the tumour is exposed to the drug [135]. Traditional chemotherapy brings systemic distribution of the drug which induces non-specific cytotoxicity and increases the risk of side effects, limiting drug concentrations, and therefore reducing the levels of drug transported to the solid tumour and surrounding tissue. Systemic therapy can also result in the development of drug resistance which represents a growing problem [136]. 3. Significantly higher concentrations of drug may be delivered with the use of DEB-TACE than can be transported systemically in non-toxic doses. This reduces the risk of cancer cells becoming aggressive at sub-lethal concentrations [51,123,135]. 4. DC Bead™ can either be used as a monotherapy or in an amalgamation of therapies, and has been proven to achieve and maintain cytotoxic conditions safely and effectively through a combination of Phase I, II and III clinical studies and randomised control trials [72,79,80,137–139]. 5. Embolisation is possible due to tumours having 95 % of their blood supplied through the hepatic artery, whilst the remaining liver parenchyma perfusion receives only 25 % of its blood supply through the hepatic artery and the additional 75 % via portal blood flow [83]. 6. Finally, as a result of reduced trauma patients recover faster with no scaring and minimal risk of infection.

DEB-TACE is considered to have an effective EPR, however local delivery of chemotherapeutic agent may not be effective against systemic disease and it is becoming increasingly common to combine DEB-TACE with systemic therapies. A poor response to DEB-TACE may be due to incomplete or ineffective treatment. Incomplete treatment can occur when only a portion of tumour feeding arteries are embolised, resulting in an adequate blood supply to the tumour. It could also arise from insufficient quantities of DEB delivered to the tumour as a result of aggregation or oversized beads, leaving areas under-dosed. Ineffective treatment could transpire because of drug or ischemia resistance [89].

1.5.5. Histology

There were no adverse reactions associated in the administration of the beads with 150 mg of Dox in a porcine model. Electrocardiography, enzyme levels and pathological examination proposed that the concentration of Dox released into systemic circulation was below the amount required to induce cardiac toxicity. Liver aminotransferase enzymes were initially greater in all treatment groups as a result of embolic beads present in the hepatic arteries and the subsequent hepatocyte damage. The increase in these enzymes is temporary and levels returned to the original measure within 1 month of the procedure. The group embolised with small particles had elevated enzyme levels, as smaller particles produced greater tissue necrosis because of the more distal occlusion. Smaller beads with higher Dox loading concentrations induced a greater degree of hepatic injury and tissue damage reduced the extent of revascularisation. The model demonstrated the combination of Dox and DEBs small in diameter create widespread tissue damage [16]. Apoptosis under hypoxic conditions caused fibrosis, inflammation and necrosis, which radiated out from the centre of DEB clusters [16,82,96]. Dox travels further through necrotic tissue because it cannot be carried away by the extensive vasculature or metabolised by the vast hepatocytes as it has been destroyed. The injured hepatoma activates the inflammatory response to stimulate the division of cell and regeneration of damaged tissue, making the organ particularly sensitive to chemotherapeutic agents such as Dox since it actively synthesises new DNA. Dox affects all cells, but the drug mechanism of action is based upon the sensitivity of rapidly dividing cancerous cells [16].

1.6. DC Bead LUMI™

Biocompatibles UK Ltd have other bead products in development and one type named DC Bead LUMI™ was recently launched onto the market. DC Bead LUMI™ builds upon the chemical structure of DC Bead™ and was developed to be a radiopaque form. It consists of iodinated polyvinyl alcohol – acrylamido methylpropane sulfonate groups, where DC Bead™ comprises polyvinyl alcohol – acrylamido methylpropane sulfonates. Simply the addition of iodine is in place of blue dye during the manufacturing process. Iodine is consistently and evenly distributed through the bead, it is covalently bonded and is therefore a permanent fixture that does not degrade. The radiopaque properties allow for visibility of the beads under all standard X-ray imaging modalities such as fluoroscopy, single-shot or cone beam CT, during and after the procedure. It was designed to improve the accuracy and control of the predicate device with bead location, coverage, targeted embolisation and precise determination of the procedural endpoint. It allows for intra-procedural adjustments and post-procedural feedback, and Figure 1.14 provides an image of the embolisation 'footprint' with DC Bead LUMI™ [140].

Figure 1.14: Distinct visualisation of occluded vessels with DC Bead LUMI™, arrow points to occluded vessels [141].

As DC Bead™ and DC Bead LUMI™ consist of the same core technology of a sulfonate ion-exchange mechanism, drug loading recommendations are the same (37.5 mg Dox/1 mL bead equivalent to 75 mg Dox/vial and 50 mg Iri/1 mL bead equivalent to 100 mg Iri/vial). DC Bead LUMI™ is purchased as 2 mL of beads suspended in 6 mL of PBS, presented in a sterile 10 mL glass vial. Detailed in Table 1.2 are the available sizes, these are identical to the two currently smallest sizes of the well-established DC Bead™ model. The only practical difference is that DC Bead™ has a 48-month shelf life compared with DC Bead LUMI™ which has a 24-month shelf life, however stability testing to extend the shelf life is ongoing. DC Bead LUMI™ is intended as an embolic device with or without the addition of drug for the treatment of malignant and non-malignant HVTs and AVMs, indicated for HCC and mCRC patients. It is compatible with Dox and Iri, and is stated to have achieved complete and controlled release [140].

Table 1.2: Available DC Bead LUMI™, their sizes and label colour [142].

Bead Reference	Bead Size (µm)	Label Colour	Product Image
M1	70-150	Black	
103	100-300	Yellow	

It is important to fully characterise such formulations to optimise their bioavailability for patients. Understanding the interaction of drug with the aforementioned polymeric carrier will allow optimisation and modification of the design of new types of DDSs for even more effective targeted drug therapy. This research project aims to investigate whether the chemical and structural properties of DC Bead LUMI™ produce different results to the standard DC Bead™.

1.7. LifePearl™

LifePearl™ is an embolisation microsphere indicated for the treatment of primary HVTs and liver metastasis. Like DC Bead™ it is designed to be used bland or for loading with drugs such as Dox or Iri. It is manufactured by Terumo Corporation and is the most recently developed DEB, it was released in Europe during 2015 but is not yet approved for use in the USA. LifePearl™ is a polyethylene glycol (PEG), biocompatible, hydrophilic, compressible, elastic, tightly calibrated and controlled release hydrogel. The product boasts enhance suspension characteristics with minimised time to suspension and maximised time in suspension. Similar to DC Bead™ drug-bead binding is through a sulfonate site, but with the addition of 3-sulfopropyl acetate sodium salt (SPA) rather than AMPS. Presented in Table 1.3 is the device in a syringe with 2 mL of beads in 4 mL of PBS [143].

Table 1.3: Available LifePearl™, their sizes and label colour [143].

Bead Reference	Bead Size (µm)	Label Colour	Product Image
100	100 ± 25	Black	
200	200 ± 50	Yellow	
400	400 ± 50	Blue	

Analysis undertaken by Biocompatibles UK Ltd reported the unpublished data summarised in Table 1.4. Using the calculated sulfonate content, the theoretical loading capacity of LifePearl™ is 47.8 mg/mL compared with a higher loading capacity of 58.4 mg/mL for DC Bead™. Solid and water content was also evaluated in the original bead packaging solution.

Table 1.4: Components of DC Bead™ and LifePearl™.

Bead Type	Sulfonate Content (mol)	Solid Content (%)	Water Content (%)
DC Bead*M1*™ (70-150 µm)	1.0×10^{-4}	6.2	93.8
LifePearl™ 100 (75-125 µm)	0.83×10^{-4}	4.1	95.9

1.8. Tandem™

The main competitor to DC Bead™ is Tandem™ (known as Oncozene™ in the USA) produced by Boston Scientific Corporation and launched in 2012. Embozene Tandem™ Microspheres are indicated for embolisation and used with 50 mg/mL Dox or Iri, however the biocompatible hydrogel is also capable of loading compounds such as epirubicin (Epi) and idarubicin (Ida) [144]. Tandem™ is a polymethacrylate (PMA) sodium coated with a patented inorganic perfluorinated polymer (Polyzene®-F). It is indicated for the treatment of AVMs, HCC, HVTs, uterine fibroids, along with tumour of the head, neck, torso and skeletal system, as well as bleeding and trauma, in addition to preoperative reduction of bleeding other than the central nervous system [145]. The benefits are defined as the smallest size bead with the tightest calibration, offering up to 3 mL beads and a 3-year shelf life. The microspheres allow fast drug loading time, superior drug loading capacity, precise drug delivery, efficient drug release rates, and a stable size during drug loading and storage (<5 % size change) [144].

The opaque beads are available in various sizes, and in 2 and 3 mL volumes. Displayed in Table 1.5 are the beads packaged in 20 mL syringes with colour coded labels and one 3 mL volume of Tandem™ is alleged to deliver 150 mg of the loaded drug. The microspheres are stored in a suspension of non-pyrogenic sterile solution of physiological saline, the total volume of material and solution inside the syringe is approximately 7 mL. This solution is removed before loading the product with the required drug. Tandem™ is not to be used with ionic contrast agent as this could lead to microsphere deformation. The vascular is evaluated using high resolution imaging and non-ionic contrast agent prior to the embolisation procedure. Each package is intended for single patient use, the size and quantity is selected by the physician according to the lesion to be treated [145].

Table 1.5: Available Tandem™, their sizes and label colour [146].

Bead Reference	Bead Size (µm)	Label Colour	Product Image
104	40 ± 10	Black	
107	75 ± 15	Burgundy	
110	100 ± 25	Orange	

1.9. Hepasphere™

Another competitor to DC Bead™ is HepaSphere™ (known as QuadraSphere™ in the USA) manufactured by Merit Medical Systems, Inc. and launched shortly after DC Bead™ [147–152]. HepaSphere™ is a PVA acrylic acid superabsorbent copolymer, which has the ability to increase up to 64 times its original size. It has a similar mechanism to DC Bead™, except the ionic interaction with the bead and drug is through carboxylate groups and not sulfate groups. It is suggested that since Dox-polymer interactions are similar, the elution profile is also akin [148]. The hydrophilic microsphere is made of two monomer units, vinyl acetate and methyl acrylate, which combine to form sodium acrylate alcohol copolymer. HepaSphere™ is indicated for the embolisation of HCC and metastases to the liver when loaded with Dox, and mCRC to the liver when loaded with Iri. The advantages are understood to be targeted delivery, fast loading, compressibility and an expanding structure [153].

The product is supplied in a 10 mL glass vial with a crimped cap, and in 25 and 50 mg options. The size of sphere in Table 1.6 is selected by the physician according to the size of the target vessel. The microspheres are supplied dry and must be reconstituted before use. 75 mg of Dox can be loaded into one HepaSphere™ vial and it is intended for practise with non-ionic contrast media [154].

Table 1.6: Available HepaSphere™, their sizes and label colour [155].

Bead Reference	Bead Size (µm)	Expanding Size (µm)	Label Colour	Product Image
200	30-60	120-240	Orange	
300	50-100	200-400	Yellow	
500	100-150	400-600	Blue	
700	150-200	600-800	Red	

1.10. Experimental Analysis of Drug-Bead Systems

It is difficult to evaluate drugs and delivery systems *in vivo*, consequently *in vitro* methods must also be developed to mimic *in vivo* conditions. *In vivo* methods are disadvantaged because data observed in a single animal species is not always equivalent to human outcomes, and different animal species have different pharmacokinetics making it difficult to extrapolate or generalise data. *In vitro* methods also have their weaknesses as homeostatic mechanisms are not present in the test, however *in vitro* tests are capable of testing specific mechanisms of action, they can be performed without the need to address ethical issues, can be quick and inexpensive to perform. Owing to these discrepancies in *in vivo* test methods it is desirable to consider the use of multiple models, and to study the differences and similarities between models and an actual tumour. When *in vivo* and *in vitro* methods correlate well they have the potential for predicting attributes required of the drug delivery device.

It is important to not only to understand how the drug and DDS interact with the tumour and the rest of the body, but also how the drug and DDS interact with one another to provide effective treatment. Understanding drug-excipient interactions is essential in light of their potential to bind and release particular drugs in a controlled and sustained manner.

1.10.1. Thermodynamics

There has been considerable data gathered both *in vivo* and *in vitro* relating to DEBs, however presently no data has been generated corresponding to the thermodynamics of the beads. Isothermal titration calorimetry (ITC) is an established analytical technique used to study the binding interactions of molecules. The instrument displays a variety of thermodynamic parameters for chemical and biological systems. The intermolecular interactions allow determination of parameters such as binding constant (K), reaction stoichiometry (N), enthalpy (ΔH), entropy (ΔS) and Gibbs free energy (ΔG) for any given system. From these units the number of binding sites, binding ratio, type of bonding (hydrogen, ionic and van der Waals), type of binding interaction (electrostatic and hydrophobic), order, spontaneity, conformation and aggregation state can be identified.

Previous studies have included the use of ITC to determine the reactive sites on active ester surfmers nanoparticle beads with the amine containing compound remazol brilliant blue. The interaction between the nuclepohilic group of the dye and the activated ester was an exothermic 1:1 reaction. The

reaction was successfully carried out at 298 K with a buffer of pH 7.5 [156]. The interaction of chemically modified Pluronic block copolymers such as poly-acrylic acid (PAA) grafted to poly-ethylene oxide (PEO) with Dox has also been evaluated. 15 mM of Dox was titrated into 0.01 % wt PEO-PAA over a pH range of 4.3 to 7.1. It was found that exothermic peaks became broader with an increase in pH, suggesting that more Dox molecules were bound to the polymer chain as the pH increased [157]. Figure 1.15 displays the main components of the ITC, in this circumstance as the syringe rotates drug is injected into beads. The bottom of the cell is coin shaped and there are two internally identical cells, one to hold the sample and the other is the reference cell. The heat difference between the two cells are measured for analysis.

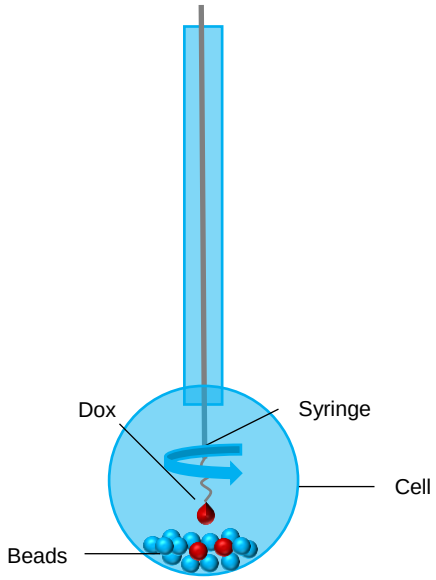

Figure 1.15: ITC cell and syringe with Dox titrated into beads.

1.10.2. Drug Loading

The amount of Dox loaded into beads can be determined by immersing a measured volume of beads into a Dox solution. Dox concentration can then be defined by measuring absorbance of the residual drug in the depleted solution and converting absorbance to concentration using a calibration plot. It has been publicised that >99 % of a 37.5 mg Dox solution can be loaded into DC Bead™. A maximum of 40 mg of Dox was loaded in 1 mL of beads and the time taken for beads to load drug was dependent upon bead size, with smaller beads loading faster due to a larger surface area. This was also associated with a reduction of water contained in the bead and the effect is more pronounced in the larger bead ranges.

The fluorescent distribution across the surface of beads showed Dox to be homogenously dispersed, however cross-section analysis revealed that the internal distribution of the drug is concentrated around the outer 20 µm of the bead, although there was Dox present in the internal structure [47].

1.10.3. Drug Elution

High performance liquid chromatography (HPLC) has shown that Dox before and after loading does not change chemical structure, i.e. it does not degrade. Furthermore, Dox was found to elute in PBS and plasma, but did not release in water as the rate of release was dependent upon the concentration of salt, i.e. at higher salt concentrations a larger amount of drug was eluted from the beads [88].

The elution of Dox in different ionic strength solutions was evaluated using the United States Pharmacopeia (USP) Type 2 Dissolution Apparatus (found in Chapter 711 of the USP), the paddle type fitting is represented in Figure 1.16 but this can be replaced with other components. The study showed 30:70 potassium chloride in 20 % w/v ethanol to be the most suitable elution media and the drug release profile to follow first order kinetics. Elution increased as the diameter of the bead decreased because of the larger surface area, therefore the elution rate was inversely proportional to bead size [88].

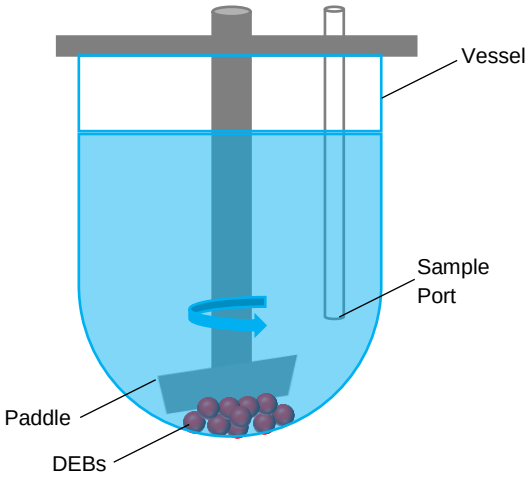

Figure 1.16: USP Type 2 dissolution apparatus.

The USP 2 guidelines state that the *in vitro* release testing of implantable drug-device combination products may be evaluated by immersing the system, usually with a stirring element such as a paddle,

in a static suitable elution medium whilst heated to 310 K. The medium may be exchanged periodically to prevent drug saturation and is sampled intermittently for analytical determination of the elution kinetics. In a closed loop system the selected drug can be eluted under sink conditions, however the drug is released via an ion-exchange mechanism, therefore it is the presence of ions which allow the drug to detach from the bead. Even if there is ample medium to dissolve the drug there may not be enough ions for the mechanism to occur once equilibrium has been reached. Under a fixed volume of elution media there is limited exchange of eluent ions, it is for his reason that it is more appropriate to perform the elution of drug from DEBs in an open loop system.

Nonetheless, in a high concentration of salt Hecq *et al.* showed that >90 % of Dox loaded in 500-700 µm DC Bead™ eluted in less than 2 hours from a USP 2 closed loop system [158]. Gonzalez *et al.* and Lewis *et al.* had similar observations with 100-300, 300-500, 500-700 and 700-900 µm DC Bead™ [88,89]. The paddle suspends beads in the elution media, yet this would not be the case in a vessel and so the method tends to exaggerate the rate of elution. This technique is more useful for quality control purposes but inappropriate for *in vivo* correlations.

An alternative method is the USP Type 4 Dissolution Apparatus (found in Chapter 711 of the USP). Figure 1.17 depicts the flow-through cell where the elution medium may be circulated around or through the system, depending on its configuration using flow-through apparatus. DEBs have been evaluated with this method, but it was unable to demonstrate complete drug elution from the systems under this study due to experimental conditions. Fuchs *et al.* suggested that 100-300 µm DC Bead™ loaded with Sunitinib in a flow-through cell released only 80% of the drug when microsphere were densely packed together, but this was using USP 4 in a closed loop system in which there was a limited number of ions available. The addition of a bed of glass beads to sit on top of the polymer spheres did not significantly change the elution profile [159]. Few beads would pack together in a vessel, therefore dense packing may not emulate the *in vivo* situation and could predict lower elution rates as the medium fails to gain access to the entirety of each microsphere underestimating the elution of drug. Nonetheless, USP 4 is an improvement on USP 2 as it better predicts drug released into systemic circulation [89].

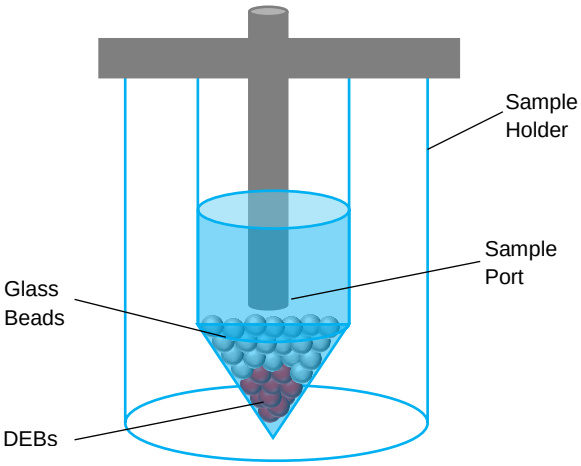

Figure 1.17: USP Type 4 dissolution apparatus.

The T-Apparatus as seen in Figure 1.18, was designed to simulate *in vivo* conditions and results fitted a slow release model. Half-life ($t_{1/2}$) was determined and was found to increase with the concentration of Dox loaded in the beads. $t_{1/2}$ also increased with bead diameter, but the increase was not proportional [88]. The T-Apparatus was proposed as an alternative method that better emulates the embolisation environment by profusion of diffusion and convection zones, representing drug diffusion from the beads through the vessel and surrounding tissues, and then its removal in blood flowing through more distant patent vessels [160]. This method proved useful in predicting the first 24 hours of drug release into systemic circulation, producing a level A *in vitro:in vivo* correlation (IVIVC). The technique is however cumbersome and not without technical limitations when forecasting elution data beyond 24 hours.

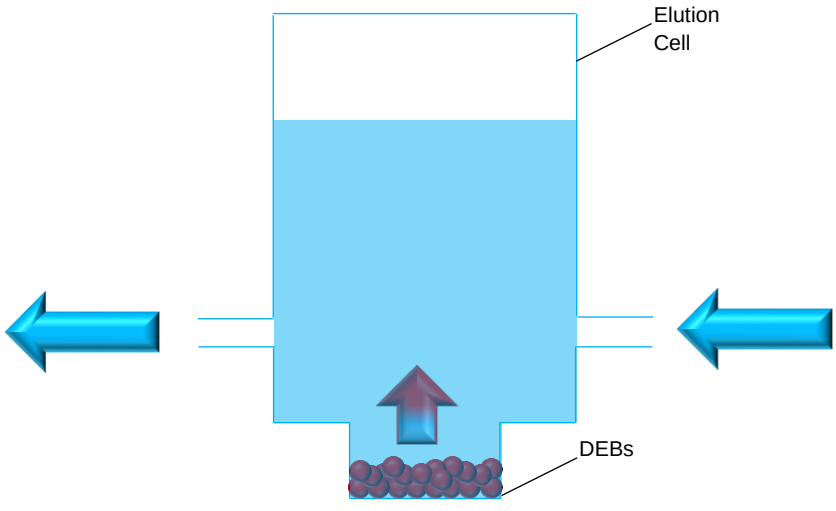

Figure 1.18: T-Apparatus for measurement of drug elution.

Several attempts have been made to standardise microsphere *in vitro* release testing [160–162]. This study reports the development of a new elution method for the evaluation of DEBs, which overcome some of the short-comings of previously reported methods and will allow a better comparison between the performances of different products despite their different characteristics. The aim was that the methods developed would distinguish between different formulations and mimic *in vivo* conditions, therefore enhancing the understanding of drug-DEB interactions.

1.10.4. *In Vivo* Studies

In a pharmacokinetic study Dox was detected in the plasma 24 hours longer in smaller beads and although the concentration of Dox was 1.5 times greater, the peak concentration was 15 times higher than larger bead groups, an effect of the larger surface area with smaller beads [16]. Crucially, Dox was found to remain in 100-300 and 700-900 µm beads for at least 90 days [96]. Dox loaded beads were found both inside and around the periphery of tumours, and an average of one bead occluded one vessel [84]. This is useful information when designing methods and making *in vivo* – *in vitro* correlations.

1.11. Project Objectives

The overarching aim of this study is to investigate drug-bead interactions, to understand how they affect binding and subsequent drug release phenomena using *in vitro* techniques to mimic *in vivo* scenarios.

This aim will be achieved through the following three objectives:

1. The application of ITC to investigate drug-bead binding interactions.

Initially, the concept of using ITC to monitor drug-bead binding will be considered, permitting calculation of drug-bead binding ratios over a range of temperatures and concentrations. Subsequently, a variety of bead sizes, bead types and a set of drugs applicable to bead-based delivery systems will be analysed to determine their effect on binding ratio. It is hoped that analysing drug binding using ITC will provide a unique and simple way to quantify such interactions.

2. The development of a novel method to determine the release of drug from DEBs.

A new release method will be investigated to overcome the limitations experienced with existing techniques. It is to incorporate an open-loop system producing standardised, characterised and reproducible *in vivo* correlated data. Primarily, various flow rates and salt concentrations will be evaluated to identify suitable method parameters. Comparisons will be made between elution data using different bead sizes and bead types, with different drugs and drug concentrations.

3. Confirmation of drug loading, drug elution and microscopic analysis.

Conclusions will be drawn from data using both methods investigated in Objectives 1 and 2, along with quantification of residual and extracted drug from DEBs, to confirm as to whether complete drug loading or elution has been achieved from both ITC and elution experiments. Visual analysis of the beads will be conducted using microscopy before, during and after elution to support the previous results.

References

1 R. Mrsny, in *Biomaterials for Cancer Therapeutics*, Elsevier, 2013, pp. 20–30.

2 A. Gilman, The initial clinical trial of nitrogen mustard, *Am. J. Surg.*, 1963, **105**, 574–578.

3 R. Siegel, D. Naishadham and A. Jemal, Cancer statistics, 2012, *CA. Cancer J. Clin.*, 2012, **62**, 10–29.

4 B. K. Lee, Y. H. Yun, K. Park and M. Sturek, in *Biomaterials for Cancer Therapeutics*, Elsevier, 2013, pp. 3–19.

5 R. Zeineldin, in *Biomaterials for Cancer Therapeutics*, Elsevier, 2013, pp. 137–164.

6 S. Bhatia, J. V Frangioni, R. M. Hoffman, A. J. Iafrate and K. Polyak, The challenges posed by cancer heterogeneity, *Nat. Biotechnol.*, 2012, **30**, 604.

7 L. Fass, Imaging and cancer: A review, *Mol. Oncol.*, 2008, **2**, 115–152.

8 S. Achilefu, Introduction to Concepts and Strategies for Molecular Imaging, *Chem. Rev.*, 2010, **110**, 2575–2578.

9 A. L. Lewis, in *Biomaterials for Cancer Therapeutics*, Elsevier, 2013, pp. 207–239.

10 Cancer today IARC, Cancer fact sheets: Liver cancer cancer, http://gco.iarc.fr/today/fact-sheets-cancers?cancer=7&type=0&sex=0, (accessed 1 June 2014).

11 Cancer today IARC, Cancer fact sheets: Colorectal cancer cancer, http://gco.iarc.fr/today/fact-sheets-cancers?cancer=6&type=0&sex=0, (accessed 1 June 2014).

12 R. Adam, V. Lucidi and H. Bismuth, Hepatic colorectal metastases: methods of improving resectability, *Surg. Clin. North Am.*, 2004, **84**, 659–671.

13 R. R. Taylor, Y. Tang, M. V. Gonzalez, P. W. Stratford and A. L. Lewis, Irinotecan drug eluting beads for use in chemoembolization: In vitro and in vivo evaluation of drug release properties, *Eur. J. Pharm. Sci.*, 2007, **30**, 7–14.

14 E. Eyol, A. Boleij, R. Holden, A. Lewis and M. Berger, Chemoembolisation of rat colorectal liver metastases with drug eluting beads loaded with irinotecan or doxorubicin, *Clin. Exp. Metastasis*,

2008, **25**, 273–282.

15 J.M Llovet, Updated treatment approach to hepatocellular carcinoma, *J. Gastroenterol.*, 2005, **40**, 225–235.

16 A. L. Lewis, R. R. Taylor, B. Hall, M. V. Gonzalez, S. L. Willis and P. W. Stratford, Pharmacokinetic and Safety Study of Doxorubicin-eluting Beads in a Porcine Model of Hepatic Arterial Embolization, *J. Vasc. Interv. Radiol.*, 2006, **17**, 1335–1343.

17 G. Fusai and B. R. Davidson, Management of colorectal liver metastases, *Color. Dis.*, 2003, **5**, 2–23.

18 A. Villanueva, V. Hernandez-Gea and J. M. Llovet, Medical therapies for hepatocellular carcinoma: a critical view of the evidence, *Nat. Rev. Gastroenterol. &Amp; Hepatol.*, 2012, **10**, 34.

19 K. Park, Controlled drug delivery systems: Past forward and future back, *J. Control. Release*, 2014, **190**, 3–8.

20 A. S. Hoffman, The origins and evolution of ‘controlled’ drug delivery systems, *J. Control. Release*, 2008, **132**, 153–163.

21 V. V Ranade and J. B. Cannon, *Drug Delivery Systems, Third Edition*, Taylor & Francis, 2011.

22 K. K. Jain, *Drug Delivery Systems - An Overview*, Humana Press, Totowa, NJ, 2008.

23 K. Park, *Biomaterials for Cancer Therapeutics: Diagnosis, Prevention and Therapy*, 2013.

24 S. Boeckle and E. Wagner, Optimizing targeted gene delivery: Chemical modification of viral vectors and synthesis of artificial virus vector systems, *AAPS J.*, 2006, **8**, E731–E742.

25 D. L. Stirland, J. W. Nichols, T. A. Denison and Y. H. Bae, in *Biomaterials for Cancer Therapeutics*, Elsevier, 2013, pp. 31–56.

26 C. Wong, T. Stylianopoulos, J. Cui, J. Martin, V. P. Chauhan, W. Jiang, Z. Popović, R. K. Jain, M. G. Bawendi and D. Fukumura, Multistage nanoparticle delivery system for deep penetration into tumor tissue, *Proc. Natl. Acad. Sci. U. S. A.*, 2011, **108**, 2426–2431.

27 E. S. Lee, Z. Gao, D. Kim, K. Park, I. C. Kwon and Y. H. Bae, Super pH-sensitive Multifunctional Polymeric Micelle for Tumor pH(e) Specific TAT Exposure and Multidrug Resistance, *J. Control. Release*, 2008, **129**, 228–236.

28 M. Silhol, M. Tyagi, M. Giacca, B. Lebleu and E. Vivès, Different mechanisms for cellular internalization of the HIV-1 Tat-derived cell penetrating peptide and recombinant proteins fused to Tat, *Eur. J. Biochem.*, 2002, **269**, 494–501.

29 Y. Ueda, S. Wang, N. Dumont, J. Y. Yi, Y. Koh and C. L. Arteaga, Overexpression of HER2 (erbB2) in Human Breast Epithelial Cells Unmasks Transforming Growth Factor β-induced Cell Motility, *J. Biol. Chem.* , 2004, **279**, 24505–24513.

30 S. Liu, S. J. Shah, L. J. Wilmes, J. Feiner, V. D. Kodibagkar, M. F. Wendland, R. P. Mason, N. Hylton, H. W. Hopf and M. D. Rollins, Quantitative Tissue Oxygen Measurement in Multiple Organs Using (19)F MRI in a Rat Model, *Magn. Reson. Med.*, 2011, **66**, 1722–1730.

31 G. U. Dachs, A. V Patterson, J. D. Firth, P. J. Ratcliffe, K. M. S. Townsend, I. J. Stratford and A. L. Harris, Targeting gene expression to hypoxic tumor cells, *Nat. Med.*, 1997, **3**, 515.

32 Y. Tang, K. Schmitt-Ott, K. Qian, S. Kagiyama and M. Ian Phillips, Vigilant vectors: adeno-associated virus with a biosensor to switch on amplified therapeutic genes in specific tissues in life-threatening diseases, *Methods*, 2002, **28**, 259–266.

33 I. F. Tannock and D. Rotin, Acid pH in Tumors and Its Potential for Therapeutic Exploitation, *Cancer Res.*, 1989, **49**, 4373 LP-4384.

34 M. E. Richardson and D. W. Siemann, Tumor cell heterogeneity: Impact on mechanisms of therapeutic drug resistance, *Int. J. Radiat. Oncol.*, 1997, **39**, 789–795.

35 S. K. Hobbs, W. L. Monsky, F. Yuan, W. G. Roberts, L. Griffith, V. P. Torchilin and R. K. Jain, Regulation of transport pathways in tumor vessels: Role of tumor type and microenvironment, *Proc. Natl. Acad. Sci. U. S. A.*, 1998, **95**, 4607–4612.

36 M. Stubbs, P. M. McSheehy and J. R. Griffiths, Causes and consequences of acidic pH in tumors: a magnetic resonance study, *Adv. Enzyme Regul.*, 1999, **39**, 13—30.

37 A. J. Thistlethwaite, G. A. Alexander, D. J. Moylan and D. B. Leeper, Modification of human tumor

pH by elevation of blood glucose, *Int. J. Radiat. Oncol.*, 1987, **13**, 603–610.

38 A. Pluen, Y. Boucher, S. Ramanujan, T. D. McKee, T. Gohongi, E. di Tomaso, E. B. Brown, Y. Izumi, R. B. Campbell, D. A. Berk and R. K. Jain, Role of tumor–host interactions in interstitial diffusion of macromolecules: Cranial vs. subcutaneous tumors, *Proc. Natl. Acad. Sci. U. S. A.*, 2001, **98**, 4628–4633.

39 D. Lu, M. G. Wientjes, Z. Lu and J. L.-S. Au, Tumor Priming Enhances Delivery and Efficacy of Nanomedicines, *J. Pharmacol. Exp. Ther.*, 2007, **322**, 80 LP-88.

40 L. Eikenes, M. Tari, I. Tufto, Ø. S. Bruland and C. de Lange Davies, Hyaluronidase induces a transcapillary pressure gradient and improves the distribution and uptake of liposomal doxorubicin (Caelyx™) in human osteosarcoma xenografts, *Br. J. Cancer*, 2005, **93**, 81–88.

41 A. M. Dvorak and D. Feng, The Vesiculo–Vacuolar Organelle (VVO): A New Endothelial Cell Permeability Organelle, *J. Histochem. Cytochem.*, 2001, **49**, 419–431.

42 T. Teesalu, K. N. Sugahara, V. R. Kotamraju and E. Ruoslahti, C-end rule peptides mediate neuropilin-1-dependent cell, vascular, and tissue penetration, *Proc. Natl. Acad. Sci. U. S. A.*, 2009, **106**, 16157–16162.

43 P. Ehrlich and C. Bolduan, *Collected studies on immunity*, J. Wiley, New York, 1906.

44 P. Ehrlich, *Über den jetzigen Stand der Karzinomforschung*, 1908.

45 R. Yamada, H. Nakatsuka, K. Nakamura, M. Sato, M. Itami, N. Kobayashi, K. Minakuchi, T. Onoyama, T. Kanno, T. Monna and S. Yamamoto, Hepatic artery embolization in 32 patients with unresectable hepatoma, *Osaka City Med. J.*, 1980, **26**, 81—96.

46 L. Marelli, R. Stigliano, C. Triantos, M. Senzolo, E. Cholongitas, N. Davies, J. Tibballs, T. Meyer, D. W. Patch and A. K. Burroughs, Transarterial Therapy for Hepatocellular Carcinoma: Which Technique Is More Effective? A Systematic Review of Cohort and Randomized Studies, *Cardiovasc. Intervent. Radiol.*, 2006, **30**, 6.

47 A. L. Lewis, M. V. Gonzalez, S. W. Leppard, J. E. Brown, P. W. Stratford, G. J. Phillips and A. W. Lloyd, Doxorubicin eluting beads − 1: Effects of drug loading on bead characteristics and drug distribution, *J. Mater. Sci. Mater. Med.*, 2007, **18**, 1691–1699.

48 K. Malagari, Drug-eluting particles in the treatment of HCC: chemoembolization with doxorubicin-loaded DC Bead™, *Expert Rev. Anticancer Ther.*, 2008, **8**, 1643–1650.

49 A. Lewis, *Drug Device Combination Products: Delivery Technologies and Applications*, 2009.

50 M.-S. Chen, J.-Q. Li, Y.-Q. Zhang, L.-X. Lu, W.-Z. Zhang, Y.-F. Yuan, Y.-P. Guo, X.-J. Lin and G.-H. Li, High-dose iodized oil transcatheter arterial chemoembolization for patients with large hepatocellular carcinoma, *World J. Gastroenterol.*, 2002, **8**, 74–78.

51 D. Struk, R. N. Rankin and S. J. Karlik, Stability studies on chemoembolization mixtures. Dialysis studies of doxorubicin and lipiodol with Avitene, Gelfoam, and Angiostat, *Invest. Radiol.*, 1993, **28**, 1024—1027.

52 T. de Baere, J. Dufaux, A. Roche, J. L. Counnord, M. F. Berthault, A. Denys and P. Pappas, Circulatory alterations induced by intra-arterial injection of iodized oil and emulsions of iodized oil and doxorubicin: experimental study., *Radiology*, 1995, **194**, 165–170.

53 Z. Kan, K. Wright and S. Wallace, Ethiodized oil emulsions in hepatic microcirculation: In vivo microscopy in animal models, *Acad. Radiol.*, 1997, **4**, 275–282.

54 S. W. Yi, Y.-H. Kim, I. C. Kwon, J. W. Chung, J. H. Park, Y. W. Choi and S. Y. Jeong, Stable lipiodolized emulsions for hepatoma targeting and treatment by transcatheter arterial chemoembolization, *J. Control. Release*, 1998, **50**, 135–143.

55 W.-S. Tzeng, R.-H. Wu, S.-C. Chang, C.-K. Chou, C.-Y. Lin, J.-J. Chen, S.-C. Yang and C.-H. Lin, Ionic Versus Nonionic Contrast Media Solvents Used with an Epirubicin-based Agent for Transarterial Chemoembolization of Hepatocellular Carcinoma, *J. Vasc. Interv. Radiol.*, 2008, **19**, 342–350.

56 E. Liapi and J.-F. H. Geschwind, Transcatheter Arterial Chemoembolization for Liver Cancer: Is It Time to Distinguish Conventional from Drug-Eluting Chemoembolization?, *Cardiovasc. Intervent. Radiol.*, 2011, **34**, 37–49.

57 D. B. Brown, J. E. Gould, D. A. Gervais, S. N. Goldberg, R. Murthy, S. F. Millward, W. S. Rilling, J.-F. S. Geschwind, R. Salem, S. Vedantham and M. C. Soulen, Transcatheter Therapy for Hepatic Malignancy: Standardization of Terminology and Reporting Criteria, *J. Vasc. Interv.*

Radiol., 2009, **20**, S425–S434.

58 M. A. Maluccio, A. M. Covey, L. Ben Porat, J. Schubert, L. A. Brody, C. T. Sofocleous, G. I. Getrajdman, W. Jarnagin, R. DeMatteo, L. H. Blumgart, Y. Fong and K. T. Brown, Transcatheter Arterial Embolization with Only Particles for the Treatment of Unresectable Hepatocellular Carcinoma, *J. Vasc. Interv. Radiol.*, 2008, **19**, 862–869.

59 H. Nakamura, T. Hashimoto, H. Oi and S. Sawada, Transcatheter oily chemoembolization of hepatocellular carcinoma., *Radiology*, 1989, **170**, 783–786.

60 Y. Sasaki, S. Imaoka, H. Kasugai, M. Fujita, S. Kawamoto, S. Ishiguro, J. Kojima, O. Ishikawa, H. Ohigashi and H. Furukawa, A new approach to chemoembolization therapy for hepatoma using ethiodized oil, cisplatin, and gelatin sponge, *Cancer*, 1987, **60**, 1194—1203.

61 D. B Brown, J.-F. H Geschwind, M. C Soulen, S. F Millward and D. Sacks, Society of Interventional Radiology Position Statement on Chemoembolization of Hepatic Malignancies, *J. Vasc. Interv. Radiol.*, 2006, **17**, 217–223.

62 J.-F. H. Geschwind, D. E. Ramsey, B. C. H. van der Wal, H. Kobeiter, K. Juluru, G. G. Hartnell and M. A. Choti, Transcatheter Arterial Chemoembolization of Liver Tumors: Effectsof Embolization Protocol on Injectable Volume of Chemotherapy andSubsequent Arterial Patency, *Cardiovasc. Intervent. Radiol.*, 2003, **26**, 111–117.

63 D. B. Brown, T. K. Pilgram, M. D. Darcy, C. E. Fundakowski, M. Lisker-Melman, W. C. Chapman and J. S. Crippin, Hepatic Arterial Chemoembolization for Hepatocellular Carcinoma: Comparison of Survival Rates with Different Embolic Agents, *J. Vasc. Interv. Radiol.*, 2005, **16**, 1661–1666.

64 R. J Lewandowski, D. Wang, J. Gehl, B. Atassi, R. Ryu, K. Sato, A. A Nemcek, F. H Miller, M. Mulcahy, L. Kulik, A. C Larson, R. Salem and R. A Omary, A Comparison of Chemoembolization Endpoints Using Angiographic versus Transcatheter Intraarterial Perfusion/MR Imaging Monitoring, *J. Vasc. Interv. Radiol.*, 2007, **18**, 1249–1257.

65 I. V Ward Small, P. R Buckley, T. Wilson, W. Benett, J. Hartman, D. Saloner and D. Maitland, Shape Memory Polymer Stent With Expandable Foam: A New Concept for Endovascular Embolization of Fusiform Aneurysms, *IEEE Trans. Biomed. Eng.*, 2007, **54**, 1157–1160.

66 J. H. Grindlay and O. T. Clagett, A plastic sponge prosthesis for use after pneumonectomy; preliminary report of an experimental study, *Proc. Staff Meet. Mayo Clin.*, 1949, **24**, 538.

67 A. L. Lewis, C. Adams, W. Busby, S. A. Jones, L. C. Wolfenden, S. W. Leppard, R. R. Palmer and S. Small, Comparative in vitro evaluation of microspherical embolisation agents, *J. Mater. Sci. Mater. Med.*, 2006, **17**, 1193–1204.

68 D. J. Kerr, Microparticulate drug delivery systems as an adjunct to cancer treatment, *Cancer Drug Deliv.*, 1987, **4**, 55—61.

69 A. L. Lewis, DC Bead™: a major development in the toolbox for the interventional oncologist, *Expert Rev. Med. Devices*, 2009, **6**, 389–400.

70 A. Lewis, M. González, A. Lloyd, B. Hall, Y. Tang, S. Willis, S. Leppard, L. C Wolfenden, R. R Palmer and P. Stratford, DC Bead: In Vitro Characterization of a Drug-delivery Device for Transarterial Chemoembolization, *J. Vasc. Interv. Radiol.*, 2006, **17**, 335–342.

71 K. Malagari, M. Pomoni, A. Kelekis, A. Pomoni, S. Dourakis, T. Spyridopoulos, H. Moschouris, E. Emmanouil, S. Rizos and D. Kelekis, Prospective Randomized Comparison of Chemoembolization with Doxorubicin-Eluting Beads and Bland Embolization with BeadBlock for Hepatocellular Carcinoma, *Cardiovasc. Intervent. Radiol.*, 2010, **33**, 541–551.

72 J. Lammer, K. Malagari, T. Vogl, F. Pilleul, A. Denys, A. Watkinson, M. Pitton, G. Sergent, T. Pfammatter, S. Terraz, Y. Benhamou, Y. Avajon, T. Gruenberger, M. Pomoni, H. Langenberger, M. Schuchmann, J. Dumortier, C. Mueller, P. Chevallier, R. Lencioni and O. B. of the P. V Investigators, Prospective Randomized Study of Doxorubicin-Eluting-Bead Embolization in the Treatment of Hepatocellular Carcinoma: Results of the PRECISION V Study, *Cardiovasc. Intervent. Radiol.*, 2010, **33**, 41–52.

73 M. Bower, T. Metzger, K. Robbins, D. Tomalty, V. Válek, J. Boudný, T. Andrasina, C. Tatum and R. C. G. Martin, Surgical downstaging and neo-adjuvant therapy in metastatic colorectal carcinoma with irinotecan drug-eluting beads: a multi-institutional study, *HPB (Oxford).*, 2010, **12**, 31–36.

74 C. Aliberti, G. Benea, M. Tilli and G. Fiorentini, Chemoembolization (TACE) of Unresectable Intrahepatic Cholangiocarcinoma with Slow-Release Doxorubicin-Eluting Beads: Preliminary

Results, *Cardiovasc. Intervent. Radiol.*, 2008, **31**, 883–888.

75 T. de Baere, F. Deschamps, C. Teriitheau, P. Rao, K. Conengrapht, M. Schlumberger, S. Leboulleux, E. Baudin and L. Hechellhammer, Transarterial Chemoembolization of Liver Metastases from Well Differentiated Gastroenteropancreatic Endocrine Tumors with Doxorubicin-eluting Beads: Preliminary Results, *J. Vasc. Interv. Radiol.*, 2008, **19**, 855–861.

76 S. C. Schiffman, T. Metzger, G. Dubel, T. Andrasina, I. Kralj, C. Tatum, K. M. McMasters, C. R. Scoggins and R. C. G. Martin, Precision Hepatic Arterial Irinotecan Therapy in the Treatment of Unresectable Intrahepatic Cholangiocellular Carcinoma: Optimal Tolerance and Prolonged Overall Survival, *Ann. Surg. Oncol.*, 2011, **18**, 431–438.

77 G. Fiorentini, C. Aliberti, A. Del Conte, M. Tilli, S. Rossi, P. Ballardini, G. Turrisi and G. Benea, Intra-arterial Hepatic Chemoembolization (TACE) of Liver Metastases from Ocular Melanoma with Slow-release Irinotecan-eluting Beads. Early Results of a Phase II Clinical Study, *In Vivo*, 2009, **23**, 131–137.

78 E. Tomlinson, Microsphere delivery systems for drug targeting and controlled release, *Int J Pharm Technol Prod Manuf*, 1983, **4**, 49–57.

79 R. T.P. Poon, W. Kuen Tso, R. W.C. Pang, K. Ng, R. Woo, K. Shing Tai and S. Tat Fan, A Phase I/II Trial of Chemoembolization for Hepatocellular Carcinoma Using a Novel Intra-Arterial Drug-Eluting Bead, *Clin. Gastroenterol. Hepatol.*, 2007, **5**, 1100–1108.

80 M. Varela, M. I. Real, M. Burrel, A. Forner, M. Sala, M. Brunet, C. Ayuso, L. Castells, X. Montañá, J. M. Llovet and J. Bruix, Chemoembolization of hepatocellular carcinoma with drug eluting beads: Efficacy and doxorubicin pharmacokinetics, *J. Hepatol.*, 2007, **46**, 474–481.

81 A. L. Lewis and R. R. Holden, DC Bead embolic drug-eluting bead: clinical application in the locoregional treatment of tumours, *Expert Opin. Drug Deliv.*, 2011, **8**, 153–169.

82 J. Namur, M. Wassef, J. P. Pelage, A. Lewis, M. Manfait and A. Laurent, Infrared microspectroscopy analysis of Ibuprofen release from drug eluting beads in uterine tissue, *J. Control. Release*, 2009, **135**, 198–202.

83 R. J. Lewandowski, J.-F. Geschwind, E. Liapi and R. Salem, Transcatheter Intraarterial

Therapies: Rationale and Overview, *Radiology*, 2011, **259**, 641–657.

84 J. Namur, S. J. Citron, M. T. Sellers, M. H. Dupuis, M. Wassef, M. Manfait and A. Laurent, Embolization of hepatocellular carcinoma with drug-eluting beads: Doxorubicin tissue concentration and distribution in patient liver explants, *J. Hepatol.*, 2011, **55**, 1332–1338.

85 T. P. Kingham, M. D'Angelica and N. E. Kemeny, Role of intra-arterial hepatic chemotherapy in the treatment of colorectal cancer metastases, *J. Surg. Oncol.*, 2010, **102**, 988–995.

86 F. Meric, Y. Z. Patt, S. A. Curley, J. Chase, M. S. Roh, J. N. Vauthey and L. M. Ellis, Surgery After Downstaging of Unresectable Hepatic Tumors With Intra-Arterial Chemotherapy, *Ann. Surg. Oncol.*, 2000, **7**, 490–495.

87 K. Hong, A. Khwaja, E. Liapi, M. S Torbenson, C. S Georgiades and J.-F. H Geschwind, New Intra-arterial Drug Delivery System for the Treatment of Liver Cancer: Preclinical Assessment in a Rabbit Model of Liver Cancer, *Clin. Cancer Res.*, 2006, **12**, 2563–2567.

88 M. V. Gonzalez, Y. Tang, G. J. Phillips, A. W. Lloyd, B. Hall, P. W. Stratford and A. L. Lewis, Doxorubicin eluting beads - 2: methods for evaluating drug elution and in-vitro:in-vivo correlation, *J. Mater. Sci. Mater. Med.*, 2008, **19**, 767–775.

89 A. L. Lewis and M. R. Dreher, Locoregional drug delivery using image-guided intra-arterial drug eluting bead therapy, *J. Control. Release*, 2012, **161**, 338–350.

90 S. M. Tadavarthy, J. Moller and K. Amplatz, Polyvinyl alcohol (Ivalon). A new embolic material, *Am. J. Roentgenol. Radium Ther. Nucl. Med.*, 1975, **125**, 609–616.

91 K. Ashrafi, Y. Tang, H. Britton, O. Domenge, D. Blino, A. J. Bushby, K. Shuturminska, M. den Hartog, A. Radaelli, A. H. Negussie, A. S. Mikhail, D. L. Woods, V. Krishnasamy, E. B. Levy, B. J. Wood, S. L. Willis, M. R. Dreher and A. L. Lewis, Characterization of a novel intrinsically radiopaque Drug-eluting Bead for image-guided therapy: DC Bead LUMI, *J. Control. Release*, 2017, **250**, 36–47.

92 B. Cylwik, J. Darewicz and B. Karasewicz, Morphometric and histological examinations of dog kidneys after embolization of the renal artery with the cyanoacrylic glue "Chirurcol-Polfa'', *Int. Urol. Nephrol.*, 1985, **17**, 303–309.

93 M. R. Dreher, K. V Sharma, D. L. Woods, G. Reddy, Y. Tang, W. F. Pritchard, O. A. Chiesa, J. W. Karanian, J. A. Esparza, D. Donahue, E. B. Levy, S. L. Willis, A. L. Lewis and B. J. Wood, Radiopaque Drug-Eluting Beads for Transcatheter Embolotherapy: Experimental study of Drug Penetration and Coverage in Swine, *J. Vasc. Interv. Radiol.*, 2012, **23**, 257–64.e4.

94 R. Martin, J. Irurzun, J. Munchart, I. Trofimov, A. Scupchenko, C. Tatum and G. Narayanan, Optimal technique and response of doxorubicin beads in hepatocellular cancer: bead size and dose, *Korean J. Hepatol.*, 2011, **17**, 51–60.

95 BTG, DC Bead™, http://bead.btg-im.com/products/turkey-315/dcbead-3/about-dc-bead, (accessed 1 October 2017).

96 J. Namur, M. Wassef, J.-M. Millot, A. L. Lewis, M. Manfait and A. Laurent, Drug-eluting Beads for Liver Embolization: Concentration of Doxorubicin in Tissue and in Beads in a Pig Model, *J. Vasc. Interv. Radiol.*, 2010, **21**, 259–267.

97 E. K. Lang and C. L. Brown, Colorectal metastases to the liver: selective chemoembolization., *Radiology*, 1993, **189**, 417–422.

98 K. Stuart, Chemoembolization in the management of liver tumors, *Oncologist*, 2003, **8**, 425—437.

99 J. Llovet and J. Bruix, Systematic review of randomized trials for unresectable hepatocellular carcinoma: Chemoembolization improves survival, *Hepatology*, 2003, **37**, 429–442.

100 Eliseu Padilha, Unloaded and loaded DC Bead™ with Doxorubicin, http://www.eliseupadilha.com.br/advogado/16122013102341-quimioembolizacao---dc-beads---100---300/index.php, (accessed 1 October 2017).

101 BTG, Unloaded and loaded DC Bead™ with Irinotecan, http://bead.btg-im.com/products/uk-322/contrast-media-test-197/visipaque-update, (accessed 1 October 2017).

102 BTG, DEBDOX™, http://bead.btg-im.com/products/uk-322/dcbead-3/stability-information-debdox, (accessed 1 June 2014).

103 BTG, DEBIRI™, http://bead.btg-im.com/visipaque-update, (accessed 1 June 2014).

104 D. Outomuro, D. R. Grana, F. Azzato and J. Milei, Adriamycin-induced myocardial toxicity: New solutions for an old problem?, *Int. J. Cardiol.*, 2007, **117**, 6–15.

105 E. Meucci, G. Minotti, A. Mordente, B. Giardina and G. E. Martorana, Human Heart Cytosolic Reductases and Anthracycline Cardiotoxicity, *IUBMB Life (International Union Biochem. Mol. Biol. Life)*, 2001, **52**, 83–88.

106 H. Lou, I. Danelisen and P. K. Singal, Cytokines are not upregulated in adriamycin-induced cardiomyopathy and heart failure, *J. Mol. Cell. Cardiol.*, 2004, **36**, 683–690.

107 K. A. Wouters, L. C. M. Kremer, T. L. Miller, E. H. Herman and S. E. Lipshultz, Protecting against anthracycline-induced myocardial damage: a review of the most promising strategies, *Br. J. Haematol.*, 2005, **131**, 561–578.

108 L. Gianni, J. L. Zweier, A. Levy and C. E. Myers, Characterization of the cycle of iron-mediated electron transfer from Adriamycin to molecular oxygen., *J. Biol. Chem.* , 1985, **260**, 6820–6826.

109 R. D. Olson and P. S. Mushlin, Doxorubicin cardiotoxicity: analysis of prevailing hypotheses, *FASEB J.*, 1990, **4**, 3076—3086.

110 J. Milei, A. Boveris, S. Llesuy, H. A. Molina, R. Storino, D. Ortega and S. E. Milei, Amelioration of adriamycin-induced cardiotoxicity in rabbits by prenylamine and vitamins A and E, *Am. Heart J.*, 1986, **111**, 95–102.

111 M. E. Ferrero, E. Ferrero, G. Gaja and A. Bernelli-Zazzera, Adriamycin: Energy metabolism and mitochondrial oxidations in the heart of treated rabbits, *Biochem. Pharmacol.*, 1976, **25**, 125–130.

112 Y. E. Earm, W. K. Ho and I. So, Effects of adriamycin on ionic currents in single cardiac myocytes of the rabbit, *J. Mol. Cell. Cardiol.*, 1994, **26**, 163—172.

113 R. D. Olson, X. Li, P. Palade, S. E. Shadle, P. S. Mushlin, H. A. Gambliel, M. Fill, R. J. Boucek and B. J. Cusack, Sarcoplasmic Reticulum Calcium Release Is Stimulated and Inhibited by Daunorubicin and Daunorubicinol, *Toxicol. Appl. Pharmacol.*, 2000, **169**, 168–176.

114 M. B. M Gosalvez, in *5th Int. Biophysics Congr*, 1975.

115 L. Lenaz and J. A. Page, Cardiotoxicity of adriamycin and related anthracyclines, *Cancer Treat. Rev.*, 1976, **3**, 111–120.

116 D. Harake, V. I. Franco, J. M. Henkel, T. L. Miller and S. E. Lipshultz, Cardiotoxicity in childhood cancer survivors: strategies for prevention and management, *Future Cardiol.*, 2012, **8**, 10.2217/fca.12.44.

117 M. Ciotti, N. Basu, M. Brangi and I. S. Owens, Glucuronidation of 7-Ethyl-10-hydroxycamptothecin (SN-38) by the Human UDP-Glucuronosyltransferases Encoded at the UGT1 Locus, *Biochem. Biophys. Res. Commun.*, 1999, **260**, 199–202.

118 A. Santos, S. Zanetta, T. Cresteil, A. Deroussent, F. Pein, E. Raymond, L. Vernillet, M.-L. Risse, V. Boige, A. Gouyette and G. Vassal, Metabolism of Irinotecan (CPT-11) by CYP3A4 and CYP3A5 in Humans, *Clin. Cancer Res.*, 2000, **6**, 2012 LP-2020.

119 C. D. Scripture and W. D. Figg, Drug interactions in cancer therapy, *Nat. Rev. Cancer*, 2006, **6**, 546.

120 A. Nicolini, L. Martinetti, S. Crespi, M. Maggioni and A. Sangiovanni, Transarterial Chemoembolization with Epirubicin-eluting Beads versus Transarterial Embolization before Liver Transplantation for Hepatocellular Carcinoma, *J. Vasc. Interv. Radiol.*, 2010, **21**, 327–332.

121 G. Fiorentini, C. Aliberti, G. Turrisi, A. Del Conte, S. Rossi, G. Benea and P. Giovanis, Intraarterial hepatic chemoembolization of liver metastases from colorectal cancer adopting irinotecan-eluting beads: Results of a phase II clinical study, *In Vivo*, 2007, **21**, 1085–1091.

122 R. C. G. Martin, J. Joshi, K. Robbins, D. Tomalty, R. O'Hara and C. Tatum, Transarterial Chemoembolization of Metastatic Colorectal Carcinoma with Drug-Eluting Beads, Irinotecan (DEBIRI): Multi-Institutional Registry, *J. Oncol.*, 2009, **2009**, 539795.

123 C. Tellez M.D, A. B. Benson III M.D, M. T. Lyster M.D, M. Talamonti, J. M.D, M. A. Braun M.D, A. A. Nemcek Jr. M.D and R. Vogelzang, Phase II trial of chemoembolization for the treatment of metastatic colorectal carcinoma to the liver and review of the literature, *Cancer*, 1998, **82**, 1250–1259.

124 A. Accardo, D. Tesauro and G. Morelli, Peptide-based targeting strategies for simultaneous

imaging and therapy with nanovectors, *Polym. J.*, 2013, **45**, 481.

125 G. L. DeNardo and S. J. DeNardo, Concepts, consequences, and implications of theranosis, *Semin. Nucl. Med.*, 2012, **42**, 147—150.

126 D. Kim and S. Jon, Gold nanoparticles in image-guided cancer therapy, *Inorganica Chim. Acta*, 2012, **393**, 154–164.

127 K. Kim, J. H. Kim, H. Park, Y.-S. Kim, K. Park, H. Nam, S. Lee, J. H. Park, R.-W. Park, I.-S. Kim, K. Choi, S. Y. Kim, K. Park and I. C. Kwon, Tumor-homing multifunctional nanoparticles for cancer theragnosis: Simultaneous diagnosis, drug delivery, and therapeutic monitoring, *J. Control. Release*, 2010, **146**, 219–227.

128 E. Terreno, F. Uggeri and S. Aime, Image guided therapy: The advent of theranostic agents, *J. Control. Release*, 2012, **161**, 328–337.

129 J. Xie, S. Lee and X. Chen, Nanoparticle-based theranostic agents, *Adv. Drug Deliv. Rev.*, 2010, **62**, 1064–1079.

130 BTG, Administration of DC Bead™, https://www.btg-im.com/en-US/Interventional-Oncology, (accessed 1 October 2017).

131 H. F. Dvorak, J. A. Nagy, J. T. Dvorak and A. M. Dvorak, Identification and characterization of the blood vessels of solid tumors that are leaky to circulating macromolecules., *Am. J. Pathol.*, 1988, **133**, 95–109.

132 H. Maeda, J. Wu, T. Sawa, Y. Matsumura and K. Hori, Tumor vascular permeability and the EPR effect in macromolecular therapeutics: a review, *J. Control. Release*, 2000, **65**, 271–284.

133 C.-H. Heldin, K. Rubin, K. Pietras and A. Östman, High interstitial fluid pressure — an obstacle in cancer therapy, *Nat. Rev. Cancer*, 2004, **4**, 806.

134 T. Konno, H. Maeda, K. Iwai, S. Tashiro, S. Maki, T. Morinaga, M. Mochinaga, T. Hiraoka and I. Yokoyama, Effect of arterial administration of high-molecular-weight anticancer agent SMANCS with lipid lymphographic agent on hepatoma: a preliminary report, *Eur. J. Cancer Clin. Oncol.*, 1983, **19**, 1053–1065.

135 W. J. Jusko, Pharmacodynamics of chemotherapeutic effects: Dose-time-response relationships for phase-nonspecific agents, *J. Pharm. Sci.*, 1971, **60**, 892–895.

136 B. Sperker, T. E. Mürdter, M. Schick, K. Eckhardt, K. Bosslet and H. K. Kroemer, Interindividual Variability in Expression and Activity of Human β-Glucuronidase in Liver and Kidney: Consequences for Drug Metabolism, *J. Pharmacol. Exp. Ther.*, 1997, **281**, 914 LP-920.

137 K. Malagari, K. Chatzimichael, E. Alexopoulou, A. Kelekis, B. Hall, S. Dourakis, S. Delis, A. Gouliamos and D. Kelekis, Transarterial Chemoembolization of Unresectable Hepatocellular Carcinoma with Drug Eluting Beads: Results of an Open-Label Study of 62 Patients, *Cardiovasc. Intervent. Radiol.*, 2008, **31**, 269–280.

138 J. M. Llovet, M. I. Real, X. Montaña, R. Planas, S. Coll, J. Aponte, C. Ayuso, M. Sala, J. Muchart, R. Solà, J. Rodés and J. Bruix, Arterial embolisation or chemoembolisation versus symptomatic treatment in patients with unresectable hepatocellular carcinoma: a randomised controlled trial, *Lancet*, 2002, **359**, 1734–1739.

139 C. Lo, H. Ngan, W. Tso, C. Liu, C. Lam, R. T. Poon, S. Fan and J. Wong, Randomized controlled trial of transarterial lipiodol chemoembolization for unresectable hepatocellular carcinoma, *Hepatology*, 2002, **35**, 1164–1171.

140 BTG, DC Bead LUMI™ FAQs, https://www.btg-im.com/en-CA/DC-Bead-LUMI/About/FAQ-s, (accessed 1 October 2017).

141 BTG, LUMI-TACE intra-procedural single-shot fluoroscopy, https://www.btg-im.com/en-SE/DC-Bead-LUMI/About/Technical-Recommendations, (accessed 1 October 2017).

142 Interventional News, DC Bead LUMI™, https://interventionalnews.com/first-european-patients-treated-with-dc-bead-lumi-radiopaque-drug-eluting-beads/, (accessed 1 October 2017).

143 Terumo, LifePearl™ Microspheres, http://www.terumo-europe.com/en-emea/interventional-oncology/loco-regional-treatment/drug-elutable-microspheres-tace/lifepearl®-microspheres, (accessed 1 October 2017).

144 Boston Scientific, Embozene Tandem™ Microspheres Information, http://www.bostonscientific.com/en-

EU/products/embolization/embozene_tandem_microspheres.html, (accessed 1 October 2017).

145 CeloNova, Embozene Tandem™ Microspheres Instructions for Use, http://celonova.com/wp-content/uploads/LAS0048-01-Artwork-08-02-2013.pdf.pdf, (accessed 1 October 2017).

146 Girlow, Embozene Tandem™, http://www.girlowusa.com/producto/embozene-tandem/?lang=en, (accessed 1 October 2017).

147 K.-H. Lee, E. A. Liapi, C. Cornell, P. Reb, M. Buijs, J. A. Vossen, V. P. Ventura and J.-F. H. Geschwind, Doxorubicin-Loaded QuadraSphere Microspheres: Plasma Pharmacokinetics and Intratumoral Drug Concentration in an Animal Model of Liver Cancer, *Cardiovasc. Intervent. Radiol.*, 2010, **33**, 576–582.

148 O. Jordan, A. Denys, T. De Baere, N. Boulens and E. Doelker, Comparative Study of Chemoembolization Loadable Beads: In vitro Drug Release and Physical Properties of DC Bead and Hepasphere Loaded with Doxorubicin and Irinotecan, *J. Vasc. Interv. Radiol.*, 2010, **21**, 1084–1090.

149 S. Gupta, K. C. Wright, J. Ensor, C. S. Van Pelt, K. A. Dixon and V. Kundra, Hepatic Arterial Embolization with Doxorubicin-Loaded Superabsorbent Polymer Microspheres in a Rabbit Liver Tumor Model, *Cardiovasc. Intervent. Radiol.*, 2011, **34**, 1021–1030.

150 H. van Malenstein, G. Maleux, V. Vandecaveye, S. Heye, W. Laleman, J. van Pelt, J. Vaninbroukx, F. Nevens and C. Verslype, A Randomized Phase II Study of Drug-Eluting Beads versus Transarterial Chemoembolization for Unresectable Hepatocellular Carcinoma, *Oncol. Res. Treat.*, 2011, **34**, 368–376.

151 M. Grosso, C. Vignali, P. Quaretti, A. Nicolini, F. Melchiorre, G. Gallarato, I. Bargellini, P. Petruzzi, C. Massa Saluzzo, S. Crespi and I. Sarti, Transarterial Chemoembolization for Hepatocellular Carcinoma with Drug-Eluting Microspheres: Preliminary Results from an Italian Multicentre Study, *Cardiovasc. Intervent. Radiol.*, 2008, **31**, 1141–1149.

152 A. Seki, S. Hori, K. Kobayashi and S. Narumiya, Transcatheter Arterial Chemoembolization with Epirubicin-Loaded Superabsorbent Polymer Microspheres for 135 Hepatocellular Carcinoma Patients: Single-Center Experience, *Cardiovasc. Intervent. Radiol.*, 2011, **34**, 557–565.

153 Merit Medical, HepaSpheres™ Microspheres Information, https://www.merit.com/interventional-oncology-spine/embolotherapy/hepatic-oncology/hepasphere-microspheres/, (accessed 1 October 2017).

154 Merit Medical, HepaSphere™ MicroSphere Instructions for Use, https://www.merit.com/ifu/?i=327962, (accessed 1 October 2017).

155 Merit Medical, HepaSphere™ MicroSpheres, https://meritemea.com/hepasphere-microspheres-absorb-mechanicall-ionically-optimal-doxorubicin-loading/, (accessed 1 October 2017).

156 A. Weber, M. Herold, H. Brunner and G. E. . Tovar, Bioconjugative polymer nanospheres studied by isothermal titration calorimetry, *Thermochim. Acta*, 2004, **415**, 69–74.

157 Y. Tian, P. Ravi, L. Bromberg, T. A. Hatton and K. C. Tam, Synthesis and Aggregation Behavior of Pluronic F87/Poly(acrylic acid) Block Copolymer in the Presence of Doxorubicin, *Langmuir*, 2007, **23**, 2638–2646.

158 J.-D. Hecq, A. L. Lewis, D. Vanbeckbergen, A. Athanosopoulos, L. Galanti, J. Jamart, P. Czuczman and T. Chung, Doxorubicin-loaded drug-eluting beads (DC Bead®) for use in transarterial chemoembolization: A stability assessment, *J. Oncol. Pharm. Pract.*, 2012, **19**, 65–74.

159 K. Fuchs, P. E. Bize, A. Denys, G. Borchard and O. Jordan, Sunitinib-eluting beads for chemoembolization: Methods for in vitro evaluation of drug release, *Int. J. Pharm.*, 2015, **482**, 68–74.

160 F. Amyot, V. Boudy, K. Jurski, J.-L. Counord, G. Guiffant, J. Dufaux and J.-C. Chaumeil, A new experimental method for the evaluation of the release profiles of drug-loaded microbeads designed for embolisation, *ITBM-RBM*, 2002, **23**, 285–289.

161 D. Carugo, L. Capretto, S. Willis, A. L. Lewis, D. Grey, M. Hill and X. Zhang, A microfluidic device for the characterisation of embolisation with polyvinyl alcohol beads through biomimetic bifurcations, *Biomed. Microdevices*, 2012, **14**, 153–163.

162 R. Y. Cheung, R. Kuba, A. M. Rauth and X. Y. Wu, A new approach to the in vivo and in vitro investigation of drug release from locoregionally delivered microspheres, *J. Control. Release*,

2004, **100**, 121–133.

Chapter 2 : Methodology

All work presented in this thesis was carried out at the University of Huddersfield. It should be noted that several sections of this work have been published in the well reputed International Journal of Pharmaceutics and European Journal of Pharmaceutical Sciences [1,2].

2.1. Isothermal Titration Calorimetry (ITC)

Isothermal titration calorimetry (ITC) measures the heat released or absorbed by an excipient as a consequence of injecting precise amounts of a reactant. The sample may be held at a selected temperature and mixed at a spin rate chosen by the user. The differential power (DP) difference between the reference cell and sample cell is measured from the temperature difference observed [3].

An exothermic reaction, where heat is released from the interaction between a ligand titrated from the syringe into a macromolecule contained in the cell, causes a negative DP. The opposite occurs in an endothermic reaction, where heat is absorbed, causing a positive DP. This measure of thermal energy (ΔH) is directly proportional to binding between the ligand and the macromolecule. At each point that the ligand (drug) is supplemented the heat signal decreases as the macromolecule (bead) becomes saturated. The signal reduces until only the background signal of dilution effects is observed [3]. The interaction of the ligand with the macromolecule solvent can be measured and subtracted from the interaction with the ligand and macromolecule. The same subtraction can be made between the macromolecule and the ligand solvent to obtain the overall binding result, in this case the sole interaction of bead and drug. Figure 2.1 illustrates the main components of the ITC instrument.

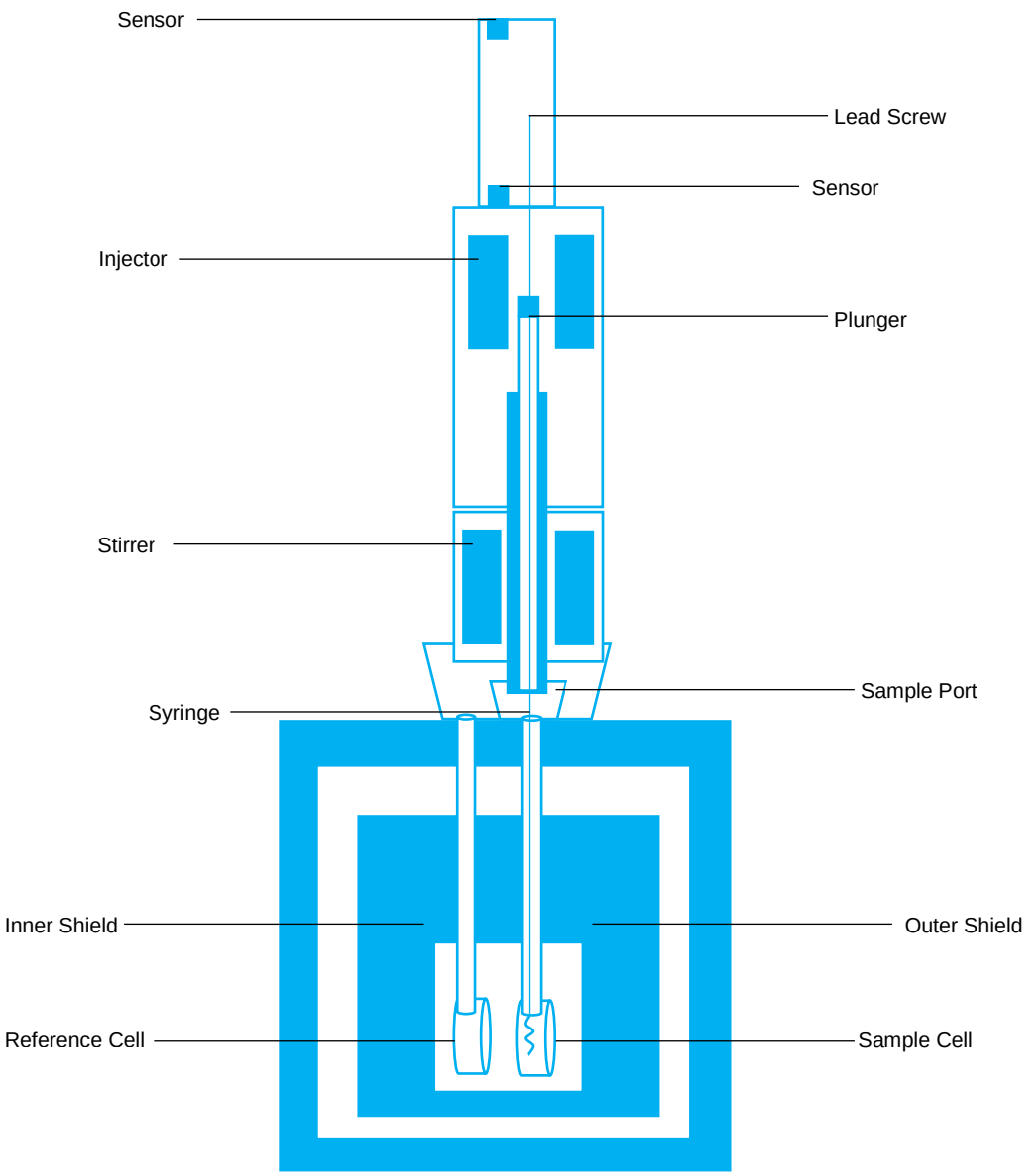

Figure 2.1: The main components in the ITC unit [3].

2.1.1. Materials

The following drugs, beads and other materials were utilised in the ITC studies:

Drugs:

Doxorubicin hydrochloride (Dox) powder, >99 % purity, product code 13773, Zhejiang Hisun Pharmaceutical Co Ltd, Zhejiang, China.

Mitoxantrone dihydrochloride (Mit) powder, ≥97 % purity, product code M6545, Sigma-Aldrich Corporation, Missouri, United States of America (USA).

Irinotecan hydrochloride (Iri) powder, >99 % purity, product code 218MF10990, ScinoPharm Taiwan Ltd, Tainan, Taiwan.

Topotecan hydrochloride (Top) powder, >99 % purity, product code 1672257, Sigma-Aldrich Corporation, Missouri, USA.

Beads:

DC Bead*M1*™, also referred to as 70-150 µm DC Bead™ (M1), additional sizes of 100-300 µm (103), 300-500 µm (305) and 500-700 µm (507), Biocompatibles UK Ltd, Surrey, United Kingdom (UK).

LifePearl™, 100 µm ± 25 (100), Terumo Corporation, Tokyo, Japan.

DC Bead LUMI*M1*™, also known as 70-150 µm DC Bead LUMI™ (M1), Biocompatibles UK Ltd, Surrey, UK.

Tandem™, 100 µm ± 25 (110), Boston Scientific Corporation, Massachusetts, USA.

HepaSphere™, 30-60 µm, expanding size 120-240 µm (200), Merit Medical System Inc, Roissy, France.

Other materials:

Hydrochloric acid (HCl), 37 % concentration, reagent grade, product code 435570, Sigma-Aldrich Corporation, Missouri, USA.

Centrifugal filters, ultrafree-MC SV, non-sterile, 5.0 µm pore size, product code UFC30SV00, Merek Millipore, Massachusetts, USA.

2.1.2. Instrument Preparation

Calibration of the equipment was undertaken periodically and tests to ensure the instruments accuracy can be found in the Appendix ‘Isothermal Titration Calorimetry (ITC) Calibrations’ Section.

Before samples were placed into the ITC the equipment was cleaned thoroughly to prevent contamination. 10 – 20 % Decon® 90 is a dilute solution known not the damage the cells, this was placed in the sample cell which was heated to 60 °C and left for >60 minutes. Decon® was removed from the cell and replaced with deionised water, the machine was then cleaned by drawing >1 L of water through the apparatus using a vacuum pump. Water was also flushed through the syringe multiple times and could be filled with methanol, then left to dry to reduce the amount of sample required to flush through the system. If additional cleaning was required water was pre-heated to 60 °C to flush through the instrument. If other compounds had been previously used in the instrument the risk of contamination was greater and so strong basic chemicals such as 3 mM (12 % v/v) NaOH were used instead of Decon®. Excessive use of NaOH can desensitise either of the identical coin shaped sample or reference cell composed of Hastelloy® C 276, therefore unnecessary use was avoided. Following this the machine was ready to use by preparing the samples and placing them inside the instrument.

Once an experiment was complete the sample cell and syringe contents were removed and replaced with deionised water if the instrument was to be left for more than 24 hours without use, as the contents may damage internal components of the equipment.

2.1.3. Sample Preparation

An investigation was conducted into the amount of time adequate for bead centrifugation. The purpose of centrifugation was to provide a mass of beads with a known solid content that could be place into the ITC cell. Beads unsuspended in water are also easier to place into the cell. Pre-washed beads, in either water or acid, were centrifuged in a 1000 µL tube with a 5.0 µm centrifugal filter unit and then weighed at intervals over 5 minutes. There are two known stages of water loss, in the first stage water is lost from outside the beads and in the second water is lost from inside the beads. For this study water must remain inside the beads in order to retain the beads structure, so ideally only the first stage of water loss would have occurred before ceasing centrifugation. When trend lines were taken from the first two and last two data points, it was determined that the intercept where the two sets of data points met confirmed that 1000 µL of beads and water required 30 seconds centrifugation at 3000 revolutions per minute (rpm). The results of this work are demonstrated in Figure 2.2.

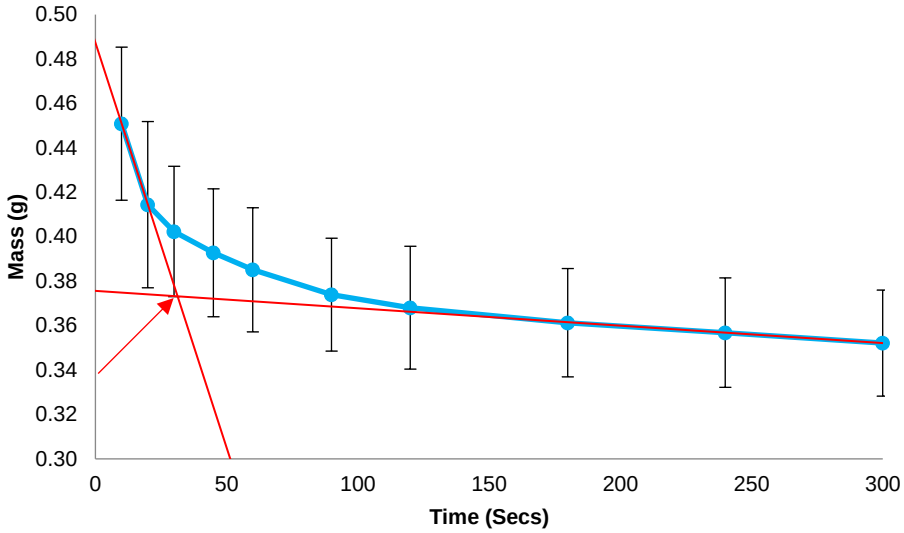

Figure 2.2: Mass of DC Bead*M1*™ after centrifugation at different time points, arrow shows point of inception (n = 3, error bars = standard deviation).

25 – 100 mg of pre-washed centrifuged beads were placed into the sample cell with a spatula. To wash the beads the packing solution was removed and replaced with either deionised water or 2M HCl, as sodium ions would interfere with bead binding properties. The beads were then shaken and left to settle for 1 minute to allow the ion-exchange process to take place. This washing step was repeated at least ten times to ensure ion-exchange equilibrium was achieved, as seen in Figure 2.3. After acid washing the beads were washed with deionised water to removal any residual HCl.

To ensure all beads were inside the sample cell, the beads were periodically washed down with small of amounts deionised water using a syringe with a needle. Air bubbles were removed from the cell by inserting and removing the syringe until no bubbles could be seen. Over time beads separate from the water as the sample sediments, the beads were left to settle until no beads could be seen in the sample cell entrance, excess water was then removed. Beads with the addition of deionised water gave a total volume of 1.4194 mL. The syringe was filled with 1 – 43 mM of drug depending upon the type of experiment and drug solubility; the syringe held a volume of 290 µL.

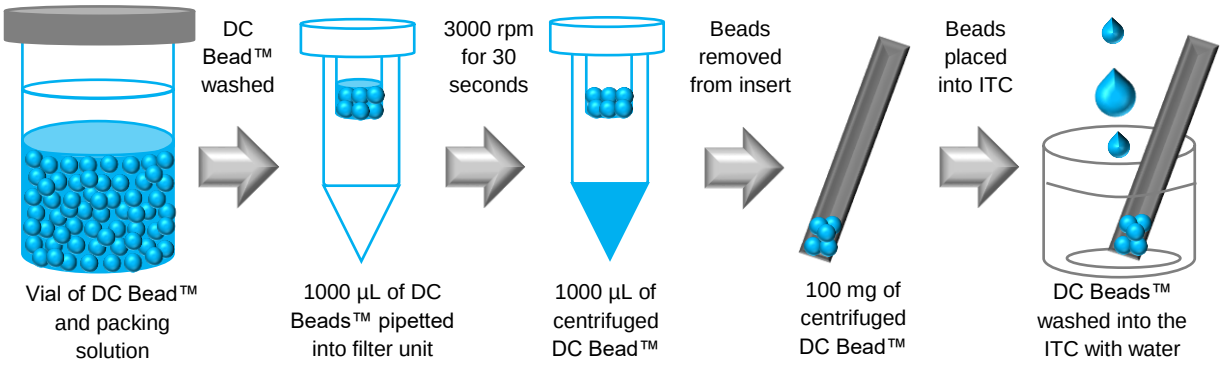

Figure 2.3: Step by step bead sample preparation for ITC experiments.

2.1.4. Instrument Parameters

The majority of experiments involved a total of 14 injections, whereby each injection volume was 20 µL for a duration of 40 seconds. Every injection had a spacing of 600 seconds and a filter period of 2 seconds, with the reference power set between 1 – 25 µcal/sec (depending on the experiment) and a stirring speed of 307 rpm. Initially, the cell temperature was set to 25 °C, with a series of temperatures studied from 20 – 40 °C. The instrument used in this study was a VP-ITC MicroCal™ unit manufactured by Malvern Instruments Inc, using Origin® 7 software for all data analysis.

2.2. Open-Loop Flow-Through Elution

Ultraviolet-Visible (UV-Vis) spectrophotometry used a method incorporating a system to evaluate the tendency of drug to release into the systemic circulation as a function of either time or embolic load from drug eluting bead (DEB) products. It measures light intensity as a function of wavelength from a beam of light passed through a sample and compares this with the reference, which can then be converted into absorbance. The main components of the UV instrument are illustrated in Figure 2.4.

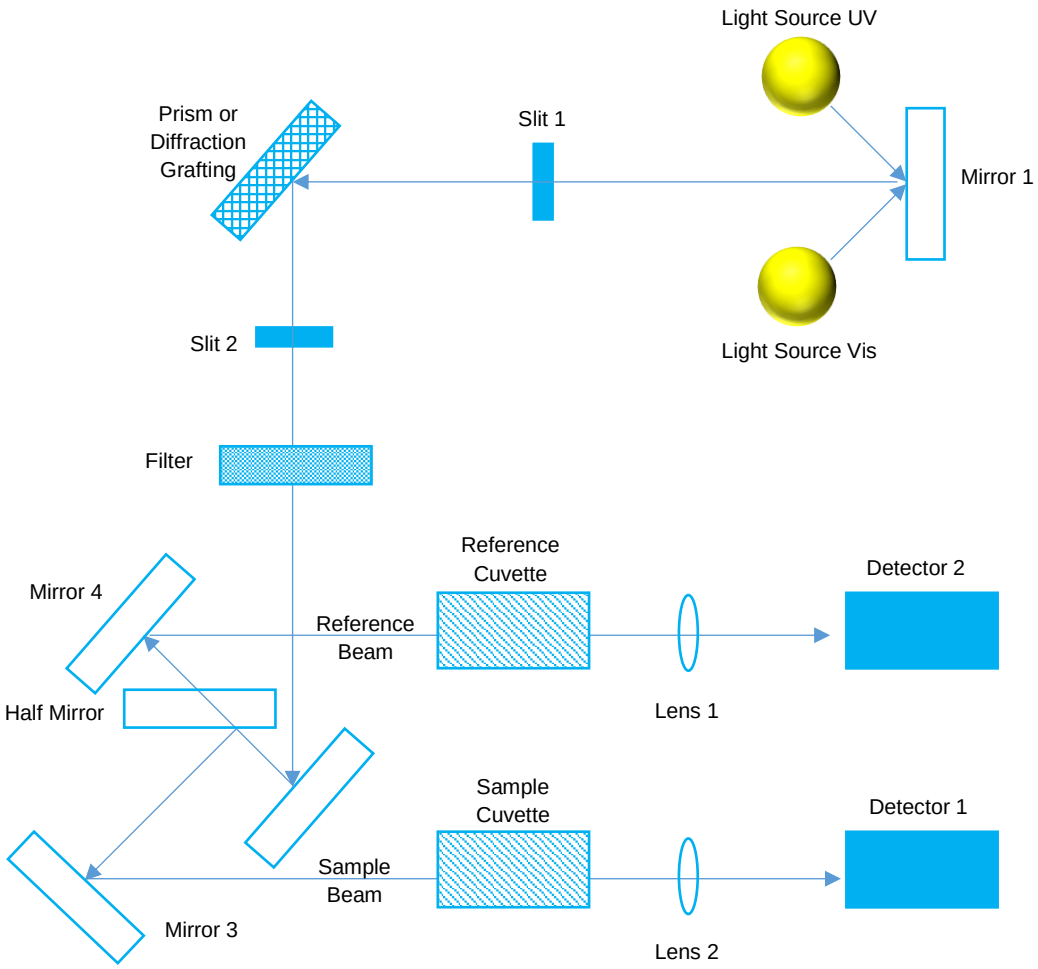

Figure 2.4: The main components in the UV-Vis unit [4].

2.2.1. Materials

Drugs used in the open-loop flow-through elution experiments were Dox HCl and Iri HCl as listed in Section 2.1.1. All beads in Section 2.1.1 were used in the elution studies, with additional bead sizes and other materials used in analysis as itemised below:

Beads:

DC Bead LUMI™, 100-300 µm (103), Biocompatibles UK Ltd, Surrey, UK.

Tandem™, 75 µm ± 15 (107), Boston Scientific Corporation, Massachusetts, USA.

Other materials:

Glass beads, 150-212 µm, product code G1145, Sigma-Aldrich Corporation, Missouri, USA.

Filter membrane, polyester, pore size 27 µm, product code 07-27/19, Sefar Medifab, Heiden, Switzerland.

Silicon tubing, platinum cured, 3/32 inch internal diameter, 5/32 inch external diameter, product code 95802-03, Cole-Parmer, Illinois, USA.

Phosphate buffered serology saline (PBSS), pH 7.0, product code 04-004, Source BioScience UK Ltd, Nottingham, UK.

Helium, A Grade, product code 110745, The BOC Group plc, Guildford, UK.

Ringer's solution ¼ strength tablets, product code 96724, Sigma-Aldrich Corporation, Missouri, USA.

Sodium chloride (NaCl), product code S7653, Sigma-Aldrich Corporation, Missouri, USA.

Sodium bicarbonate ($NaHCO_3$), product code 71631, Sigma-Aldrich Corporation, Missouri, USA.

Potassium chloride (KCl), product code P9333, Sigma-Aldrich Corporation, Missouri, USA.

Potassium phosphate dibasic trihydrate ($K_2HPO_4 \cdot 3H_2O$), product code P5504, Sigma-Aldrich Corporation, Missouri, USA.

Magnesium chloride hexahydrate ($MgCl_2 \cdot 6H_2O$), product code M2393, Sigma-Aldrich Corporation, Missouri, USA.

HCl, 37 % concentration, reagent grade, product code 435570, Sigma-Aldrich Corporation, Missouri, USA.

Calcium chloride hexahydrate ($CaCl_2.6H_2O$), product code 442909, Sigma-Aldrich Corporation, Missouri, USA.

Sodium sulfate (Na_2SO_4), product code 798592, Sigma-Aldrich Corporation, Missouri, USA.

Tris(hydroxymethlyl)aminomethane ($(CH_2OH)_3CNH_2$), product code T1378, Sigma-Aldrich Corporation, Missouri, USA.

2.2.2. Instrument Preparation

The overall setup as shown in Figure 2.5, consisted of an open-loop flow-through system which encompassed eluent solution, a peristaltic pump, a water bath with temperature controlled unit, an air collection unit, a flow-through cell, a Cary 60 UV-Vis spectrophotometer with an 18 cell holder accessory (so that samples could be tested in triplicate with standards simultaneously), quartz cuvettes, silicon tubing, a container to syphon water and a waste collection system.

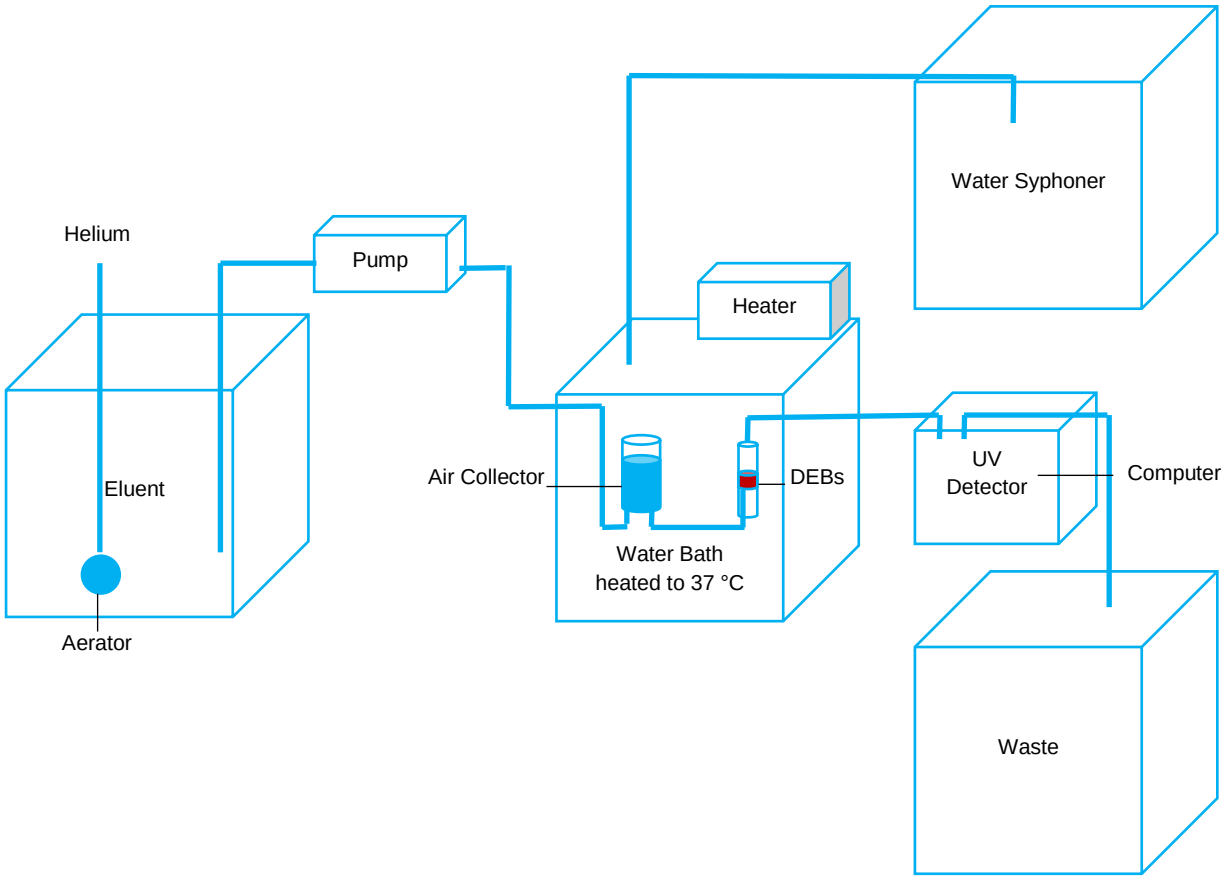

Figure 2.5: Experiment set up of the open-loop flow-through elution.

Tubing inside the pump was replaced every experiment to ensure a constant flow rate. The flow rate was checked before and after experiments, and an average taken for the calculations. Flow rate was measured by pre-weighing a glass vial, filling the vial with flowing eluent for one minute and then re-weighing the vial to give the volume per minute. The instrument has room light immunity and so can work with the compartment door open, allowing tubing to go to and from the flow-through cuvettes. Cuvettes to analyse Dox had a path length of 10 mm, whereas Iri cuvettes had a shorter path length of 5 mm because the absorbance of this drug was >>1 under the same conditions.

2.2.3. Sample Preparation

A 25 mg/mL stock solution of Dox in deionised water was prepared. Beads were initially loaded with 37.5 mg/mL by the addition of 1.5 mL Dox stock to 1 mL of beads, once the bead packing solution had been removed as demonstrated in Figure 2.6. To ensure full saturation the beads were left to load in a cool dark area overnight. When the bead volume was changed to 0.5 and 0.2 mL the volume of Dox was altered accordingly. The concentration of Dox in the beads was studied at 25, 37.5, 45, 50 and 75 mg/mL depending on the type of bead. Further experiments were conducted using Iri at a loaded concentration of 50 mg/mL with a 12.5 mg/mL stock solution, i.e. 4 mL Iri stock solution in 1 mL of beads.

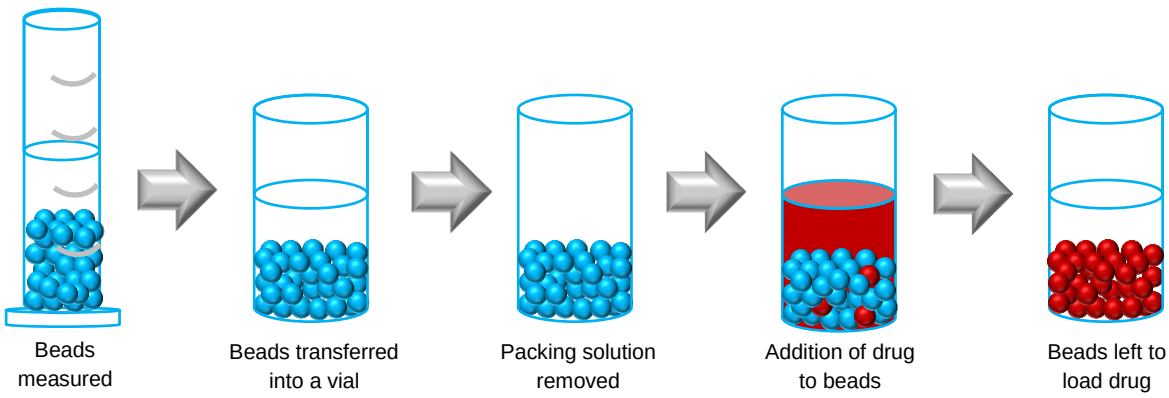

Figure 2.6: Step by step bead sample preparation for elution experiments.

Beads with packing solution removed were loaded with the drug of choice at the desired concentration. Beads were then transferred into tubes which allowed eluent through one end and out the other with the

eluted drug. Loaded beads were prepared with and without sand or glass beads for packing, and at various DEB:packing material ratios (1:0, 1:3 and 1:5).

To insert beads into the flow-through cell deionised was water heated to 37 °C with care taken to avoid creating air bubbles within the sample. A ring with a filter membrane one third of the way inside the elution cell held beads within the plastic tube. If the experiment contained no packing material an adequate space was left to allow the beads to expand. A second ring and membrane resided after the measured space to retain the beads (e.g. for DC Bead™ this was 6 – 7 mm per mL of beads). As discussed, packing material was required in some cases to produce interstitial space between DEBs, with the aim of separating and suspending beads as well as allowing for any size changes during elution to be accommodated. The most suitable technique of mixing DEBs with packing material can be seen in Figure 2.7, which was to start with the packing substance and layer beads with packing one layer at a time until all the beads were in the cell. As each level was added the two were mixed to create a homogenous mixture. As beads were lighter than packing care was taken to avoid over-mixing as the beads would separate. The final layer was more packing material before the second ring and filter membrane was fitted on top. A third membrane was commonly used to prevent air being introduced to the beads, this was positioned with a space between the second filter membrane. The cell was then topped up with deionised water and the top of the cell fitted. The methods were initially developed using Dox loaded DEBs at 37 ºC with degassed eluent (physiological saline [154 mM NaCl (0.9 % w/v)]). However, a second drug viz. Iri, and additional eluent solutions such as various concentrations of NaCl, Ringer's solution and simulated body fluid (SBF) were analysed.

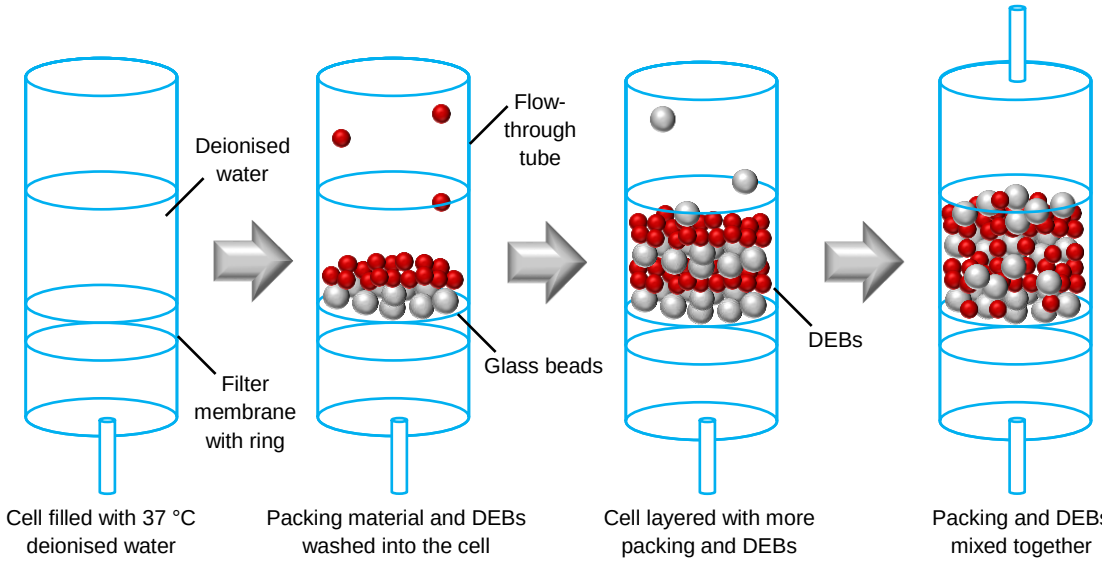

Figure 2.7: Step by step bead packing preparation for elution.

Several concentrations of NaCl solutions were prepared to identify elution behavior under different concentrations of salt. Table 2.1 displays the concentrations in each buffer solution.

Table 2.1: NaCl buffer composition for elution studies.

Percent of NaCl (%)	0.45	0.9	1.35	1.8	4.5
Quantity of Salt (g/L)	4.5	9.0	13.5	18.0	45.0
Concentration (mM)	77	154	231	308	770

Ringer's solution ¼ strength tablets were used to prepare eluent for the flow-through apparatus. The mixture contains several salts producing an isotonic solution related to bodily fluids. Ringer's solution was created by Sydney Ringer who determined the precise concentration of salts required [5]. The product data sheet recommends dissolving 1 tablet in 500 mL of deionised water and to adjust the pH to 7.0, therefore a solution of 2 tablets in 1 L was prepared to give a half-strength Ringer's solution. A second Ringer's solution was prepared by dissolving 4 tablets in 1 L of deionised water to give a full-strength Ringer's solution. A third solution was prepared with 8 tablets in 1 L to give a double-strength Ringer's solution. The compounds contained in Ringer's tablets and the composition in each solution can be found in Tables 2.2, 2.3 and 2.4. The ionic strength of half-strength, full-strength and double-strength Ringer's solution was 52.08 mM, 104.16 mM and 208.32 mM, respectively.

Table 2.2: Half-strength Ringer's solution composition [6].

Compound	**2 Tablets in 1 L (g/L)**	**Concentration (%)**	**Concentration (mM)**
NaCl	2.25	0.225	38.50
KCl	0.105	0.0105	1.41
$CaCl_2$	0.12	0.012	1.08
$NaHCO_3$	0.05	0.005	0.60
Total	2.53	0.25	41.59

Table 2.3: Full-strength Ringer's solution composition [6].

Compound	4 Tablets in 1 L (g/L)	Concentration (%)	Concentration (mM)
NaCl	4.50	0.45	77.00
KCl	0.21	0.021	2.82
$CaCl_2$	0.24	0.024	2.16
$NaHCO_3$	0.10	0.010	1.19
Total	5.05	0.505	83.17

Table 2.4: Double strength Ringer's solution composition [6].

Compound	8 Tablets in 1 L (g/L)	Concentration (%)	Concentration (mM)
NaCl	9.00	0.900	154.00
KCl	0.42	0.042	5.63
$CaCl_2$	0.48	0.048	4.33
$NaHCO_3$	0.20	0.020	2.39
Total	10.10	1.010	166.34

A solution of SBF was also prepared as flow-through eluent. The synthetic solution was developed by Kokubu *et al*. to imitate human blood plasma (HBP), with similar inorganic ion concentrations to human extracellular fluid and pH at physiological temperature [7]. SBF contains the same ions as Ringer's solution but with additional ions prepared in a specific way. The ion concentrations of SBF in comparison with HBP are detailed in Table 2.5. Each SBF reagent was placed in a 1 L volumetric with deionised water in the order provided by Table 2.6. The addition of reagent 9 was gradual in order to avoid local increase in pH of the solution. The ionic strength of SBF was 330.81 mM.

Table 2.5: SBF and HBP ion concentration [8].

Ion	Concentration in SBF (mM)	Concentration in HBP (mM)
Sodium (Na^+)	142.0	142.0
Potassium (K^+)	5.0	5.0
Magnesium (Mg^{2+})	1.5	1.5
Calcium (Ca^{2+})	2.5	2.5
Chloride (Cl^-)	147.8	103.0
Bicarbonate (HCO_3^-)	4.2	27.0
Hydrogen phosphate (HPO_4^{2-})	1.0	1.0
Sulfate (SO_4^{2-})	0.5	0.5

Table 2.6: SBF composition [8].

Reagent Number	Compound	Quantity	Concentration (%)	Concentration (mM)
1	NaCl	7.996 g/L	0.7996	136.82
2	$NaHCO_3$	0.350 g/L	0.0350	4.17
3	KCl	0.224 g/L	0.0224	3.00
4	$K_2HPO_4 \cdot 3H_2O$	0.228 g/L	0.0228	1.00
5	$MgCl_2 \cdot 6H_2O$	0.305 g/L	0.0305	1.50
6	HCl (1 kmol/dm^3)	40 cm^3	0.1641	45
7	$CaCl_2$	0.278 g/L	0.0278	2.50
8	Na_2SO_4	0.071 g/L	0.0071	0.50
9	$(CH_2OH)_3CNH_2$	6.057 g/L	0.6057	50.00
10	HCl (1 kmol/dm^3)	Adjusted to pH 7.25 at 36.5 °C	N/A	N/A
Total		19.00	1.90	244.50

2.2.4. Instrument Parameters

A scan of the compound of interest identified the wavelength at the maximum absorbance; known as λ_{max}. The UV then was set at a wavelength of 483 nm for Dox and 369 nm for Iri, readings were taken every minute for the first hour and every five minutes after the first hour for a maximum of 7999 minutes. If the experiment hadn't completed within the allocated time frame the instrument was re-started as required. The software used to analyse data was Cary WinUV using the Kinetics program.

Different parameters were analysed to optimise the method: de-gassing (to reduce air bubbles), packing with sand and glass beads (to eliminate swelling and flow artefacts), flow rate (to measure the effect on drug diffusion within DEBs), concentration of salt solution (to confirm flow rate effects), eluent solution (to measure the effect of different ion-exchange mechanisms) and bead volume (to measure the effect of packing density and bead geometry on the elution pattern).

2.3. Three-Dimensional Microscopy during Elution

To identify changes in bead size during elution the flow-through method was conducted under a three-dimensional microscope (3DM) at a magnification of x 20.

2.3.1. Materials

The drug used in this study was Dox HCl and the bead used was DC Bead™ 103, the other materials used were the same as described in Section 2.2.1.

2.3.2. Instrument Preparation

The microscope lens was tilted at a 90 ° angle to allow the flow-through cell to stand vertical. The equipment set up was similar to the open-loop flow-through elution method, but with the eluent heated to 70 °C rather than the flow-through cell to allow the beads to be imaged and so that beads during elution were 37 ° C. The DEBs were videoed and/or images were captured as depicted in Figure 2.8.

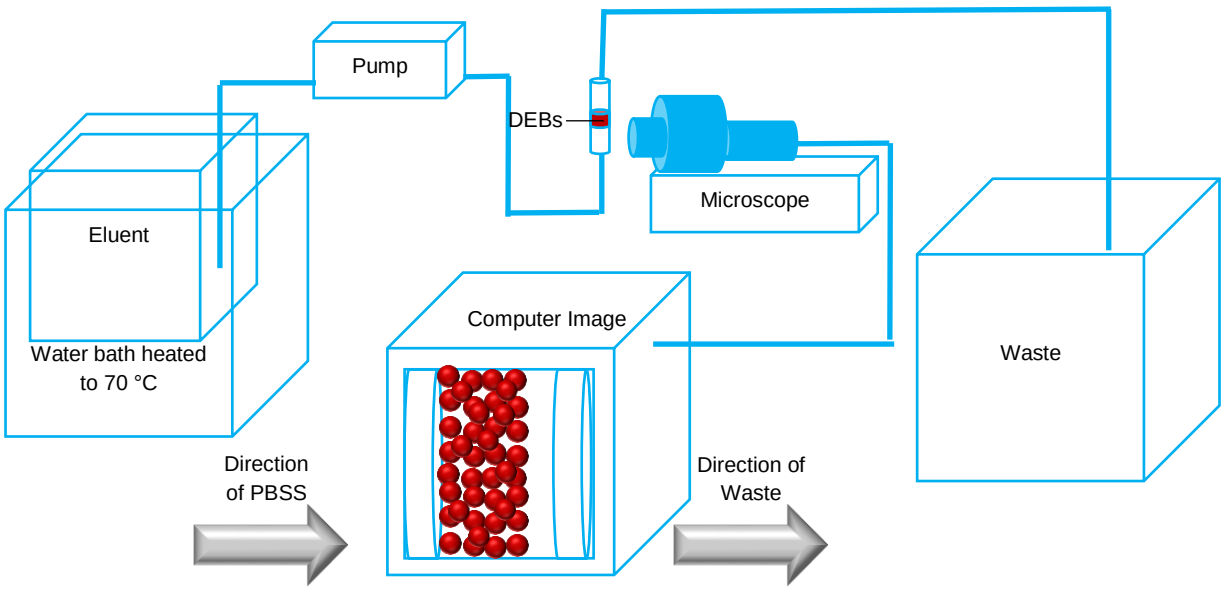

Figure 2.8: Experiment set up of the open-loop flow-through elution with 3DM.

2.3.3. Sample Preparation

Samples were prepared as in Section 2.2.3 without glass beads for packing. 0.5 mL of 100-300 µm DC Bead™ were used loaded with 37.5 mg/mL of Dox.

2.2.4. Instrument Parameters

The digital microscope employed for these experiments was a VHX-2000 unit using the Keyence VHX software program, this captured the images at magnifications of x 20 with options of: auto focus, remove glare, light shift, high-dynamic-range (HDR), high resolution HDR, optimize (with 9 different automatic settings of normal mode, normal mode + light shift, sharpening image mode, sharpening image mode + light shift, glare removal, glare removal + light shift, HDR (clear image), HDR (clear image) + light shift and high resolution HDR), image stitch, measurement, 3D (three-dimensional) display and live depth up used to enhance the image. The programme was set to capture images every 15 seconds over 1 day and 17 hours for a maximum of 9999 images. If required the timer was re-set until the experiment was complete. The pump was set at a flow rate of 2 mL/min with 154 mM (0.9 % w/v) NaCl.

2.4. Residual Solution

UV-Vis spectrophotometry was used to determine the concentration of drug in the residual solution of DEBs after loading, this confirmed the loaded concentration of drug in the beads.

2.4.1. Instrument Preparation

A Cary 60 UV-Vis spectrophotometer was used to analyse the concentration of drug. The cuvette for both Dox and Iri had a path length of 10 mm to ensure a high signal-to-noise ratio. The software used for analysis was Cary WinUV using the Concentration program.

2.4.2. Sample Preparation

After beads had been saturated in a drug solution and left to sequester overnight to ensure complete drug loading, the residual solution was then removed using a glass pipette with glass wool in the tip to prevent beads from being sampled as portrayed in Figure 2.9. The residual solution was then analysed using UV to identify the amount of drug recovered from the sample.

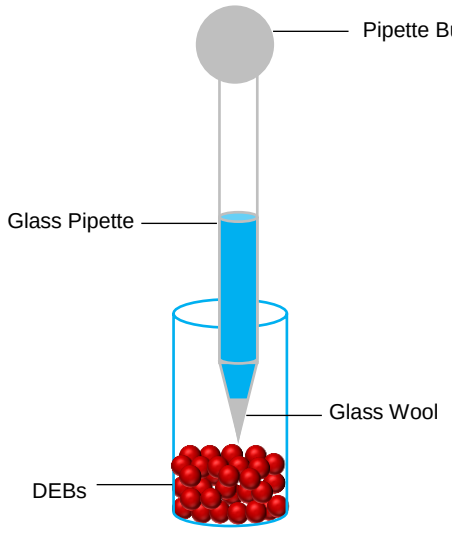

Figure 2.9: Collection of residual solution.

2.4.3. Instrument Parameters

Dox samples were recorded at an absorbance of 483 nm and Iri samples were recorded at 369 nm. Absorbance was converted to concentration using a previously established calibration curve which included seven standards at 0.001, 0.005, 0.01, 0.02, 0.03, 0.04 and 0.05 mg/mL for Dox, and 0.01, 0.05, 0.1, 0.2, 0.3, 0.4 and 0.5 mg/mL for Iri, standard curves can be found in the Appendix 'Ultra-Violet Visible (UV-Vis) Spectrophotometry Calibrations' Section. The concentration of drug was then converted to a percent of the unloaded drug to identify the drug loaded concentration of each sample, which was then correlated with the percent of drug eluted from the open-loop flow-through and ITC results.

2.5. Forced Extraction

An established method used a solution of 1 % (w/v) NaCl in dimethyl sulfoxide (DMSO) to extract any unreleased drug from elution samples [2]. This facilitated a calculation of the amount of drug bound to samples using UV-Vis spectrophotometry. Additional methods were performed using 15 % (w/v) NaCl in deionised water, 0.1 M HCl in deionised water and 20 % (w/v) KCl in deionised water in a 50:50 (v/v) ethanol (EtOH) solution to identify the most suitable chemical combination for drug extraction.

2.5.1. Materials

KCl, NaCl and HCl details are as described in Section 2.2.1. Additional materials used of DMSO anhydrous, ≥99.9 %, product code 276855, Sigma-Aldrich Corporation, Missouri, USA and EtOH, product code 459836-1L, Sigma-Aldrich Corporation, Missouri, USA.

2.5.2. Instrument Preparation

A Cary 60 UV-Vis spectrophotometer was used to analyse the concentration of drug in the samples. The cuvette for both Dox and Iri had a path length of 10 mm to ensure a high signal-to-noise ratio. The software used for analysis was a Cary WinUV using the Concentration program.

2.5.3. Sample Preparation

In Figure 2.10 eluted beads along with any packing material were washed into a separation column with deionised water. Any residual drug and the deionised water was drained into a waste container from the column. This was followed by adding an extraction solution of 10 mL 1 % NaCl/DMSO prepared by producing a 20 % (w/v) NaCl solution in deionised water, i.e. 10 g in 50 mL, then transferring this into 1 L DMSO. The column was agitated to ensure that the beads were mixed in the extraction solution. During this procedure the solution became the colour of the loaded drug and the beads began to return to their original colour. The beads were left for at least 10 minutes before the solution was collected in a vial below the column. The addition of extraction media was repeated until drug could not be seen in the solution or beads. The extracted drug was analysed using UV to identify the amount of drug

recovered. If required the solutions were occasionally diluted by known concentrations to record a value within the standard range and to record an absorbance of ≤ 1. If the drug was not extractable with this method 15 % NaCl, 0.1 M HCl or a solution of 10 % KCl/EtOH was used. To prepare the KCl ethanol solution a 20 % (w/v) KCl solution in deionised water was produced, i.e. 20 g KCl in 100 mL. This solution was then mixed in a ratio of 80:20 or 50:50 (v/v) KCl solution:ethanol, however the 50:50 solution was found to be a superior mixture for drug extraction from DEBs.

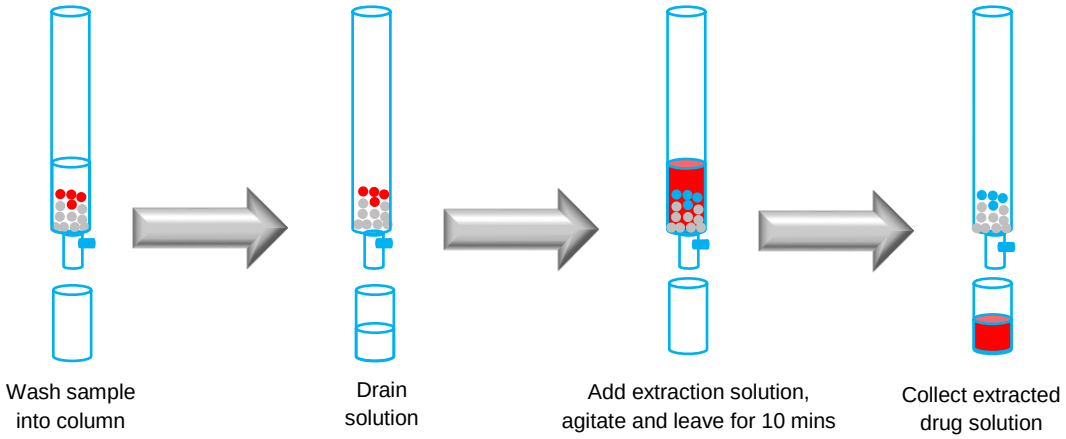

Figure 2.10: Step by step bead sample preparation for forced extraction analysis.

2.5.4. Instrument Parameters

Dox samples were recorded at an absorbance of 483 nm and Iri samples were recorded at 369 nm. Absorbance was converted to concentration using a previously established calibration curve which included seven standards at 0.001, 0.005, 0.01, 0.02, 0.03, 0.04 and 0.05 mg/mL for Dox, and 0.01, 0.05, 0.1, 0.2, 0.3, 0.4 and 0.5 mg/mL for Iri, standard curves can be found in the Appendix 'Ultra-Violet Visible (UV-Vis) Spectrophotometry Calibrations' Section. The concentration of drug was then converted to a percent of the unloaded drug to identify the drug loaded concentration of each sample, which was then correlated with the percent of drug eluted from the open-loop flow-through and ITC results.

2.6. Three-Dimensional Microscopy (3DM) of Drug-Eluting Beads (DEBs)

To identify the distribution of drug and to ascertain the extent of any aggregation and/or fragmentation the beads were analysed using a 3DM before loading, after loading and after the flow-through method was conducted. Analysis was completed at a magnification of x 250, 500, 1000 and 2500.

2.6.1. Instrument Preparation

Unlike microscopic during elution in which the microscope lens was tilted at a 90 ° angle (see method 2.3) the lens in these experiments was left horizontal at a 180 ° angle to capture the images.

2.6.2. Sample Preparation

Samples of beads were placed in a petri dish or on a glass slide under the microscope lens. In the eluted bead samples glass beads were avoided in the analysis of the cross section as shown in Figure 2.11. Samples were removed from the flow-through cell by piercing the filter membrane and washing the beads into a vial. Mechanical force of removing beads out of the cell caused bead destruction.

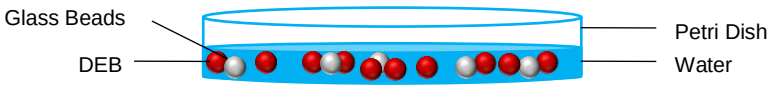

Figure 2.11: Petri dish of beads.

2.6.3. Instrument Parameters

In the ‘Optimize’ setting glare was removed in order to visualise the beads, however this gave a green effect to the bland samples. The microscope employed for these experiments was a VHX-2000 unit using the Keyence VHX software program which captured the images.

2.7. Hot Stage Microscopy (HSM)

Hot stage microscopy (HSM) is a technique which combines microscopy and thermal analysis of samples. Samples can be heated and images can be captured with the increase in temperature over a period of time. Through recording images at designated time/temperature points the equipment can also record any corresponding changes in colour and light intensity.

2.7.1. Materials

The drug used in the HSM study was Dox HCl and the bead used was DC Bead*M1*™ with NaCl.

2.7.2. Instrument Preparation

The sample was heated either to room temperature (25 °C) or to average normal internal body temperature (37 °C) and images were captured every minute for 30 minutes.

2.7.3. Sample Preparation

10 mg of beads were placed in a crucible which was located inside the sample holder. 10 µL of 1 mM Dox was added to the beads for drug-bead binding studies and 10 µL of 15 mM NaCl was added to 37.5 mg/mL drug loaded beads for elution the studies.

2.7.4. Instrument Parameters

Figure 2.12 shows the optical microscope arrangement which was an Olympus SZ11 model coupled with a Stanton-Redcroff hot-stage. The software was written in-house using Visual Basic.

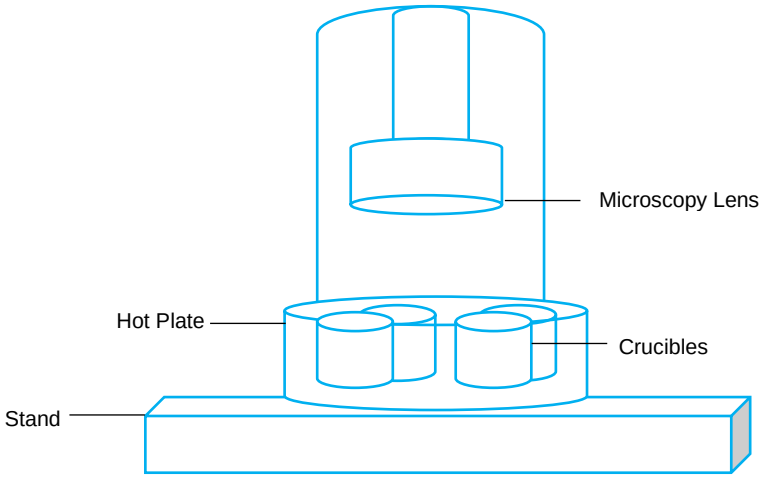

Figure 2.12: Elements of the HSM.

References

1 L. J. Waters, T. S. Swaine and A. L. Lewis, A calorimetric investigation of doxorubicin–polymer bead interactions, *Int. J. Pharm.*, 2015, **493**, 129–133.

2 T. Swaine, Y. Tang, P. Garcia, J. John, L. J. Waters and A. L. Lewis, Evaluation of ion exchange processes in drug-eluting embolization beads by use of an improved flow-through elution method, *Eur. J. Pharm. Sci.*, 2016, **93**, 351–359.

3 MicroCalorimeter User's Manual, VP-ITC MicroCal, http://www.biophysics.bioc.cam.ac.uk/files/ITC_VPITC_user_manual.pdf, (accessed 1 October 2017).

4 Michigan State University, UV-Visible Spectroscopy Chemistry, https://www2.chemistry.msu.edu/faculty/reusch/virttxtjml/spectrpy/uv-vis/uvspec.htm, (accessed 1 October 2017).

5 J. A. LEE, Sydney Ringer (1834-1910) and Alexis Hartmann (1898-1964), *Anaesthesia*, 1981, **36**, 1115–1121.

6 Sigma-Aldrich, Ringers solution 1/4 strength tablets, https://www.sigmaaldrich.com/content/dam/sigma-aldrich/docs/Sigma-Aldrich/Datasheet/1/96724dat.pdf, (accessed 6 June 2016).

7 T. Kokubo, H. Kushitani, S. Sakka, T. Kitsugi and T. Yamamuro, Solutions able to reproduce in vivo surface-structure changes in bioactive glass-ceramic A-W3, *J. Biomed. Mater. Res.*, 1990, **24**, 721–734.

8 Kyoto University, Protocol for Preparing Simulated Body Fluid (SBF), http://www.life.kyutech.ac.jp/~tmiya/SBF-e.html, (accessed 6 June 2016).

Chapter 3 : Method Development of Drug-Bead Binding Interactions using Isothermal Titration Calorimetry (ITC)

3.1. Introduction

Isothermal titration calorimetry (ITC) has previously been employed to determine the saturation of surfactants with several drugs. A method was developed to provide data which was unusual to traditional practice, whereby a change in the isotherm such as an increase in the enthalpy change from a negative value (exothermic response) to a positive value (endothermic response) was identified as the saturation limit rather than diminished signals [1]. Typically, the middle of the isotherm is attained as the binding ratio as seen in Figure 3.1, but alternatively the point of change was selected.

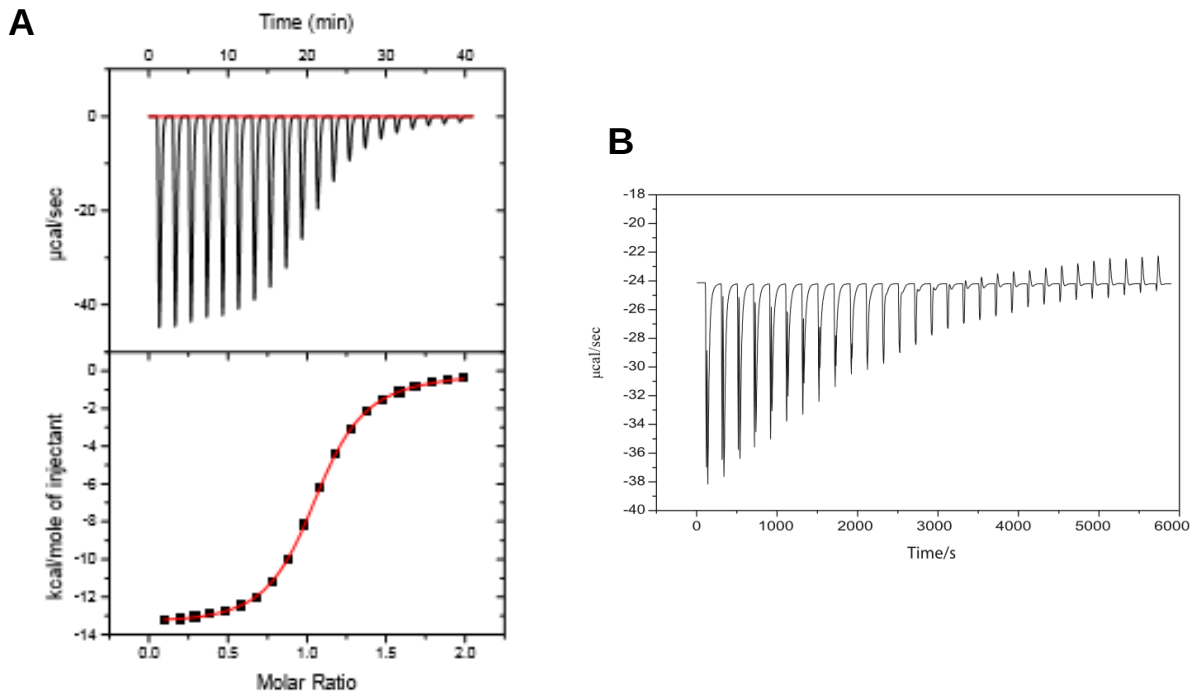

Figure 3.1: Typical example of ITC data with plateau saturation point (A) [2] and alternative example of ITC data with a change in enthalpy from exothermic to endothermic as the point of saturation (B) [1].

Preliminary work for this study suggested a similar enthalpy change in the isotherm with drug eluting beads (DEBs). One particular bead is DC Bead™, this is a polyvinyl alcohol (PVA) hydrogel with 2-acrylamido-2-methylpropane sulfonate sodium salt (AMPS) binding sites. This study investigates the binding ratio of drug to AMPS. The beads are commonly used with the chemotherapeutic agent doxorubicin (Dox) and this was the initial compound of interest. The beads are known to consist of 55.55 % PVA macromer 45.45% AMPS monomer, and earlier research has shown 1 mL of beads has a theoretical binding capacity of 44.77 mg if 1 mole of sulfonate was to react with 1 mole of Dox. The actual binding capacity was found to be 37.04 mg with a standard deviation of 0.377. Considering that the water content of these beads is 95 % in packing solution, this equates to a ratio of 0.836:1 Dox to AMPS using the technique of ultraviolet-visible (UV-Vis) spectroscopy [3]. ITC has the potential to produce accurate and precise data with further information about the binding characteristics of DEBs.

ITC has the ability to conduct experiments at set temperatures from 275 – 353 K. DEBs are loaded prior to the medical procedure at room temperature, but it was of interest to study the effects of temperatures outside of this range. Standard ITC experiments are run at 298 K and so four additional temperatures were chosen which were 293, 303, 310 and 313 K.

A further variable to be considered is pH as this can alter the binding interaction. Not only can the results be of an acid-base titration, but they can depend on the amount of ionised compound. Any changes must be investigated, but with careful contemplation in extremely low and high pH environments as unstable baselines and pH shifts are common.

The concentration of Dox loaded into DC Bead™ prior to the medical procedure is generally 37.5 mg in 1 mL of beads. This requires 1 mL of beads saturated in 1.5 mL of a 25 mg/mL (43 mM) Dox solution [4]. As the ITC syringe only holds 290 µL it requires an extremely small number of beads. The ITC also has a maximum detection limit which is +/- 38.799 µcal/sec and a minimum of +/- 3 – 5 µcal/sec [5], therefore an appropriate concentration of drug and mass of beads is required for analysis along with discovering whether any changes influenced the results.

The volume of injectant and the number of injections may be altered during instrumental set up. The instrument manual advises a volume between 3 – 15 µL and 10 – 15 injections [5], a set of experiments were undertaken to examine this recommendation.

Finally, the saturation of beads, aggregation state of Dox and the ITC limit of Dox detection (LOD) was confirmed. The saturation test was completed by evaluating the residual solution collected from the ITC experiment for the concentration of drug unloaded, in addition to extracting the drug from the beads to confirm whether the concentration of drug expected to have loaded into the beads was achieved during analysis. Rather than Dox titrated into water, water was titrated into Dox to determine to self-association of the drug. Minute concentrations of Dox were titrated into the ITC, the concentration was reduced until the differential power (DP) was close to 0.1 µcal/sec which is the instruments LOD. This experiment determined the lowest concentration of Dox required for a visible interaction on the ITC.

3.2. Results and Discussion

3.2.1. Effect of Temperature

ITC was used to investigate drug-bead interactions, whereby drug was injected into the sample cell containing polymer beads, namely DC Bead*M1*™. To calculate the moles of DC Bead*M1*™ binding sites, specifically the moles of AMPS in the ITC sample cell, the solid content was first determined using Equation 3.1. For this calculation 1000 µL of water washed beads were placed in a pre-weighed centrifugal filter insert and were centrifuged for 30 seconds at 3000 rpm. The beads and the centrifugal filter insert were then weighed and placed in a vacuum oven for 24 hours at 313 K. After 24 hours in the vacuum oven the beads were allowed to cool to room temperature, then the beads and the insert were weighed for a second time. These weights were used to calculate the percentage solid and water content of beads which have been centrifuged for 30 seconds at 3000 rpm. The test was conducted in triplicate and the results of DC Bead*M1*™ are found in Table 3.1.

Equation 3.1: Calculation of solid content.

$$\%\ Solid\ Content = \frac{(Weight\ of\ Dry\ Beads + the\ Insert) - (Weight\ of\ the\ Empty\ Insert)}{(Weight\ of\ the\ Wet\ Beads + the\ Insert) - (Weight\ of\ the\ Empty\ Insert)} \cdot 100$$

Table 3.1: The percentage solid content of DC Bead*M1*™ in water prepared for the ITC (sample number = 3).

Weight of Empty Insert (mg)	Weight of Wet Beads + insert (mg)	Weight of Dry Beads + Insert (mg)	% Water Content	% Solid Content
908.90	1167.52	916.75	96.96	3.04
908.45	1184.28	916.82	96.97	3.03
926.52	1159.54	933.58	96.97	3.03

The average percentage solid content of DC Bead*M1*™ in water centrifuged for 30 seconds at 3000 rpm was 3 % to the nearest whole number. To confirm the percentage solid content the method was performed in packing solution and compared with results in water. The solid content of beads in packing solution is known to be ~5 %, and so performing the method in saline as well as in water was to confirm accuracy of the method. The test was executed in triplicate and the results are shown in Table 3.2.

Table 3.2: The percentage solid content of DC Bead*M1*™ in saline (sample number = 3).

Weight of Empty Insert (mg)	Weight of Wet Beads + insert (mg)	Weight of Dry Beads + Insert (mg)	% Water Content	% Solid Content
900.82	999.78	908.50	92.24	7.76
926.45	1041.20	935.08	92.48	7.52
891.15	1004.38	899.92	92.25	7.75

The average percentage solid content of DC Bead*M1*™ in saline centrifuged for 30 seconds at 3000 rpm is 7 % to the nearest whole number. Although the solid content of beads in saline was expected to be 5 % and this study presents a larger value, the discrepancy in the results could be caused by a difference in the removal of water test method. Some choose to wick the water off the beads, others pipette the water off and a variation in the amount of water removed from the beads would result in a disparity between the solid content. If the beads were centrifuged for an extended amount of time than required, water would then be removed from inside the bead along with outside presenting a higher solid content. Nevertheless, it was important to establish the solid content of beads used in the testing of drug-bead binding, and it does indicate that there is a difference in the solid content of beads in water and beads in saline which was anticipated. While there was variation between the expected value of beads in saline the difference is relatively small, and so long as the value used was the solid content of beads in the experiment it will ensure the accuracy of the results contained in this report.

For all ITC experiments a decrease in exothermic signals was selected as the saturation of AMPS binding sites from the binding of Dox. The volume of Dox titrated to achieve the exothermic endpoint was calculated (mL) by multiplying the number of exothermic injections by the volume per injection (mL). The concentration of Dox (g/mL) was then multiplied by the volume of injections at the endpoint (mL) to equal the mass of Dox at the said endpoint (g). Since the mass of Dox used (g) and the relative molecular mass (RMM) was known ($(C_{27}H_{29}NO_{11}.HCl)$ 579.99 g), the number of moles was calculated by dividing the mass of Dox bound to AMPS by the RMM of Dox.

The solid mass of beads in the sample cell was the weight of centrifuged beads (g) divided by 100 and multiplied by the 3 % solid content. However, Dox binds to AMPS groups situated on DC Bead™ and not to the whole bead structure. DC Bead™ contains 45.45 % AMPS, therefore the mass of AMPS is equal to the mass of beads (g) divided by 100 and multiplied by 45.45 %. Since the mass of AMPS

has been calculated and the RMM is known ($(C_7H_{12}NNaO_4S)$ 229.23 g), the number of moles was calculated by dividing the mass of AMPS by the RMM of AMPS.

Therefore, the moles of Dox at the endpoint divided by the moles of AMPS in the sample cell equalled the molar ratio of AMPS bound to Dox. The Dox-water interaction and the bead-water interaction were subtracted from the Dox-bead results to produce the true Dox-DC Bead™ values. A selection of raw ITC data is displayed in Figures 3.2, 3.3, 3.4 and 3.5.

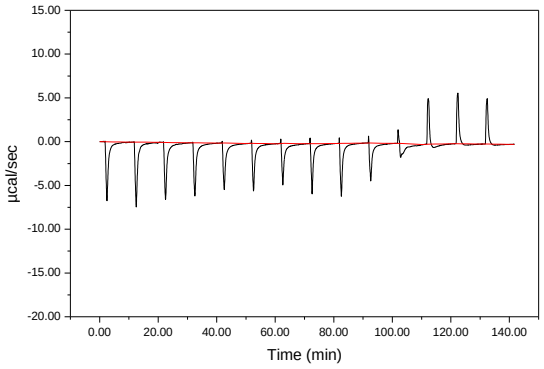

Figure 3.2: 10 mM Dox into 100 mg DC Bead*M1*™ at 298 K – the syringe contained Dox, the sample cell contained beads with deionised water and the reference cell also contained deionised water.

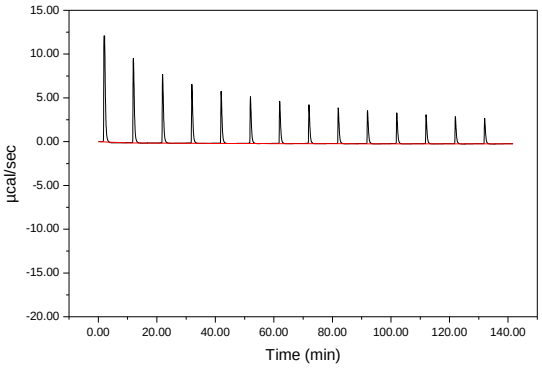

Figure 3.3: 10 mM Dox into water at 298 K – the syringe contained Dox, the sample cell and reference cell contained deionised water.

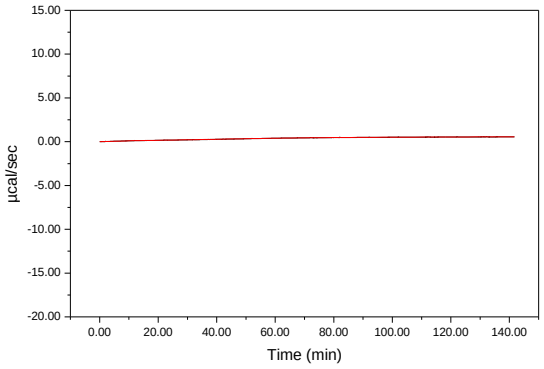

Figure 3.4: Water into 100 mg DC Bead*M1*™ at 298 K – the syringe contained deionised water, the sample cell contained beads with deionised water and the reference cell contained deionised water.

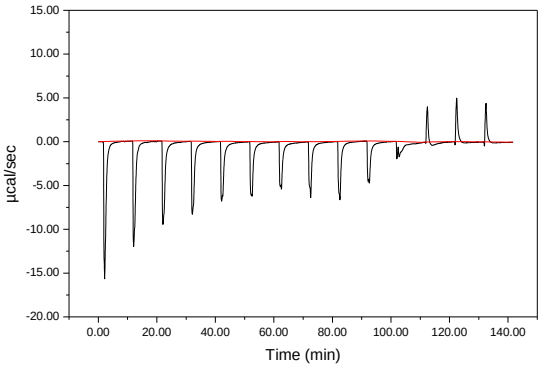

Figure 3.5: Subtraction of Figures 3.3 and 3.4 from 3.2.

Five temperatures were selected (293, 298, 303, 310 and 313 K) to encompass typical temperatures encountered during sample preparation, through to those encountered by the formulated product *in vivo*. The signals for Dox-bead binding were exothermic, whereas the interaction of Dox-water was endothermic as this process includes the dissociation of Dox-Dox aggregates under water dilution, water-bead was discovered to have a negligible trace. Where the thermogram changed from exothermic to endothermic the beads were considered saturated with drug. It was also found that the binding ratio was temperature independent as presented in Figure 3.6, this was expected since there were a set number of binding sites on the bead for the drug to bind. 303 K has a slightly different profile to the other temperatures and this could be a consequence of the small number of replicates.

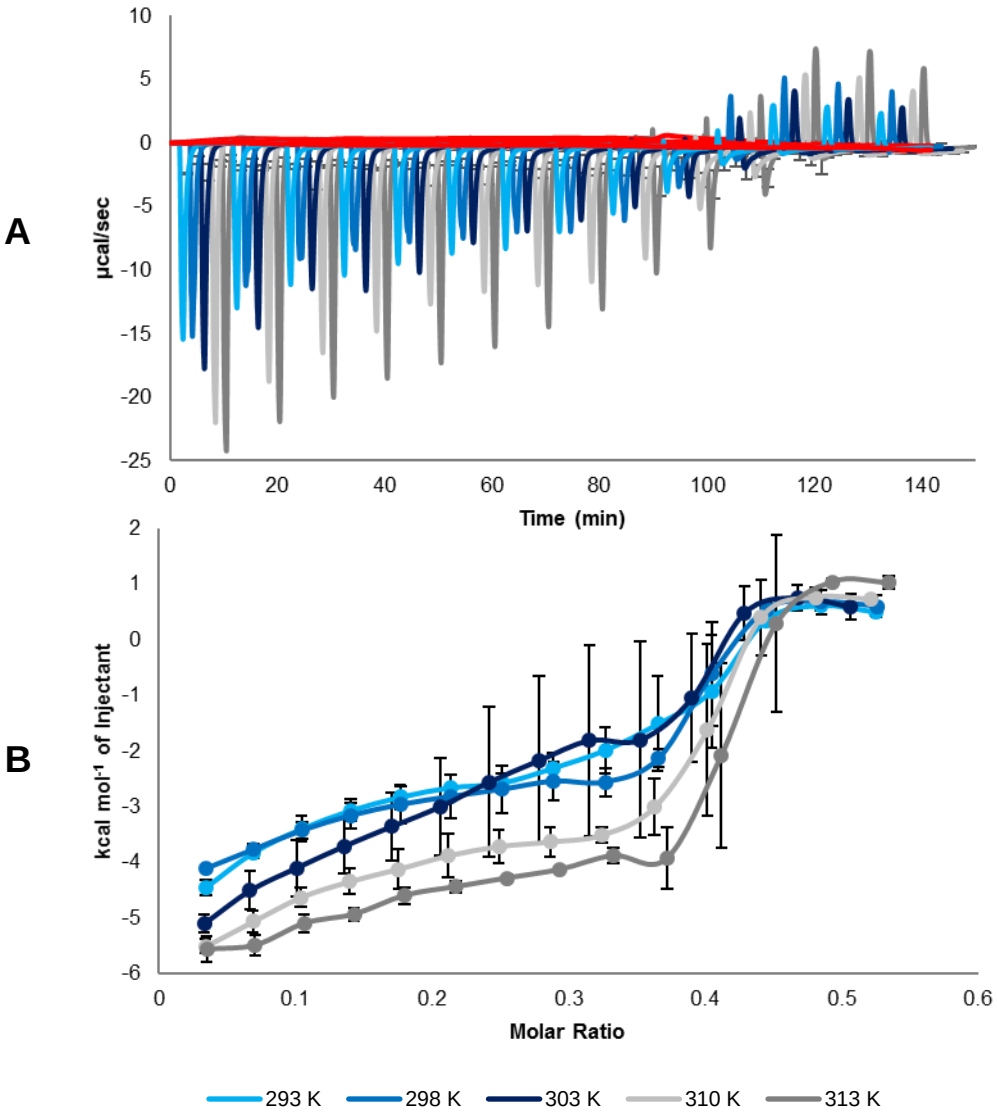

Figure 3.6: The interaction of Dox-water was subtracted from Dox-beads, the top graph shows the DP of each injection (A) and bottom graph is the matching binding isotherms (B), with 43 mM Dox titrated into 100 mg water washed beads at 293, 298, 303, 310 and 313 K (sample number = 3, error bars = standard deviation, time has been adjusted by two minutes so the details of each trace can be identified).

It was concluded that ITC was a suitable method for the investigation of drug-excipient binding interactions. Whilst studying the thermodynamic data of bead binding at different temperatures the average molar ratio (*n*) of Dox molecules bound to AMPS sites was 0.43:1 ± 0.02. Origin® displays incorrect *n* values as it sets the middle injection at half the molar ratio, a manual calculation of Dox to AMPS can be found earlier in this chapter and in a preceding paper [6]. An R^2 value of 0.12 demonstrated in Figure 3.7 suggests that there is no change in binding with a change in temperature and an ANOVA test provided evidence that there was no statistical significance within the population.

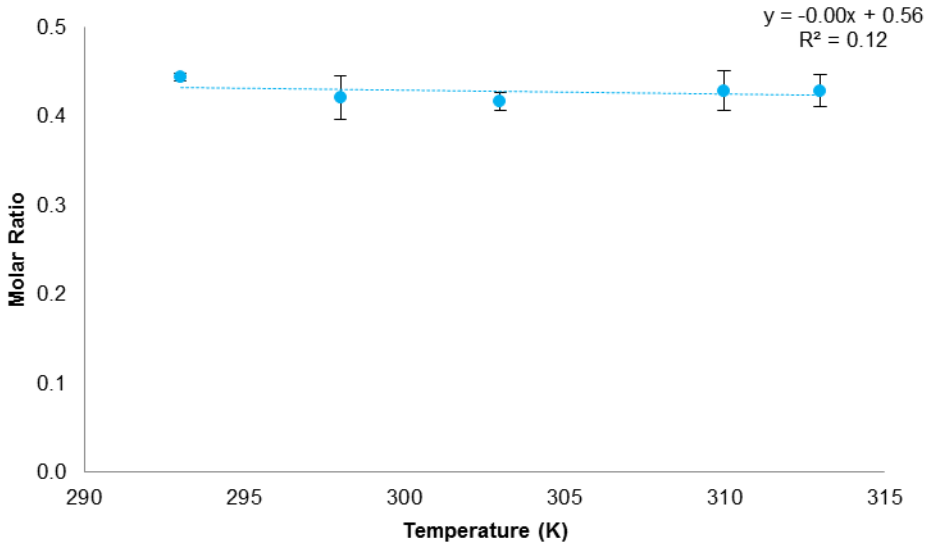

Figure 3.7: Molar ratio of Dox to AMPS at temperatures of 293, 298, 303, 310 and 313 K (sample number = 3, error bars = standard deviation).

The ratio of Dox bound to AMPS was expected to be much closer to 1:1 according to previous work completed by Gonzalez [3]. It was suggested that as the ITC adds extremely small amounts of Dox over time, that Dox binds to the outside of the beads and prevents Dox from binding to the inside, which ultimately affects the binding ratio [6]. However, on further investigation it seems that the preparation of beads is of immense importance, as explained in detail further in the chapter.

Upon analysing the individual injections more closely it seems that at higher temperatures the reaction occurred at a faster rate, this was noted in Figure 3.8 and can be identified by the reduced time taken for the trace to reach the baseline after the injection. This occurs as Dox needs to diffuse into the

beads before interaction with the binding groups. Diffusion rate increases with temperature and this can only be seen in each individual injection since injected time is controlled, i.e. every 10 minutes.

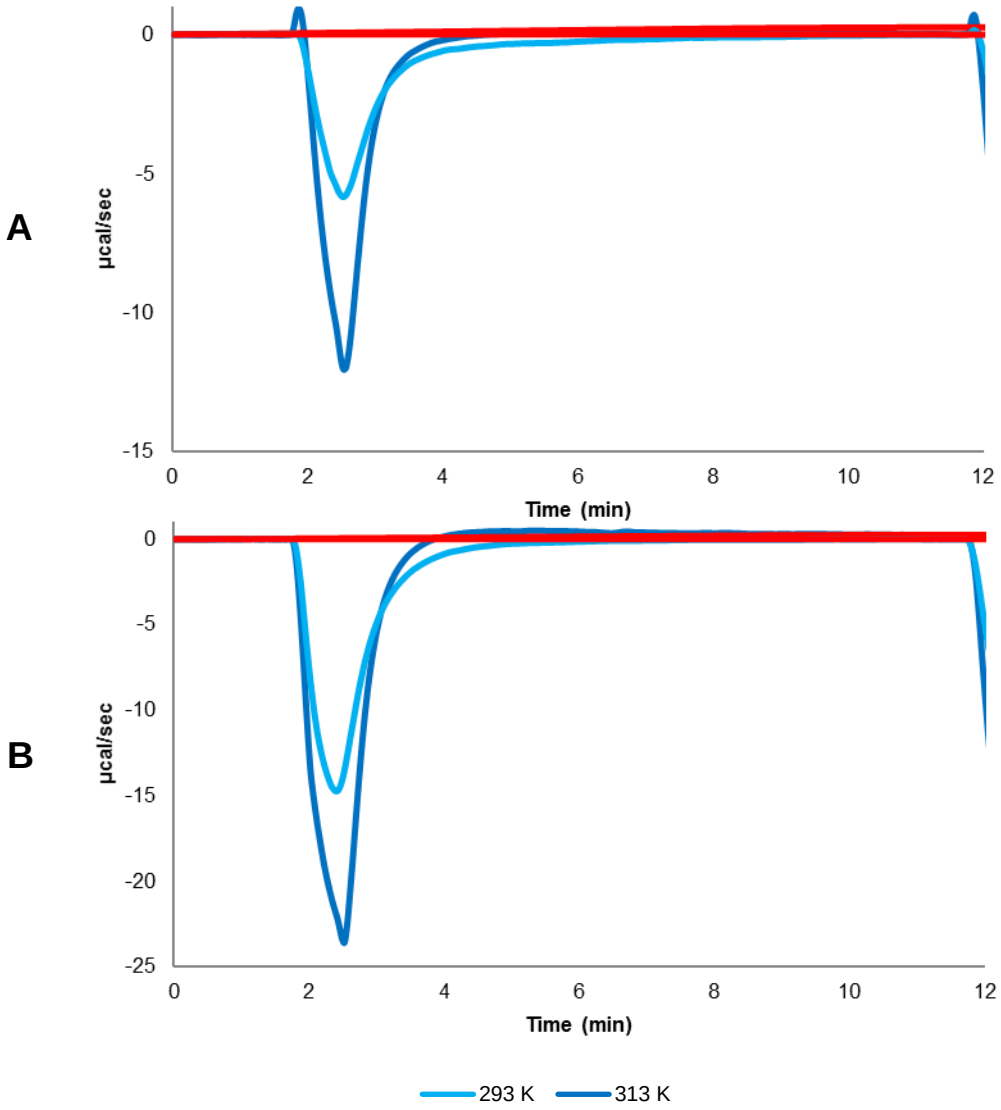

Figure 3.8: Illustration of the first injection in an ITC experiment where 20 µL of 10 mM Dox was titrated into 100 mg beads at 293 K, unsubtracted trace (A) and Dox-water subtracted from Dox-bead (B).

Note that the peak height of experiments at different temperatures varied due to the rate at which the experiment occurred, however peak area was comparable. At higher temperatures molecules move faster, the rate of diffusion is greater, the interaction occurs quicker and the peaks are more pronounced, but the total area at each temperature was the same as the amount of Dox bound to the beads at each temperature is equivalent. Occasionally Dox interacted with water more than with beads, producing a small initially endothermic signal before it exothermically interacted with beads, over time Dox was then

absorbed by beads switching the signal from endothermic to exothermic. This is apparent at 313 K in the unsubtracted trace and disappeared in the subtraction, but was evident at various temperatures in several runs possibly depending on the arrangement of binding sites within and on the surface of beads.

Data in Table 3.3 indicates normal distribution and a significant difference was found using Minitab® software. This was used to calculate an unpaired *t*-test between the time taken for the reaction to complete in the first injection by the trace retrieving to the baseline at 293 and 313 K ($p = 0.0049$). At higher temperatures molecules move faster and an increase in collisions leads to more diffusion. This data shows that the reaction takes place over a shorter period of time, most likely as the drug finds binding sites quicker at higher temperatures within the range of 293 – 313 K.

Table 3.3: Time taken for the first injection of an ITC experiment to return to the baseline at 293 and 313 K (sample number = 3, error = standard deviation).

Temperature (K)	Time to Reach Baseline (mins)	Average Time (mins)
293	7.4	8.6 ± 1.1
	9.5	
	9.0	
313	4.5	4.0 ± 0.9
	4.6	
	3.0	

Origin® calculates the thermodynamic values of stoichiometry (*n*), binding constant also known as the equilibrium constant (*K* (M^{-1})), enthalpy change (ΔH (cal/mol)) and entropy change (ΔS (cal/mol/deg)). *K* is associated with binding and unbinding of the receptor (R) and ligand (L) molecules in a reaction. If $K >> 1$ the product is favoured in the reaction and thus is spontaneous in the forward direction of Equation 3.2. If $K << 1$ the reactant is favoured and thus is non-spontaneous in the forward direction of Equation 3.2. If $K \approx 1$ the system is at equilibrium and *K* is never a negative value for any given reaction. The average experimental value for *K* was 4.45×10^5 M^{-1} and in Table 3.4 there seemed to be no correlation between temperature and equilibria, however *K* is a function of temperature and the large error bars make this temperature effect inconclusive.

Equation 3.2: Binding (equilibrium) constant, where R is the receptor and L is the ligand.

$$R + L \rightleftharpoons RL$$

Table 3.4: Binding constant of Dox to AMPS at temperatures of 293, 298, 303, 310 and 313 K (sample number = 3, error = standard deviation).

Temperature (K)	*K* (x 10^5 M^{-1})
293	0.25 ± 0.06
298	6.43 ± 9.76
303	0.44 ± 0.25
310	7.29 ± 10.11
313	7.82 ± 7.70

Change in enthalpy is a measure of the heat content of a system, which can be released (exothermic) or absorbed (endothermic). At closer inspection of change in enthalpy there was in general a decline as the temperature increased in Figure 3.9 and R^2 was close to 1 at 0.83. A statistical difference was noted between 293 and 313 K ($p = 0.0016$), showing that enthalpy change is temperature dependent. Binding was an exothermic process which became more exothermic upon an increase in temperature, as the change in free energy behind the partitioning phenomenon became more favourable.

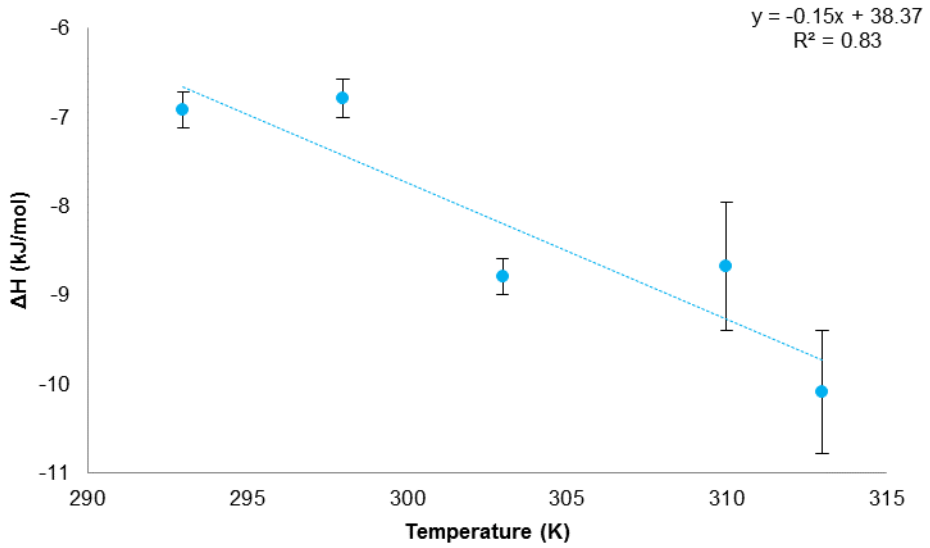

Figure 3.9: Enthalpy change of Dox to AMPS at temperatures of 293, 298, 303, 310 and 313 K (sample number = 3, error bars = standard deviation).

Entropy change is the measure of the disorder in a given system. As this was positive at each tested temperature with an average of 8.91 ± 4.24 kJ/mol.K in Table 3.5, entropy change thus increases as the reaction progresses and the change in entropy seemed not to be affected by temperature. As $\Delta S_{universe} = \Delta S_{system} + \Delta S_{surrounding} = >0$, the reactions are therefore spontaneous. If ΔS was equal to the measured reaction would be considered reversible at equilibrium.

Table 3.5: Entropy change of Dox to AMPS at temperatures of 293, 298, 303, 310 and 313 K (sample number = 3, error = standard deviation).

Temperature (K)	***T*∆*S* (kJ/mol.K)**
293	6.59 ± 0.68
298	13.53 ± 4.94
303	4.51 ± 2.33
310	10.40 ± 4.39
313	9.55 ± 1.88

As both change in enthalpy and change in entropy are known values as outputs from the software Origin®, the change in Gibbs free energy can be determined using Equation 3.3. This calculates the change in favourability of a reaction. Negative values in Table 3.6 with an average of -17.16 ± 4.34 kJ/mol propose a spontaneous reaction in the forward direction of the equation, this indicates that there is no correlation between temperature and the change in free energy. The reactions are therefore not reversible in their current state, this statement is well documented as salt present in blood is required to release drug from the bead using an ion-exchange mechanism [7,8].

Equation 3.3: Calculation of the change in Gibbs free energy, where ΔG is the change in Gibbs free energy, ΔH is the change in enthalpy, T is Temperature and ΔS is the change in entropy.

$$\Delta G = \Delta H - T\Delta S$$

Table 3.6: Free energy change of Dox to AMPS at temperatures of 293, 298, 303, 310 and 313 K (sample number = 3, error = standard deviation).

Temperature (K)	**ΔG (kJ/mol)**
293	-13.50 ± 0.60
298	-20.32 ± 5.00
303	-13.30 ± 2.39
310	-19.07 ± 4.71
313	-19.63 ± 2.53

Spontaneity of a process can be determined when temperature and pressure are constant values using Table 3.7. As ΔH was negative, ΔS positive and ΔG negative for all temperatures, the reaction of Dox into water washed beads is always spontaneous regardless of the systems temperature.

Table 3.7: Determining spontaneity of a system, colour blue corresponds to low temperature (L) and the red colour corresponds to high temperature (H).

ΔH	**ΔS**	**T**	**ΔG**	**Spontaneity**
+	+	L/H	+/-	Non-Spontaneous at Low Temperature/Spontaneous at High
+	-	L/H	+	Always Non-Spontaneous
-	+	L/H	-	Always Spontaneous
-	-	L/H	-/+	Spontaneous at Low Temperature/Non-Spontaneous at High

The interaction of Dox-water has been subtracted from the interaction between Dox solubilised in water and titrated into beads in water. Due to unforeseen circumstances with the equipment Dox into water was only completed once at each temperature, however enthalpy change was plotted to ensure correct values were obtained. As R^2 specified in Figure 3.10 is equal to 0.99 it was sufficient assurance for a

sample number of 1. Each signal in the thermodynamic profile for water titrated into beads in Figure 3.11 was <0.1 µcal/sec, signifying that no binding was present.

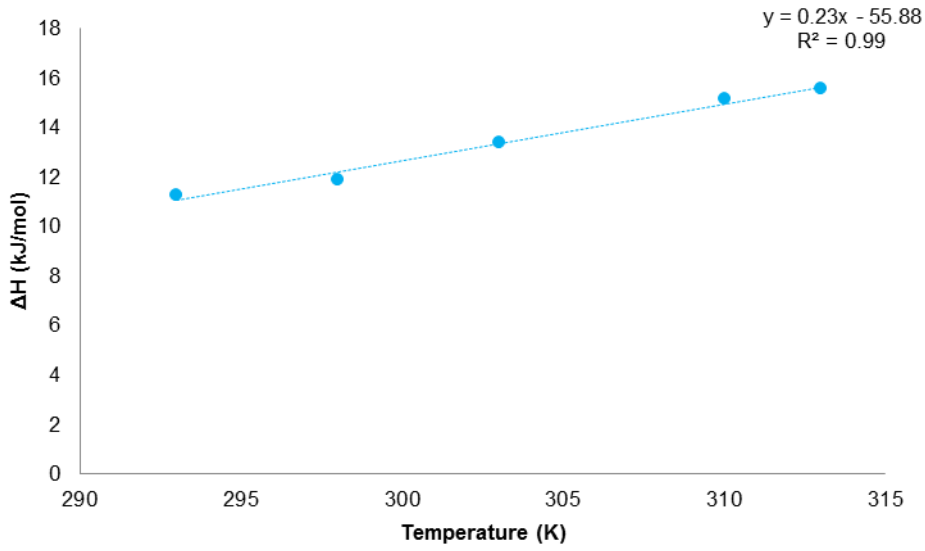

Figure 3.10: Enthalpy change of Dox to water at temperatures of 293, 298, 303, 310 and 313 K (sample number = 1).

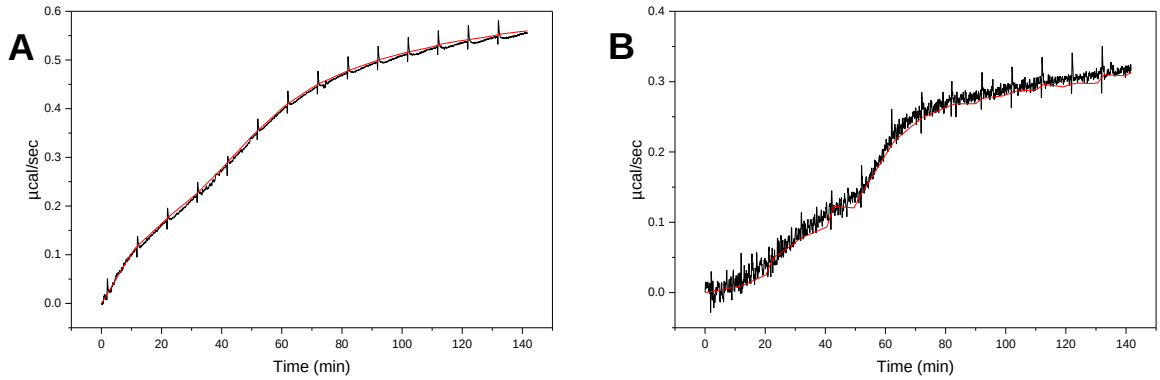

Figure 3.11: Isotherm of water into beads at 293 (A) and 313 K (B).

3.2.2. Binding Ratio Study

The ratio of Dox molecules to SO_3^- groups was previously reported to be 0.42:1 with a standard deviation of 0.02 [6], however a further study found the ratio much closer to data obtained by Gonzales using UV-Vis where the binding ratio was quantified as 0.836:1 and a standard deviation of 0.377 [3].

Firstly, it was ascertained that the presents of residual Decon® existed in the temperature experiments. The manual suggests washing the ITC cell with 200 – 400 mL of detergent and rinsing with 300 mL of water. By thoroughly washing the cell with at least 1 L of water and removing all traces of Decon® a decrease in binding was observed. Higher ratios were then obtained by washing the beads in hydrochloric acid (HCl). The beads arrive stored in saline and it was believed that washing the beads in deionised water during the first study removed free excess sodium ions from around the beads, but that sodium ions bound within the bead would remain and interfere with bead binding properties. Different washing processes were found to produce varying results. Washing the beads in acid improved reproducibly and led to an increased drug-bead interaction. This acid washing step does not take place in the clinic and yet a similar binding ratio was achieved which was demonstrated by the UV method. However, in the clinic Dox is loaded into beads in one simple step where a high concentration of drug is added in one go, whereas the ITC injects small amounts of Dox over time. The concentration of Dox in the one step process could drive the Dox-bead interaction. Washing the beads in 2 M HCl exchanges the sodium for a proton. The hydrogen bond on the protonated bead is weaker, less energy is required to break the bond and it is therefore easier for Dox to displace than the ionic bond on the sodium ion.

The water content changed when acid washed beads compared with water washed beads and the results can be found in Table 3.8. The new percentage solid content value of 6 % was replaced with 3 % in the molar ratio calculations for all further analysis.

Table 3.8: The percentage solid content of DC Bead*M1*™ in HCl prepared for the ITC (sample number = 3).

Weight of Empty Insert (mg)	**Weight of Wet Beads + insert (mg)**	**Weight of Dry Beads + Insert (mg)**	**% Water Content**	**% Solid Content**
906.97	1153.46	921.71	94.02	5.98
887.76	1150.71	903.40	94.05	5.95
922.57	1149.20	935.91	94.11	5.89

Figure 3.12 illustrates Dox binding to sulfonic acid on the bead in contrast with a sulfonate salt. It was difficult to determine the endpoint of bead loading using a change in exothermic to endothermic signal with this new method of bead preparation. Consequently, the highest ΔH value was used as the point of bead saturation where there was a plateau or fall in ΔH after this point. The ratio of Dox to acid

washed beads was 0.81:1, whereas Dox to water washed beads with no Decon® present was 0.29:1 (water washed beads data varied greatly but for clarity not all data is shown). Clearly there was an increase in activity with the elimination of ions when using the ITC.

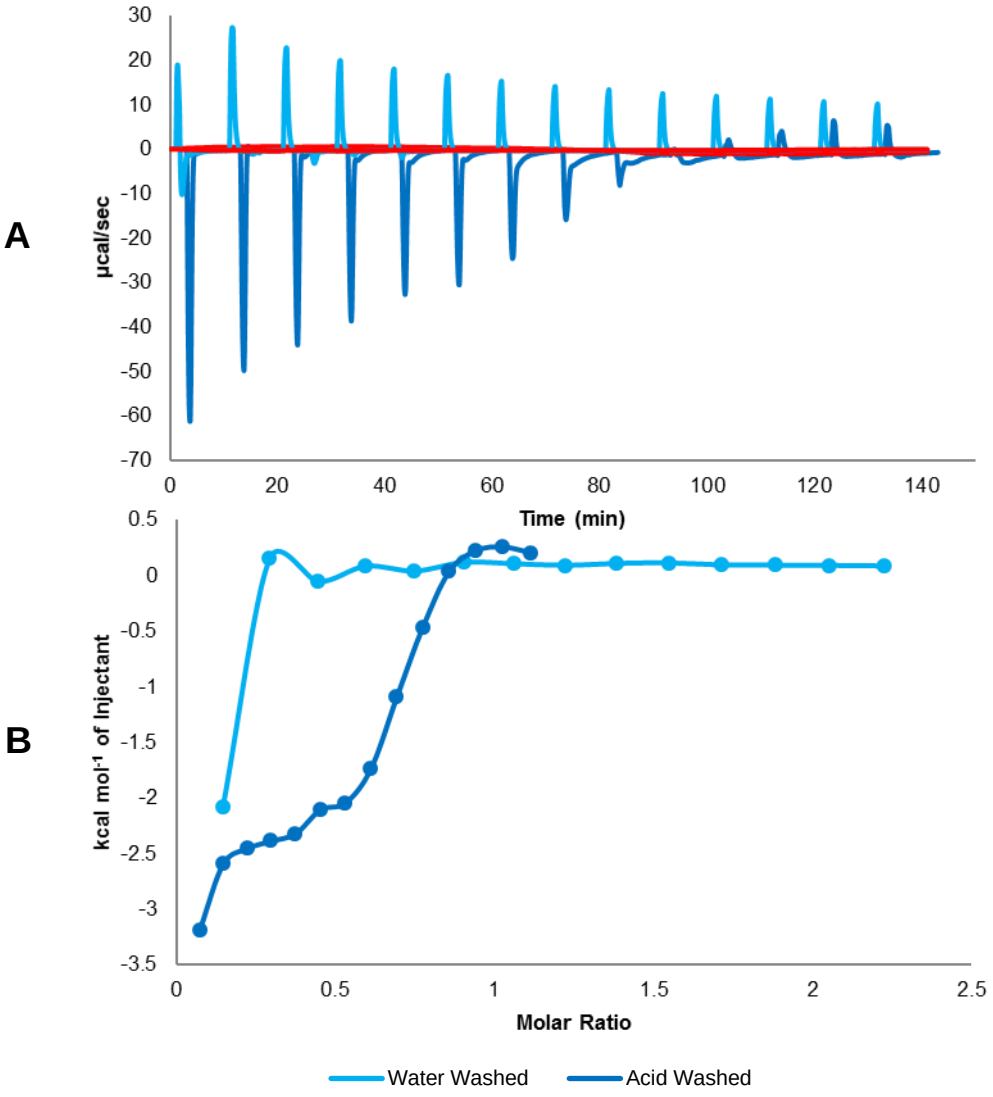

Figure 3.12: 43 mM Dox titrated into 100 mg water washed beads and 100 mg acid washed beads (sample number = 1, time has been adjusted by two minutes so the details of each trace can be identified).

Binding constant is an indication of the extent of binding interaction in that the larger the *K* value the greater the binding affinity. The binding constants for both preparations of beads are given in Table 3.9. The affinity was much smaller in the acid washed sample, therefore the extent of binding appears to be greater in the water washed beads. This is a consequence of the extended binding event observed in the water washed sample and does not reflect the fact that acid washed beads are available for binding.

Table 3.9: Binding constant of Dox to AMPS with beads washed in either water or acid (sample number = 1).

Bead Preparation	***K* (M^{-1})**
Water Washed	7.73×10^{8}
Acid Washed	1.19×10^{4}

The thermodynamic data for the two washing preparations of beads is available in Figure 3.13. Both bead preparations were discovered to be exothermic, but water washed beads released a greater amount of heat than acid washed beads. Consequently, more energy was required to break the bonds in the water washed sample when sodium ions were present in comparison to hydrogen ions in the acid washed sample. The entropy change for water washed beads was negative and for acid washed beads was positive. This reveals that for the water washed sample change in entropy decreased towards the product, whereas entropy change of the system increased in the acid washed sample resulting in a much more spontaneous reaction. This is possible because more protons are released from the acid washed beads and hence entropy is greater. The change in free energy is negative, and so is spontaneous in the forward direction and subsequently non-spontaneous in the reverse.

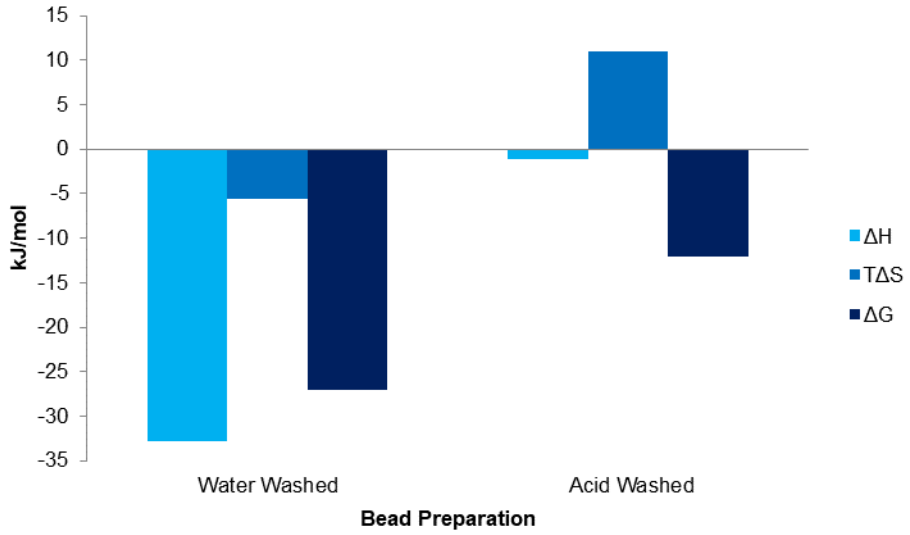

Figure 3.13: Thermodynamics of Dox to AMPS with beads washed in either water or acid (sample number = 1).

As ΔH, ΔS and ΔG were negative for water washed beads the reaction is spontaneous at low temperature and non-spontaneous at high, in these experiments the temperature was relatively low and

so the process was spontaneous. For acid washed beads ΔH was negative, ΔS positive and ΔG negative, and so the reaction was always spontaneous regardless of the systems temperature. Binding affinity is influenced by non-covalent intermolecular interactions such as electrostatic interactions, hydrogen bonding, hydrophobic and Val der Waals forces between the two molecules [9]. The thermodynamics of water washed beads indicate favourable hydrogen and hydrophobic interaction, whilst acid washed beads exhibit good hydrogen bonding with unfavourable conformational change. The reaction of water washed beads was enthalpically driven, whereas acid washed beads were both enthalpically and entropically driven. The enthalpy contribution is due to hydrogen bonding, electrostatic and van der Waals interactions. The entropy contribution is due to due to hydrophobic interactions. Moreover, water molecules which surround the bead binding sites are replaced by the drug and the bead changes conformation during binding to create binding sites which can accommodate the drug. This is exactly what is known to happen during the drug loading process of DEBs and is another indication that binding occurs as expected in the acid washed sample [10,11].

This study was to identify the binding characteristics and provide a method whereby different types of bead can be distinguished. It was not to mimic the binding method produced in the clinic, and so this technique provides a way of understanding the drug-excipient interaction and a possibility of demonstrating the binding properties of different beads. It would be easier for future analysis to differentiate between different product and types of binding with a method that produces a higher binding ratio, and so the process of washing the beads with 2 M HCl was adopted as the preferred technique.

Without washing the beads very small interactions were seen, as when sodium ions are replaced with hydrogen a greater amount of Dox has the potential to bind. The strong binding of the sodium ion with the sulfonic group may need to absorb more energy to exchange with Dox in comparison to hydrogen. The protonated form of the bead has a non-ionic bond, which is weaker and will need to absorb less energy to exchange with Dox compared with the ionic bond between sodium and the bead. The energy required for Dox to exchange with sodium compared with Dox to exchange with a proton is larger and may not be detectable in the current method. Standard enthalpy of formation for the cation sodium (Na^+) was discovered in various literature to be -239.7 and -240.34 kJ/mol in a 1 M aqueous solution at 298 K, the compound sulfur trioxide (SO_3) was exposes to be -395.2 and -395.7 kJ/mol under the same conditions and the anion hydroxide (OH^-) was revealed as -229.9 and -230.015 kJ/mol [12,13]. As values for Na^+ are greater than OH^- more energy is required for breaking bonds with SO_3.

3.2.3. Effect of pH

Dox has six pKa values of 8.1, 9.8, 11.8, 13.6, 14.2 and 15.7 as illustrated in Figure 3.14 in its protonated form. To confirm whether binding was a result of a change in pH of the beads, the pH of Dox was altered to the same pH of the acid washed beads. The pH of 43 mM Dox was 3.788, the pH of water washed beads in 1.4194 mL water was 5.612 and 100 mg of acid washed beads in 1.4194 mL water was pH 1.824. At pH 3.8 and 1.8 the ionisation of the amine group on Dox theoretically corresponded to 99.99 and 100 %, respectively. The pH of the Dox solution was consequently adjusted to 1.8 with the addition of HCl. The pH of the beads was not increased to 3.8 as this would have involved the addition of ionic compounds such as sodium hydroxide (NaOH), which would have led to the inhibition of Dox binding.

In another experiment the pH of water washed beads was decreased to 1.8, whilst the pH of Dox was unchanged at 3.8. This was to reveal whether the presence of acid rather than the removal of sodium was the result of the exothermic response. A similar amount of Dox was bound to the beads when the pH of Dox was 1.8 compared with the pH of Dox remaining unchanged, as the ratio was 0.94:1 this indicates that the results are not the effect of an acid-base titration. On the other hand, the baseline drifted from ~0 to ~15 µcal/sec in the raw data profile producing unreliable thermodynamic parameters and suspected isotherm imperfections. Less binding was observed in the experiment where the cell was filled with water washed beads and pH 1.8 deionised water, the ratio was reduced to 0.72:1 showing that the presence of HCl may have removed some but not all the ions from the beads, and therefore the results were not the cause of acid but the insufficient removal of ions demonstrated in Figure 3.15.

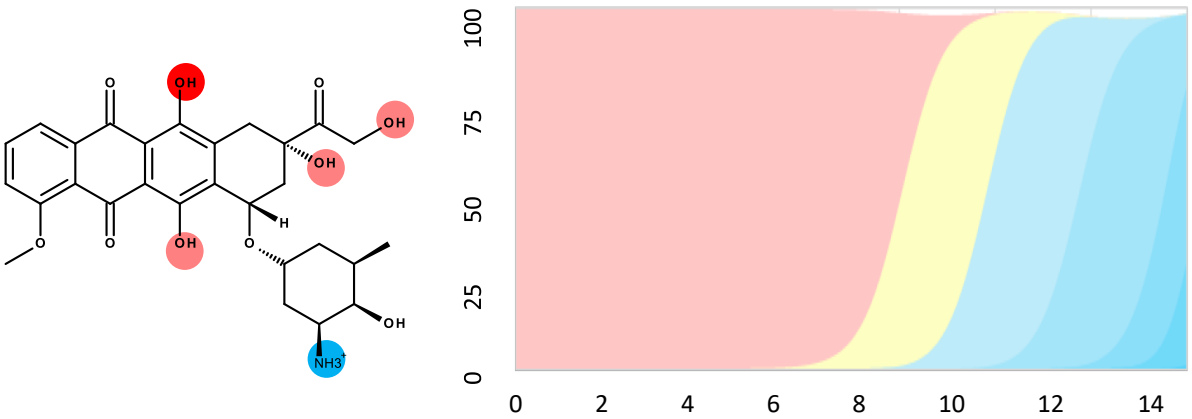

Figure 3.14: Structure and pKa groups of Dox (left) and plot of net charge versus pH (right) [14].

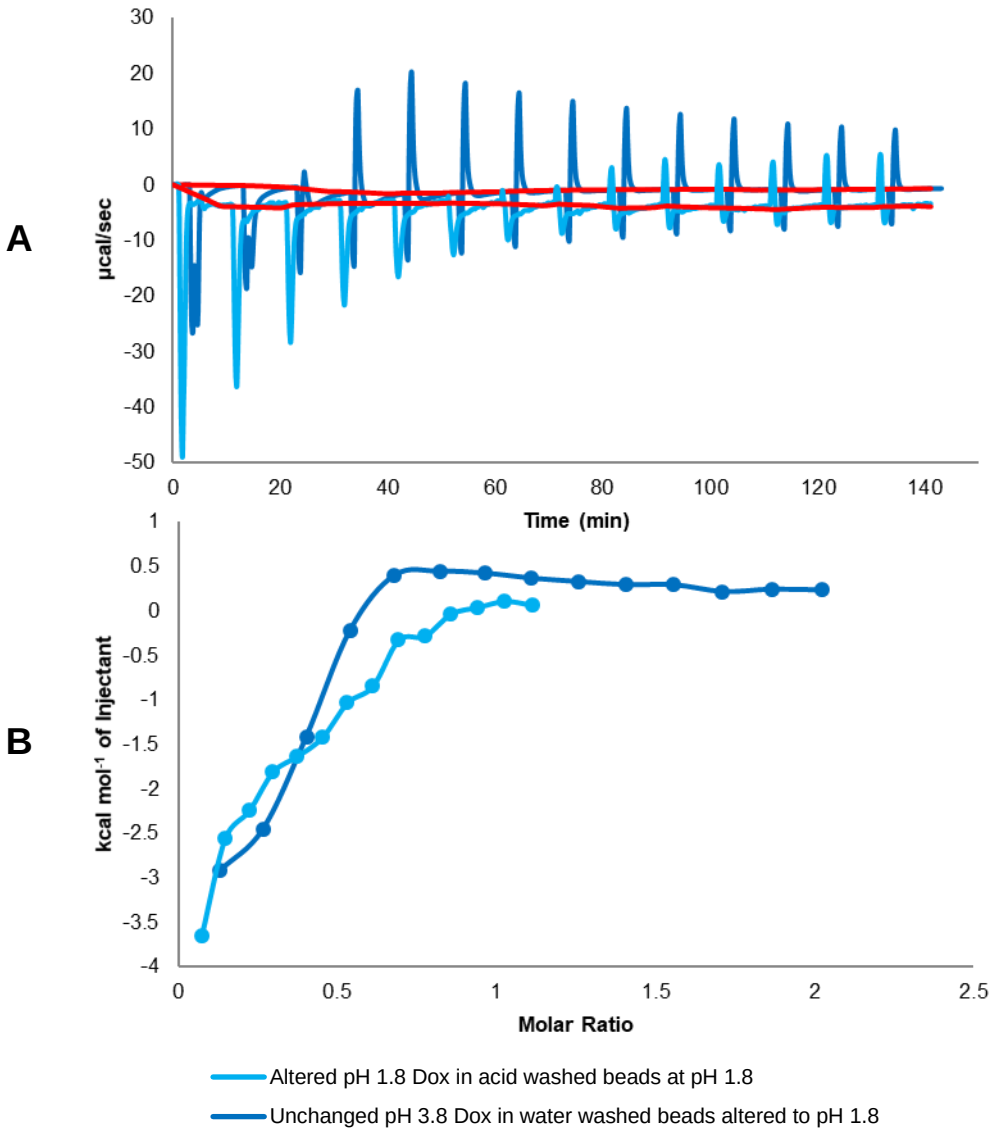

Figure 3.15: 43 mM Dox unchanged pH (3.8) into 100 mg water washed beads altered to pH 1.8, and 43 mM Dox adjusted to pH 1.8 into unchanged pH (1.8) 100 mg acid washed beads (sample number = 1, time has been adjusted by two minutes so the details of each trace can be identified).

The binding constant displayed in Table 3.10 is much smaller in the sample where the pH of Dox had been altered to 1.8 with acid washed beads which innately had a pH of 3.8, in comparison to the pH 3.8 Dox with water washed beads altered to pH 1.8. Combined with Table 3.9 the data revealed that the binding constant was reduced in the presence of a lower pH, however binding was weaker with acid washed beads, thought to be a consequence of the extended binding event observed in the water washed samples and does not reflect the fact that acid washed beads are available for binding.

Table 3.10: Binding constant of Dox to AMPS at different pH values (sample number = 1).

Drug and Bead Preparation	*K* (M^{-1})
Altered pH 1.8 Dox into acid washed beads at pH 1.8	8.62×10^{2}
pH 3.8 Dox into water washed beads altered to pH 1.8	1.74×10^{4}

Thermodynamic data of Dox at pH 3.8 into water washed beads at pH 1.8 and of Dox at pH 1.8 into acid washed beads at pH 1.8 is expressed in Figure 3.16. The change in enthalpy was similar at both pH's and a negative value stipulates an exothermic reaction. A negative entropy change with pH 1.8 Dox indicates that the disorder of a system decreases as the reaction develops, a positive entropy change with pH 3.8 Dox illustrates the system has a more disorder spontaneous state. The change in Gibbs free energy with Dox at pH 1.8 is a positive value implying a non-spontaneous process in the forward direction and with Dox at pH 3.8 is a negative value implying a spontaneous event in the forward route.

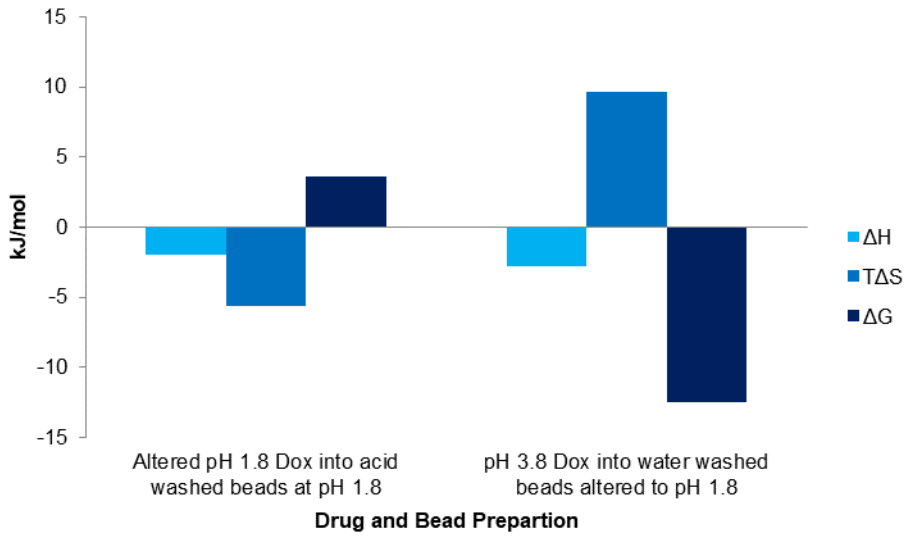

Figure 3.16: Thermodynamics of Dox to AMPS binding with Dox at different pH values (sample number = 1).

The experiment conducted with Dox at pH 3.8 had a negative ΔH, positive ΔS and negative ΔG, thus the process is spontaneous at all temperatures. The experiment conducted with Dox at pH 1.8 was also spontaneous, but only at low temperatures as ΔH and ΔS were both negative whilst ΔG was positive. Dox at pH 3.8 exhibits good hydrogen bonding with unfavourable conformational change. The Dox at pH 3.8 experiment is both entropically and enthalpically driven, whereas Dox at pH 1.8 is entropically

unfavourable. This means the reaction is not spontaneous and therefore cannot occur, it is possible that a shift in the baseline caused by the pH being too far away from neutral has produced unreliable results.

3.2.4. Effect of Concentration

Signal size is partially related to concentration and can be modified to some extent by varying the volume and concentration per injection. Based on initial experiments it was difficult to identify measurable signals using 14 injections with each injection 20 µL of 10 mM and 43 mM Dox into water washed beads. However, upon reducing this to 2 injections of 10, 20, 30 and 43 mM Dox where each injection was 140 µL, this produced signals above the equipment detection limit. The number of beads in the experiment was designed to form an exothermic and endothermic peak as expressed in Figure 3.17. An increase in signal strength was discovered as the concentration increased. The first injection generated two exothermic peaks, which can clearly be identified in the raw data. The first interaction shoulders a second, once Dox-water has been subtracted from Dox-beads. This indicates two binding events that could be attributed to either Dox diffusing through the bead, the collapsing of the PVA structure preventing some Dox from internal binding or the distance between Dox-Dox groups changing as bead stiffness and compressibility transform. Gonzales defined two distinctive densities of matter concentrated around the external and the internal structure of the bead using a scanning electron microscope (SEM), and the microscopic image is illustrated in Figure 3.18 [3]. The first peak could be Dox binding to the denser more crosslinked outer structure, Dox then diffuses through the concentrated layer of SO_3^- and a second peak occurs as Dox then binds to the inner less dense less crosslinked matter. As the outer layer is more crosslinked the binding event would be more intense than the second. The endothermic peak in the raw data is the interaction of Dox with water.

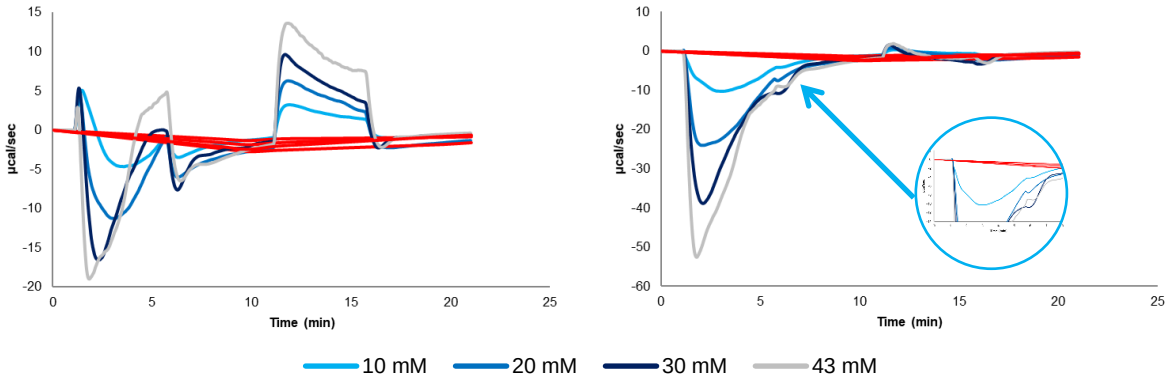

Figure 3.17: Raw ITC data (left) and subtracted ITC trace (right) of 2 injections of 10, 20, 30 and 43 mM Dox into a respective mass of 15, 30, 40 and 60 mg water washed beads, where each injection was 140 µL to obtain one exothermic and one endothermic response, inset is a rescaled graph of the shouldering peak (sample number = 1).

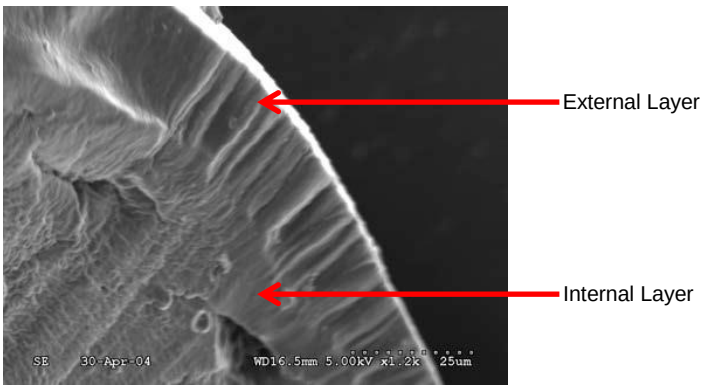

Figure 3.18: SEM image displaying the internal and external structure of a bead [3].

An investigation was then conducted where the injection number was increased with 10 mM Dox to discover the concentration required to create visible binding. Dox binding was present in Figure 3.19 with 2 injections of 140 µL of 10 mM Dox, 4 injections of 70 µL 10 mM Dox and 7 injections of 40 µL 10 mM Dox. Significantly less binding was observed with 14 injections of 20 µL 10 mM Dox, and so 40 µL of 10 mM Dox was required for binding without acid washing to protonate the beads. As analysis requires 10 – 15 injections to define a binding isotherm the molar ratios calculated in Table 3.11 are estimations, however it seems that with higher concentrations of drug there is more competition of binding.

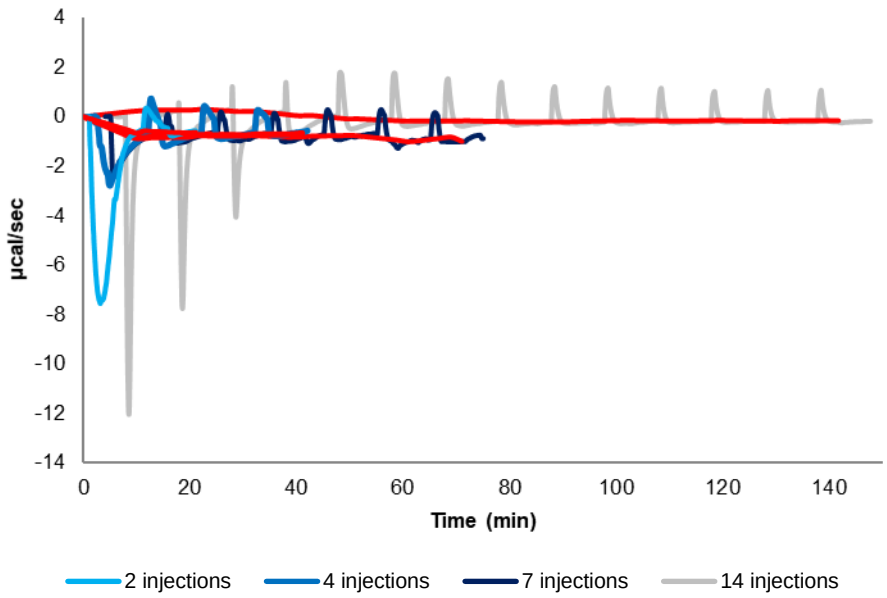

Figure 3.19: 2, 4, 7 and 14 injections of 10 mM Dox into water washed beads (sample number = 1, time has been adjusted by the addition of two minutes per injection profile so the details of each trace is displayed).

Table 3.11: Estimated molar ratios of 2, 4, 7 and 14 injections of 10 mM Dox into water washed beads (sample number = 1).

Number of Injections in Experiment	Injection Volume (µL)	Injection Number at Point of Bead Saturation	Molar Ratio
2	140	1	0.88:1
4	70	2	0.90:1
7	40	5	0.88:1
14	20	6	0.21:1

As Dox was injected into the beads two effects were seen; initially Dox interacted with water breaking Dox-Dox bonds (an endothermic event), Dox then immediately bound to beads and bonds were formed (an exothermic event). As the experiment continued and more Dox was bound to the beads the time taken for the signal to reach the baseline increased. This could be due to Dox requiring time to diffuse through the bead when surface binding sites are occupied. The endothermic signal increased during the experiment as the exothermic signals decreased, this might also be due to the occupation of beads sites. Eventually, as beads become saturated during the experiment only the effects of Dox interacting with water can be seen through endothermic signals, here the change in enthalpy decreased and this point was used for the calculation of Dox bound to beads. If this wasn't seen within the 14 injections of the experiment the syringe was reloaded and the experiment was started again with the same sample

in the cell until saturation of the beads occurred. The interaction of Dox-water was subtracted from Dox-beads, the interaction of water-beads was negligible and so was not required in the subtraction equation.

In Figure 3.20 with an increase in beads from 25 to 50 and 100 mg a similar ratio was calculated, but larger heat signals were detected because there were more beads for the drug to interact with. Four titrations of 10 mM Dox were required for saturation of 100 mg beads, two titrations of 10 mM Dox for 50 mg beads and one titration of 10 mM Dox for 25 mg beads. Where each titration was fit together the adjoining connection was visible, this could be due to experiments situated in the cell for an extensive period of time before another titration was initialised, the impact of which is not fully understood.

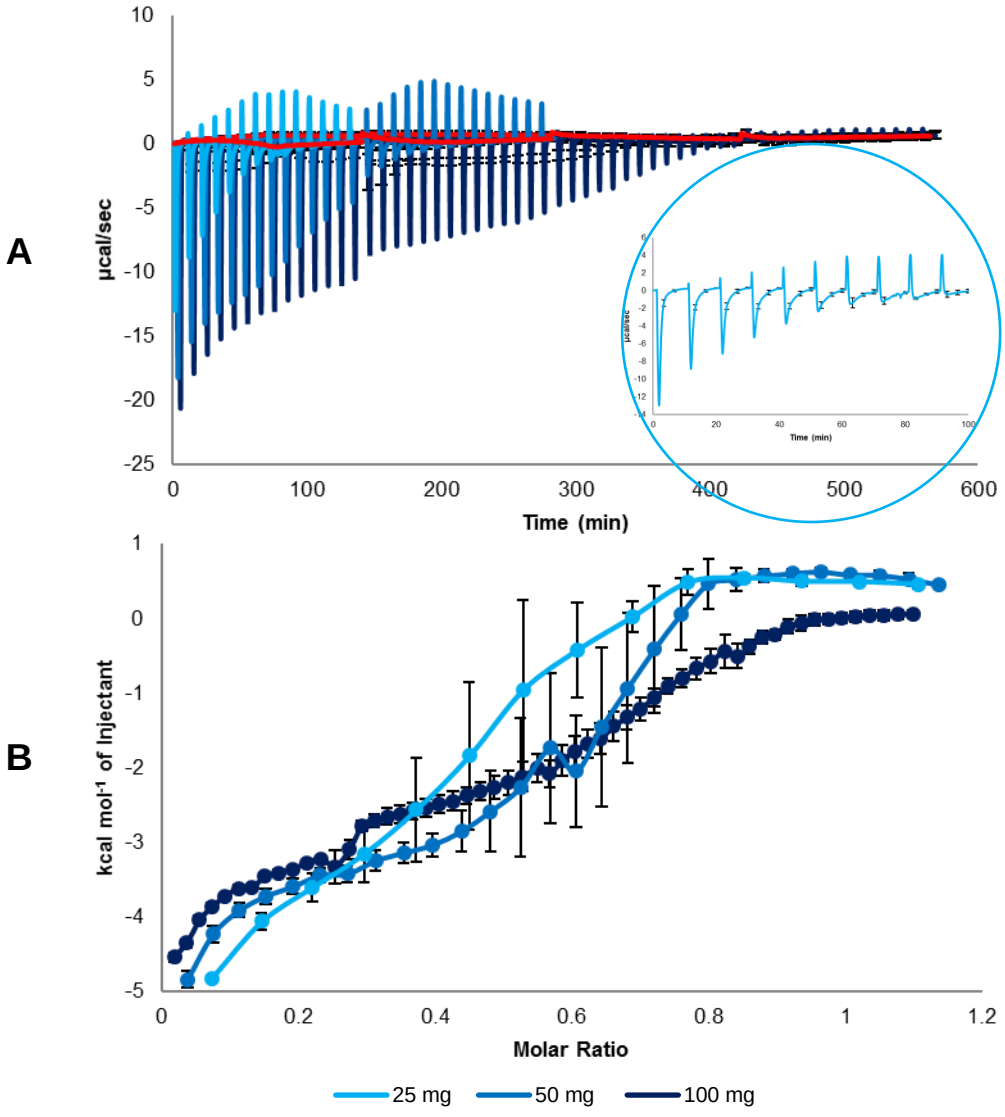

Figure 3.20: 10 mM Dox to 25, 50 and 100 mg beads with inset graph of 25 mg exposing the time taken for each injection to return to the baseline (sample number = 3, error bars = standard deviation, time has been adjusted by the addition of two minutes per mass profile so the details of each trace is displayed).

Although the ratio of Dox bound to AMPS increased with mass of beads in Figure 3.21, an increase in bead mass most likely improved the reproducibility of the experiment. Some beads were lost outside the sample cell and mass variation will contribute a larger error with a smaller number of beads, therefore 100 mg was a preferred bead mass rather than 25 mg. An average calculated resultant ratio of 0.86:1 is similar to the value of 0.836:1 reported by Gonzales using UV-Vis, however the standard deviation of 0.09 was much smaller than the previous work of 0.377.

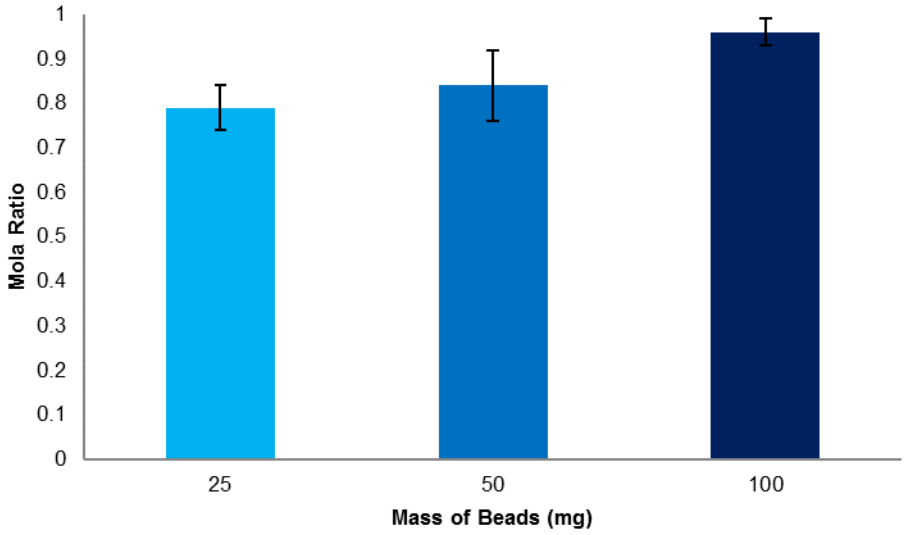

Figure 3.21: Molar ratio of Dox to AMPS with 10 mM Dox and 25, 50 and 100 mg beads (sample number = 3, error bars = standard deviation).

The average binding constant of 10 mM Dox into 25, 50 and 100 mg beads was 1.62 x 10^4, and the data exhibited in Table 3.12 exposes no correlation between bead mass and binding affinity.

Table 3.12: Binding constant of Dox to AMPS with 10 mM Dox and 25, 50 and 100 mg beads (sample number = 3, error = standard deviation).

Bead Mass (mg)	***K* (x 10^4 M^{-1})**
25	2.53 ± 1.63
50	1.27 ± 0.13
100	1.07 ± 0.76

All integers for enthalpy change were negative and increased with bead mass, yet there are only three data points therefore more experimental data is required to verify this statement. Entropy change also increased with bead mass and a positive change in entropy shows that the reaction was spontaneous in the forward direction. Yet again, with three data points and larger error bars more data requires collection to verify this statement. The change in free energy was negative and implies a spontaneous system, the data infers no relationship with bead mass. Thermodynamic data for bead mass is expressed in Figure 3.22 and demonstrates that ΔH is negative, ΔS positive and ΔG negative in all bead masses, consequently the reaction is always spontaneous regardless of the systems temperature. All reactions were enthalpically and entropically driven, which includes hydrogen bonding, electrostatic, van der Waals and hydrophobic interactions resulting in conformational changes.

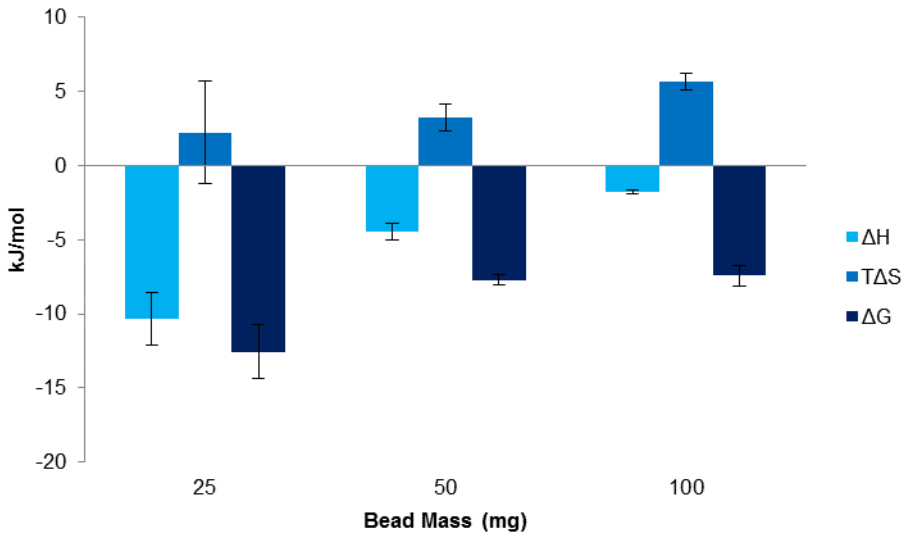

Figure 3.22: Thermodynamics of 10 mM Dox to 25, 50 and 100 mg beads (sample number = 3, error bars = standard deviation).

With higher concentrations of Dox such as 30 and 43 mM, two exothermic effects were recognised with one injection. With a more concentrated solution there was a large, sharp and rapid exothermic signal with a shallower, broader exothermic signal. The first exothermic signal is thought to be Dox binding to the surface of the bead, the second exothermic signal is then thought to be Dox penetrating the internal sites which was a much slower and less intense binding process. The break between these two signals is the time taken for the drug to diffuse through the hydrogel. As the experiment continued the two exothermic signals merged as there were less surface groups. Ultimately, the experiment developed in

a similar manner to the previously described test such as 10 and 20 mM Dox, with decreasing exothermic signals and emerging endothermic signals.

With an increase in Dox from 10 to 20, 30 and 43 mM in Figure 3.23 a similar ratio was calculated, but larger heat signals were detected with an increase in concentration because there were more Dox molecules for the beads to interact with. Most binding isotherms are sigmoidal, however the trace for Dox into beads has a rapid uptake in the initial section of the curve. One explanation could be the structure of the bead and how the surface differs from the internal segment. As the external layer is more crosslinked Dox would bind more tightly, with greater energy and would encounter this primarily. As this section becomes more saturated Dox binds to the less crosslinked internal layer with less energy.

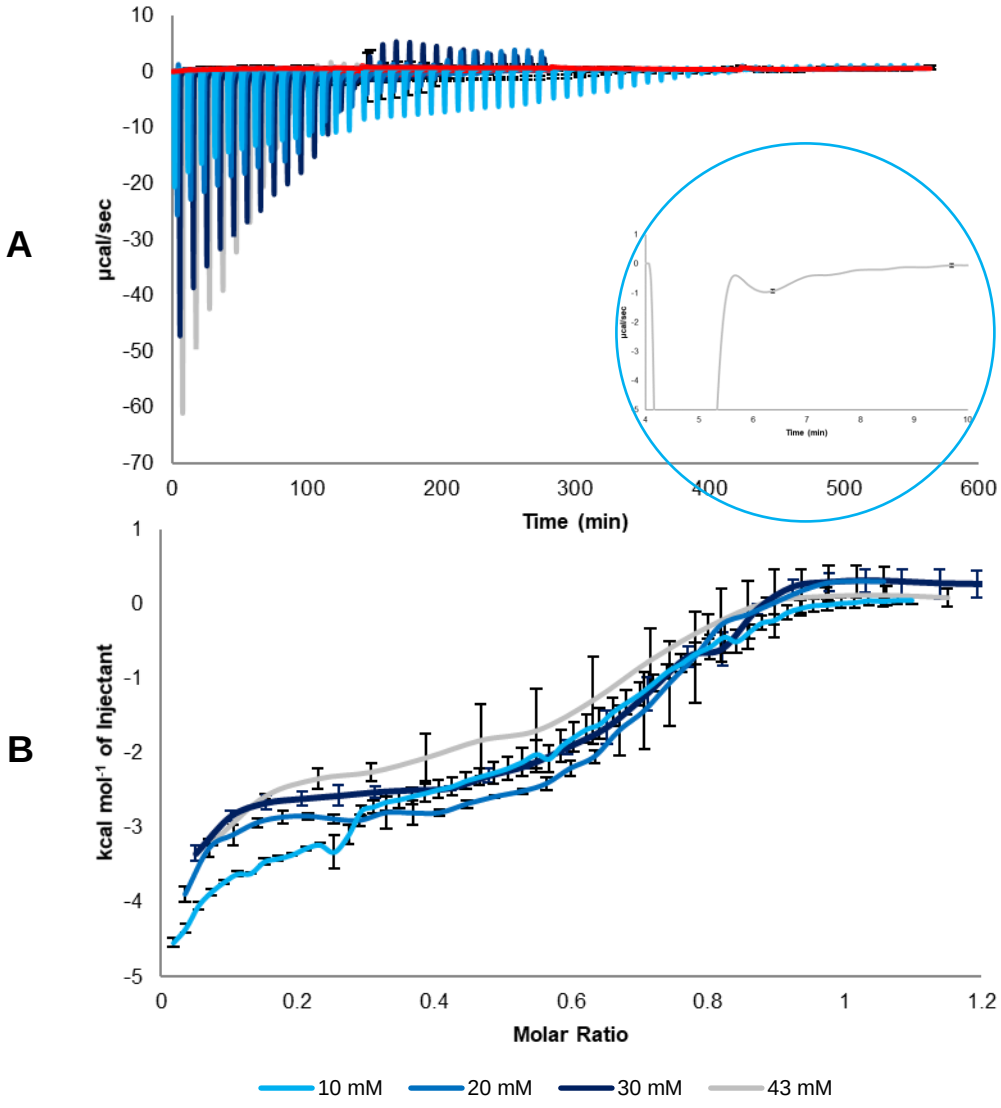

Figure 3.23: 10, 20, 30 and 43 mM Dox to 100 mg beads with inset graph of the first injection at 43mM (sample number = 3, error bars = standard deviation, time has been adjusted by the addition of two minutes per concentration profile so the details of each trace is displayed).

The average molar ratio for Dox at different concentrations was slightly higher than beads at different masses, with an average ratio of 0.94:1 ± 0.06 exhibited in Figure 3.24. Nevertheless, the difference by conventional criteria is not considered statistically significant (p = 0.0911), and the data suggests no relationship between molar ratio and drug concentration.

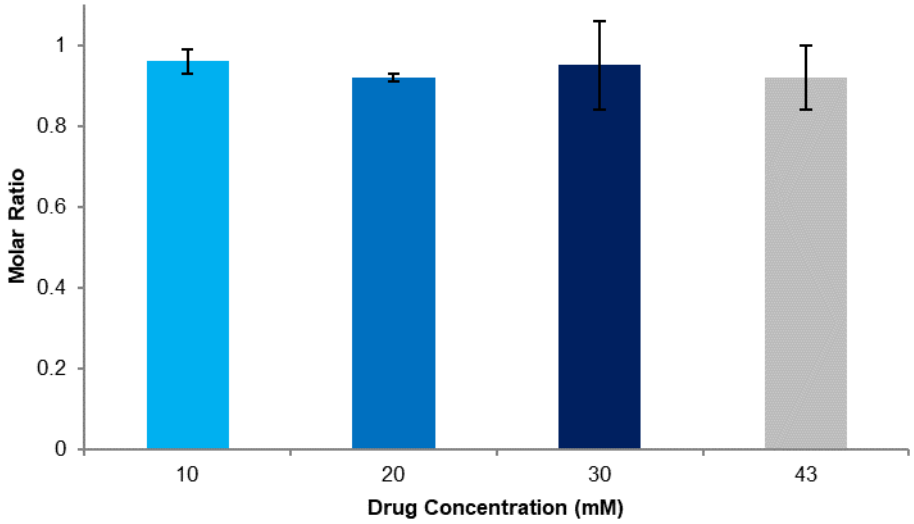

Figure 3.24: Molar ratio of Dox to AMPS with 100 mg beads and 10, 20, 30 and 43 mM Dox (sample number = 3, error bars = standard deviation).

Table 3.13 presents the average binding constant of 10, 20, 30 and 43 mM Dox into 100 mg beads which was 8.17 x 10^3, and indicates no correlation between drug concentration and binding strength.

Table 3.13: Binding constant of Dox to AMPS with 100 mg beads and 10, 20, 30 and 43 mM Dox (sample number = 3, error = standard deviation).

Drug Concentration (mg)	***K* (x 10^4 M^{-1})**
10	1.07 ± 0.76
20	0.49 ± 0.24
30	0.87 ± 0.14
43	0.84 ± 0.51

The values for enthalpy change were negative and so binding was exothermic. The data insinuates that the change in enthalpy increased with concentration of drug, however more data is required to validate

this statement. A positive change in entropy infers a spontaneous reaction as the experiment proceeds. The calculated change in entropy also increased as the concentration of drug increases, nevertheless the error bars at 43 mM are rather large and need further investigation. The values for changes in Gibbs free energy were negative and decreased as the concentration of drug increased, but again the errors bars of 43 mM were particularly large in comparison with other values for this assumption. Like the data for bead mass Figure 3.25 reveals ΔH is negative, ΔS is positive and ΔG is negative, the experiments studied were therefore spontaneous at both low and high temperatures. At each drug concentration the reactions were enthalpically and entropically driven, which includes hydrogen bonding, electrostatic, van der Waals and hydrophobic interactions resulting in conformational changes.

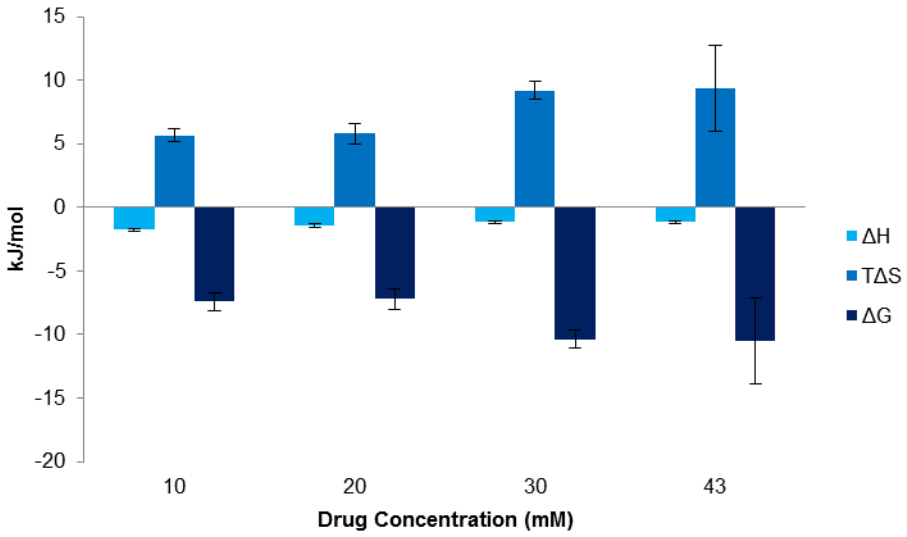

Figure 3.25: Thermodynamics of 10, 20, 30 and 43 mM Dox to 100 mg beads (sample number = 3, error bars = standard deviation).

Illustrated in Figure 3.26 is enthalpy change of experiments performed with Dox titrated into water examined against concentration to determine how precise and accurate results were gathered for subtraction from Dox into beads. R^2 was 0.98 and so it was decided that a sample number of 1 was an acceptable collection of data. It is worth noting that 10 mM Dox into water includes four titrations of 280 µL, 20 mM and 30 mM include two titrations of 280 µL and 43 mM includes one titration of 280 µL. Change in enthalpy decreases with an increase in drug concentration because Dox aggregates depending upon the concentration, which in-turn alters the thermodynamic processes. Aggregation

occurs to a greater extent at higher concentrations allowing Dox-Dox bonds to be broken and then formed, which is limited at the lower concentrations.

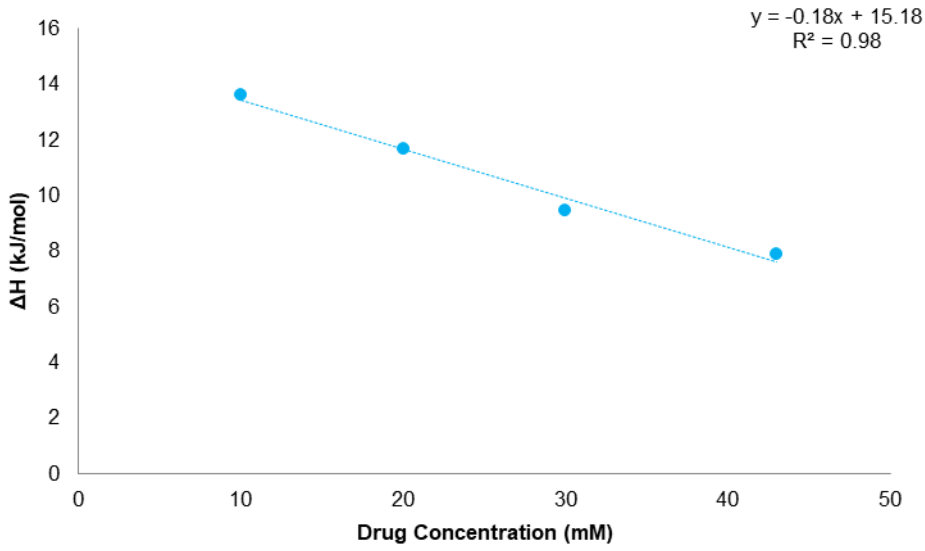

Figure 3.26: Enthalpy of Dox to water at selected concentrations of 10, 20, 30 and 43 mM (sample number = 1).

3.2.5. Effect of Volume and Number of Injections

With an increase in the volume of each injection the number of injections must decrease, as the syringe has a set capacity. Decreasing the number of injections decreases the accuracy, as the drug-bead ratio can only be accurate to one injection. In other words, one more or one less injection when the total number of injections is reduced has a much larger effect on the binding ratio. With an increase in the number of injection there is less change in DP between injections and so a greater error incurs due to the inability to pin point the number of injection required to saturate the beads. To maintain experimental success there was a decrease in the amount of beads loaded into the sample cell when the volume of injection decreased, this could contribute to the difficulty in determining the saturation point and the error associated with a small sample. Malvern Instruments Inc (the manufacturer of the ITC), recommends that for reproducible results the total number of injections should be 10 – 15 to define a binding isotherm. An injection volume generally of 3 – 15 µL is required to ensure high volumetric accuracy, signals above the sensitivity of the VP-ITC which is 0.1 µcal/sec but preferably heat of at least 3 – 5 µcal/sec absorbed or evolved for precise measurements and a *c* value between 5 – 500 for ideal measurements of *K* [5].

Since the time between injections could not be adjusted from 600 seconds to allow the signal to retrieve back to the baseline, a 2 injection experiment takes 20 minutes to complete, whereas a 290 injection experiment requires at least 48 hours 20 minutes, as illustrated in Figures 3.27 and 3.28, respectively. It was therefore possible to finish three experiments in one working day, including cleaning, preparation and equilibration time, hence for practical feasibility 14 injections were chosen as the appropriate length of study. To improve the accuracy of the test experiments could have been increased to 29 injections, which would have taken 4 hours 40 minutes for the run to terminate.

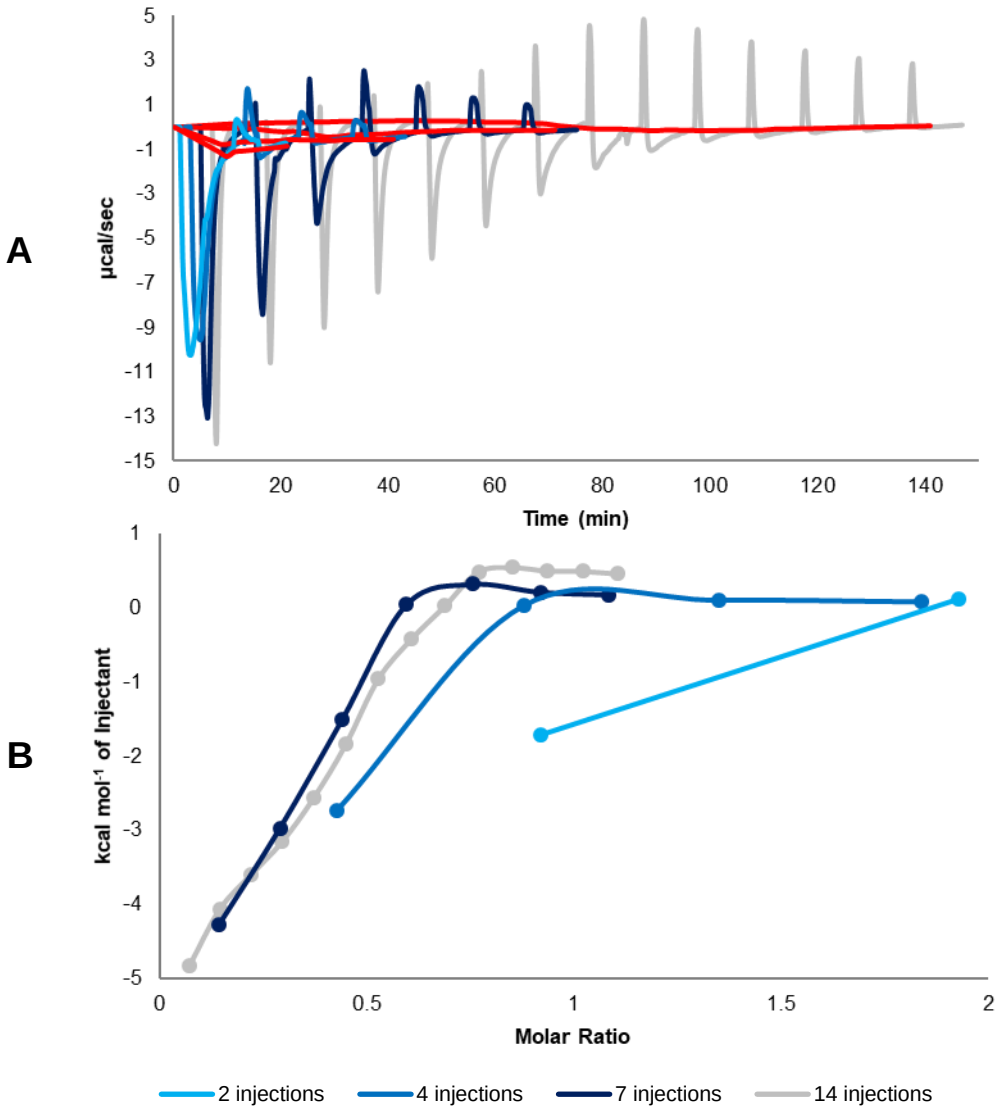

Figure 3.27: 10 mM Dox to 25 mg beads with 2, 4, 7 and 14 injection binding isotherm (sample number = 1, time has been adjusted by the addition of two minutes per injection profile so the details of each trace is displayed).

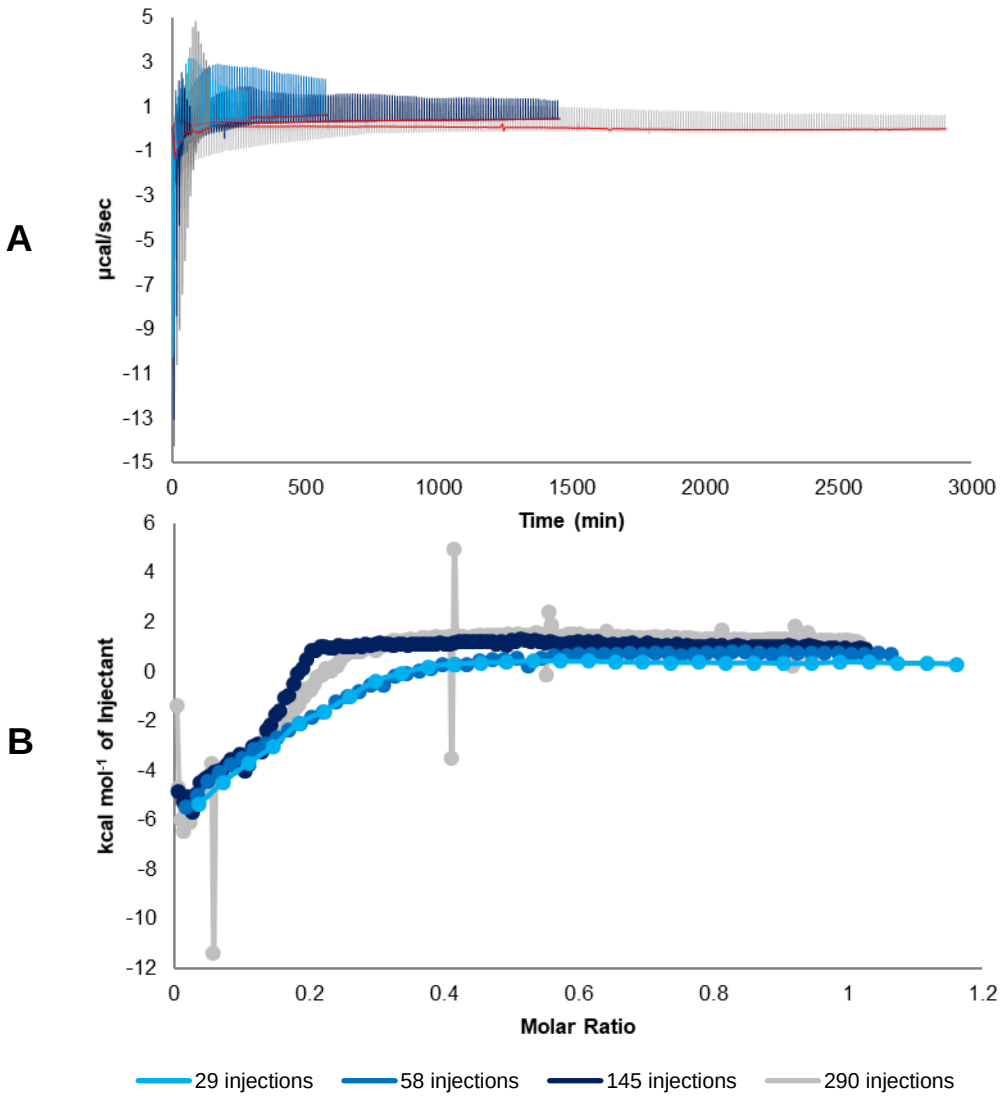

Figure 3.28: 10 mM Dox to 25 mg beads with 29, 58, 145 and 290 injection binding isotherm (sample number = 1, time has been adjusted by the addition of two minutes per injection profile so the details of each trace is displayed).

The data in Table 3.14 confirms that an injection volume of 1 and 2 µL is an inappropriate use of the instrument. An early 7 injection experiment gave a ratio 1.26:1 (data not shown) proving that too few injections runs a risk of over or under shooting the ratio by a large amount, as the ratio can only be accurate to one injection. A suitable number of injections was found to be between 14 and 58.

Table 3.14: Molar ratio of 10 mM Dox to 25 mg beads with different numbers of injections (sample number = 1).

Number of Injections	Injection Volume (µL)	Ratio of Dox to AMPS	Experimental Time
2	140	0.88:1	20 min
4	70	0.84:1	40 min
7	40	0.71:1	1 h 10 min
14	20	0.79:1	2 h 20 min
29	10	0.73:1	4 h 50 min
58	5	0.83:1	9 h 40 min
145	2	0.49:1	24 h 10 min
290	1	0.60:1	48 h 20 min

Table 3.15 lists calculated *c* values, this number determines the shape of the binding isotherm using Equation 3.4, where *K* is the binding constant, M_{tot} is the total macromolecule concentration and *n* is stoichiometry. An ideal *c* value for measuring *K* is between 5 and 500 [5]. This means anything above 7 injections provided an adequate *c*, however in 145 and 290 injections there were a number of imperfections, and it was difficult to determine the point of bead saturation. As the manual for this equipment suggests, this many injections cannot be recommended. The volume in 2 – 7 injections was too large, and so over saturation and under saturation was common (data not shown). As stated in the manual a preference would be to set the instrument parameters with 5 – 20 µL of reactant per injection, which allows for 14 – 58 injections with a one syringe loaded test.

Equation 3.4: Calculation of *c*, where *c* is the shape of the binding isotherm, *K* is the binding constant, M_{tot} is the total macromolecule concentration and *n* is stoichiometry.

$$c = K M_{tot} n$$

Table 3.15: *c* values of 10 mM Dox to 25 mg beads with different numbers of injections (sample number = 1).

Number of Injections	*C*
2	43736
4	8034
7	49
14	59
29	39
58	26
145	130
290	46

3.2.6. Saturation, Aggregation and Limit of Detection (LOD) Study

Origin® software identifies the midpoint of the sigmoidal ITC trace as *n*, this is used by many in literature at the molar ratio, as these reactions are reversible it would be correct to use the point of equilibrium. However, the reactions in this study were not reversible without intervention, i.e. the addition of salt occurring naturally in blood elutes drug from the bead. It is for this reason the point where the change in enthalpy decreased was believed to be where Dox interacted with water after beads were fully loaded.

To check whether this was indeed the case a standard experiment was conducted of 43 mM Dox into 100 mg DC Beads™. A deviation was made whereby the experiment was discontinued midway on the 7th 20 µL injection, where the Origin® molar ratio was around 0.55 (close to the point where the software stated was equal to *n*), indicated by an example ITC trace in the red boxed sections of Figure 3.29. The residual solution, as well as beads were collected from the ITC sample cell. Dox was then extracted from the sample with a 20 % (w/v) potassium chloride (KCl) solution into 50:50 (v/v) ethanol (see Chapter 2 for extraction solution preparation). Standard samples, the ITC residual solution and extracted sample were analysed on the UV-Vis spectrophotometer.

The amount of Dox calculated to have entered the cell and expected to be in the beads was 3.5 mg/mL. The amount of Dox extracted from the beads was 3.2124 mg/mL and the amount in the residual solution was 0.0101 mg/mL, which equates to 92 % of the titrated solution. 8 % could have been lost during removal of the sample from the ITC or bound to the ITC cell. The amount of Dox was equivalent to 5.54 mM into 11.30 mM AMPS, a ratio of 0.49:1. Therefore, the software calculation of *n* at ~0.55 (the midpoint of the sigmoidal curve) was not the point of bead saturation as would be expected for an

equilibrium reaction. The endpoint was then much further on and since the absorbance matched close to the expected value of 0.53:1 when the concentration of Dox titrated into the cell should have been 6.03 mM into 11.30 mM AMPS, this confirmed that the top of the sigmoidal curve (and not the middle) is the saturation point closer to the expected 1:1 ratio.

A report found that dimers were formed at 0.1 mg/mL in Dox solution and 1.0 mg/mL in Dox loaded beads [15,16], the studies in this document contained Dox at concentrations of 58 – 580 mg/mL. Therefore, these concentrations of Dox in aqueous solution will self-associate to form aggregate structures of dimers and trimer though π-π hydrophobic stacking of the dihydroxyanthraquinone ring.

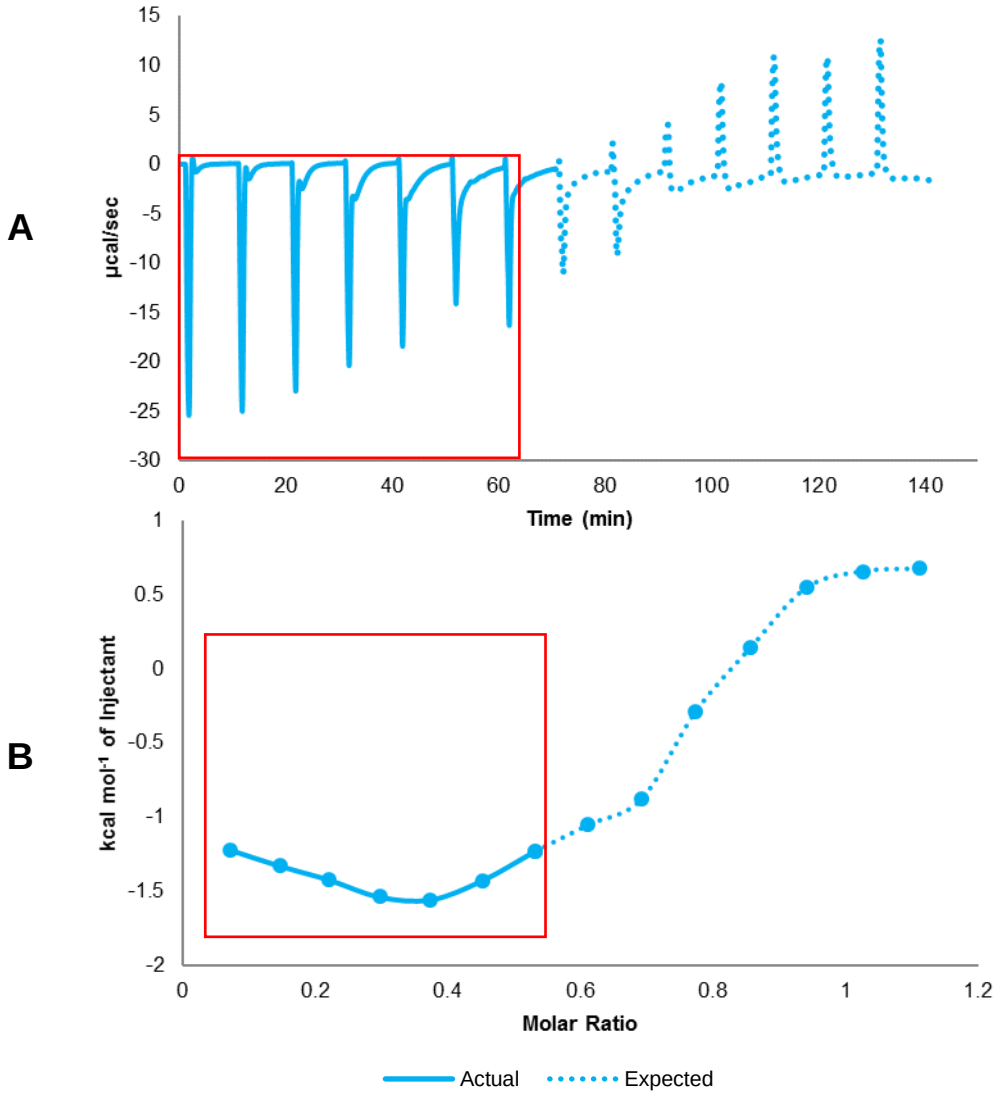

Figure 3.29: Saturation test to determine the concentration of Dox at midpoint of experiment (sample number = 1).

It is well known that Dox aggregates [16], a test for confirmation was conducted where water was titrated into 43 mM Dox. Figure 3.30 is a clear example of a non-constant monotonously decreasing heat of dilution without sigmoidal behaviour, suggesting Dox self-association in this solution. The absence of sigmoidal behaviour suggests Dox does not self-associate cooperatively.

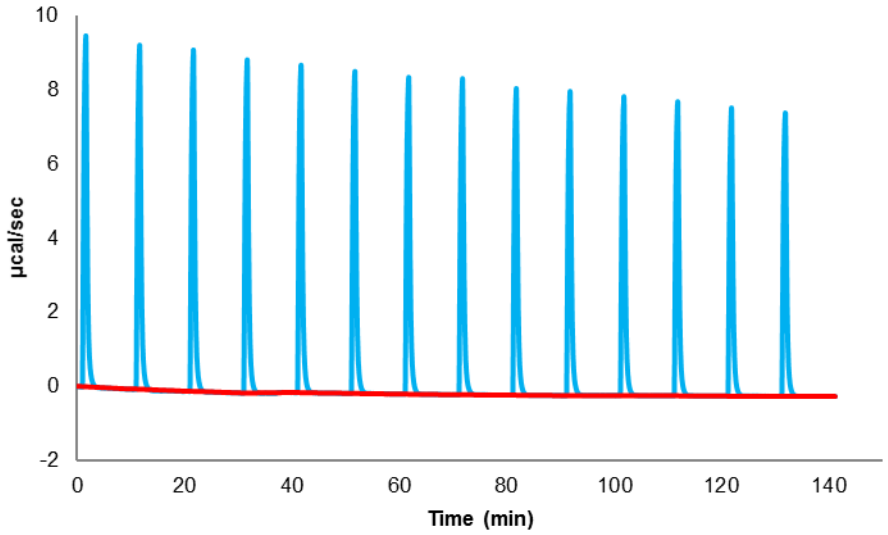

Figure 3.30: Aggregation test to determine the formation of Dox (sample number = 1).

In Figure 3.31 1 µL of 10 mM Dox into the ITC cell initially produced a signal intensity of ~0.19 µcal/cec, the first injection is not included as this can be inaccurate especially as such low concentrations. The ITC LOD is known to be 0.1 µcal/sec, so 1 µL of 10 mM Dox is close to this limit. As the cell contained 1.4194 mL deionised water and the mass of Dox in one injection is known to be 0.58 µg, the concentration in the cell was 704.41 nM. The amount of Dox could be further reduced to reach 0.1 µcal/sec, but this experiment does show that any interaction of 0.58 µg Dox should be visible. However, Dox signals decrease due to aggregation and this should be considered when working at such low concentrations. This information will prove useful when analysing the interactions with different types of drugs.

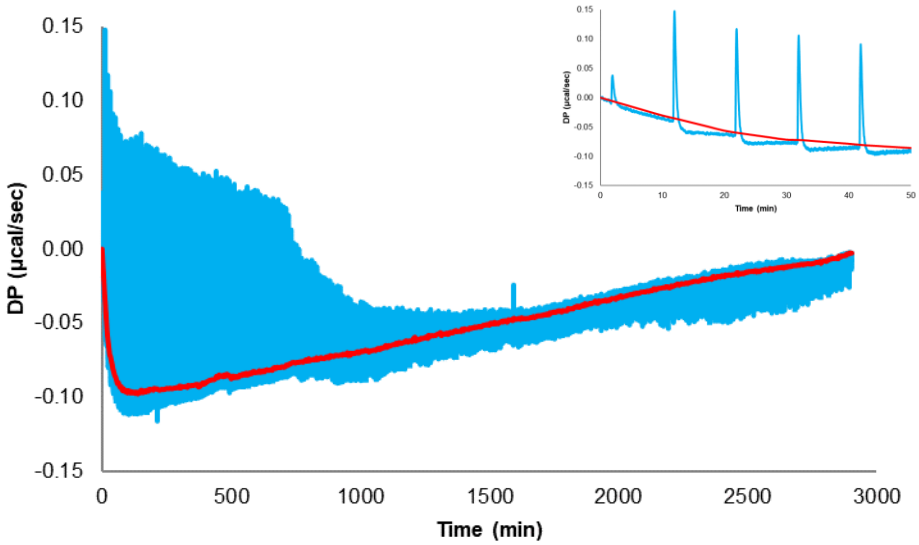

Figure 3.31: 1 mM Dox into deionised water with 290 injections and each injecton a volume of 1 µl, inset is a closer view of the first five injections (sample number = 1).

3.3. Conclusion

Although temperature didn't affect the binding ratio of Dox to beads it did affect the rate of reaction, which can be seen in each injection by the length of time taken for the reaction to complete. At higher temperatures there were a larger number of high energy collisions, as molecules move faster, collisions were more frequent and diffusion was quicker, which resulted in an increase in the rate of the reaction.

It was thought that the binding ratio of AMPS to Dox was 0.42:1 with a standard deviation of 0.02, however removing the sodium ions from the beads by washing them in 2 M HCl increased the binding to 0.90:1 and a standard deviation of 0.09, when both bead mass and drug concentration results were combined. As previously explained the packing solution of the DEBs must be removed before the mixture of chemotherapeutic agent is loaded, this packing solution contain sodium chloride and sodium ions interfere with drug-bead binding. Larger concentrations of drugs achieved saturation by adding the drug in one stage, such as those used when preparing the device for patient use. This could drive the Dox-bead binding interaction without the need of acid washing, which has been reported by Gonzales to be 0.836:1 [3]. Not only has the ITC method found the binding 0.90:1 to be slightly higher than previously reported, but the standard deviation was much lower at 0.09 compared with the UV method of 0.377 [3], showing that the new method is more precise and accurate in comparison with UV analysis.

Dox at pH 4 and water washed beads adjusted to pH 2 the stoichiometry decreased in comparison to acid washed beads, which confirmed that the response was not an acid-base titration and that the presence of acid does not create the results. Altering the pH of Dox to 2, which then matched the pH of acid washed beads, caused a drift in the baseline which started 15 µcal/sec higher than it was set and continued drifting during the run. A drift larger than 1 µcal/sec is not considered suitable fitting.

Once the binding ratio had been identified Origin software® was employed to calculate K, ΔH and ΔS, then from this calculate ΔG. Output values for n were not suitable for analysis, as the reactions in these instances without the presence of salt were not reversible. The software takes the midpoint of the reaction as equilibrium, but of interest in these circumstances was the endpoint, hence n was calculated manually. The data was analysed to determine the stoichiometry of the drug–polymer interaction and the highest molar ratio was reported with the beads washed in acid.

Spontaneity is related to enthalpy change, entropy change and change in free energy of binding associated with the interaction. In the experiments where residual Decon® was suspected to be present

the reaction was considered spontaneous at all temperatures, water washed beads were spontaneous only at low temperatures and acid washed beads were spontaneous at both low and high temperatures.

An increase in the molar ratio was expressed with an increase in bead mass, a correlation could be due to a small number of beads being lost as they were placed into the sample cell. With a small sample the percentage of beads lost outside of the sample port would be greater than a larger sample. The binding interaction was independent of concentration. 10 mM Dox to 25 mg beads and 43 mM Dox to 100 mg beads were preferred, as saturation occurred in one experiment without the syringe being re-filled for additional titrations. The binding constant appeared independent of temperature, bead mass and drug concentration. The change in enthalpy decreased with temperature, alternatively it increased with both bead mass and drug concentration. While a conclusive statement cannot be made as, this does indicate that temperature, mass and concentration could affect enthalpy, yet this needs additional work as the sample number was small. An increase in the change in enthalpy during temperature could be connected to an increase in endothermic signals in the reaction of Dox to water. As temperature increased and more heat was absorbed into the system, the drug into bead reaction consequently became more exothermic. Correspondingly, in the mass and concentration experiments the Dox to water interaction became less endothermic and so the exothermic signals of Dox to bead became more endothermic. The change in entropy was also an independent variable for the temperature, whereas for beads mass and drug concentration although some relationship was possible, when the data was gathered together large error bars prevented stating that the change in entropy increased by the increase of either of these variables. Any increase in entropy change with an increase in mass and concentration could be attributed to an increase in the number of molecules in the system. The energy available in the system to do useful work seems an independent variable in the temperature study and in bead mass, though for an increase in drug concentration there was a decline in the Gibbs free energy change, nonetheless this could be due to large error bars in one of the data points. Although often conducted, technically three data points are not enough for an exact calculation standard deviation, replicating some of this work would remedy these queries.

At least 14 injections, each 20 µL, were found mandatory to provide accurate data. Less injections would require an increase in volume to saturate the beads and this would dramatically shift the ratio. More injections than 58 would decrease the volume and in-turn decrease the signal size,

forcing the change in exothermic to endothermic peaks to be much more difficult to discover, and consequently rendering the bead saturation point and hence the ratio more inaccurate.

Saturation is usually the midpoint of the experiment, however analysis of drug concentration using UV-Vis at the midpoint following collection from the ITC and extraction of the drug found that the endpoint is much later, as only half the concentration of drug had loaded. This is a consequence of the reaction being irreversible under the experimental conditions. At the experimental concentrations Dox forms aggregates, which explains the endothermic interaction and the decrease heat signals, as the drug is supplemented into the cell as Dox-Dox bonds are broken. A mass of 0.58 µg Dox from 1 µL of a 1 mM solution titrated into the ITC cell was just over the instruments LOD. interactions between concentrations much lower than conducted in the LOD experiment maybe not be detected, and the decrease in DP as the experiment progresses during Dox dilution must also be considered. 1µL of 1 mM Dox might be treated as an exploration into the limit of the method.

In summary, there are multiple methods which provide the binding characteristics of drug to bead, this study describes a preferred method where a higher binding potential was achieved with acid washed beads. This study paves the way for further research into DEBs.

References

1 L. J. Waters, T. Hussain and G. M. B. Parkes, Titration calorimetry of surfactant–drug interactions: Micelle formation and saturation studies, *J. Chem. Thermodyn.*, 2012, **53**, 36–41.

2 University of Oxford, ITC Data Analysis in Origin®, https://www.bioch.ox.ac.uk/aspsite/services/equipmentbooking/biophysics/ITC_data_analysis.pdf, (accessed 1 June 2014).

3 M. V. G. Fajardo, University of Brighton, 2006.

4 BTG, Loading of DC Bead™ using Doxorubicin Solution in syringe, http://bead.btg-im.com/uploads/document_r/DCB(R) Dox Solution in syringe_EC10-160 v2.pdf, (accessed 1 June 2014).

5 MicroCalorimeter User's Manual, VP-ITC MicroCal, http://www.biophysics.bioc.cam.ac.uk/files/ITC_VPITC_user_manual.pdf, (accessed 1 October 2017).

6 L. J. Waters, T. S. Swaine and A. L. Lewis, A calorimetric investigation of doxorubicin–polymer bead interactions, *Int. J. Pharm.*, 2015, **493**, 129–133.

7 A. L. Lewis, M. V. Gonzalez, S. W. Leppard, J. E. Brown, P. W. Stratford, G. J. Phillips and A. W. Lloyd, Doxorubicin eluting beads − 1: Effects of drug loading on bead characteristics and drug distribution, *J. Mater. Sci. Mater. Med.*, 2007, **18**, 1691–1699.

8 M. V. Gonzalez, Y. Tang, G. J. Phillips, A. W. Lloyd, B. Hall, P. W. Stratford and A. L. Lewis, Doxorubicin eluting beads - 2: methods for evaluating drug elution and in-vitro:in-vivo correlation, *J. Mater. Sci. Mater. Med.*, 2008, **19**, 767–775.

9 Malvern Instruments Ltd, Binding affinity and Kd, https://www.malvern.com/en/products/measurement-type/binding-affinity, (accessed 1 October 2017).

10 R. R. Taylor, Y. Tang, M. V. Gonzalez, P. W. Stratford and A. L. Lewis, Irinotecan drug eluting beads for use in chemoembolization: In vitro and in vivo evaluation of drug release properties, *Eur. J. Pharm. Sci.*, 2007, **30**, 7–14.

11 D. Struk, R. N. Rankin and S. J. Karlik, Stability studies on chemoembolization mixtures. Dialysis studies of doxorubicin and lipiodol with Avitene, Gelfoam, and Angiostat, *Invest. Radiol.*, 1993, **28**, 1024—1027.

12 Newton South High School, Standard Enthalpy of Formation for Various Compounds, http://nshs-science.net/chemistry/common/pdf/R-standard_enthalpy_of_formation.pdf, (accessed 1 October 2017).

13 Jeff Bigler, Standand Enthalpies of Formation & Standard Entropies of Common Compounds, www.mrbigler.com/misc/energy-of-formation.PD, (accessed 1 October 2017).

14 ACD/I-Lab, Doxorubicin pKa, https://ilab.acdlabs.com/iLab2/index.php, (accessed 1 October 2017).

15 Gaurav Raval, University of Toronto, 2012.

16 Laura Ellen, University of Southampton and Biocompatibles UK Ltd, 2011.

17 Z. Fülöp, R. Gref and T. Loftsson, A permeation method for detection of self-aggregation of doxorubicin in aqueous environment, *Int. J. Pharm.*, 2013, **454**, 559–561.

Chapter 4 : Characteristic Determination of the Effect of Bead Size, Bead Type and Drug Type using Isothermal Titration Calorimetry (ITC)

4.1. Introduction

DEBs (drug eluting beads) are available to purchase in assorted dimensions, the size range is selected depending upon the size of the vessel to be embolised. There are currently four sizes of DC Bead™, all work thus far has been completed on the smallest bead size of 70-150 µm labelled M1. The other sizes are 100-300, 300-500 and 500-700 µm (termed 103, 305 and 507, respectively) [1].

These assorted sizes have been found to elute the drug differently and so it is conceivable that they may also bind differently [2]. However, it has been well documented that each bead size is able to bind to the same total amount of drug and still achieve complete elution [3]. Yet the pattern of elution and binding, in particular the length of time, differs due to smaller bead having a large surface area to volume ratio and therefore a faster binding and elution [4,5]. Table 4.1 summarises data supplied by the manufacturer regarding the length of time required for beads to load doxorubicin (Dox) according to their size, along with Table 4.2 which displays the predicted period of time required for the concentration of drug in the body to be reduced by half for each size of bead. Half-life is predicted from *in vitro-in vivo* correlation and proposes that the smallest size of bead elutes the fastest into the body, and thus metabolises at a quicker rate. The predicted half-life data was derived from T-apparatus experiments, the values decrease with an increase in bead size, except for the largest bead. The data does not follow a trend and could be affected by many factors such as bead packing, shape of cell, flow and convection etc. Details of this method are given in Chapters 1 and 5.

Table 4.1: Manufacturer suggested loading instructions, clinical loading of 37.5 mg Dox per mL of DC Bead™ at 98 % uptake (75 mg Dox per 2 mL vial of beads) [1].

Bead Name	Bead Size (µm)	Loading Time (min)
M1	70-150	30
103	100-300	45
305	300-500	90
507	500-700	90

Table 4.2: Half-life values for DC Bead™ loaded with Dox at 37.5 mg/mL [6].

Bead Name	Bead Size (µm)	Predicted Half-life ($t_{1/2}$) (h)
103	100-300	1505
305	300-500	2478
507	500-700	3658
709	700-900	2557

There are several types of DEBs available on the market, Some from the same and alternative suppliers. Some DEBs are made from similar materials and behave alike whilst other are somewhat different. To date there are few methods to distinguish drug-binding properties from different beads, therefore in this work the ITC was employed to determine whether this could be used as a method to identify bead characteristic differences exhibited from different bead properties. This project focused on five distinctive bead types named DC Bead™, DC Bead LUMI™, LifePearl™, Tandem™ and HepaSphere™.

Firstly, comparing DC Bead™ and LifePearl™, it was discovered that DC Bead™ is produced from a polyvinyl alcohol (PVA) crosslinked with N-acrylol-aminoacetaldehyde dimethylacetal (NAAADA) [7], whereas LifePearl™ is made of polyethylene glycol (PEG) crosslinked with polyethylene glycol diacrylate (PEGDA) [8]. Both products are modified with sulfonate groups the former been 2-acrylamido-2-methylpropane sulfonate sodium salt (AMPS) [7], and the latter been 3-sulfopropyl acetate sodium salt (SPA) [8]. Certain properties between the two are alike, for instance both are hydrophilic, compressible, elastic hydrogels. Furthermore, both types of beads have comparable solid and water content in saline solution, as discovered by Biocompatibles Ltd and summarised in Table 4.4 (data unpublished).

Table 4.3: Components of DC Bead™ and LifePearl™ [7,8].

Feature	DC Bead™	LifePearl™
Polymer Backbone	PVA 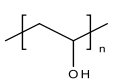	PEG 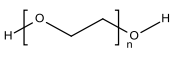
Crosslinker	NAAADA 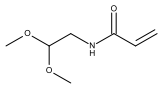	PEGDA 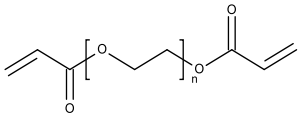
Binding Site	AMPS 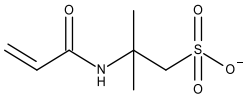	SPA 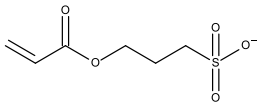
Solid Content	6.2 %	4.1 %
Water Content	93.8 %	95.9 %

The third type of bead considered in this work was DC Bead LUMI™, which builds on the predicate device of DC Bead™. This bead uses the well-established technology with the addition of a radiopaque moiety, used to enhance clinical performance with the ability to visualise the procedure under x-ray imaging modalities. The chemistry of DC Bead LUMI™ is identical to DC Bead™, with the exception of a covalently bonded iodine and without the addition of blue dye. Because of this the colour, density and time in suspension differs, illustrated in Table 4.4 [9,10].

Table 4.4: Attributes of DC Bead™ and DC Bead LUMI™ [9,10].

Feature	DC Bead™	DC Bead LUMI™
Radiopacity	No, but contains blue dye 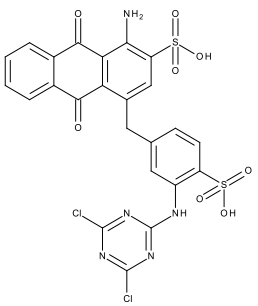	Yes, contains iodine 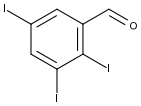
Colour	Blue	Golden
Density	1.03 g/cm^3	1.30 g/cm^3
Suspension	Suspends more than DC Bead LUMI™ because it is lighter	Suspends less than DC Bead™ because it is denser
Size Change	Shrinks up to 25 % with Dox loading and 30 % with Iri loading	No change upon drug loading

The fourth type of bead considered in this work was Embozene Tandem™. Referred to as Tandem™ it is polymethacrylate (PMA) sodium coated with Polyzene®-F (poly(bis[trifluoroethoxy]phosphazene) [11]. Like DC Bead LUMI™, Tandem™ is a more crosslinked product (i.e. has a higher solid content and lower water content) which changes little in size after loading by < 5 % [12], where DC Bead™ is said to reduce in size by ≤ 20 % [13,14]. The drug loading capacity of Tandem™ is indicated as higher than DC Bead™, for use with 50 mg of Dox for each mL of beads compared with 37.5 mg/mL in the equivalent loading period for DC Bead™ [12], however internal studies have concluded that DC Bead™ has the potential to load 60 mg Dox per mL of beads and DC Bead LUMI™ 178 mg per mL (data unpublished).

The fifth and final type of bead considered in this work was HepaSphere™, made from a sodium acrylate alcohol (SAA) copolymer formed from the combination of two monomers, vinyl acetate and methyl acrylate. Hepasphere™ microspheres conform to the shape of the vessel lumen *in vivo*, unlike the other beads it is supplied dry and is alleged to expand approximately four time in diameter when reconstituted in saline [15]. A maximum dose of 75 mg of Dox can be loaded into a 25 mg vial of Hepasphere™, which must be placed in either 0.9 % (w/v) sodium chloride (NaCl) or non-ionic contrast media before use [16]. The polymeric structures of Tandem™ and HepaSphere™ are shown in Table 4.5.

Table 4.5: Composition of Tandem™ and HepaSphere™ [12,15].

Feature	Tandem™		HepaSphere™
	PMA (core)	Polyzene-F (shell)	SAA
Polymer			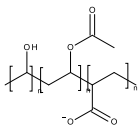

It was important to understand the binding process of DEBs to different drugs to identify specific drug-bead interactions. The previously mentioned beads are indicated for use with both Dox and irinotecan (Iri), hence both these compounds were chosen for analysis. It was understood that Dox and Iri have one potential binding site per drug molecule. In contrast, mitoxantrone (Mit), a compound similar in structure to Dox and an associated topoisomerase II (TOPII) inhibitor, exhibits two potential binding sites and was therefore selected for investigation. It was then reasonable to compare Iri with a corresponding structure and an alternative topoisomerase I inhibitor (TOPI), hence topotecan (Top) was also evaluated.

In summary, this work investigated the ability of ITC to provide data that would allow analytical comparisons to be made with respect to drug-bead binding for four sizes of bead (70-150, 100-300, 300-500 and 500-700 µm), five types of bead (DC Bead™, DC Bead LUMI™, LifePearl™ Tandem™ and HepaSphere™) and four drugs (Dox, Iri, Mit and Top).

4.2. Results and Discussion

4.2.1. Effect of Bead Size

During preliminary testing of the obtainable sizes of DC Bead™, it seemed that the larger beads bound to less drug, conversely preceding studies have opposed this statement [3]. It is possible that during experimental bead preparation sodium ions had not been entirely removed from the larger beads, as a smaller surface area to volume ratio would require this process to take an increased amount of time. Larger beads were left to soak in acid for 1 hour and this did improve drug loading, but not to the expected quantity, as demonstrated in Figure 4.1. Allowing the beads to soak for even longer from 1 hour to overnight, affected the bead structure. The beads became translucent, highly swollen and the loading did not improve further but diminished. The effect of leaving the beads to soak in 2 M hydrochloric acid (HCl) influences the bead binding properties because the structure is acid labile and the polymer degrades upon hydrolysis of the amide group. Optimum time for soaking in HCl could be a focus of investigation for future work on the use of calorimetry to analyse DEBs.

The solid content and water content of 103, 305 and 507 beads were presumed to be the same as the previously tested M1 beads, since the beads are produced by the same supplier, with the same materials and by the same manufacturing process, with the only deviation being the beads were from a segment of a different sized sieve at the final stage of production. Based on experimental data presented in Figure 4.1 the four bead sizes achieved different final drug-bead binding ratios and displayed differences in the kinetic profiles, such as the rate of each injection completing the binding process. However, the rate of binding didn't not correlate to bead size with the largest beads binding the slowest, which could indicate that either there was incomplete binding or that larger beads have more internal binding sites compared to smaller beads with more surface sites. The difference in the density of the outer and inner layer of different sized beads changes the difficulty of the penetration of Dox. Slower binding could lead to signals under the limit of detection.

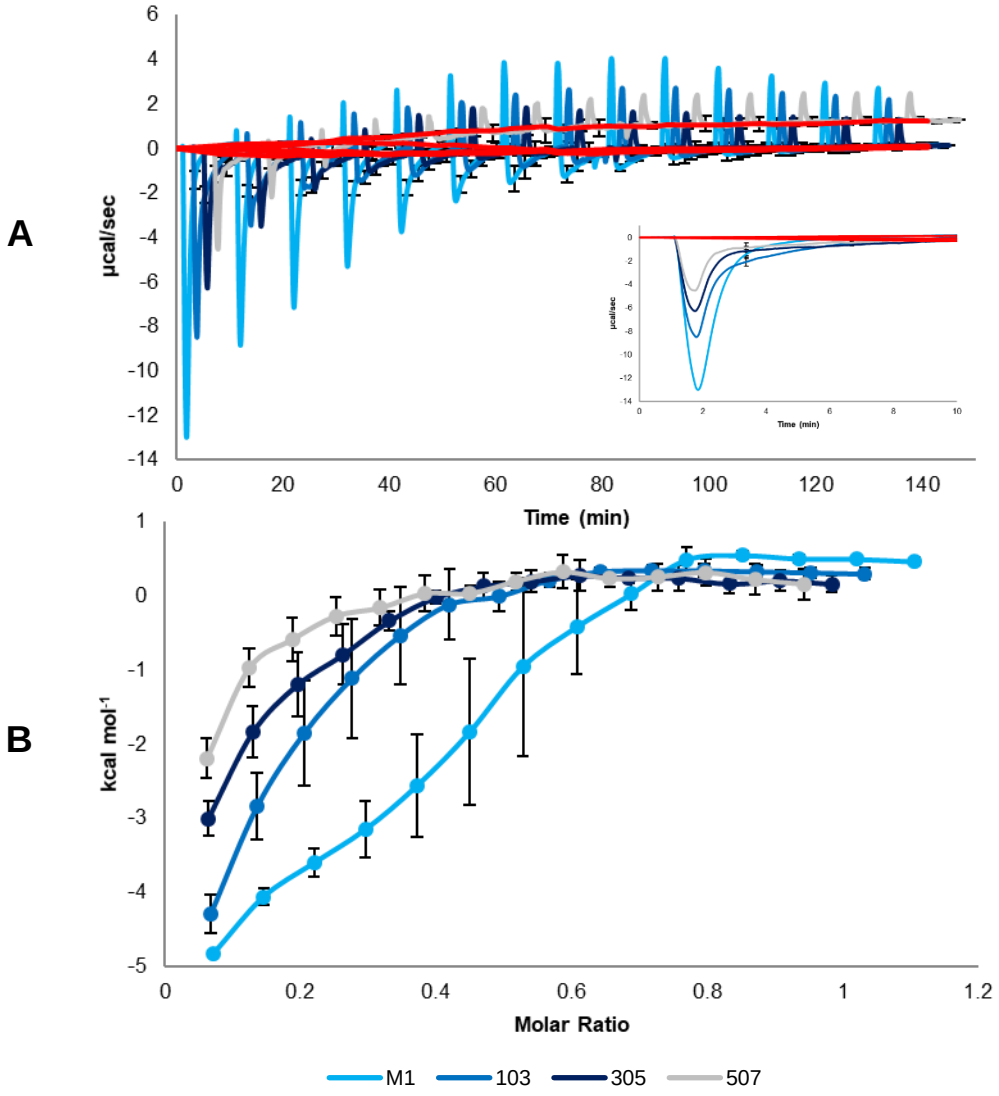

Figure 4.1: Binding of different sized beads with 10 mM Dox to 25 mg beads (sample number = 3, error bars = standard deviation, time has been altered by two minutes for each sample for visibility). Please note that the baseline of 507 beads drifts but does not exceed 1 µcal/sec and is therefore valid data. Inset is a replicate of the first injection at a closer scale and all injections starting at the same timepoint to identify the rate at which each injection completes the binding process.

Using data obtained from Figure 4.1, it was possible to calculate overall drug-bead binding ratios in Table 4.6. From this, 103 beads were found to have a lower average molar ratio than M1 beads, but the two group are not statistically different using Minitab® software to calculate the values of an unpaired *t*-test ($p = 0.7056$). M1 is made from a similar distribution size of beads as 103, therefore similar results were anticipated. In contrast, the difference between M1 and 305 as well as M1 and 507 were found to be significantly different ($p = 0.0098$ and $p = 0.0446$, respectively).

Table 4.6: Molar ratios of different sized bead with 10 mM Dox into 25 mg beads using the highest ΔH value for the calculation (sample number = 3, error = standard deviation).

Bead Size	Run	Molar Ratio	Average
M1	1	0.82:1	0.79:1 ± 0.05
	2	0.73:1	
	3	0.83:1	
103	1	0.78:1	0.76:1 ± 0.13
	2	0.62:1	
	3	0.88:1	
305	1	0.56:1	0.58:1 ± 0.06
	2	0.64:1	
	3	0.52:1	
507	1	0.60:1	0.53:1 ± 0.15
	2	0.63:1	
	3	0.36:1	

The concentration of Dox was increased to observe whether binding would also increase, with the theory being that an increased concentration would force the removal of sodium. Interestingly, an increase in the molar ratio was observed in Table 4.7, but with both 10 mM and 43 mM Dox the 103, 305 and 507 beads appeared to have a different isotherm shape compared with M1 beads, as is visible in Figure 4.2.

Overall, the increased Dox concentration did further increase the binding ratio for all four bead sizes to achieve values much closer to the anticipated 1:1 ratio, but it is possible since the rate of binding again did not correlate with bead size, that the ratio is less than recorded and that full binding could not be achieved. The inset graph of Figure 4.2 displays the rate of reaction for the first injection, all four bead sizes reach the baseline at roughly the same time, so rate of binding was regarded as the same regardless of bead size. There are at least two conceivable explanations for the larger bead size results, one is that sodium ions were not completely removed from the larger beads. The other is that there are two mechanisms at play, one being initial binding on surface of the bead that the ITC picks up well, and a secondary mechanism as the drug skips through the bead matrix. It was plausible that larger beads tend to bind drug on surface and possibly build a barrier to slow down drug diffusion and binding. The later slow binding could generate less heat due to the low level of drug diffusion and this lower energy could be under the limit of detection, resulting in increased measurement error.

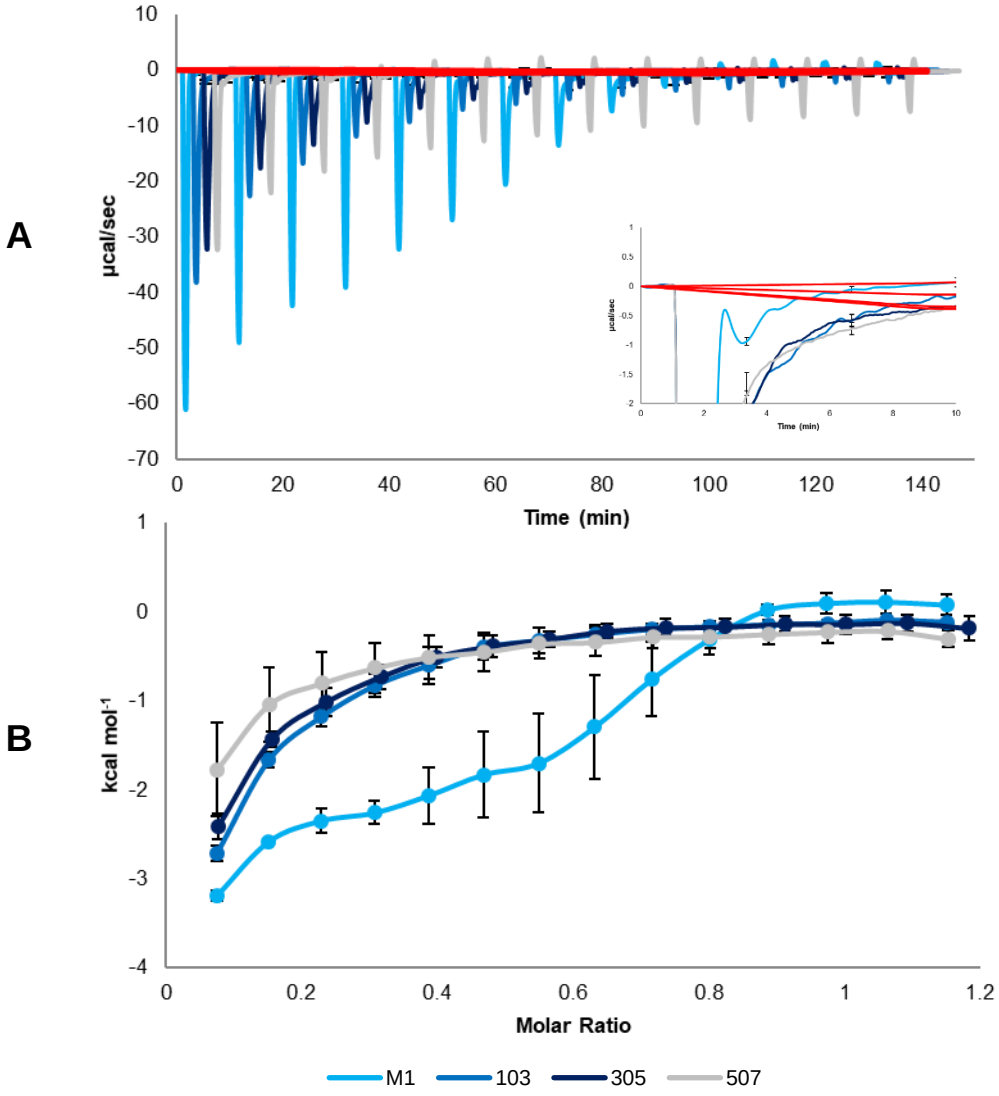

Figure 4.2: Binding of different sized beads with 43 mM Dox to 100 mg beads (sample number = 3, error bars = standard deviation, time has been altered by two minutes for each sample for visibility). Inset is a replicate of the first injection at a closer scale and all injections starting at the same timepoint to identify the rate at which each injection completes the binding process.

Currently the point of saturation selected is the highest value on the enthalpy (ΔH) curve, a unit which has until now descended at the end of the experiment, unfortunately this was not the case with the larger beads as ΔH levelled off. It is possible that the beginning of the plateau rather than a latter point is the saturation site. If a much earlier point in the experiment was chosen as the position of completely loaded bead, then the calculated molar ratio of the larger beads would decrease significantly. Therefore, in these experiments full binding may not have been achieved which would explain the change in the shape of the isotherm and is potentially the result of the inability to protonate the beads.

The peaks showed that drug binding with 43 mM Dox and 507 beads did finish in 140 min however, further binding would indicate a 2:1 binding ratio which is known not to be the case. It would

appear that either incomplete removal of acid, or slower binding of the drug to the surface of bead has extended the binding process, of which is more prominent in the larger bead size. In any case, larger beads were unable to achieve expected drug loading, which therefore requires further investigation.

Residual and extracted drug analysis of the ITC samples confirmed that a significantly lower portion of the titrated drug had bound to the larger beads than in Table 4.7. M1 was calculated to have an average ratio of 0.89 (standard deviation of 0.07), any discrepancy could be drug bound to the ITC cell or inefficient removal of all beads. 103 was found to have a ratio of 0.86:1, 307 was 0.61:1 and 507 at 0.59:1 (corresponding standard deviations were 0.18, 0.78 and 0.76, respectively).

Table 4.7: Molar ratios of different sized bead with 43 mM Dox into 100 mg beads using the highest ΔH value for the calculation (sample number = 3, error = standard deviation).

Bead Size	Run	Molar Ratio	Average
M1	1	0.92:1	0.92:1 ± 0.08
	2	1.00:1	
	3	0.84:1	
103	1	0.98:1	0.97:1 ± 0.02
	2	0.95:1	
	3	0.99:1	
305	1	0.97:1	1.00:1 ± 0.04
	2	0.99:1	
	3	1.04:1	
507	1	0.93:1	0.95:1 ± 0.02
	2	0.94:1	
	3	0.97:1	

Single injection method (SIM) experiments were then conducted to simplify the investigation with just one injection of drug into the various bead sizes. This would establish the time taken for each sample to return to the baseline, hence the loading speed. The SIM experiments equate to 1.68 mg Dox in the cell with ~0.13 mL beads when reconstituted in saline. When compared with clinical loading concentrations of 37.5 mg Dox in 1 mL beads, 4.88 mg Dox would be required to saturate the same volume of bead in the ITC cell. In the SIM experiments beads were under saturated to create one exothermic peak, however this requires much lower concentrations of Dox than in the clinical setting.

The SIM experiments in Figure 4.3 signify each bead size reached the baseline at approximately the same time of 50 mins. It was expected that the larger beads would take longer to completely bind, the results may be attributed to smaller concentrations and volumes used compared with clinical loading. In agreement with previous data, a larger portion of the drug had bound to the M1 bead in the first ten minutes, and a general pattern can be seen to correlate bead size with increasingly slower binding.

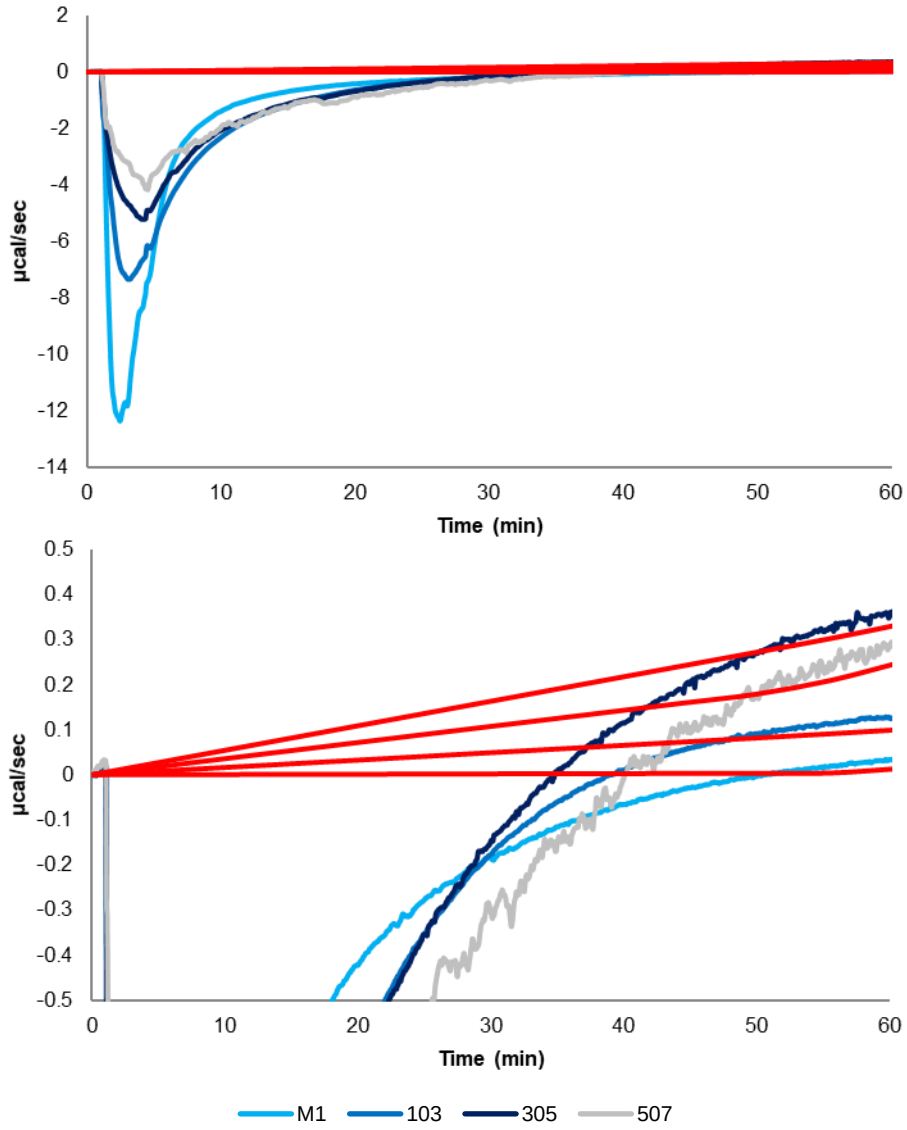

Figure 4.3: SIM experiment with 100 µL 10 mM Dox into 25 mg beads of different sizes. The bottom graph is a replication of the top graph exposing the baseline of each bead size (sample number = 1).

Tables 4.8 and 4.9 reveal that the binding constant and free energy remained much the same with a change in bead size. In Figures 4.4 and 4.5 both enthalpy and entropy increased as the diameters of

the bead also increased. Although the R^2 values are either > 0.96 or < 0.01 for each parameter, there is only one replicate of each experiment and therefore definitive conclusions cannot be made. However, this data does permit an initial relationship to be explored.

Table 4.8: Binding constant of SIM experiments with 100 µL 10 mM Dox into 25 mg M1, 103, 305 and 507 beads (sample number = 1).

Bead Size	***K* (x 10^5 M^{-1})**
M1	1.73
103	1.74
305	1.72
507	1.74

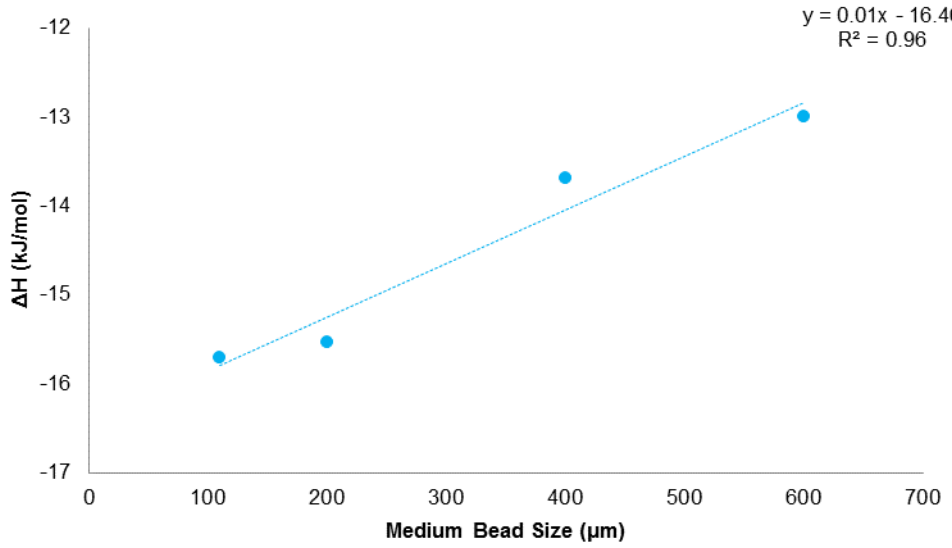

Figure 4.4: Enthalpy of SIM experiments with 100 µL 10 mM Dox into 25 mg M1, 103, 305 and 507 beads (sample number = 1).

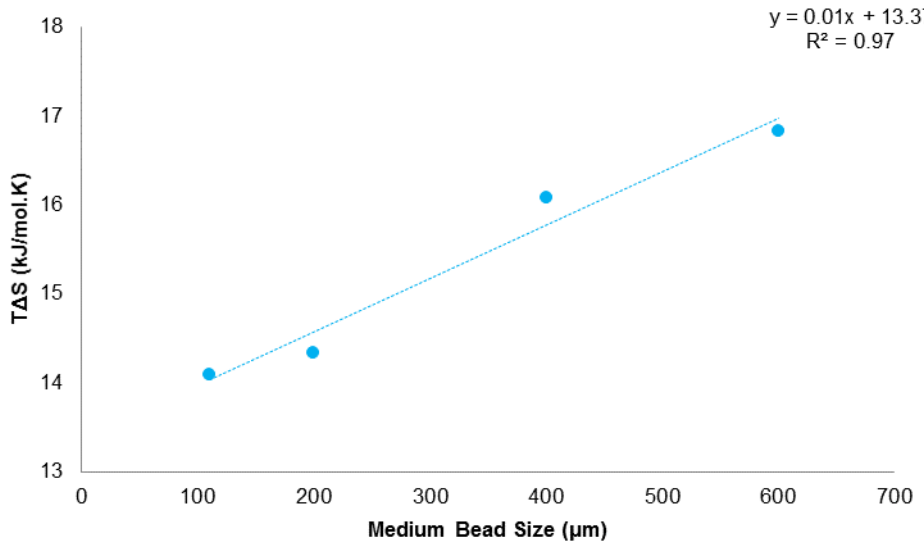

Figure 4.5: Entropy of SIM experiments with 100 µL 10 mM Dox into 25 mg M1, 103, 305 and 507 beads (sample number = 1).

Table 4.9: Free energy of SIM experiments with 100 µL 10 mM Dox into 25 mg M1, 103, 305 and 507 beads (sample number = 1).

Bead Size	**Δ*G* (kJ/mol)**
M1	-29.8
103	-29.9
305	-29.8
507	-29.8

If it is considered that the larger beads bound to less drug, possibly due to inefficient removal of sodium with the current bead washing process, then there would be a decrease in the heat released from the reaction as less binding transpires. Entropy can change depending on the number of molecules in a system, and as larger beads are thought to be bound to a greater number of sodium ions there will be a larger number of molecules in the system, which is likely to increase the change entropy.

In summary, it would appear that bead size does affect the binding process, as evidenced using ITC, although it concerns the kinetics of binding rather than the absolute binding ratio achieved.

4.2.2. Effect of Bead Type

In this study five bead types were investigated to consider the effect of bead type on drug-bead binding, firstly comparing DC Bead™ and LifePearl™, the most recent DEB to be released into the market. The average solid content of DC Bead™ washed in 2 M HCl and centrifuged for 30 seconds at 3000 rpm was 6 %, and for LifePearl™ under the same experimental conditions was 5 % with no significant difference between the values in Table 4.10 and 4.11 ($p = 0.2269$). DC Bead M1™ (70-100 µm) was selected for analysis as it was closest in size to LifePearl™ 100 µM (75-125 µm). It's important to think about this topic in terms of solid content, as water content is essentially the same (94 – 95 %), whereas the solid content is 5 or 6 %, i.e. DC Bead has 20% more solid present.

Table 4.10: Solid content of DC Bead™ prepared for use in the ITC (sample number = 3).

DC Bead™	Insert (mg)	Wet Beads (mg)	Dry Beads (mg)	% Water Content	% Solid Content
Sample 1	932.38	993.90	936.25	93.71	6.29
Sample 2	910.50	973.58	913.79	94.78	5.22
Sample 3	910.32	983.36	914.91	93.72	6.28

Table 4.11: Solid content of LifePearl™ prepared for use in the ITC (sample number = 3).

LifePearl™	Insert (mg)	Wet Beads (mg)	Dry Beads (mg)	% Water Content	% Solid Content
Sample 1	908.65	946.11	910.32	95.54	4.46
Sample 2	917.66	952.66	919.40	95.03	4.97
Sample 3	914.87	946.45	916.75	94.05	5.95

It was vital to identify the number of binding sites on the beads, the DC Bead™ formulation was known to be 45.45 % AMPS sites from the manufactures calculations. This value was investigated by washing a known mass of beads in 10 mM HCl to remove sodium ions, and with deionised water to remove any residual acid. A salt solution consisting of NaCl was filtered through the beads and then washed with a known volume of deionised water to removed free NaCl, followed by an acid-base titration with the collected solution. This facilitated a calculation of the amount of salt bound to the beads, and the value equates to the total number of binding sites when subtracted from the standardisation.

For DC Bead™ the average titrated volume in Table 4.13 subtracted from the average standardisation titration in Table 4.10 and fit to 100 mg of beads was 8.17 mL, which is known to equate to 45.45 % AMPS sites in the 6 % solid content of DC Bead™. 8.17 mL divide by 45.45 and multiplied by 100 is 17.98. An identical test was then conducted for the LifePearl™ product. So, in 100 mg of LifePearl™ an average titrated volume in Table 4.14 subtracted from the average standardisation is 10.33 mL and this divided 17.98 and multiplied by 100 equates to 57.44 % binding sites in the 5 % of solid content of LifePearl™. An attempt has been made to standardise the calculation of the number of binding sites on the beads, however the different configuration of binding sites within each bead make the uniform penetration of acid and salt problematic. Insufficient removal of sodium ions from the packing solution, beads sites not bound back to sodium and sodium not completely removed for a second time could all contribute to inaccurate results, leading to incorrect binding site and molar ratio calculations.

Table 4.12: Standardisation for determining binding sites of different bead types (sample number = 3, error = standard deviation).

Standardisation	**Mass of NaOH (mg)**	**8.38 mM HCl (mL)**
Sample 1	10.05	23.70
Sample 2	10.15	24.20
Sample 3	9.99	24.00
Average Fit to 10.00 mg NaOH		23.82 ± 0.25

Table 4.13: Number of binding sites on DC Bead™ prepared for use in the ITC (sample number = 3, error = standard deviation).

DC Bead™	**Mass of Beads**	**Mass of NaOH (mg)**	**8.38 mM HCl (mL)**
Sample 1	100.92	10.07	15.70
Sample 2	100.92	10.04	15.70
Sample 3	100.92	10.27	15.90
Average Fit to 100.00 mg Beads 10.00 mg NaOH			15.57 ± 0.07

Table 4.14: Number of binding sites on LifePearl™ prepared for use in the ITC (sample number = 3, error = standard deviation).

LifePearl™	**Mass of Beads**	**Mass of NaOH (mg)**	**8.38 mM HCl (mL)**
Sample 1	97.65	10.53	14.50
Sample 2	97.65	10.15	13.90
Sample 3	97.65	10.12	13.90
Average fit to 100.00 mg Beads 10.00 mg NaOH			13.73 ± 0.03

A separate calculation was performed to compare with the titration data using element analysis and the solid content of beads by applying Equation 4.1. Comparisons could then be made between the binding site values of the two different methods of titration data and element analysis.

Equation 4.1: Calculation of moles of binding sites per mL of hydrated DC Bead™.

$$\% \text{ of Sulfur} = \frac{\text{Relative Molecular Mass (RMM) of Sulfur (32.06)}}{\text{RMM of AMPS (229.23)}} \cdot 100 = 13.99$$

$$\% \text{ of AMPS (w/w)} = \frac{\% \text{ Solid Content (6)}}{\% \text{ of Sulfur (13.99)}} \cdot 100 = 42.89$$

$$\% \text{ of PVA (w/w)} = 100 - \% \text{ of AMPS} = 57.11$$

$$\text{AMPS mol/g} = \frac{\% \text{ of AMPS (42.89)}}{\text{RMM of AMPS (229.23)}} / 100 = 1.87 \times 10^{-3}$$

$$\text{PVA mol/g} = \frac{\% \text{ of PVA (57.11)}}{\text{RMM of PVA (44.05)}} / 100 = 1.30 \times 10^{-2}$$

$$\text{AMPS mol/mL} = \text{AMPS mol/g } (1.87 \times 10^{-3}) \cdot 50 / 1000 = 9.35 \times 10^{-5}$$

$$\text{PVA mol/mL} = \text{PVA mol/g } (9.35 \times 10^{-5}) \cdot 50 / 1000 = 6.48 \times 10^{-4}$$

$$\text{Capacity of Dox mg/mL} = \text{AMPS mol/mL } (9.35 \times 10^{-5}) \cdot 579.99 \cdot 1000 = 54.26$$

A calculation of the percentage binding sites of DC Bead™ was 42.89 %, the moles of sites per mL was 9.35 x 10^{-5} mol/mL, which means a loading capacity of 54.24 mg/mL Dox. There is a small difference between these values and the manufacturers data, which may be due to different procedures to define the solid content. If the same equations were used with the DC Bead™ titration data, 45.45 % AMPS from DC Bead™ is equal to 9.91 x 10^{-5} mol/mL and 57.50 mg/mL Dox loading.

LifePearl™ was calculated to 35.74 % binding sites, which is 9.20 x 10^{-5} mol/mL and a Dox loading capacity of 53.37 mg/mL, by substituting the solid content with 5 % and the RMM of AMPS with the RMM SPA of 194.21 g. Again, the values were substituted with the LifePearl™ titration data of 57.44 % sites, which was calculated to be 1.48 x 10^{-4} mol/mL and a Dox loading capacity of 85.77 mg/mL. There is a vast difference between the LifePearl™ data of these two methods, the solid content to calculate the element analysis data could be incorrect as the ratio of Dox-AMPS was much greater than

1:1 and it is known that theoretically only one sulfonate group can bind to a molecule of Dox. It is for the reason that the titration values were used in the molar ratio calculation.

Figure 4.6 exposes LifePearl™ to have a similar ITC profile to that of DC Bead™. The interaction of water with LifePearl™ was found to be negligible with each signal <0.1 µcal/sec in Figure 4.7, thus confirming the similarity in thermodynamic profiles of water-bead binding.

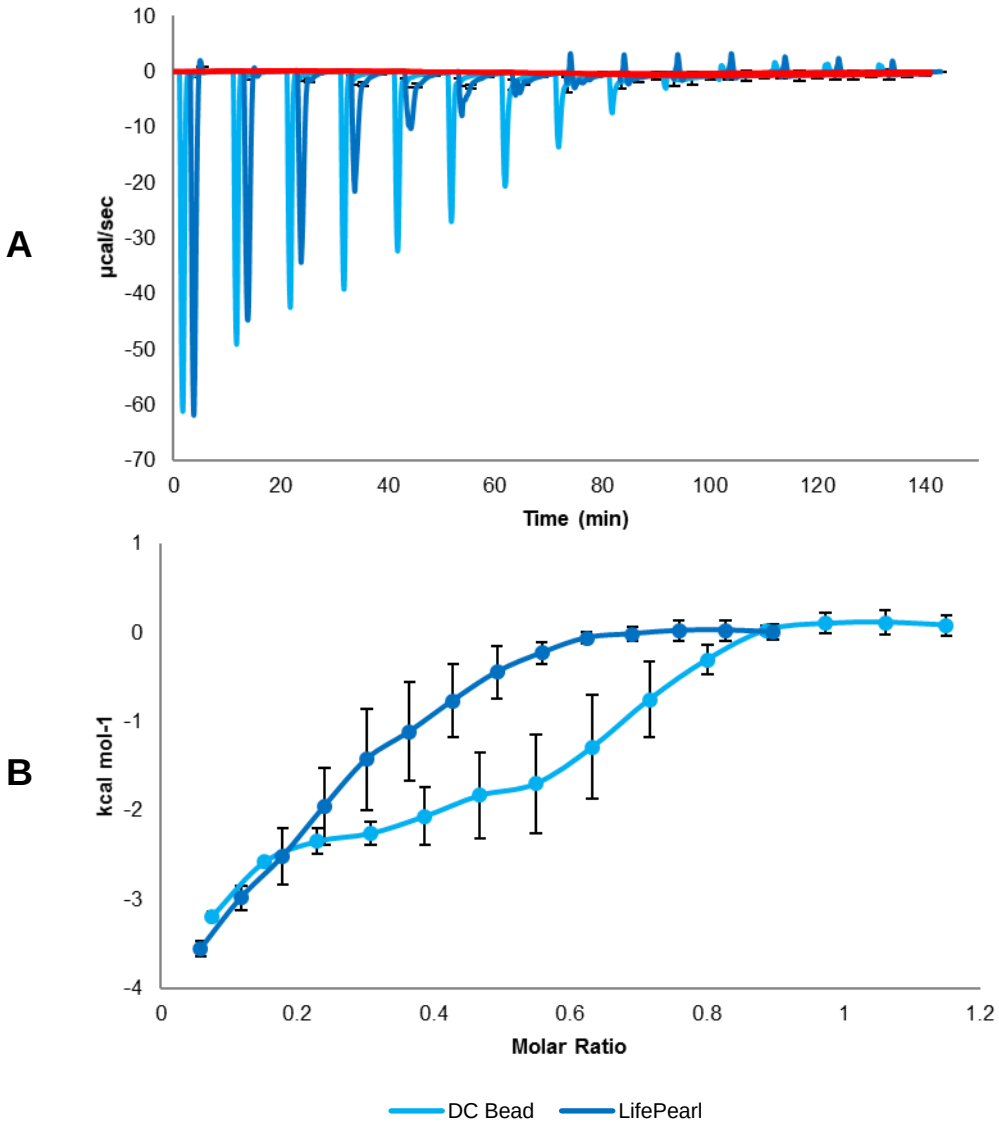

Figure 4.6: Binding of LifePearl™ in comparison to DC Bead™ with 43 mM Dox to 100 mg beads (sample number = 3, error bars = standard deviation, time has been altered by two minutes for visibility).

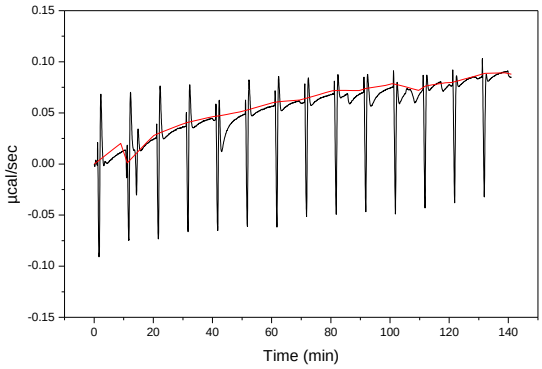

Figure 4.7: Isotherm of water into 100 mg LifePearl™.

As presented in Table 4.15, the average molar ratio of 43 mM Dox to 100 mg LifePearl™ beads was determined to be 0.78:1, with an average (previously determined) ratio of 0.92:1 for DC Bead™. Statistical analysis found these two groups to be significantly different ($p = 0.0221$) thus, confirming that DC Bead™ was able to accommodate a greater drug loading.

Table 4.15: Molar ratios of DC Bead™ versus LifePearl™ with 43 mM Dox into 100 mg beads (sample number = 3, error = standard deviation).

Product	**DC Bead™**	**LifePearl™**
Molar Ratio	0.84:1	0.74:1
	1.00:1	0.70:1
	0.92:1	0.77:1
Average	0.92:1 ± 0.08	0.74:1 ± 0.04

The shape of the isotherm between the two bead types was different, the signals began with a similar intensity but LifePearl™ rapidly declined with smaller interactions compared with DC Bead™ after the first injection. The area of the combined exothermic peaks was approximately comparable, and so LifePearl™ in general has much shallower broader signals than DC Bead™, as seen in Figure 4.8. This slower binding process affects the overall shape of the binding profile.

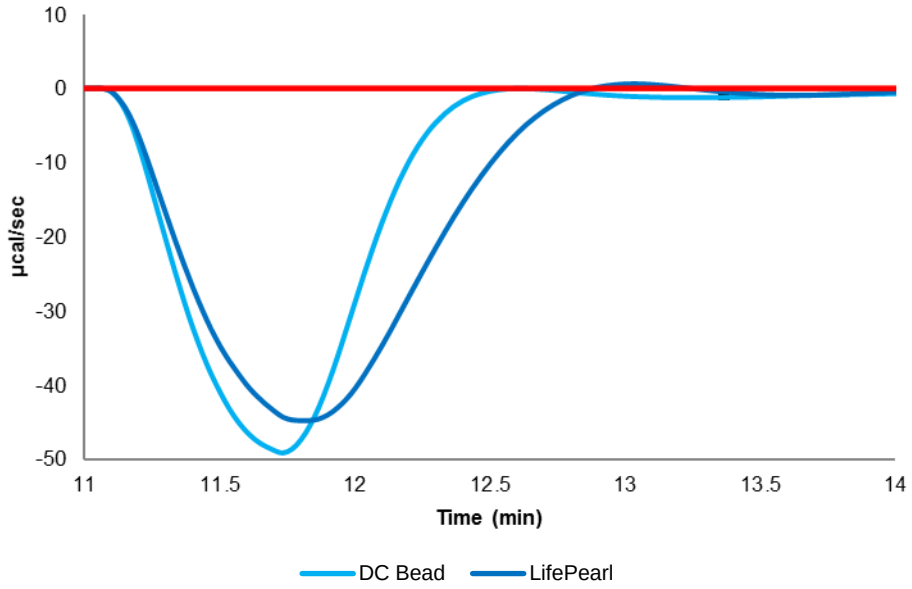

Figure 4.8: A magnification of an injection of DC Bead™ and LifePearl™ binding with 43 mM Dox to 100 mg beads (sample number = 3).

Figure 4.9 suggests both processes are exothermic as the change in enthalpy values are negative. It should be noted that the change in entropy are presented as $T\Delta S$, for both beads this is positive and therefore increases as the reaction proceeds, but the value is greater in DC Bead™ and consequently the system is more disordered. Since the actual size in the change in entropy is comparatively large in comparison with the change in enthalpy, both Dox binding to DC Bead™ and LifePearl™ are enthalpy driven processes. The change in the Gibbs free energy is a negative value thus is spontaneous for drug-bead binding, but again is more so in DC Bead™. Based on these findings it is proposed that the two reactions are spontaneous regardless of the system temperature. Both reactions are entropy and enthalpy driven, from hydrogen bonding, electrostatic or van der Waals interactions, in addition to hydrophobic interactions resulting in conformation changes. There are greater entropic and enthalpic forces in Dox-DC Bead™ compared with Dox-LifePearl™, and differences are considered significant (ΔH p = 0.0018, $T\Delta S$ p = 0.0386 and ΔG p = 0.0435).

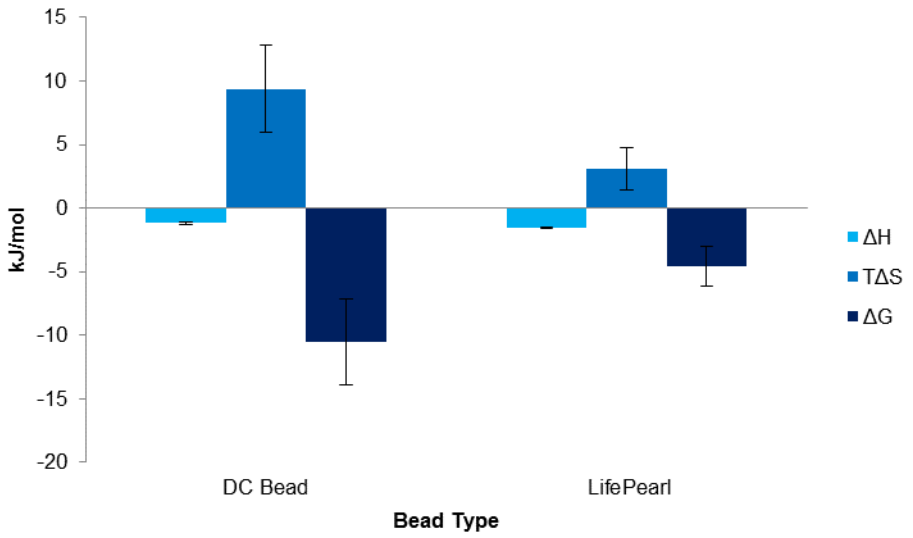

Figure 4.9: Thermodynamics of Dox into DC Bead™ and LifePearl™ (sample number = 3).

The third and fourth beads to be evaluated, namely DC Bead LUMI™ and Tandem™, were found to behave quite differently to the previously discussed beads. Tables 4.16 and 4.17 identifies these beads to be much denser, with solid contents of 33 % for DC Bead LUMI™ and 38 % for Tandem™. They do not have as substantial swelling properties during binding and elution compared with DC Bead™ and LifePearl™. The size of DC Bead LUMI™ under investigation was M1 (70-150 µm) and the size of Tandem™ selected for analysis was 100 µm (75-125 µm) to correspond with previous testing.

Table 4.16: Solid content of DC Bead LUMI™ prepared for use in the ITC (sample number = 3).

DC Bead LUMI™	Insert (mg)	Wet Beads (mg)	Dry Beads (mg)	% Water Content	% Solid Content
Sample 1	930.80	1012.17	957.10	67.68	32.32
Sample 2	906.13	1017.50	942.65	67.21	32.79
Sample 3	930.76	1053.90	972.64	65.99	34.01

Table 4.17: Solid content of Tandem™ prepared for use in the ITC (sample number = 3).

Tandem™	Insert (mg)	Wet Beads (mg)	Dry Beads (mg)	% Water Content	% Solid Content
Sample 1	906.87	964.49	982.87	61.82	38.18
Sample 2	911.44	977.98	937.71	62.02	37.98
Sample 3	897.58	955.50	919.22	62.64	37.36

The average titrated volume of DC Bead LUMI™ in Table 4.18 subtracted from the average standardisation titration in Table 4.10 and fit to 100 mg of beads was 4.66 mL, the percent of binding sites was then calculated to be 25.90 %, which is 3.39 x 10^{-4} mol/mL and 196.59 mg/mL Dox capacity. Elemental analysis values were calculated from DC Bead LUMI™ and found to be 23.59 % AMPS and 3.09 x 10^{-4} mol/mL with a Dox capacity of 179.05 mg/mL. The small difference from the projected values could again be due to the errors in the solid content analysis or error in the volume of solution titrated, as it could only be precise to 0.1 mL or 0.05 mL at best.

With 100 mg Tandem™, the average titrated volume in Table 4.19 subtracted from the average standardisation in Table 4.10 was 3.40 mL, and this equates to 18.49 % binding sites and 8.55 x 10^{-5} mol/mL, therefore the maximum loading capacity of Dox was calculated as 49.62 mg/mL. When AMPS in Equation 4.1 was replaced with Polyzene-F, the percentage binding sites was calculated as 17.45 % and 8.07 mol/ mL, the total amount of Dox which could bind to Tandem™ was 46.81 mg/mL.

Table 4.18: Number of binding sites on DC Bead LUMI™ prepared for use in the ITC (sample number = 3, error = standard deviation).

DC Bead LUMI™	Mass of Beads	Mass of NaOH (mg)	8.38 mM HCl (mL)
Sample 1	102.05	10.50	19.90
Sample 2	102.05	10.05	19.30
Sample 3	102.05	10.12	19.20
Average Fit to 100.00 mg Beads 10.00 mg NaOH			19.04 ± 0.11

Table 4.19: Number of binding sites on Tandem™ prepared for use in the ITC (sample number = 3, error = standard deviation).

Tandem™	Mass of Beads	Mass of NaOH (mg)	8.38 mM HCl (mL)
Sample 1	102.16	10.44	21.10
Sample 2	102.16	10.08	20.70
Sample 3	102.16	10.14	20.80
Average Fit to 100.00 mg Beads 10.00 mg NaOH			20.42 ± 0.15

With a known solid and salt content of DC Bead LUMI™ the ITC should have required ~25 mg of centrifuged beads with 43 mM Dox. Several bead masses were studied in Figure 4.10, to optimise and identify the method restrictions. A mass of > 5 mg beads was difficult to place into the ITC cell without losing beads on the outside of the sample port, thus creating caution with further data analysis.

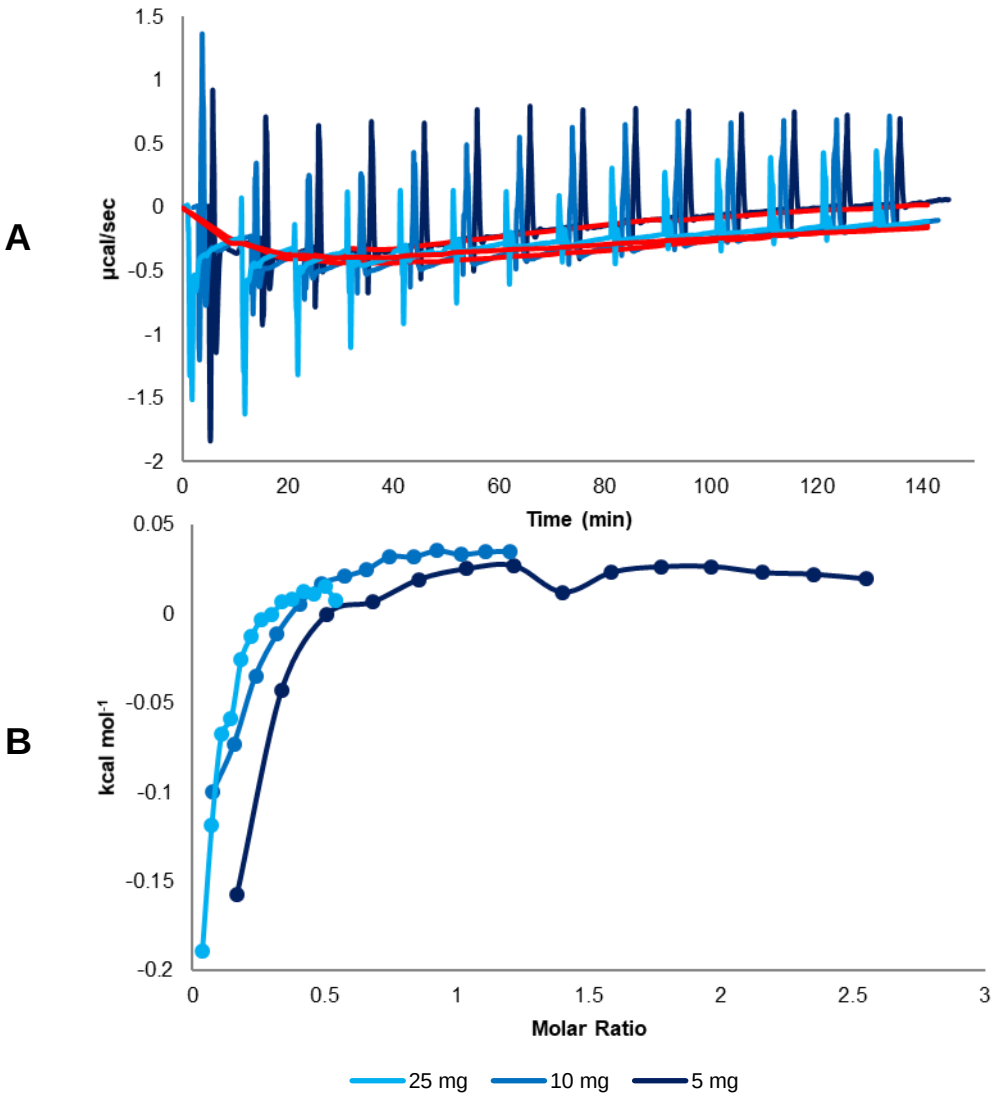

Figure 4.10: Binding of DC Bead LUMI™ with 43 mM Dox to 25, 10 and 5 mg beads (sample number = 3, error bars = standard deviation, time has been altered by two minutes for each sample for visibility).

Unexpectedly the number of injections needed for bead saturation did not coincide with the molar ratio. When the mass of beads decreased the molar ratio continually shifted with both water washed, and acid washed beads causing unreliable results, apparent in Table 4.20. Based on the comparatively small signals associated with this particular bead, caution should be expressed regarding this data.

Table 4.20: Molar ratios of DC Bead LUMI™ with 43 mM Dox into 25, 10 and 5 mg beads (sample number = 3).

Mass of DC Bead LUMI™ (mg)	Concentration of Dox (mM)	Injection Number at Point of Bead Saturation	Molar Ratio
25	43	13	1.37:1
10	43	11	2.34:1
5	43	11	4.84:1

Equivalent results were found with the product Tandem™, that with both water washed and acid washed beads many signals were too small for analysis, evident in Figure 4.11.

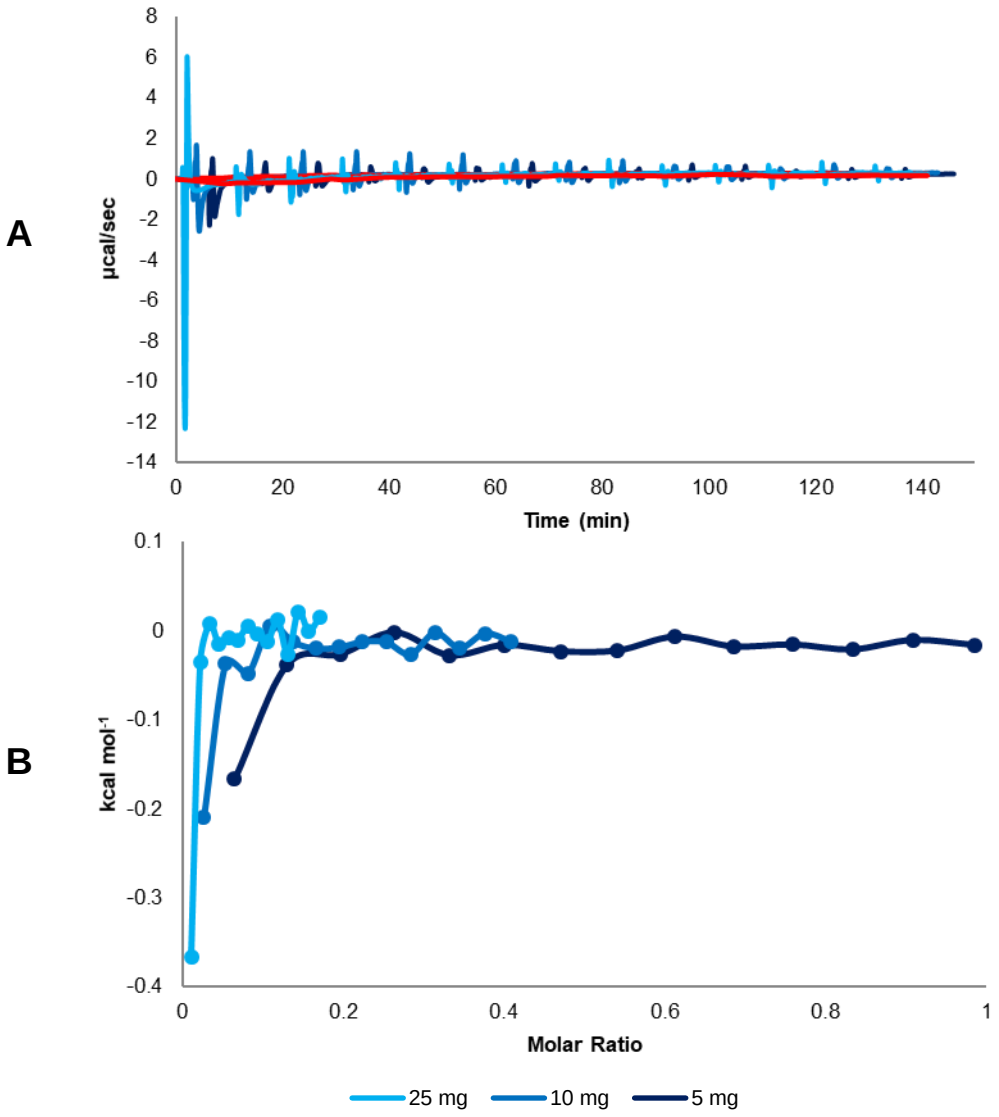

Figure 4.11: Binding of Tandem™ with 43 mM Dox to 25, 10 and 5 mg beads (sample number = 3, error bars = standard deviation, time has been altered by two minutes for each sample for visibility).

With several beads masses the molar ratio was found to be inconsistent, as displayed in Table 4.21. In Figure 4.12 the interaction of DC Bead LUMI™ into water, along with Tandem™ into water, was considered negligible, thus confirming the water-bead interaction to be thermodynamically insignificant.

Table 4.21: Molar ratios of Tandem™ with 43 mM Dox into 25, 10 and 5 mg beads (sample number = 3).

Mass of Tandem™ (mg)	Concentration of Dox (mM)	Injection Number at Point of Bead Saturation	Molar Ratio
25	43	12	0.47:1
10	43	3	1.17:1
5	43	4	2.00:1

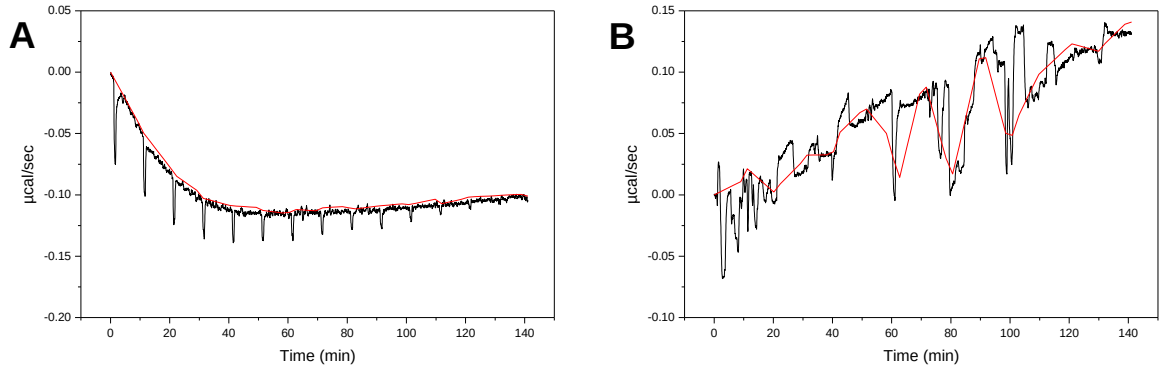

Figure 4.12: Isotherm of water into 100 mg DC Bead LUMI™ (A) and Tandem™ (B).

It was thought possible that the interaction of Dox with DC Bead LUMI™ and Tandem™ was under the instruments limit of detection, therefore samples were collected after completion of the experiment and the residual, in addition to the extracted solution tested. UV analysis of the residual solution confirmed that there were 3.7564 mg/mL Dox present, and this equates to 91 % of the drug that entered the ITC cell was unbound to the beads. The concentration of drug that had bound to the beads and extracted from them was 0.2378 mg/mL and equates to 6 % of Dox that entered the ITC cell. The extra 3 % was most likely bound to the ITC cell or was lost during collection of the beads. These results imply that only a very small amount of drug had bound to the beads during the experiment.

HepaSphere™ was the fifth and final bead was selected for binding analysis. Unfortunately, no experimental data was obtained for this bead as it was momentarily removed from the test samples. This bead was not inserted into the ITC as the product formed a gel, and it wasn't understood whether the microspheres could be easily removed and whether the syringe would be blocked causing damage to the internal components of the instrument. Preliminary testing to identify bead and instrument preparation is required before this bead can be thermodynamically analysed.

Overall, it was found that bead type does play an influential role in the binding and can be a significant factor in controlling drug-bead binding ratios as well as the kinetic profile obtained.

4.2.3. Effect of Drug Type

In total, four drugs were analysed to investigate the effect of drug choice on binding. For comparison of different drugs into DEBs, 43 mM drug into 100 mg beads was initially chosen as the most suitable concentration and mass. This is because in initial studies it gave the largest signals and best chance to differentiate between similar compounds. DC M1 Bead™ was used in the evaluation of several drugs as this had been studied the most extensively with the ITC in previous work.

One such structurally related drug to Dox is Mit, both contain an anthracene however Dox consists of a 1,4-dihydroxyanthraquinone and Mit a 1,4-dihydroxy-5,8-bisaminoanthraquinone, indicated in Figures 4.13 and 4.14. Mit has four potential basic binding sites, the two that are attached to the aromatic ring can protonate, but the charge is delocalised around the ring structure and hence it is not strong enough to interact with the beads. This is technically there are only 2 possible interactions with Mit and Dox has just the one binding site. The pH of Mit in deionised water was 3.799 and the pH of 100 mg acid washed beads in 1.4194 mL deinoised water was 1.824. Three of the Mit sites are ionised at the pH of the drug with the addition of acid washed beads of ~1.8. At pH 1.8 the ionised sites of Mit would include the strongest base, the group directly opposite and the adjacent basic group the number of ionised sites would consist of 11.57 %, then the strongest base and opposing group were ionised at 88.43 % of formulations. Dox has just one basic site at the pH Dox combined with acid washed beads of ~1.8 and this is 100 % ionised. As the majority of Mit has at least two possible binding sites, only half the concentration of drug should, in theory, be required to create a comparable profile to Dox.

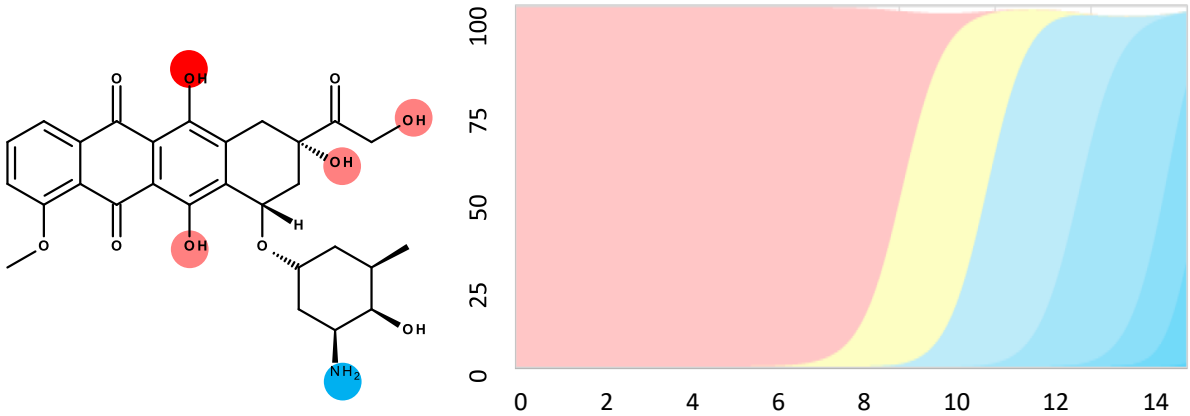

Figure 4.13: Dox chemical structure with ionisation sites (left) and pka graph (right) – red circles indicate an acid whilst blue is a base; the darker shades denote the strongest acid and base [17].

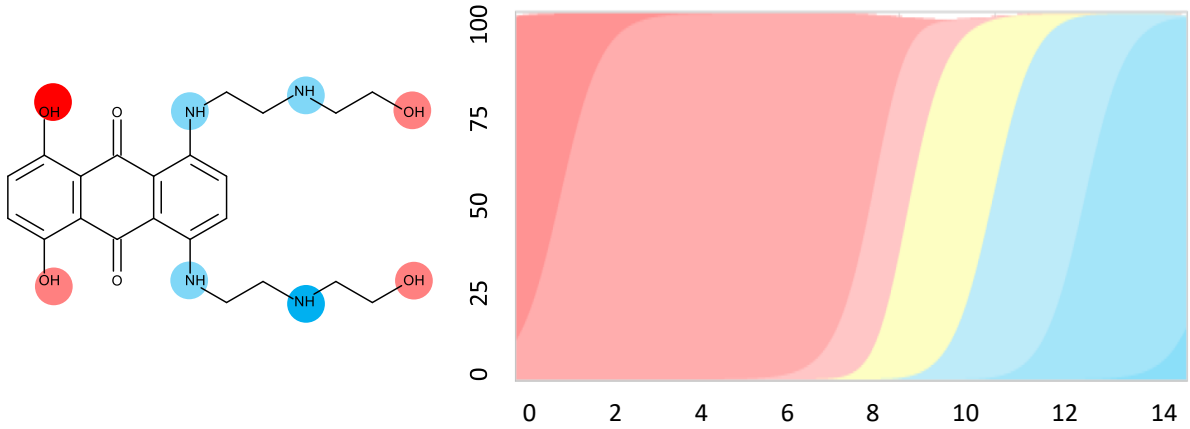

Figure 4.14: Mit chemical structure with ionisation sites (left) and pka graph (right) – red circles indicate an acid whilst blue is a base; the darker shades denote the strongest acid and base [18].

Calorimetric data of both Dox and Mit binding to beads can be seen in Figure 4.15. The Mit-bead graph implies a 0.4:1 ratio, which can also be written as 0.8:2 AMPS to drug sites as there are two Mit sites are involved with binding and the bead has only one site. If the data was considered as the ratio of AMPS to drug rather than drug sites, this could be easier compared with Dox and was calculated as 0.8:1. The ITC results for Mit show that the two sites that are involved with binding are identical, and with half the concentration of drug in comparison with Dox, the isotherm fits a two-site model [19,20]. With two identical sites engaged with binding, this must consist of the strongest base and the opposite basic site. The signal intensity is larger in Mit compared with Dox for the first three injections but is then roughly the same for the rest of the experiment. The isotherm shapes are different as Dox has two distinctive curves in the trace, Mit also has two curves although it is much more discrete. These finding implies Dox-bead binding, in addition to Mit-bead binding consist of a two-step process.

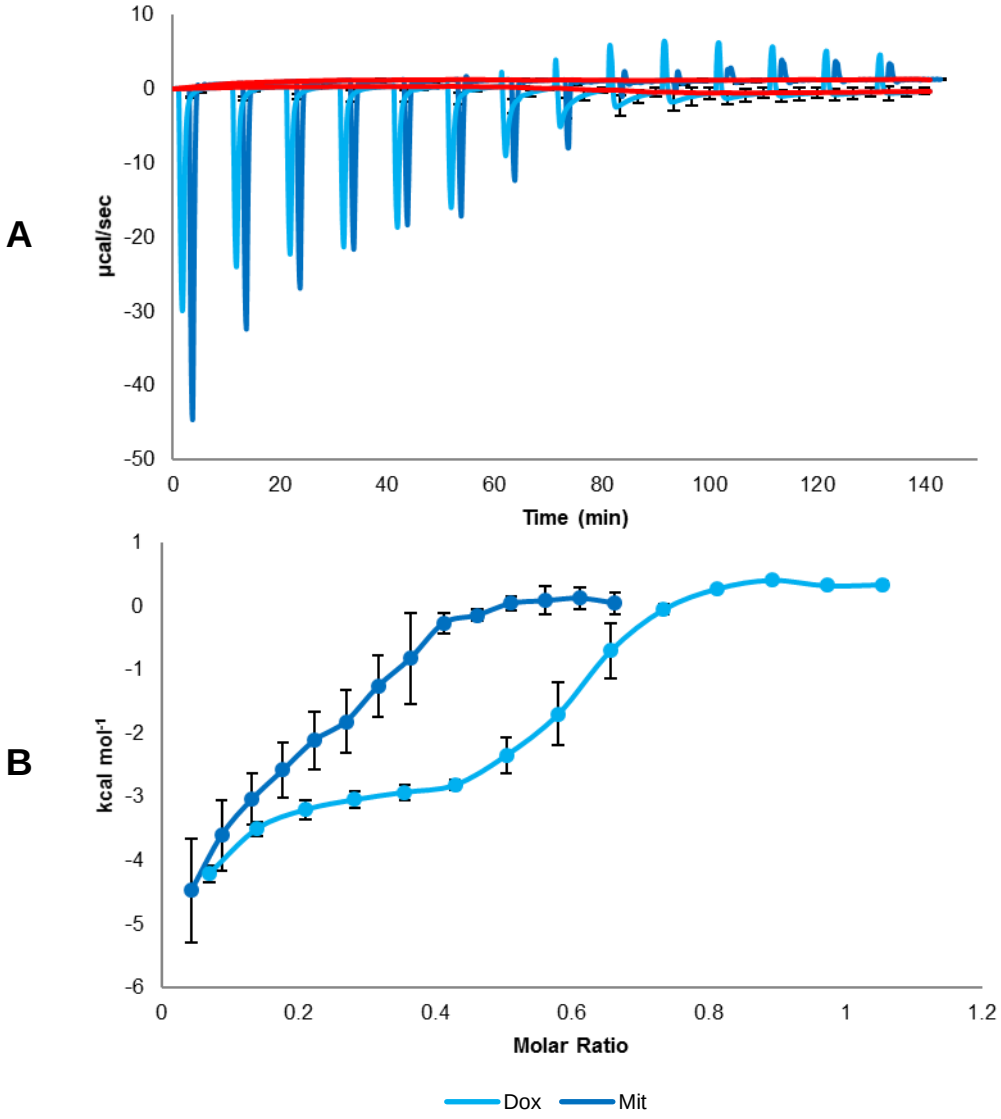

Figure 4.15: Binding of Mit in comparison to Dox with 43 mM Dox and 20 mM Mit to 100 mg beads (sample number = 3, error bars = standard deviation, time has been altered by two minutes for visibility).

A calculation of Mit-AMPS binding sites was performed using the same calculation used for Dox-AMPS, only that the RMM of Dox HCl was substituted with the RMM of Mit HCl which was 517.404 g ($C_{22}H_{30}Cl_2N_4O_6$). With half the concentration of Mit and two binding sites on the drug, a similar ratio is noted to that of Dox in Table 4.22, when comparing the whole Dox structure to individual Mit sites occupied, and this difference was not considered significant ($p = 0.2149$). Comparison of these two drugs is particularly striking, as it displays the considerable difference in binding ratios that can be observed when binding to beads. Furthermore, this result confirms that each Mit molecule can span across two AMPS molecules, therefore double binding is sterically possible.

Table 4.22: Molar ratios of Dox versus Mit with 43 mM Dox and 20 mM Mit into 100 mg beads (sample number = 3, error = standard deviation).

Drug	Dox	Mit (Whole Drug)	Mit (Individual Sites)
Molar Ratio	0.84:1	0.44:1	0.89:1
	1.00:1	0.41:1	0.83:1
	0.92:1	0.41:1	0.81:1
Average	0.92:1 ± 0.08	0.42:1 ± 0.02	0.84:1 ± 0.04

Iri is another drug licenced for use with these types of DEBs. Previous data has shown it is a drug which exhibits a very different elution profile to Dox and it is therefore conceivable that it has a different binding process. The pH of 50 mg acid washed bead in 1.4194 mL of deionised water was 2.175, and the pH of 20 mM Iri in deionised water was 4.325. 20 mM was the chosen concentration as Iri was not soluble at 43 mM (solubility is ~12.5 mg/mL). An experiment was conducted where the pH of acid washed beads was measured with irrigation and the addition of 20 µL Iri every ten minutes to a total of 14 times to replicate conditions inside the ITC. When investigating the pKa values of Iri using Figure 4.16, there were two potential basic binding sites. The results provided in Table 4.23 show that as Iri enters the ITC cell, the pH is forced from 4.3 to 2.0-2.2. At the average experimental pH of 2.1 with Iri in acid washed beads 99.33 % of both sites were ionised in the solution and 0.67 % of the strongest base individually. Since the vast majority of the two sites on Iri were ionised, this creates two potential binding sites.

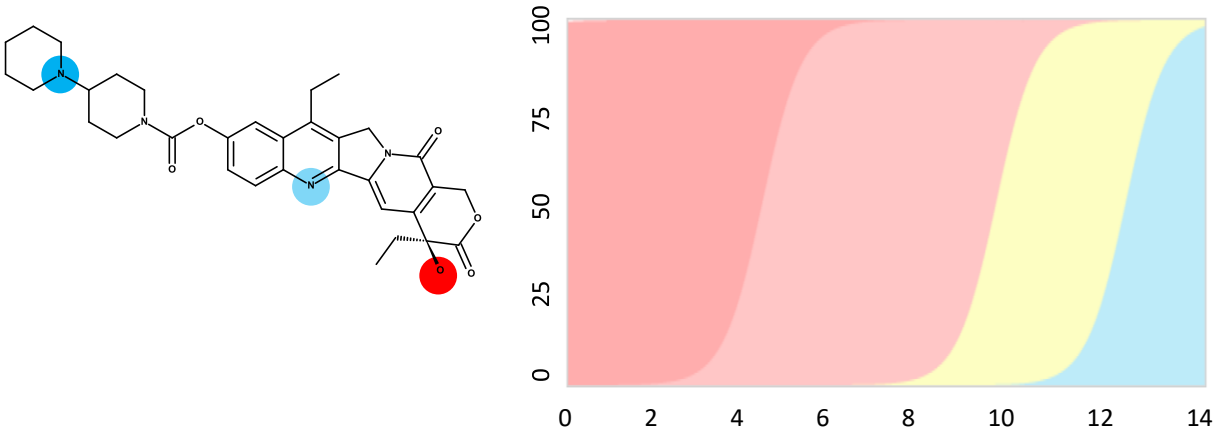

Figure 4.16: Iri chemical structure with ionisation sites (left) and pka graph (right) – red circles indicate an acid whilst blue is a base; the darker shades denote the strongest acid and base [21].

Table 4.23: pH of 20 µL Iri injected 14 times into 50 mg acid washed bead in 1.4194 mL deionised water (sample number = 1).

Injection Number	Volume of Iri in the Beads (µL)	pH
1	20	2.143
2	40	2.157
3	60	2.127
4	80	2.116
5	100	2.086
6	120	2.040
7	140	2.069
8	160	2.022
9	180	2.062
10	200	2.026
11	220	2.055
12	240	2.128
13	260	2.118
14	280	2.101
Average pH		2.089

Figure 4.17 indicates that Dox and Iri are two compounds that each have a unique way of binding to DEBs, as the shape of the Dox isotherm is completely different to Iri. Another usual phenomenon noticed was the different shape of the raw data of Iri into beads without the subtraction of Iri into water, expressed in Figure 4.18. This is not the effect of an acid base titration, as in another experiment the pH of Iri was adjusted to 2.2 into pH 2.2 beads and the same effect was, displayed in Figure 4.19.

The subtracted drug into water run was not altered in pH as previous data demonstrated an unstable baseline, and it is for this reason that the effect fails to exist after the subtraction. The shape is attributed to a two-site model [19,20], and it is the pH of 2.2 which creates an environment for two binding sites on Iri. It was assumed that Iri had only one binding site for the bead to attach, and this statement is correct in a clinical situation as the pH of beads would not altered, but a new phenomenon was discovered where at a pH of 2.2 the bead bound to two sites at different points of the loading process.

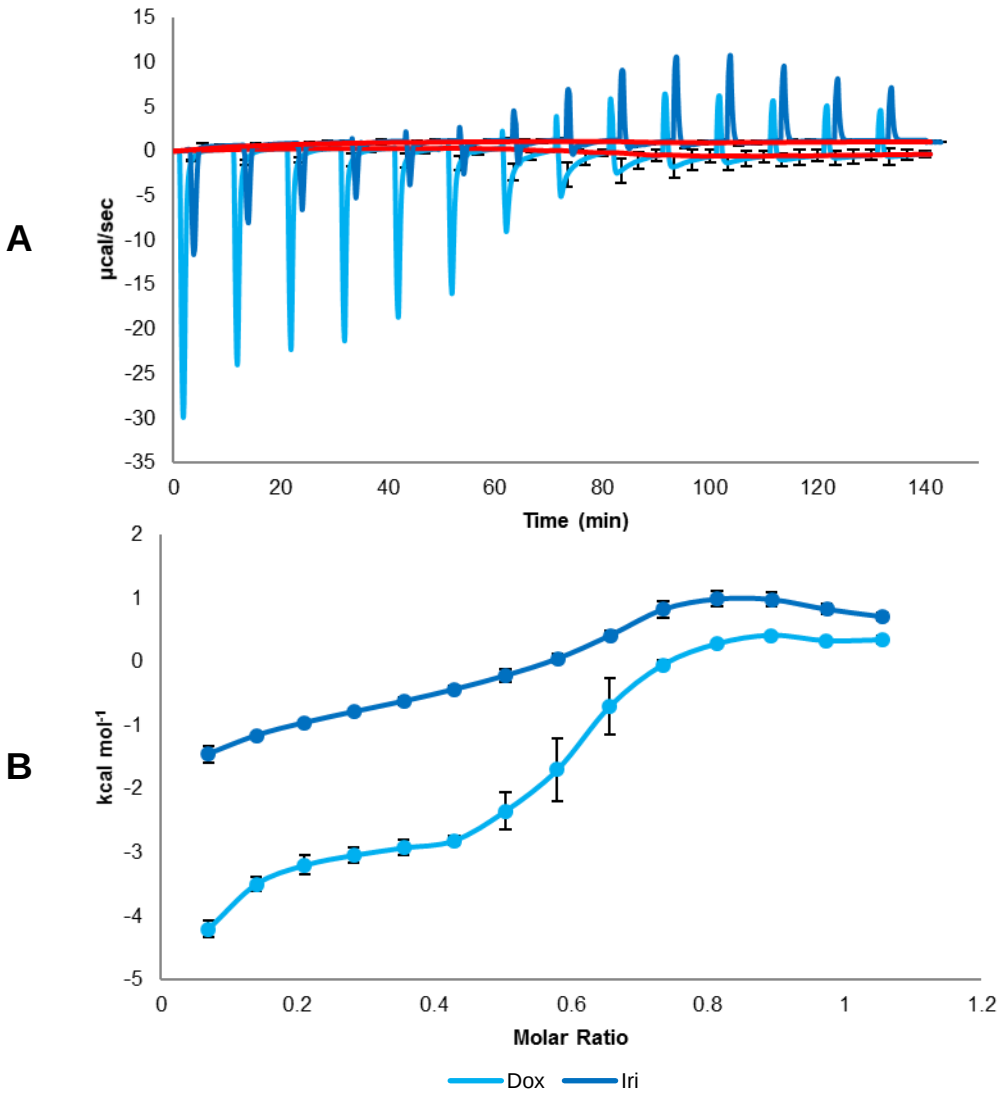

Figure 4.17: Binding of Iri in comparison to Dox with 20 mM drug to 50 mg beads (sample number = 3, error bars = standard deviation, time has been altered by two minutes for visibility) – following subtraction of water dilution data.

The predominant piperidino Iri site is likely to interact with beads during approximately the first four injections, then the quinoline group is involved in roughly the next seven, at the end of the experiment the drug interacts with water once the beads are saturated. Possibly each group binds at different points in the experiment, and it is conceivable that only one drug site is occupied at any one-time because of size constraints. Another explanation is that bead is bound across both sights and flips to one site during the experiment. The switch from one binding site to another cannot be pKa related, as the pH has been shown to stay relatively the same throughout the experiment. The second Iri site binds to nearly twice as many AMPS sites than the first, yet the switch from one site to another is currently unknown.

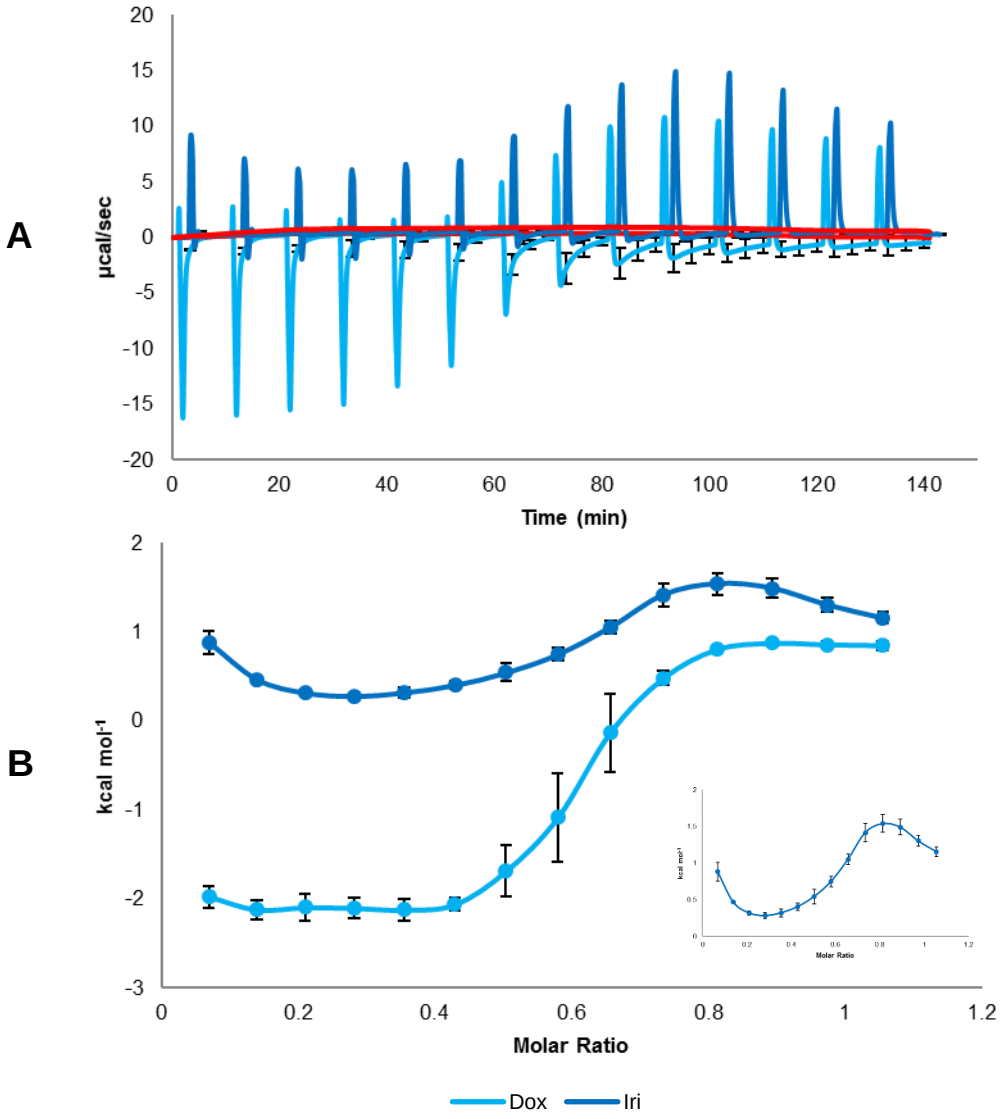

Figure 4.18: Raw binding data of Iri in comparison to Dox with 20 mM drug to 50 mg beads, inset is the Iri raw data on a closer scale (sample number = 3, error bars = standard deviation, time has been altered by two minutes for visibility) – excluding subtraction of water dilution data.

A calculation of Iri-AMPS binding sites was performed using the same calculation used for Dox-AMPS, only that the RMM of Dox HCl was substituted with the RMM of Iri HCl which was 623.147 g ($C_{33}H_{39}ClN_4O_6$). The ratio shows that AMPS are bounds only one site per Iri molecule, demonstrated in Table 4.24, and the ratios of Dox and Iri are not considered to be statistically significant (p = 0.1268).

Table 4.24: Molar ratios of Dox versus Iri with 20 mM drug into 50 mg beads (sample number = 3, error = standard deviation).

Drug	Dox	Iri
Molar Ratio	0.82:1	0.79:1
	0.82:1	0.81:1
	0.83:1	0.73:1
Average	0.80:1 ± 0.00	0.78:1 ± 0.04

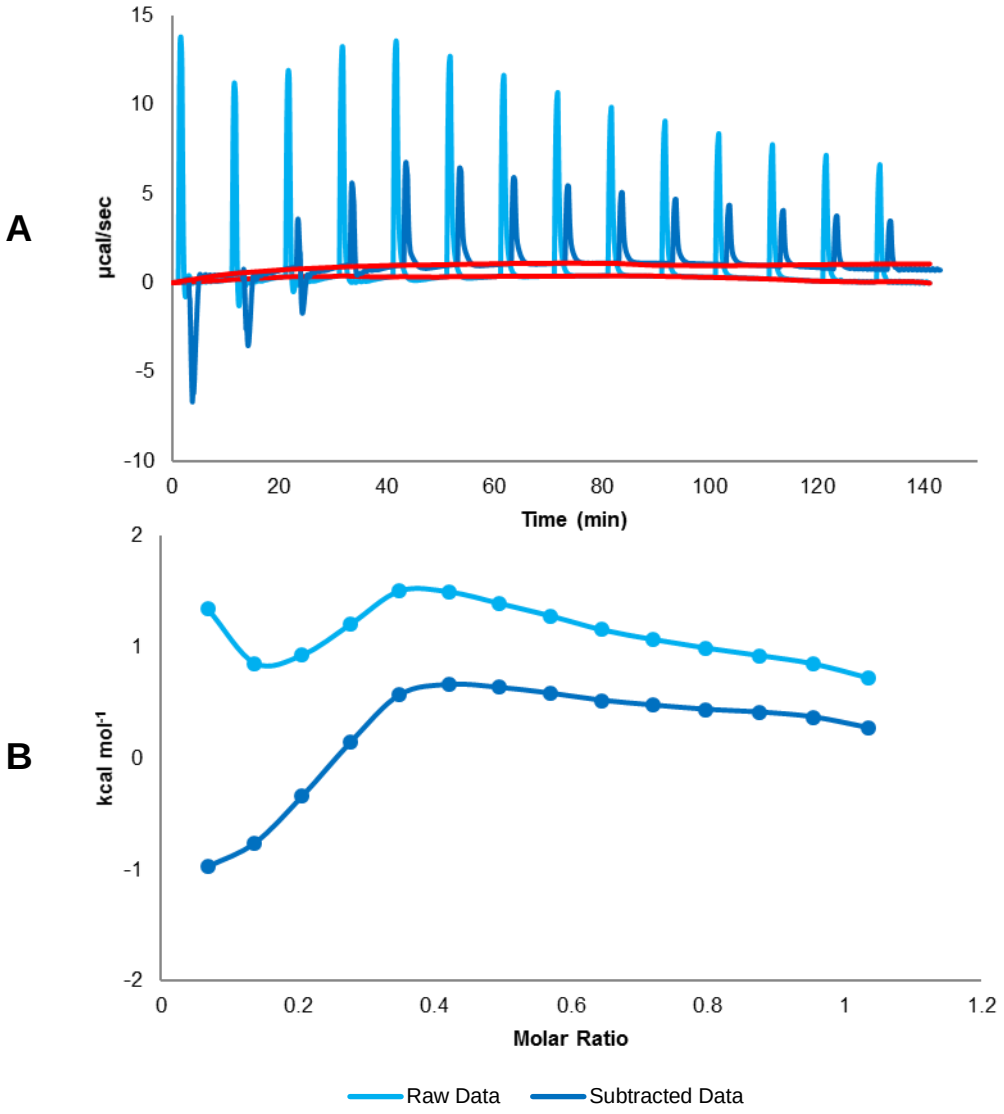

Figure 4.19: Binding of Iri at pH2 and raw data plot at pH 2 with 20 mM drug to 50 mg beads (sample number = 3, error bars = standard deviation, time has been altered by two minutes for visibility).

The final drug to be evaluated was Top. This is a compound similar in nature to Iri, in that there is potential for two-site binding, although there is a different orientation of one of the ionisable groups both include camptothecin. The pH of Top in deionised water was 2.386, and so there were minor changes

when combined with acid washed beads to pH ~2.2. Top has two possible binding sites apparent in Figure 4.20, and at a pH of 2.2 66.19 % of both basic sites are ionised in the formulation, whilst the strongest base in the solution is additionally ionised by 33.7 %.

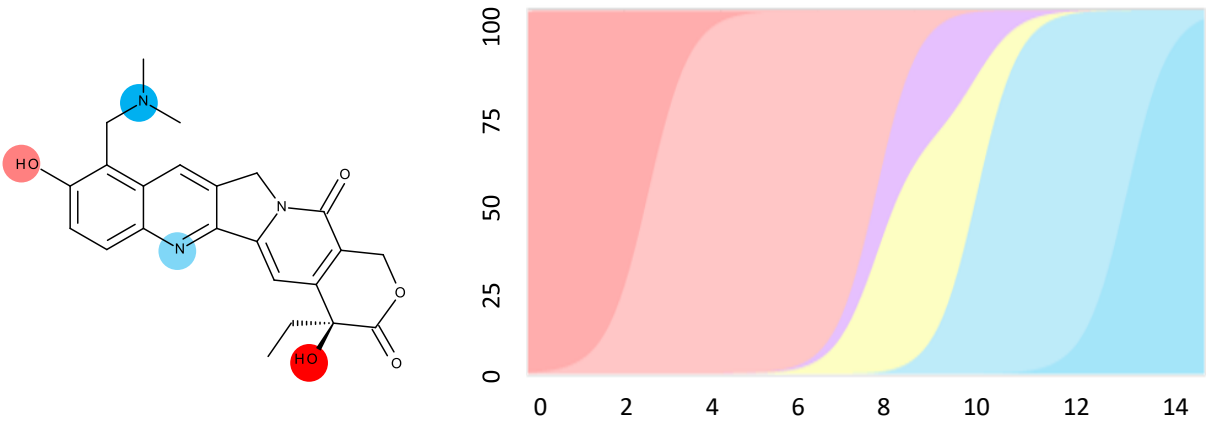

Figure 4.20: Top chemical structure with ionisation sites (left) and pka graph (right) – red circles indicate an acid whilst blue is a base; the darker shades denote the strongest acid and base [22].

Figures 4.21 and 4.22 illustrate the calorimetric data for Top-bead binding. Although the results are similar to Iri, there isn't a significant pH change and so unlike Iri the two-site model is present after the subtraction of Top into water [19,20]. Yet again, the beads bound to one site during approximately the first fours injections of the experiment and the other site in around the next eight injections. The tertiary amine is the strongest ionised group, which binds before the quinolone site. Twice as much Top bound with the second site than the first, and to only one site per drug prior to interaction with water.

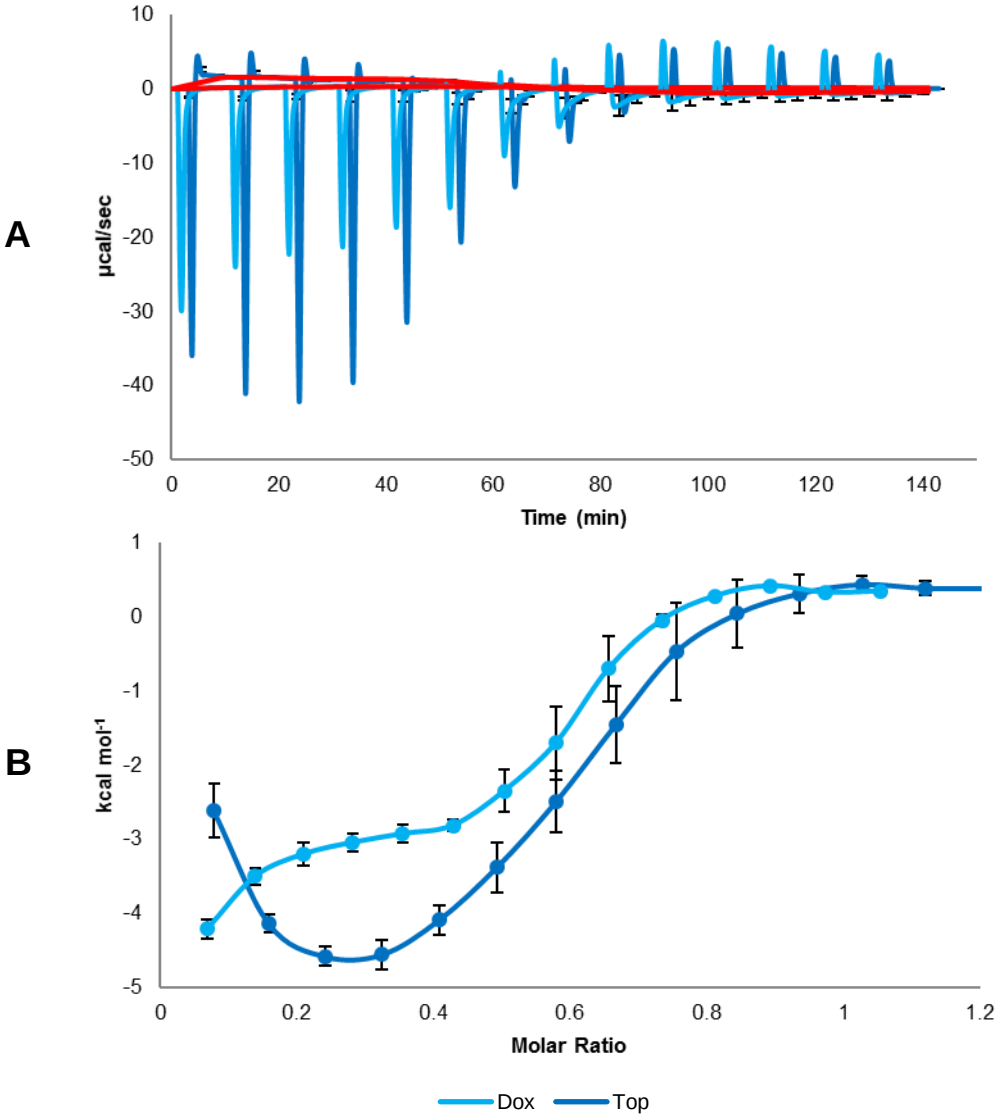

Figure 4.21: Binding of Top in comparison to Dox with 20 mM drug to 50 mg beads (sample number = 3, error bars = standard deviation, time has been altered by two minutes for visibility) – after subtraction of water of dilution data.

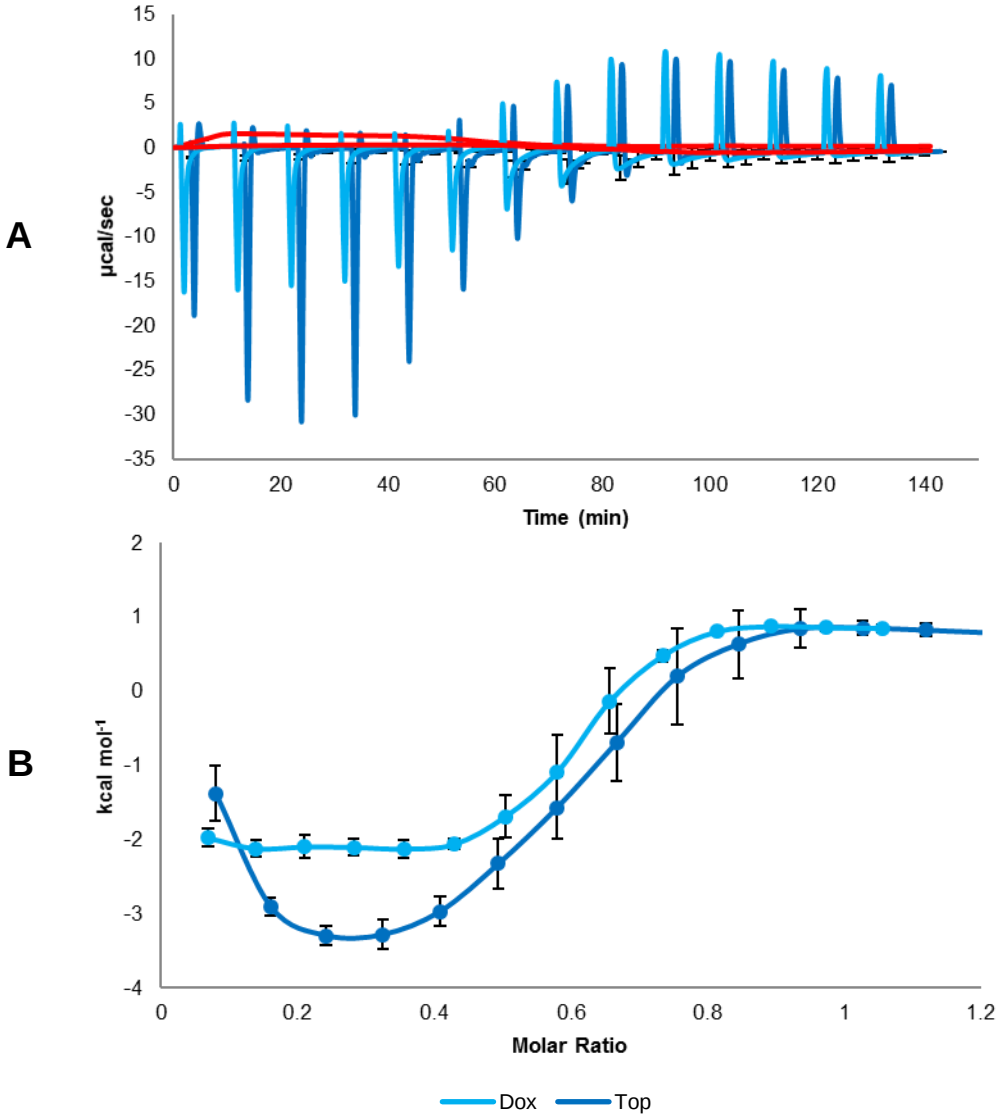

Figure 4.22: Raw binding data of Top in comparison to Dox with 20 mM drug to 50 mg beads (sample number = 3, error bars = standard deviation, time has been altered by two minutes for visibility) – prior to subtraction of water dilution data.

A calculation of Top-AMPS binding sites was performed using the same calculation used for Dox-AMPS, only that the RMM of Dox HCl was substituted with the RMM of Top HCl which was 457.911 g ($C_{23}H_{24}ClN_3O_5$ g). The molar ratio in Table 4.25 reveals that AMPS bound to only one Top site per drug molecule and was considered statistically different from the ratio of Iri ($p = 0.0188$).

Table 4.25: Molar ratios of Iri versus Top with 20 mM drug into 50 mg beads (sample number = 3, error = standard deviation).

Drug	Iri	Top
Molar Ratio	0.79:1	0.97:1
	0.81:1	0.87:1
	0.73:1	0.92:1
Average	0.78:1 ± 0.04	0.92:1 ± 0.05)

In summary, it would appear that Top, even with two binding sites, was only able to bind one AMPS site per drug molecule, as was the case for Dox and Iri yet not for Mit. Overall, each compound expressed an exothermic response with a negative change in enthalpy. Dox and Top have the highest molar ratio, whilst Iri has the smallest. Dox, Iri and Top were identified in Figure 4.23 to be spontaneous processes at all temperatures, where Mit was the anomalous compound as it was discovered in Figure 4.24 to only be spontaneous at low temperatures. Positive values for changes in entropy with Dox, Iri and Top signify that entropy increases as the reaction proceeds and decreases for Mit as the system becomes more ordered. Iri has the greatest change in entropy and so the most disordered system. Dox-bead, Iri-bead and Top-bead are entropically and enthalpically driven processes, whereas Mit-bead is enthalpically driven. Therefore, Dox-bead, Iri-bead and Top-bead contain hydrogen bonds, electrostatic or van der Waals interactions with hydrophobic interactions, while in Mit-bead the driving forces are limited to hydrogen bonds, electrostatic or van der Waals interactions. The change in Gibbs free energy is negative for Dox, Iri and Top and so binding is spontaneous, yet since it is positive for Mit it appears non-spontaneous. This is of thermodynamically interest as Mit was the only drug capable of displaying a double binding phenomenon. Although this finding is unusual (and non-spontaneous reaction would imply binding could not occur) it can be explained by solvent effects and a comparatively small change in entropy and free energy where there could be erroneous measurements.

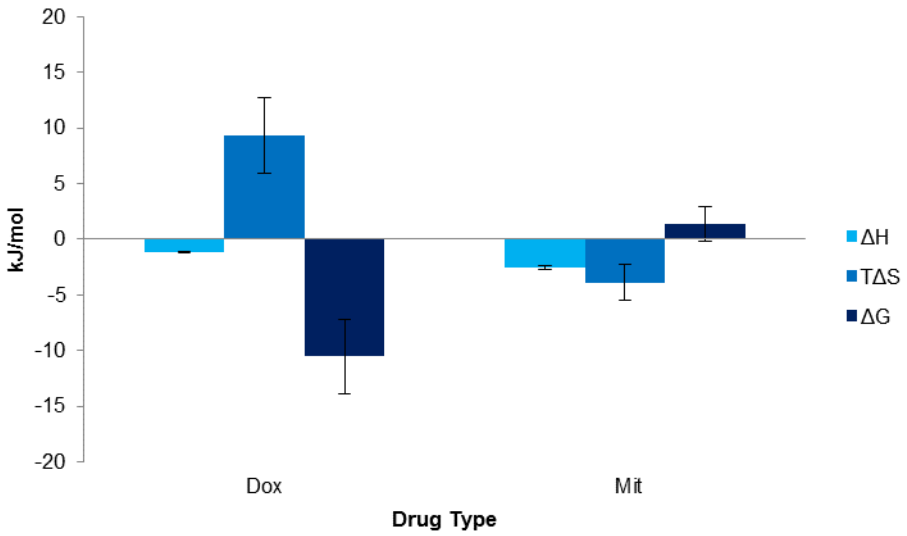

Figure 4.23: Thermodynamics of 43 mM Dox and 20 mM Mit into DC Bead™ (sample number = 3).

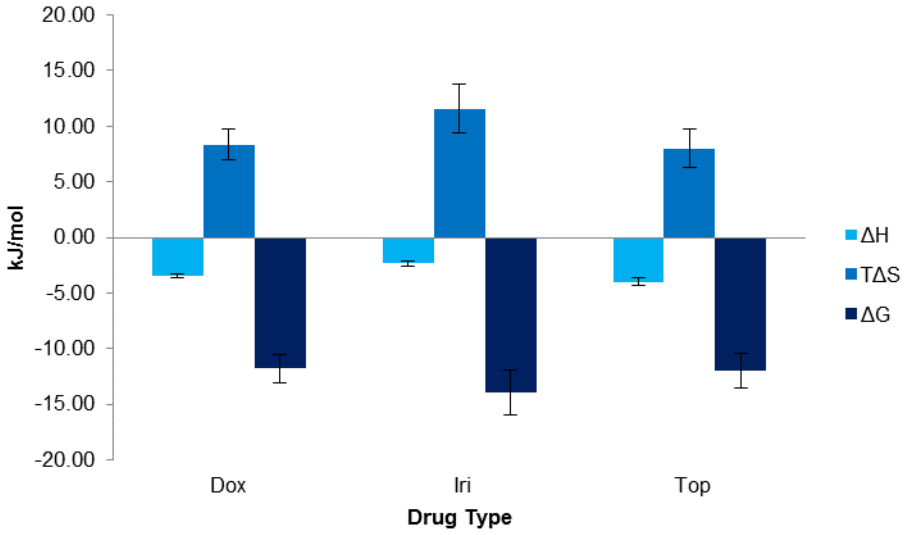

Figure 4.24: Thermodynamics of 20 mM Dox, 20 mM Iri and 20 mM Top into DC Bead™ (sample number = 3).

4.3. Conclusion

ITC data produced varying molar ratios for the different bead sizes of DC Bead™. As the shape of the isotherm changed for the lager beads, this could signify that the beads were unable to partake in complete binding. It is possible that sodium ions were not entirely removed from the larger beads, as this would take longer due to the surface area. Further work could be done to ascertain the level of sodium ions that effect drug binding. A slight improvement was observed when the beads were washed for longer, but the ratio diminished after a certain point. The inefficient removal of salt is well-known to inhibit the binding process. SIM experiments also suggested that the larger beads bound to less drug, as there was a decrease in the heat released with an increase in bead size, and this would coincide with a reduction in binding. An improved method to remove salt from the beads is crucial.

It is possible to use the ITC and the methods of this study to differentiate between different types beads, such as DC Bead™ and LifePearl™. There are various similarities between PVA and PEG beads such hydrophilicity, compressibility and elasticity [23,24]. Like DC Bead™, LifePearl™ bindings to Dox via a sulfonate group, except that the publicised activate site is SPA instead of AMPS. It is to no surprise that these two bead types behave similarly but differences could arise from the scale of hydrophilicity, compressibility and elasticity, including the strength and capacity of the binding site. The technology behind DC Bead LUMI™ and Tandem™ differs such as the iodinated group, however some physical properties are similar such as increased solid content and reduced compressibility. This suggests there may be a diffusion effect necessary for ITC methodology, and that the slow binding process to these beads may be outside the instruments limit of detection. It is also a possibility that sodium inhibits binding to Dox with water washed beads, and that acidified DC Bead LUMI™ and Tandem™ could lead to the formation of a hydrogen bond which cannot be substituted for Dox [25,26]. Similar to DC Bead LUMI™, Tandem™ is a product of high solid content which changes little in size after loading by < 5 % [12], whereby DC Bead™ reduces in size by what is said to be ≤ 20 % [13,14]. This shows that these two products have very different shrinking and swelling properties which match among DC Bead™ and LifePearl™, and amid DC Bead LUMI™ and Tandem™, perhaps grouping these devices with the ITC data.

Four different chemotherapeutic compounds produced thermodynamic data displaying one and two-site binding models. Mit bound to twice as many AMPS sites compared with Dox as it has two loading locations. Iri and Top bound to two sites in an overall 1:1 ratio, possibly one site was involved with the first portion of the experiment and another in the second section. Two-site binding to non-

identical sites occurred when the compounds were approximately pH 2. Top was originally this pH and Iri was altered due to pH of acid washed beads. Iri loaded beads would not bind to two different sites when prepared for use on a patient as the beads in this situation do not require acid washing, however Top loaded beads would bind using two sites even when if prepared for a patient using manufacturer loading instructions, as the drug is already at the pH were this binding phenomenon occurs.

In summary, ITC has been shown to be an effective analytical technique to acquire thermodynamic data relating to drug-bead binding with respect to bead type and drug choice, a synopsis of this data can be found in Tables 4.26 and 4.27.

Table 4.26: Comparison of bead type thermodynamic data and drug capacity calculated with elemental analysis equation (sample number = 3, error = standard deviation).

Bead Type and Size	**Molar Ratio**	**ΔH (kJ/mol)**	**$T\Delta S$ (kJ/mol.K)**	**ΔG (kJ/mol)**	**Dox Loading Capacity (mg/mL)**
DC Bead™ (70-150)	0.92:1 ± 0.08	-1.18 ± 0.08	9.36 ± 3.42	-10.54 ± 3.36	57.50
LifePearl™ (75-125 µm)	0.74:1 ± 0.04	-1.52 ± 0.01	3.07 ± 1.08	-4.60 ± 1.08	53.37
DC Bead LUMI™ (70-150)	Insufficient Data				179.05
Tandem™ (75-125 µm)	Insufficient Data				46.81

Table 4.27: Comparison of drug type thermodynamic data and DC Bead™ loading capacity calculated with elemental analysis equation. *Mit bound with two sites and molar ratio to individual sites was 0.84:1 ± 0.04 (sample number = 3, error = standard deviation).

Drug Compound	**Molar Ratio**	**ΔH (kJ/mol)**	**$T\Delta S$ (kJ/mol.K)**	**ΔG (kJ/mol)**	**DC Bead™ Loading Capacity (mg/mL)**
Dox (43 mM)	0.92:1 ± 0.08	-1.18 ± 0.08	9.36 ± 3.42	-10.54 ± 3.36	57.50
Mit (20 mM)*	0.42:1 ± 0.02	-2.51 ± 0.16	-3.88 ± 1.65	1.37 ± 1.54	24.20
Dox (20 mM)	0.82:1 ± 0.00	-3.49 ± 0.16	8.31 ± 1.39	-11.80 ± 1.24	57.50
Iri (20 mM)	0.78:1 ± 0.04	-2.43 ± 0.22	11.57 ± 2.20	-13.91 ± 2.02	58.29
Top (20 mM)	0.92 ± 0.05	-4.00 ± 0.36	7.99 ± 1.73	-11.98 ± 1.51	42.84

References

1 BTG, DC Bead™ and DC BeadM1™ loading instructions, http://bead.btg-im.com/uploads/document_r/Loading Instructions Folder v4 web DEBDOX.pdf, (accessed 1 October 2017).

2 T. Swaine, Y. Tang, P. Garcia, J. John, L. J. Waters and A. L. Lewis, Evaluation of ion exchange processes in drug-eluting embolization beads by use of an improved flow-through elution method, *Eur. J. Pharm. Sci.*, 2016, **93**, 351–359.

3 M. V. G. Fajardo, University of Brighton, 2006.

4 R. R. Taylor, Y. Tang, M. V. Gonzalez, P. W. Stratford and A. L. Lewis, Irinotecan drug eluting beads for use in chemoembolization: In vitro and in vivo evaluation of drug release properties, *Eur. J. Pharm. Sci.*, 2007, **30**, 7–14.

5 A. L. Lewis, M. V. Gonzalez, S. W. Leppard, J. E. Brown, P. W. Stratford, G. J. Phillips and A. W. Lloyd, Doxorubicin eluting beads − 1: Effects of drug loading on bead characteristics and drug distribution, *J. Mater. Sci. Mater. Med.*, 2007, **18**, 1691–1699.

6 M. V. Gonzalez, Y. Tang, G. J. Phillips, A. W. Lloyd, B. Hall, P. W. Stratford and A. L. Lewis, Doxorubicin eluting beads - 2: methods for evaluating drug elution and in-vitro:in-vivo correlation, *J. Mater. Sci. Mater. Med.*, 2008, **19**, 767–775.

7 K. Ashrafi, Y. Tang, H. Britton, O. Domenge, D. Blino, A. J. Bushby, K. Shuturminska, M. den Hartog, A. Radaelli, A. H. Negussie, A. S. Mikhail, D. L. Woods, V. Krishnasamy, E. B. Levy, B. J. Wood, S. L. Willis, M. R. Dreher and A. L. Lewis, Characterization of a novel intrinsically radiopaque Drug-eluting Bead for image-guided therapy: DC Bead LUMI, *J. Control. Release*, 2017, **250**, 36–47.

8 T. de Baere, S. Plotkin, R. Yu, A. Sutter, Y. Wu and G. M. Cruise, An In Vitro Evaluation of Four Types of Drug-Eluting Microspheres Loaded with Doxorubicin, *J. Vasc. Interv. Radiol.*, 2016, **27**, 1425–1431.

9 BTG, DC Bead™ FAQs, http://bead.btg-im.com/products/uk-322/dcbead-3/debdox-dc-bead, (accessed 1 October 2017).

10 BTG, DC Bead LUMI™ FAQs, https://www.btg-im.com/en-CA/DC-Bead-LUMI/About/FAQ-s, (accessed 1 October 2017).

11 S. Anandhan and S. Bandyopadhyay, *Advances in Polymer Materials and Technology*, 2016.

12 CeloNova, Embozene Tandem™ (Microspheres for Embolization), http://tecnicasintervencionistas.com/presentacion_cursos/PRESENTACION TANDEM.pdf, (accessed 1 October 2017).

13 K. Hong, A. Khwaja, E. Liapi, M. S Torbenson, C. S Georgiades and J.-F. H Geschwind, New Intra-arterial Drug Delivery System for the Treatment of Liver Cancer: Preclinical Assessment in a Rabbit Model of Liver Cancer, *Clin. Cancer Res.*, 2006, **12**, 2563–2567.

14 A. Lewis, M. González, A. Lloyd, B. Hall, Y. Tang, S. Willis, S. Leppard, L. C Wolfenden, R. R Palmer and P. Stratford, DC Bead: In Vitro Characterization of a Drug-delivery Device for Transarterial Chemoembolization, *J. Vasc. Interv. Radiol.*, 2006, **17**, 335–342.

15 Merit Medical, HepaSpheres™ Microspheres Information, https://www.merit.com/interventional-oncology-spine/embolotherapy/hepatic-oncology/hepasphere-microspheres/, (accessed 1 October 2017).

16 Merit Medical, HepaSphere™ Microspheres instructions for use - 2, https://meritemea.com/wp-content/uploads/2013/11/730142001-001.pdf, (accessed 1 October 2017).

17 ACD/I-Lab, Doxorubicin pKa, https://ilab.acdlabs.com/iLab2/index.php, (accessed 1 October 2017).

18 ACD/I-Lab, Mitoxantrone pKa, https://ilab.acdlabs.com/iLab2/index., (accessed 1 October 2017).

19 V. H. Le, R. Buscaglia, J. B. Chaires and E. A. Lewis, Modeling complex equilibria in isothermal titration calorimetry experiments: Thermodynamic parameters estimation for a three-binding-site model, *Anal. Biochem.*, 2013, **434**, 233–241.

20 S. L. Reichow, D. M. Clemens, J. A. Freites, K. L. Németh-Cahalan, M. Heyden, D. J. Tobias, J. E. Hall and T. Gonen, Allosteric mechanism of water-channel gating by Ca2+–calmodulin, *Nat. Struct. &Amp; Mol. Biol.*, 2013, **20**, 1085.

21 ACD/I-Lab, Irinotecan pKa, https://ilab.acdlabs.com/iLab2/index., (accessed 1 October 2017).

22 ACD/I-Lab, Topotecan pKa, https://ilab.acdlabs.com/iLab2/index., (accessed 1 October 2017).

23 BTG, DC Bead™ instructions for use, http://bead.btg-im.com/uploads/document_r/DCB(R) IFU English_CN00103.4CN000164.1 dox irino.pdf, (accessed 1 October 2017).

24 Terumo, LifePearl™ Microspheres, http://www.terumo-europe.com/en-emea/interventional-oncology/loco-regional-treatment/drug-elutable-microspheres-tace/lifepearl®-microspheres, (accessed 1 October 2017).

25 Gaurav Raval, University of Toronto, 2012.

26 Y. Tian, K. Tam, T. Hatton and L. Bromberg, Titration Microcalorimetry Study: Interaction of Drug and Ionic Microgel System, *J. Control. Release*.

Chapter 5 : Method Development of Drug-Bead Elution Characteristics using a Method of Open-Loop Flow-Through Elution

5.1. Introduction

A method was developed for evaluating drug release behaviour of drug-eluting beads (DEBs). Previous methods such as United States Pharmacopeia (USP) 2, USP 4 and the T-apparatus have proved useful for quality control, however have limitations for method development when analysing the different compositions of DEBs and are inappropriate for long-term *in vivo* correlations [1,2].

The improved method consisted of an open-loop flow-through system, whereby elutant was passed through drug loaded beads under a controlled flow rate and was able to extract drug from the beads, this flowed to an ultraviolet-visible (UV-Vis) detector and then was collected into waste with fresh elutant going through the beads. The elution medium must be replaced to prevent saturation of the drug and an underestimation of drug release. The majority of work thus far has been completed on DC Bead™, and so this device in particular size 103 (100-300 µm) as it is the most commonly use in the clinic, was chosen for development experiments. The binding and release of drug to and from DC Bead™ is through an ion-exchange mechanism, therefore in the elution experiments the medium must contain ions for the process to occur. The solution in the majority of these experiments was phosphate buffered saline (PBS), until the concentration and type of eluent was investigated. Unlike the previously discussed methods, beads were packed in an occlusive mass to emulate the embolisation of a vessel, which is closer to the in vivo situation than that of existing methods. The USP 2 instrument immerses the device allowing particles to float in a liquid phase usually with stirring allow particulates to circulate the system depending on particle size and density, resulting in an overestimation of drug release and compromises the reproducibility of the test method. The USP 4 type design hold the particles with a support matrix such as a bed of sand or glass beads, but the method led to in incomplete drug elution.

Sand was eliminated from the selection of packing materials as it was established an unsuitable material for the method. Glass beads were mixed with DEBs in order to improve reproducibility by compensating for swelling phenomena. The effects of different glass bead ratios (1:0, 1:3 and 1:5 DEB:glass bead), the elution flow rate (0.5, 1, 2, 5, 10, 20 and 45 mL/min), ion concentration (77, 154,

231, 308 and 770 mM) type of elution medium (PBS, Ringer's solution, simulated body fluid (SBF)) and bead volume (0.2, 0.5 and 1 mL) was investigated to identify the most suitable method parameters.

The following chapter establishes the method development of elution, specifically for the evaluation of DEBs which overcomes some of the limitations of the previously reported methods, and ascertains the effects of degassing with helium, glass beads, flow rate, salt concentration, eluent type and bead volume. The schematics of the different dissolution apparatus and the experimental set up of elution can be found in Chapters 1 and 2, however Figure 5.1 provides various systems used in the quantification of drug release with UV-Vis spectroscopic analysis.

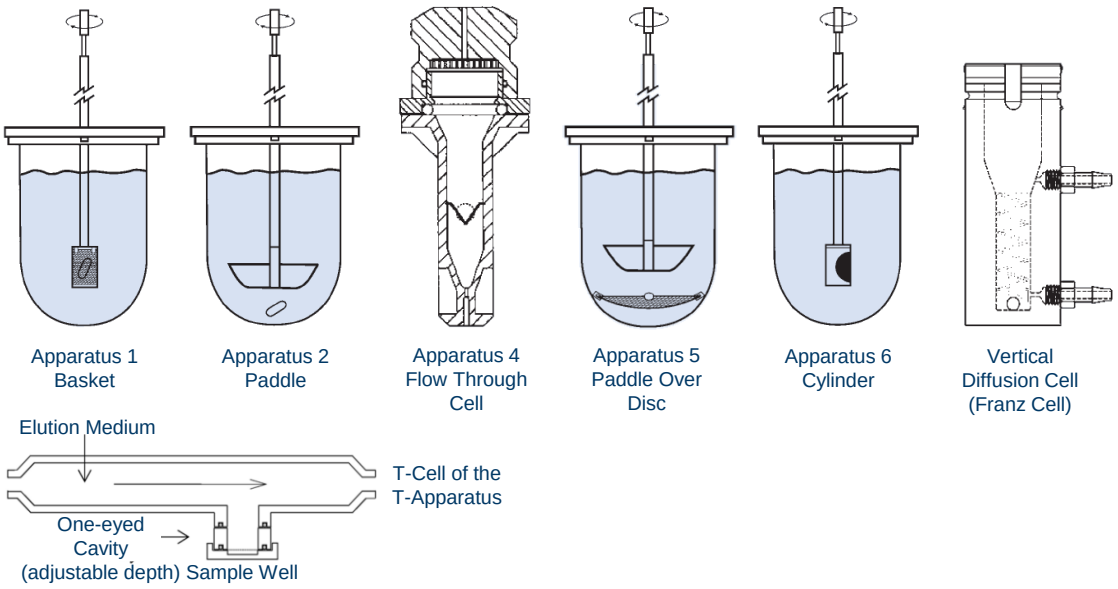

Figure 5.1: 7 types of dissolution apparatus previously used for DEB analysis.

5.2. Results and Discussion

5.2.1. Effect of Packing Material

To calculate the amount of doxorubicin (Dox) eluted, absorbance from each sample was converted into concentration, using standards analysed at the same time with a known concentration of drug. Then the area under the curve (AUC) and accumulative amount of drug was calculated with time and by defining the flow rate throughout the experiment. Three typical elution profiles can be seen in Figure 5.2.

Initially 1 mL of beads were loaded with 37.5 mg/mL Dox, PBS flowed through the elution system to facilitate ion-exchange and remove drug from the beads at a flow rate aimed for 1.3 mL/min. These parameters were selected from previous elution methods.

During method development, experiments were conducted to observe the influence of the use of helium for degassing the eluent. At this stage optimised conditions, such as the use of helium, were fixed to continue evaluation of drug elution from drug eluting beads. Without helium aerated through the PBS solution, air collects around the beads, which eventually travels to the UV-Vis detector causing spikes throughout the elution trace. Another marked effect with air that existed, was that the air bubbles were easily trapped between beads, which cause drug release restriction and nonuniform flow rate.

The swelling of beads produced artifacts and the constant disruption of beads under flow conditions caused an irregular UV-Vis profile, this is evident in Figure 5.2 particularly in sample number 3. A void between the beads and the top filter membrane of ~6 – 7 mm was present to hold the beads in place but allow them to swell without restriction. The filter mesh pore size was small enough to prevent beads from passing through the system, but large enough for solution to flow without constraint. The beads sat in layers on the bottom filter membrane, as the beads eluted drug the size increased, the beads packed tightly against each other and the rate of elution slowed. The bead expanded until the capacity reached a limit, where the beads instantly rearranged into the void provided and a large amount of drug was released as eluent could flow more freely.

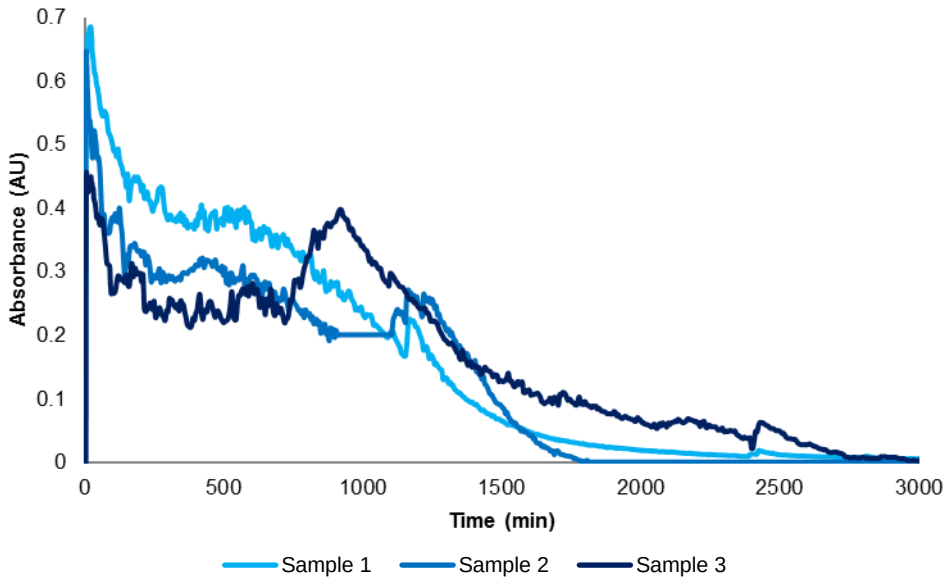

Figure 5.2: Examples of flow-through elution raw data during development of the method. The experiments were conducted using 1 mL 100-300 µm DC Bead™ loaded with 37.5 mg/mL Dox mixed with no glass beads and a flow rate of 1.3 mL/min in PBS (154 mM).

The new elution method mimics embolisation more than the previously published methods, but it is not a replica of a blood vessel. Blood vessels are much smaller than the equipment used in this study, and this many beads would not be packed into one vessel, and so any swelling is reduced and accommodated by the compliance of the vessel, which is softer than the equipment tubing. Therefore, the effects of swelling were to be eliminated in the subsequent study.

To overcome swelling artifacts and fluctuations, the effect of packing DEBs with sand and glass beads was observed. However, acid on the sand and glass seemed to bind some of the drug, as the mixture with DEBs turned them red in colour. This didn't not occur once glass beads were thoroughly washed in deionised water, and so the investigation moved forwards with glass beads at various DEB:glass bead ratios of 1 mL DEB to 0, 3 and 5 mL glass beads. Rather than a void between the DEBs and top filter membrane, the samples that contained glass beads were compressed with the top filter membrane in order to sandwich the bead mixture. The results of packing ratio are highlighted in Figure 5.3 at a flow rate of ~1.3 mL/min. With no glass beads imperfections were visible in the trace, with 3 and 5 mL glass beads the elution profiles were smoother and similar enough to suggest the different amounts do not affect the elution of drug. Although the profiles differ and only two profiles reach ~100 % eluted, the other sample was still steadily increasing and was likely to completely elute. A 1:5 ratio of DEBs to glass beads was selected for further experiments, as this produced reproducible data and a more homogenous distribution of beads. To obtain an accurate calculation of flow rate throughout the

experiment, the mass of solution eluted in 1 min was collected at the beginning, middle and end of each experiment, then an average taken of the three results.

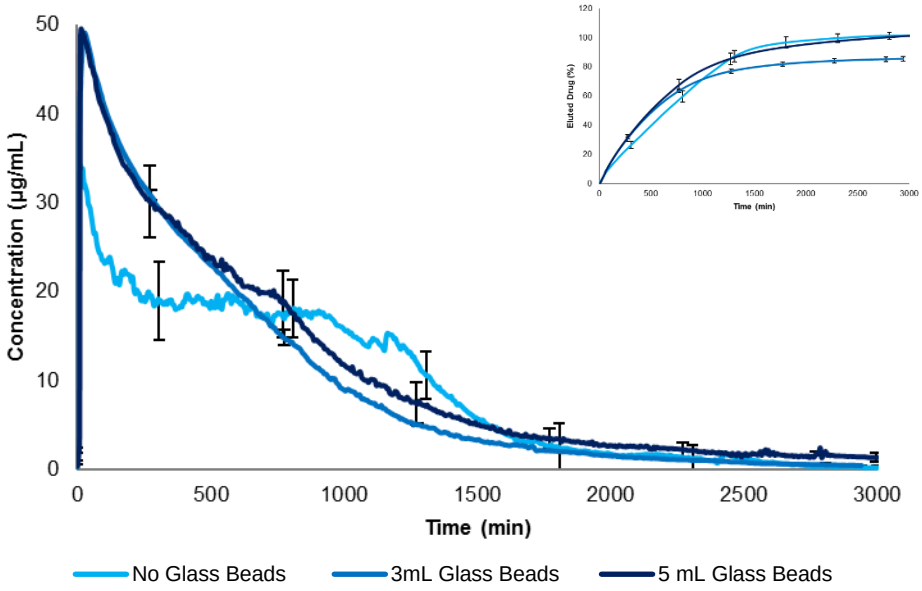

Figure 5.3: Beads mixed with and without glass beads in several ratios. The experiment was conducted using 1 mL 100-300 µm DC Bead™, loaded with 37.5 mg/mL Dox and a flow rate of 1.3 mL/min in PBS (154 mM), inset is the data presented as percent drug eluted instead of concentration (sample number = 3, errors = standard deviation every 100 data points).

The packing study of different DEB:glass bead ratios was repeated at an increased flow rate of 2 mL/min rather than 1.3 mL/min. This was to identify whether the flow rate could be increased and investigate the difference between 3 and 5 mL glass beads in the earlier experiments. Figure 5.4 illustrates that the two preparations containing glass beads elute the drug as a percent in a similar amount of time. The sample containing no glass beads had a slightly slower elution, but more importantly the same imperfections in the smoothness of the curve can be seen. The previously mentioned swelling effect was not visible, possibly due to the increased flow rate which sped up the swelling process. With 3 and 5 mL glass beads and at a flow rate of 2 mL/min, the results were closer than that at 1 mL/min. This is probably a result of better handling experience of the method and again suggested that the two amounts of glass beads do not vastly affect the elution profile. Each sample eluted more than 97 % of the drug.

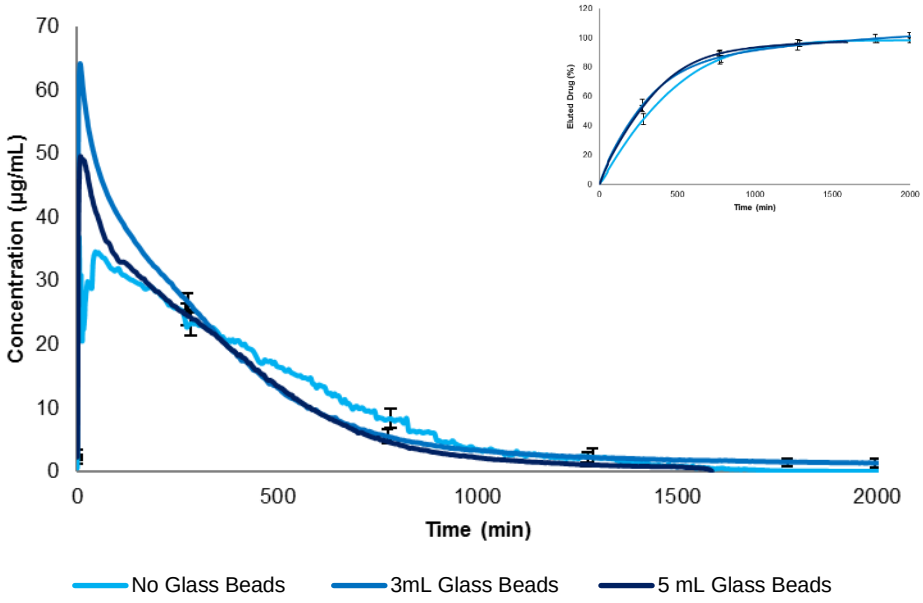

Figure 5.4: Beads mixed with and without glass beads in several ratios. The experiment was conducted using 1 mL 100-300 µm DC Bead™, loaded with 37.5 mg/mL Dox and a flow rate of 2 mL/min in PBS (154 mM) inset is the data presented as percent drug eluted instead of concentration (sample number = 3, errors = standard deviation every 100 data points).

5.2.2. Effect of Flow Rate

The rate of Dox elution from DEBs was determined by eluent flow rate, demonstrated in

Figure 5.5 5.5. A flow rate of 2 mL/min was selected for further studies as it correlated with *in vitro* study data [3]. It was also an advantage to prepare and run an experiment in one day, with 2 mL/min the experiment could be prepared at the start of the working day, initiated with the pump and UV towards the end of the day and the results would be ready at the start of the next morning. At 2 mL/min the trace was not too fast to give a full and complete profile, as the flow rate increased the time for 100 % of the drug to elute decreased, however after 2 mL/min the next result to complete was 45 mL/min. With an increased flow rate, more ions reached the beads quicker and were able to remove the drug from the beads at a faster rate, until an increase in flow rate could not match the rate of diffusion at >5 mL/min. The 5 – 45 mL/min flow rates group together and also required a considerable amount of medium which can be problematic when needing to refill the equipment with an adequate amount of fluid that will last overnight. For a 45 mL/min flow rate that lasted for 500 min, the experiment required at least 22.5 L PBS.

At lower flow rates there was a larger concentration and a slower decrease of drug detected as the samples were less diluted than the faster flows which decreased rapidly in concentration, however

the cumulative amount of drug eluted was smaller at lower flow rates as flow is taken into consideration. The 0.5 mL/min flow rate was run until just over 6800 min where it eluted slightly over 97 % of the drug (data not shown). Each experiment achieved complete or very nearly complete elution of >97 %.

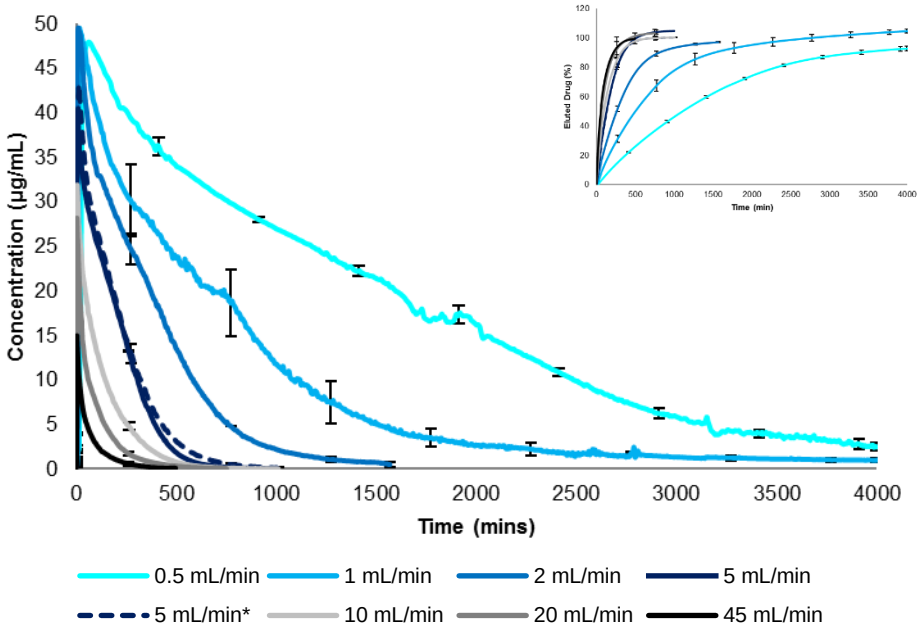

Figure 5.5: Effect of flow rate on Dox elution. The experiments were conducted at 310 K using 1 mL 100-300 µm DC Bead™, loaded with 37.5 mg/mL Dox, mixed with 5 mL glass beads and in PBS (154 mM). Inset is the data presented as the percent of Dox eluted. *Repeat experiment of the 5 mL/min flow rate (sample number = 3, error bars = standard deviation every 100 data points).

Table 5.1 specifies the "pseudo pharmacokinetic" measurements for the flow kinetics such as, C_{max} which is the maximum (peak) concentration, t_{max} which is the time that C_{max} is observed and $t_{50\,\%}$ which is the time taken for 50 % of the drug to be eluted. C_{max} decreased with an increase in flow rate, but reached t_{max} and $t_{50\,\%}$ in a shorter period. At a flow rate of 0.5 mL/min the average highest concentration was 48.33 µg/mL which was achieved at an average of 47.67 min and took an average of 1108.33 min for 50 % of the loaded drug to elute from the beads, whereas at 45 mL/min the highest concentration was 14.92 µg/mL achieved at 3.36 min and took 56.02 min for 50 % to elute. The elution kinetics of flow rate fitted a first order rate law using Equation 5.1, where *k* is the rate constant and *t* is the time.

Equation 5.1: Rate law, where $M_{Drug\ Eluted}$ is the concentration of drug eluted and $M_{Drug\ Loaded}$ is the concentration of drug loaded.

$$\frac{M_{Drug\ Eluted}}{M_{Drug\ Loaded}} = 1 - e^{-kt}$$

Table 5.1: Elution concentration and timings with flow rate. The experiments were conducted at 310 K using 1 mL 100-300 µm DC Bead™, loaded with 37.5 mg/mL Dox, mixed with 5 mL glass beads and in PBS (154 mM) (sample number = 3, error = standard deviation).

Eluent Type	Flow Rate (mL/min)	Salt Concentration (mM)	C_{max} (µg/mL)	t_{max} (min)	$t_{50\ \%}$ (min)	k (x 10^{-3} min^{-1})
PBS	0.5	154	48.33 ± 2.36	47.67 ± 11.02	1108.33 ± 34.04	0.66 ± 0.02
PBS	1	154	49.85 ± 6.50	18.00 ± 6.08	500.33 ± 43.68	1.49 ± 0.16
PBS	2	154	50.78 ± 8.94	11.33 ± 5.77	258.67 ± 12.58	2.78 ± 0.06
PBS	5	154	40.11 ± 3.11	5.34 ± 2.31	131.67 ± 2.89	5.79 ± 0.05
PBS	10	154	32.01 ± 2.11	2.67 ± 0.58	94.00 ± 5.00	7.35 ± 0.66
PBS	20	154	28.77 ± 2.86	3.67 ± 2.08	66.34 ± 8.08	10.52 ± 0.48
PBS	45	154	14.93 ± 0.72	3.36 ± 1.12	56.02 ± 16.55	12.74 ± 1.32

5.2.3. Effect of Salt Concentration

To understand the influence of saline concentration on elution, five specific concentrations of sodium chloride (NaCl) were considered, namely 77 mM (0.45 % w/v), 154 mM (0.9 % w/v), 231 mM (1.35 % w/v), 308 mM (1.8 % w/v) and 770 mM (4.5 % w/v), and release profiles were generated in Figure 5.6. Once more, the 77 mM NaCl experiment lasted until just over 3700 min where it eluted slightly >99 % of the drug (data not shown). Each experiment displayed complete or very nearly complete elution of >97 %. As the concentration of salt increased, more ions exchanged with drug quicker, removing the drug at a faster rate. This occurred until 308 mM where an increase in concentration could no longer impact the diffusion rate. The mass of beads in the experiment was reduced from 1 mL to 0.5 mL to conserve beads, drug and decrease the experimental time with the hope to still produce valid data.

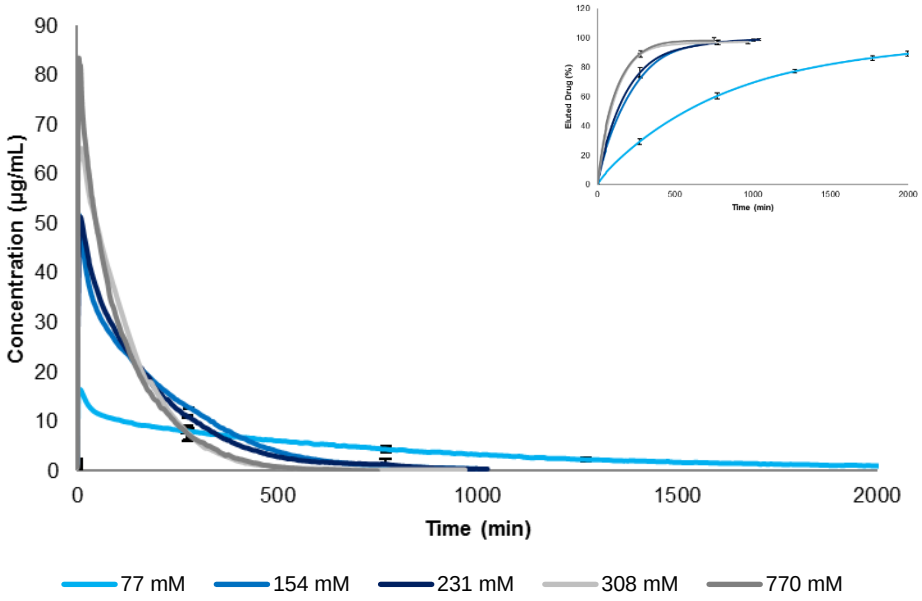

Figure 5.6: Effect of saline concentration on Dox elution. The experiments were conducted at 310 K using 0.5 mL 100-300 µm DC Bead™, loaded with 37.5 mg/mL Dox, mixed with 2.5 mL of glass beads and at a flow rate of 2 mL/min. Inset is the data presented as the percent of Dox eluted (sample number = 3, error bars = standard deviation every 100 data points).

Figure 5.7 was created to compare data in Figure 5.5 and Figure 5.6 of flow rate with fixed salt concentration of 154 mM and salt concentration at a fixed flow rate of 2 mL/min. 77 mM NaCl at a flow rate of 2 mL/min was the closer result to 1 mL/min in PBS (154 mM). 154 and 231 mM at 2 mL/min were most similar to 5 mL/min in PBS (154 mM). 308 and 770 mM at 2 mL/min were closer to the higher flow rates of 10, 20 and 45 mL/min in PBS (154 mM). The two studies followed the same trend, as the samples which completely eluted in ~500 min (5 mL/min, 10 mL/min, 20 mL/min, 45 mL/min, 308 mM and 770 mM) reached a limit in the rate of diffusion. Therefore, it would be advantageous to perform comparative experiments below a flow rate of 5 mL/min and a salt concentration of 308 mM.

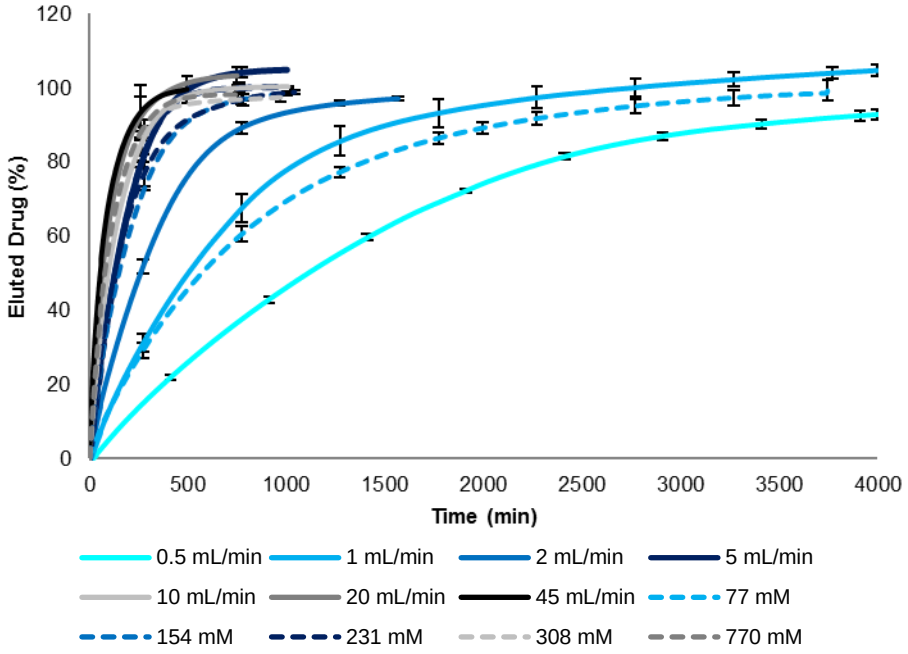

Figure 5.7: Effects of flow rate and saline concentration Vs. time on Dox elution. The flow rate experiments were conducted at 310 K using 1 mL 100-300 µm DC Bead™, loaded with 37.5 mg/mL Dox, mixed with 5 mL glass beads and in PBS (154 mM). *Repeat experiment of the 5 mL/min flow rate. The saline experiments were conducted using 0.5 mL 100-300 µm DC Bead™, loaded with 37.5 mg/mL Dox, mixed with 2.5 mL of glass beads and at a flow rate of 2 mL/min (sample number = 3, error bars = standard deviation every 100 data points). This graph uses data from Figure 5.5 and Figure 5.6.

Although the flow rate study used 1 mL of beads and the salt study used 0.5 mL, the two were analysed as a percent of the eluted drug and are therefore comparable. As hypothesised, an increase in flow rate is equivalent to an increase in salt concentration in this particular elution method and suggests that the same ion-exchange mechanism is in operation. Table 5.2 is a direct comparison of salt levels in the flow rate and salt study, which suggests flow rates of 0.5, 1, 2 and 5 mL/min should respectively correspond to 77, 154, 308 and 770 mM in the salt concentration study. The difference between these two parameters could be attributed to flow rate not being consistent throughout the experiment.

Table 5.2: Comparison of salt levels in the flow rate and salt concentration study.

Flow Rate (mL/min)	Salt Concentration in Flow rate Study (mM/min)	Salt Concentration in Salt Study (mM/min)
0.5	77	77
1	154	154
		231
2	308	308
5	770	770
10	1540	
20	3080	
45	6930	

The pharmacokinetic measurements for salt concentration in Table 5.3 confirms that C_{max} increased with an increase in salt concentration and reached $t_{50\,\%}$ in a shorter period. t_{max} was independent of salt, as more salt eluted the drug from the beads quicker providing higher concentration readings, but the flow rate of each experiment was the same and thus was achieved at approximately the same time. At an NaCl concentration of 77 mM the average highest concentration was 66.74 µg/mL which took an average of 500.22 min for 50 % of the loaded drug to elute from the beads, whereas at 770 mM the highest concentration was 85.70 µg/mL and took 77.65 min for 50 % to elute. 154 mM NaCl correlates well with PBS at the same flow rate, as the two elution solutions have an identical amount of salt. Like flow rate, the effect of salt on the elution kinetics also fitted a first order profile.

Table 5.3: Elution concentration and timings with salt concentration. The experiments were conducted at 310 K using 0.5 mL 100-300 µm DC Bead™, loaded with 37.5 mg/mL Dox, mixed with 2.5 mL glass beads and in PBS (154 mM) (sample number = 3, error = standard deviation).

Eluent Type	Flow Rate (mL/min)	NaCl Concentration (mM)	C_{max} (µg/mL)	t_{max} (min)	$t_{50\,\%}$ (min)	k (x 10^{-3} min^{-1})
PBS	2	77	16.74 ± 2.28	6.67 ± 3.05	500.22 ± 52.68	1.18 ± 0.07
PBS	2	154	51.76 ± 1.25	4.33 ± 1.15	148.33 ± 2.89	4.75 ± 0.09
PBS	2	231	51.38 ± 1.34	8.00 ± 0.00	127.67 ± 7.64	5.26 ± 0.52
PBS	2	308	65.40 ± 3.94	9.00 ± 1.73	85.00 ± 5.00	7.71 ± 0.46
PBS	2	770	85.70 ± 4.84	6.00 ± 2.65	77.65 ± 5.77	8.51 ± 0.34

5.2.4. Effect of Eluent Type

Different types of salt solutions were analysed under elution to identify variations and discover which was most comparable with *in vivo* data. The solutions evaluated in Figure 5.8 were PBS (154 mM [0.9 % salt w/v]), half strength Ringer's solution (42 mM [0.25 % salt w/v]), full strength Ringer's solution (83 mM [0.51 % salt w/v]), double strength Ringer's solution (166 mM [1.01 % salt w/v]), SBF (295 mM [1.9 % salt w/v] adjusted to pH 7.25) and 0.9 % salt w/v SBF (154 mM adjusted to pH 7.25). Composition and preparation of the eluent solutions can be found in Chapter 2.

PBS and 0.9 % SBF have similar elution profiles. This is to no surprise as they both contain the same salt concentration of 154 mM. Interestingly, with double the number of tablets in the Ringer's solution (accordingly to the preparation instructions), there is a decrease in total amount of drug eluted. Neither of the Ringer's solution experiments completely eluted the drug, even when the experiments were extended for ~2000 min (data not shown). The total percent of eluted drug from half strength, full strength and double strength Ringer's solution was 72, 74, and 56 %, respectively. Double strength Ringer's solution contains a similar amount of salts to PBS and 0.9 % SBF, clearly something inhibited the elution process, however this is not yet fully understood. Future work could be completed on individual ions contained in Ringer's solution. Ringer's solution was prepared from Ringer's tablets, which contained sodium chloride, potassium chloride, calcium chloride and sodium bicarbonate. These same components of NaCl, potassium chloride (KCl), calcium chloride ($CaCl_2$) and sodium bicarbonate ($NaHCO_3$) are found in SBF and in similar concentrations in either the full strength or double strength Ringer's solutions, however SBF contains extra chemical elements of potassium phosphate dibasic trihydrate ($K_2HPO_4{\cdot}3H_2O$), magnesium chloride hexahydrate ($MgCl_2{\cdot}6H_2O$), hydrochloric acid (HCl), sodium sulfate (Na_2SO_4) and tris(hydroxymethyl)aminomethane ($(CH_2OH)_3CNH_2$). It is possible that there is competition for certain ions, particularly an affinity for either monovalent, divalent, trivalent or tetravalent ions. PBS and SBF both eluted >99 % of the drug, whilst 0.9 % SBF eluted >91 % but an increase in the elution curve was still visible, therefore it is expected that this sample would have fully eluted if the experiment had not been stopped prematurely.

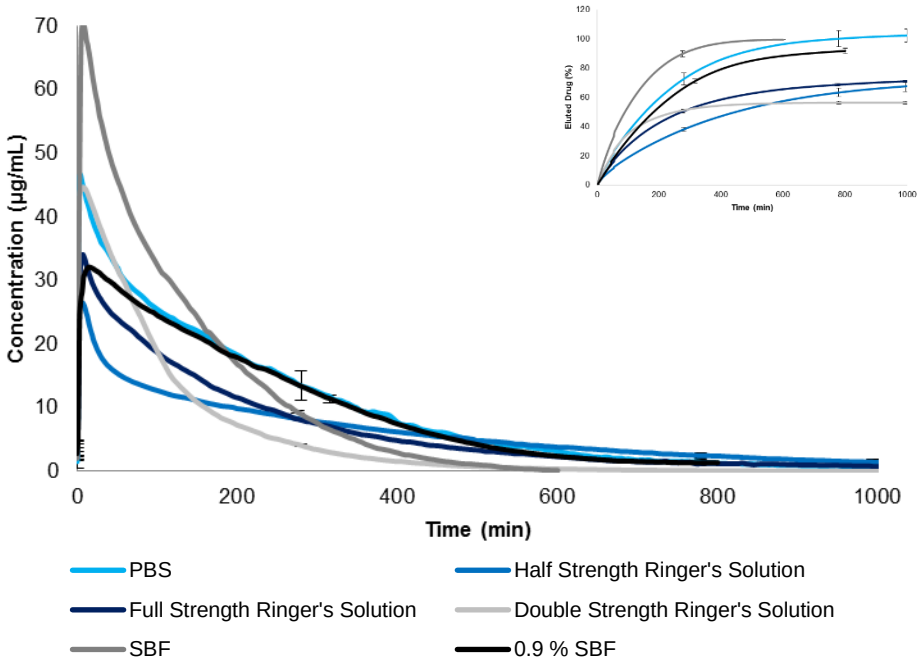

Figure 5.8: Effect of eluent on Dox elution. The experiments were conducted at 310 K using 0.5 mL 100-300 µm DC Bead™, loaded with 37.5 mg/mL Dox, mixed with a 1:5 ratio of DEBs to glass beads and a flow rate 2 mL/min. Inset is the data presented as the percent of Dox eluted (sample number = 3, error bars = standard deviation every 100 data points).

Figure 5.9 was created to compare data in Figure 5.6 and Figure 5.8 of salt concentration and eluent type. 154 mM NaCl was found equivalent to the experiment conducted in PBS, PBS also contains 154 mM salts and so comparable results were expected. The SBF results were similar to 308 and 770 mM NaCl, displaying that the concentration of SBF, as with 308 and 770 mM NaCl, produced a higher rate of diffusion. 77 mM NaCl corresponds closely to the concentration of salt in the half strength Ringer's solution at 42 mM, however the results were vastly different. This is further evidence that a component of the Ringer's solution was preventing elution of drug from the beads.

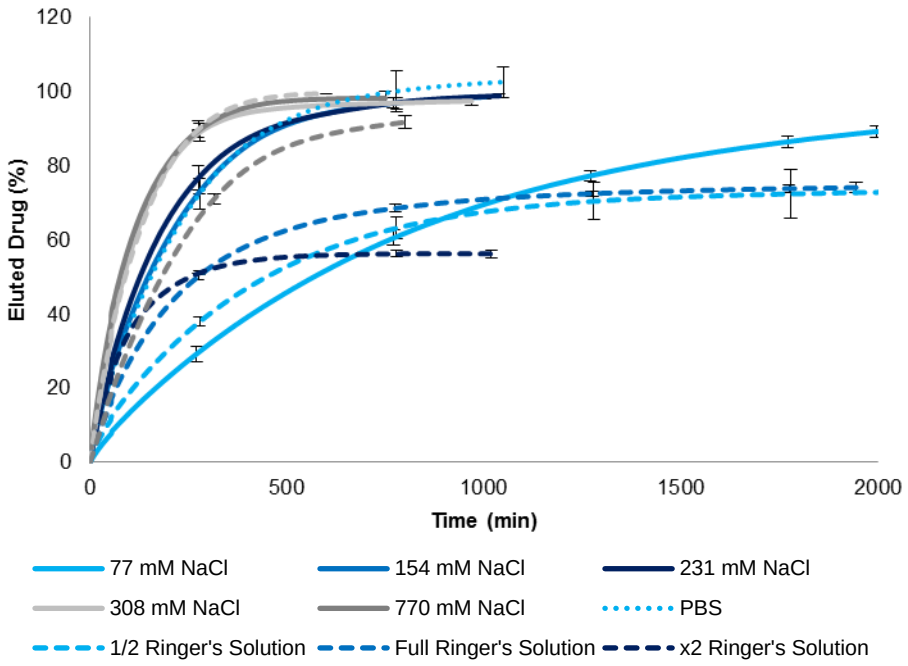

Figure 5.9: Eluent solution comparison. The experiments were conducted at 310 K using 0.5 mL 100-300 µm DC Bead™, loaded with 37.5 mg/mL Dox, mixed with a 1:5 ratio of DEBs to glass beads and a flow rate 2 mL/min (sample number = 3, error bars = standard deviation every 100 data points). This graph uses data from Figure 5.6 and Figure 5.8.

It is possible that calcium in Ringer's solution interacts with Dox, as Dox complexes with alkaline earth metals like calcium (Ca^{2+}), magnesium (Mg^{2+}), poor metals like zinc (Zn^{2+}) [4] and transition metals like manganese (Mn^{2+}) and iron (Fe^{2+}) [5]. An experiment was conducted were a UV-Vis scan of 0.5 mg/mL Dox in deionised water was obtained and compared with 0.5 mg/mL Dox in 0.9% (w/v) calcium chloride hexahydrate ($CaCl_2.6H_2O$). The absorbance of Dox was greater with calcium ions than without, suggesting that upon intercalation a hyperchromic effect and bathochromic shift occurred due to calcium complexation with Dox, causing structural changes as proposed in Figure 5.10 [6], which could limit Dox elution with Ringer's solution. In Figure 5.11 absorbance increased from ~0.6 to ~0.8 AU and λ_{max} shifted from ~480 to ~500 nm with the addition of $CaCl_2.6H_2O$, perhaps an extra component of SBF prevents Ca^{2+} binding to Dox as complete elution was achieved with this type of eluent solution.

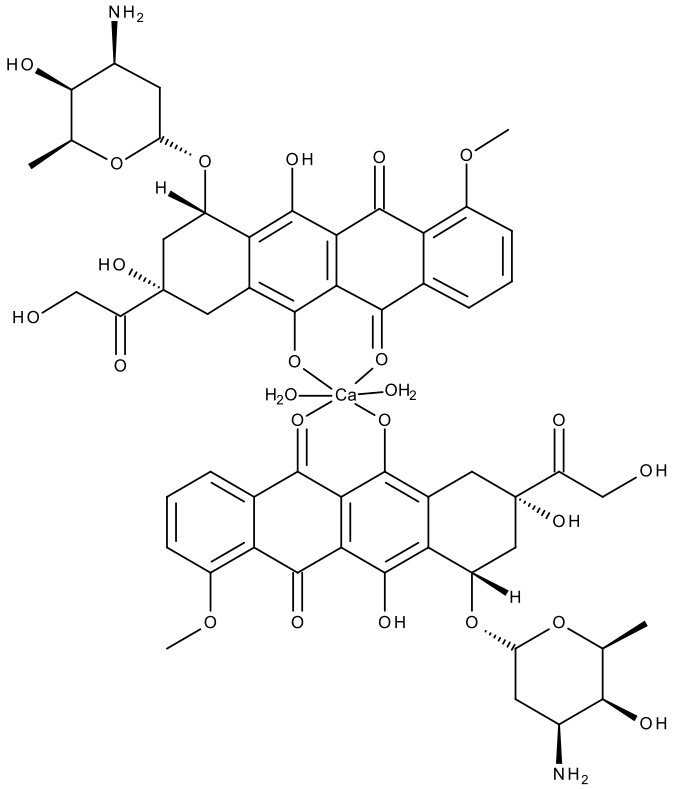

Figure 5.10: Predicted bidentate chelation structure form between Ca^{2+} and Dox.

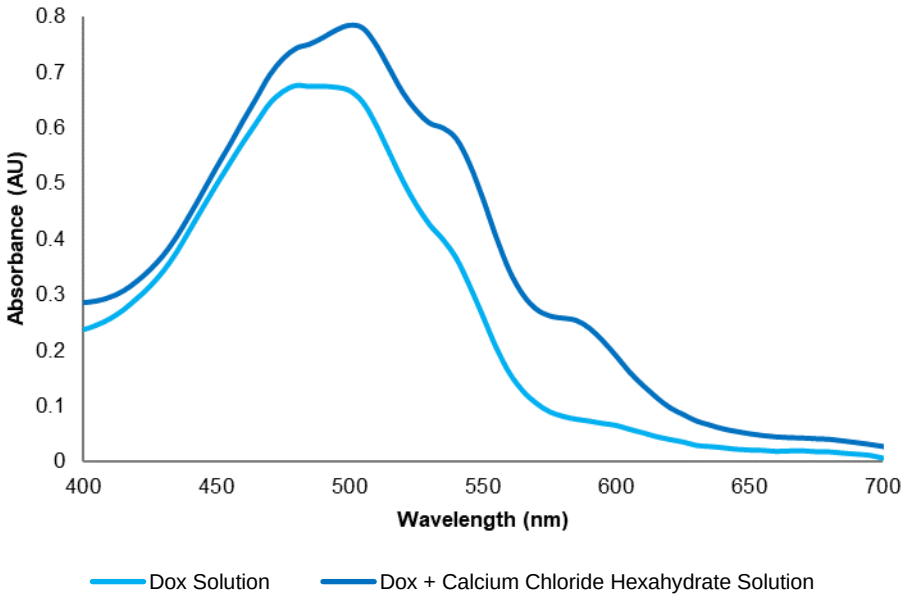

Figure 5.11: UV-Vis scan of Dox compared with Dox and calcium hexahydrate.

The pharmacokinetic measurements for eluent type in Table 5.4 demonstrates that C_{max} increased with an increase in salt concentration, as was seen with the data at different concentrations of NaCl. Again,

t_{max} was independent of eluent. Ringer's solution at a salt concentration of 83 mM had an average C_{max} of 34.12 µg/mL, which took an average of 274.35 min for 50 % of the loaded drug to elute from the beads. The salt concentration of Ringer's solution was similar to the 77 mM NaCl solution, however the average C_{max} was much lower at 16.74 µg/mL and $t_{50\ \%}$ took longer with an average 500.22 min. 154 mM NaCl, PBS and 0.9 % SBF all contained 154 mM salts and had similar C_{max} and $t_{50\ \%}$ values, whereas full strength Ringer's solution contained similar salt levels of 166 mM but took much longer for 50 % of the drug to elute. Natural SBF solution includes 295 mM salts which matches closely with 308 mM NaCl, C_{max} for 308 mM NaCl was 65.40 µg/mL which took 85.00 min for 50 % to elute, and for SBF was 70.73 µg/mL which took 91.00 min for $t_{50\ \%}$. The results for SBF and 308 mM are so similar they could be considered equivalent. From the elution curve it can be seen that Ringer's solution does not correlate with the other solutions and indicates an initial fast release of drug with a later inhibitory effect as the double strength solution took more than 70 min to elute 50 %.

Table 5.4: Elution concentration and timings with eluent type. The experiments were conducted at 310 K using 0.5 mL 100-300 µm DC Bead™, loaded with 37.5 mg/mL Dox, mixed with 2.5 mL glass beads and in PBS (154 mM) (sample number = 3, error = standard deviation).

Eluent Type	**Flow Rate (mL/min)**	**Salt Concentration (mM)**	**C_{max} (µg/mL)**	**t_{max} (min)**	**$t_{50\ \%}$ (min)**	***k* (x 10^{-3} min^{-1})**
PBS	2	154	46.73 ± 3.18	3.67 ± 0.58	155.00 ± 5.00	4.81 ± 0.67
1/2 Ringer's	2	42	27.43 ± 2.36	2.67 ± 0.58	450.00 ± 31.22	2.56 ± 0.42
Full Ringer's	2	83	34.12 ± 0.14	6.68 ± 0.56	274.35 ± 7.64	3.95 ± 0.00
x2 Ringer's	2	166	45.18 ± 0.96	4.67 ± 2.08	255.00 ± 13.23	9.14 ± 0.24
SBF	2	295	70.73 ± 4.43	7.67 ± 1.53	91.00 ± 0.00	7.83 ± 0.25
0.9 % SBF	2	154	32.19 ± 0.95	16.33 ± 2.08	184.33 ± 2.89	3.76 ± 0.18

Note that as Ringer's solution did not show complete elution, *k* could only be calculated when the culminated concentration was also considered the loaded concentration. These results may not necessarily be comparable to the other elution solutions.

5.2.5. Effect of Bead Volume

To conserve the bead samples, it was necessary to establish the most suitable total bead volume required for elution. Figure 5.12 displays flow through experiments with 0.2, 0.5 and 1 mL beads.

A bead volume of around 0.5 mL was considered the most appropriate amount for further experimentation in the elution test method as both 0.5 and 1 mL eluted >97 % of the drug. 0.2 mL beads did not completely elute the drug, possibly because smaller volumes incur greater error.

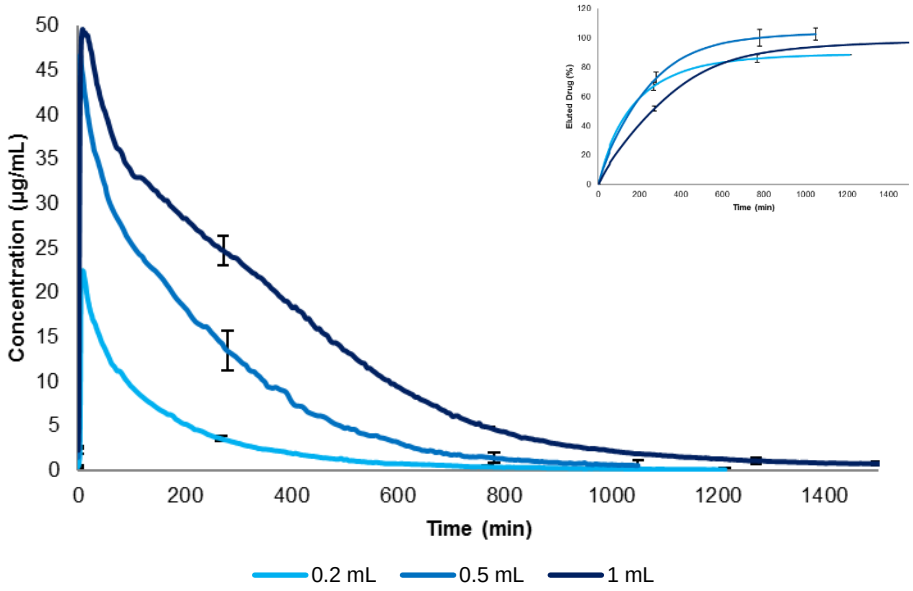

Figure 5.12: Effect of bead volume on Dox elution. The experiments were conducted at 310 K using 100-300 µm DC Bead™, loaded with 37.5 mg/mL Dox, mixed with a 1:5 ratio of DEBs to glass beads, in PBS (154 mM) and a flow rate 2 mL/min. Inset is the data presented as the percent of Dox eluted (sample number = 3, error bars = standard deviation every 100 data points).

5.2.6. Difference and Similarity Factors

For dissolution profile comparisons, FDA guidelines suggest a model independent approach using a difference factor (f_1) and similarity factor (f_2) [7]. f_1 calculates the percentage difference between two curves at each time point and is a measurement of the relative error between the two curves using Equation 5.2, where n is the number of time points, R is the dissolution value of one sample at time t, and T is the dissolution value of a second sample at time t. f_2 is a logarithmic reciprocal square root transformation of the sum of squared error and is a measurement of the similarity in the percentage dissolution between two curves using Equation 5.3. For curves to be considered similar, f_1 values should

be close to 0, and f_2 values should be close to 100. In general, f_1 values <15 and f_2 values >50 ensures the equivalence of two curves. f_1 and f_2 values for glass beads, flow rate, salt concentration, eluent type, and bead volume can be found in Table 5.5. Figure 5.2 is the standard for similarity and difference calculations, and is therefore not included in the statistical analysis.

Equation 5.2: Difference factor (f_1) calculation, where R is the dissolution value of one sample at time t and T is the dissolution value of a second sample at time t.

$$f_1 = \{[\sum_{t=1}^{n}|R_t - T_t|]/[\sum_{t=1}^{n} R_t] \cdot 100\}$$

Equation 5.3: Similarity factor (f_2) calculation, where R is the dissolution value of one sample at time t and T is the dissolution value of a second sample at time.

$$f_2 = 50 \cdot \log\left\{\left[1+(1/n)\sum_{t=1}^{n}(R_t - T_t)^2\right]^{0.5} \cdot 100\right\}$$

The data concludes that with the exception of the experiment conducted without glass beads and at a flow rate of 1 mL/min, as well as the 45 mL/min flow rate, there was no significant difference between replicate curves, as the average f_1 values were >15 and the average f_2 values were <50 for all other samples, and hence the method is robust and able to be used to investigate experimental differences in the method. Without the use of glass beads the curves are not uniform and samples tested together do not run parallel to each other, this was less visible at a flow rate of 2 mL/min as imperfections and swelling effects between curve are not as extended at faster flows. The 45 mL/min flow rate was possibly too fast for precise and accurate results of drug elution.

Table 5.5: Difference and similarity calculations between elution curves. Highlighted red are f_1 values greater than 15 and f_2 values less than 50 (sample number = 3, error = standard deviation).

Figure Number	Figure Name	Data Label	f_1 Value	f_2 Value
Figure 5.3	Effects of Glass Beads at 1 mL/min	No Glass	22.99 ± 11.97	39.85 ± 11.96
		3 mL Glass	2.25 ± 1.21	83.95 ± 9.47
		5 mL Glass	7.90 ± 2.68	70.32 ± 5.08
Figure 5.4	Effects of Glass Beads at 2 mL/min	No Glass	6.45 ± 2.11	80.29 ± 5.92
		3 mL Glass	8.75 ± 4.14	74.06 ± 8.61
		5 mL Glass	4.29 ± 1.36	87.86 ± 5.23
Figure 5.5	Effects of Flow Rate	0.5 mL/min	1.80 ± 0.35	89.60 ± 2.57
		1 mL/min	7.90 ± 2.68	70.32 ± 5.08
		2 mL/min	4.29 ± 1.36	87.86 ± 5.23
		5 mL/min	2.53 ± 0.24	97.39 ± 0.45
		*5 mL/min	1.17 ± 0.19	99.02 ± 0.40
		10 mL/min	5.61 ± 2.83	88.05 ± 6.95
		20 mL/min	8.54 ± 4.16	82.12 ± 9.15
		45 mL/min	19.93 ± 14.77	71.28 ± 21.37
Figure 5.6	Effect of Salt Concentration	77 mM	4.28 ± 1.64	79.68 ± 6.47
		154 mM	1.40 ± 0.75	98.54 ± 1.13
		231 mM	5.69 ± 2.62	86.75 ± 8.56
		308 mM	4.29 ± 0.44	92.34 ± 2.93
		770 mM	4.10 ± 2.99	92.56 ± 6.23
Figure 5.8	Effects of Eluent Type	PBS	5.48 ± 3.96	85.07 ± 12.68
		½ Ringer's	9.89 ± 5.12	54.96 ± 16.01
		Full Ringer's	4.92 ± 5.72	68.21 ± 32.75
		x2 Ringer's	1.86 ± 0.72	95.05 ± 3.30
		SBF	3.54 ± 1.58	94.81 ± 3.02
		0.9 % SBF	2.52 ± 0.91	93.68 ± 2.62
Figure 5.12	Effect of Bead Volume on Dox elution	0.2 mL	14.29 ± 9.20	61.39 ± 19.31
		0.5 mL	5.48 ± 3.96	85.07 ± 12.68
		1 mL	4.29 ± 1.36	87.86 ± 5.23

5.3. Conclusion

In summary, sand and glass beads were evaluated for their suitability as packing material. Dox bound to the sand and glass particles rendering it an inappropriate material for packing, however washing the glass bead with deionised water produced an inert material. When testing the most suitable bead packing configuration it was found that the addition of glass beads mixed with DEBs generated more reproducible and consistent results. Various volume ratios of DEBs to glass beads were included in the experimental test design, although the elution profile did not markedly change with different volumes of glass beads, a ratio of 1:5 was a more convenient volume for the practicality of producing an even mixture of beads. Glass beads allowed DEBs to expand without being compressed. Certain DEBs increase in size as the drug is eluted and water is drawn in. When DEBs are restricted from swelling the flow rate will alter as the beads become tightly packed. Glass beads allow PBS to travel around DEB no matter whether the beads are prone to expansion. The introduction of helium de-gassed the eluent, removed dissolved air and in-turn reduced air bubbles in the system which improved the flow of medium.

During each experiment there was an initial steep increase in the elution profile, followed by a sharp drop in concentration and a period of slow release. As the elution of drug from DC Bead™ is an ion-exchange process [7,1], the drug elution rate depends upon the cation present in the eluent. The flow of eluent was found to be proportional to the availability of sodium ions, the higher the flow rate the faster the rate of elution. Higher flow rates eluted the drug faster and so would increase the number of experiments which could be completed in a set amount of time. However, much larger volumes of PBS were required for each test, this created a greater risk running out of elutant and made each experiment more expensive. Lower flow rates used much smaller amounts of PBS, but the experiments took much longer to complete. Various flow rates have been used by a number of people with different methods, and it was important to select the best parameter for this particular method. Therefore, the chosen flow rate of 2 mL/min was not only better for comparative analysis, but had a balance of retrieving the data in a suitable amount of time with regards the practicality of equipment setup and completing a test within 24 hours, whilst using a suitable amount of material. A flow rate of 2 mL/min could also correlate well with *in vivo* data; nonetheless higher flow rates could be acceptable for other types of comparative analysis for instance bead type, bead size and type of drug.

Concentrations of NaCl were investigated to confirm flow rate effects. If at higher flow rates more sodium ions pass by the beads and so the drug can elute quicker, then varying the concentration

of NaCl should have the same influence. Altering the concentration of NaCl confirmed that elution is proportional to the availability of sodium ions. The composition of the release medium influenced the release kinetics, and this drug ion-exchange as a mechanism of loading and release has been previously demonstrated by Gonzalez et al, Jordon et al and Biondi et al [1,2,8]. Both flow rate and salt concentration followed a similar trend and increased the elution rate up to a point where rate of diffusion becomes the controlling factor, this appeared to be above 5 mL/min and 308 mM NaCl, as these curves are similar to 10 mL/min and 770 mM NaCl. An increase of more than 308 mM NaCl or a flow rate higher than 5 mL/min does not seem to increase the rate of elution.

Different eluents eluted different concentrations of drug, SBF was selected as this has similar ion concentrations as those found in HBP (human blood plasma). SBF contains 295 mM salts, the data appears comparable to the 308 mM NaCl elution. However, this is at a point whereby an increase of salt no longer increases the rate of elution. Ringers solution has previously demonstrated the ability to elute drugs, however in this case a maximum of 74 % of the drug was eluted and this decreased to 56 % when the concentration of Ringer's solution was doubled. In Ringer's solution the different elution profiles where complete elution of the drug was not achieved could be due to Dox-Ca^{2+} binding.

Owing to a limited availability of certain beads, bead volume was studied to evaluate the lowest amount of beads which could be employed for elution experiments. To conserve the bead samples, 0.5 mL was found an adequate quantity, which gave precise and accurate results, as 0.2 mL did not display a 100 % elution. This could be down to a larger error in loading with a smaller volume of beads.

Packing material, flow rate, salt concentration, eluent type, and bead volume each confirmed that elution was dependent on diffusion which in turn affected the rate that drug eluted. These parameters can now be used to evaluate the elution profile of different beads, bead sizes, drugs and drug concentrations. The new elution method overcomes limitations of the previous ones and mimics embolisation, this would be useful for the comparisons of bead technology and the development of new bead devices, in addition to *in vivo* correlated studies. A calculation of f_1 and f_2 values shows that there is large similarity between most of the elution curves using this elution method.

References

1 M. V. Gonzalez, Y. Tang, G. J. Phillips, A. W. Lloyd, B. Hall, P. W. Stratford and A. L. Lewis, Doxorubicin eluting beads - 2: methods for evaluating drug elution and in-vitro:in-vivo correlation, *J. Mater. Sci. Mater. Med.*, 2008, **19**, 767–775.

2 O. Jordan, A. Denys, T. De Baere, N. Boulens and E. Doelker, Comparative Study of Chemoembolization Loadable Beads: In vitro Drug Release and Physical Properties of DC Bead and Hepasphere Loaded with Doxorubicin and Irinotecan, *J. Vasc. Interv. Radiol.*, 2010, **21**, 1084–1090.

3 J. Namur, M. Wassef, J.-M. Millot, A. L. Lewis, M. Manfait and A. Laurent, Drug-eluting Beads for Liver Embolization: Concentration of Doxorubicin in Tissue and in Beads in a Pig Model, *J. Vasc. Interv. Radiol.*, 2010, **21**, 259–267.

4 A. Das, C. Adhikari and A. Chakraborty, Interaction of Different Divalent Metal Ions with Lipid Bilayer: Impact on the Encapsulation of Doxorubicin by Lipid Bilayer and Lipoplex Mediated Deintercalation, *J. Phys. Chem. B*, 2017, **121**, 1854–1865.

5 S. A. Abraham, K. Edwards, G. Karlsson, S. MacIntosh, L. D. Mayer, C. McKenzie and M. B. Bally, Formation of transition metal–doxorubicin complexes inside liposomes, *Biochim. Biophys. Acta - Biomembr.*, 2002, **1565**, 41–54.

6 T. T. T. Nguyen, Y. J. Lim, M. H. M. Fan, R. A. Jackson, K. K. Lim, W. H. Ang, K. H. K. Ban and E. S. Chen, Calcium modulation of doxorubicin cytotoxicity in yeast and human cells, *Genes to Cells*, 2016, **21**, 226–240.

7 U.S. Department of Health and Human Services Food and Drug Administration Center for Drug Evaluation and Research (CDER), Guidance for Industry Dissolution Testing of Immediate Release Solid Oral Dosage Forms, https://www.fda.gov/downloads/drugs/guidances/ucm070237.pdf, (accessed 1 June 2014).

8 A. L. Lewis, M. V. Gonzalez, S. W. Leppard, J. E. Brown, P. W. Stratford, G. J. Phillips and A. W. Lloyd, Doxorubicin eluting beads − 1: Effects of drug loading on bead characteristics and drug distribution, *J. Mater. Sci. Mater. Med.*, 2007, **18**, 1691–1699.

9 M. Biondi, S. Fusco, A. L. Lewis and P. A. Netti, Investigation of the mechanisms governing doxorubicin and irinotecan release from drug-eluting beads: mathematical modeling and experimental verification, *J. Mater. Sci. Mater. Med.*, 2013, **24**, 2359–2370.

Chapter 6 : Determination of the Effect of Bead Size, Bead Type, Drug Type and Drug Concentration using a Method of Open-Loop Flow-Through Elution

6.1. Introduction

Chapter 6 confirmed suitable elution parameters to be: a drug eluting bead (DEB) to glass bead ratio of 1:5, an elution flow rate of 2 mL/min, a bead volume of 0.5 mL and an ion concentration of 154 mM phosphate buffer saline (PBS) an as appropriate elution medium. Bead size has been a well investigated characteristic with the calorimetric method of earlier chapters, and so the evaluation of four sizes of DC Bead™ (70-150, 100-300, 300-500 and 500-700 µL) and the comparison with binding data is of interest.

The elution of drug from four bead types (DC Bead™, DC Bead LUMI™, Tandem™ and HepaSphere™) has been well documented using methods such as USP II and USP IV, however there has been some indication that Tandem™, in particular, may not completely elute the loaded drug under these conditions. The aim of this work was to establish whether beads can fully elute a drug using an alternative system and differentiate patterns of elution from different beads.

Doxorubicin (Dox) was analysed at loading concentration of 25, 37.5 and 45 mg/mL with DC Bead™ and Bead LUMI™, then at 25, 50 and 75 mg/mL with Tandem™ because of the differing loading instructions. To create comparable data, DC Bead™ and DC Bead LUMI™ experiments contained 0.5 mL of beads, whereas Tandem™ experiments contained ~0.4 mL of beads. This meant that 0.75 mL of a 25 mg/mL Dox solution would be required in all three bead types regardless of the bead chemistry.

Drug type was evaluated to identify whether the composition of different chemical compounds impact the drug eluting capabilities of DEBs. Most DEBs are licenced for use with both Dox and Irinotecan (Iri), and so it is important to understand how these two drugs elute.

Although 2 mL/min was selected as a practical flow rate for elution, this does not correlate to the flow rate of an embolised blood vessel at 0.01 mL/min [1]. The aim was to reduce the flow rate to 0.1 mL/min and identify the feasibility of elution at a flow rate closer to that of an occluded vessel. The rationale behind a flow rate of 0.1 mL/min, is to first attempt a slow flow rate that would not challenge

the equipment and detection limits. The slow flow experiments were conducted with the various combinations of the parameters tested such as bead size (70-150 and 100-300 μm), bead type (DC Bead™, DC Bead LUMI™, Tandem™ and LifePearl™) and drug concentration (37.5 and 75 mg/mL).

The open-loop flow-through method was used to allow a better comparison between the performances of different DEB sizes, different DEB products despite their differing characteristics, with different drug concentrations, different drugs and at slower flow rates.

6.2. Results and Discussion

6.2.1. Effect of Bead Size

The previous chapter described an adequate method for the elution of drug from DEBs. DEBs are available in a range of sizes, as was detailed in Chapter 4 for the binding of drug to beads using isothermal titration calorimetry (ITC). For the first study of this section the same bead sizes M1 (70-150 µm), 103 (100-300 µm), 305 (300-500 µm) and 507 (500-700 µm) were evaluated for drug elution, illustrated in Figure 6.1. Smaller beads bind to the drug faster than larger beads due to the larger surface area to volume ratio [2,3], and it was hypothesised that this may also affect subsequent drug elution. Based upon the elution data, at 500 min M1 beads had released ~95 % of Dox, 103 beads ~92 %, 305 beads ~65 %, whereas 507 beads only ~50 %. At the end of the experiments, when the absorbance readings of all bead sizes were close to zero, each had eluted >99% of Dox.

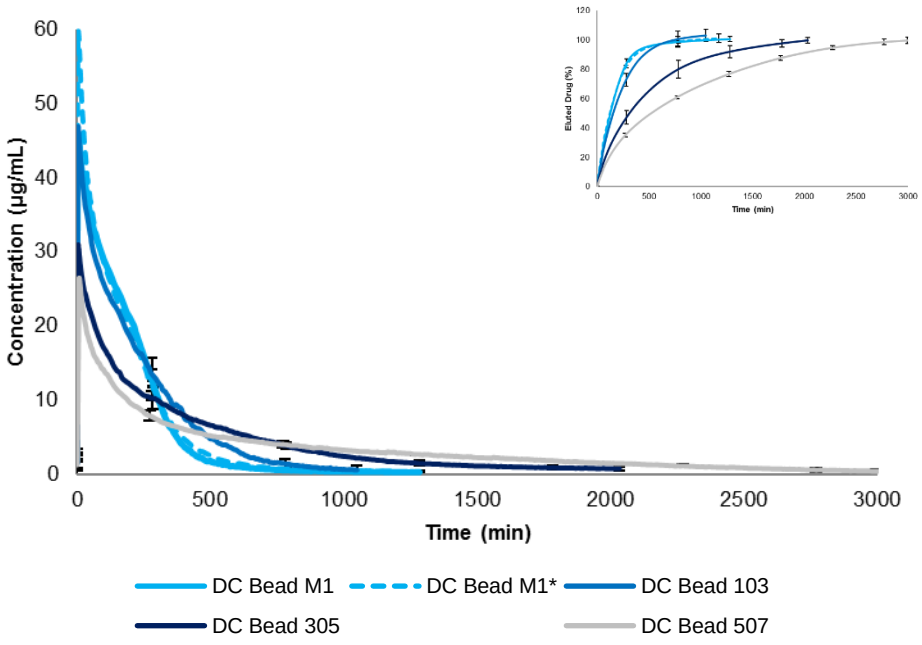

Figure 6.1: Effect of bead size on Dox elution. The experiment was conducted using 0.5 mL of 70-150, 100-300, 300-500 and 500-700 µm DC Bead™, loaded with 37.5 mg/mL Dox, mixed with 2.5 mL glass beads, in PBS (154 mM) and a flow rate of 2 mL/min. Inset is the data presented as the percent of Dox eluted. *Repeat experiment of DC Bead*M1*™ (sample number = 3, error bars = standard deviation every 100 data points).

Interestingly the shape of the 70-150 µm (M1) sample bares some similarity to the inverted ITC profile. The comparison of elution data with ITC binding data is displayed in Figure 6.2 for M1 beads. This non-

linear shape is not replicated in the larger beads of 103, 305 and 507 either in the elution or binding experiments, however the other beads do match in shape with a conventional release profile between binding and elution. The similarity between binding and elution could be because the mechanistics of the interaction are the same as both drug binding and drug release is of an ion-exchange mechanism which happens near the surface of the bead. As the two are reversed processes, the initial burst in elution be correlated with the large heat released in the beginning of titration.

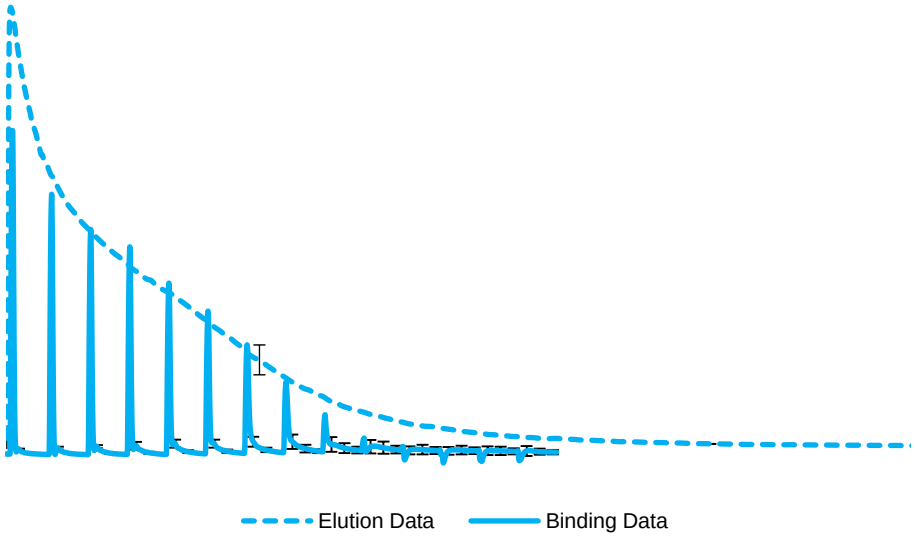

Figure 6.2: Comparison of open-loop flow-through elution data (0.5 mL 70-150 µm DC Bead™, loaded with 37.5 mg/mL Dox, mixed with 2.5 mL glass beads, in PBS (154 mM) and a flow rate of 2 mL/min) and inverted binding results from ITC (43 mM Dox into 100 mg 70-150 µm DC Bead™) (sample number = 3, error bars = standard deviation every 100 data points). There are no units as one experiment measures concentration and the other power, time is partially controlled by either flow rate or injection time in each experiment and so is irrelevant for comparison.

Although elution data has confirmed that each bead size is ultimately capable of eluting the total amount of loaded drug, the ITC results differed as they did not consistently show that same amount of drug binding, however this is thought to be a limitation of the method. Elution was able to prove that surface area is crucial to the rate of elution, but this was not observed in the binding data and was thought to be the result of the amounts of Dox added to the beads being too small to make a significant difference.

6.2.2. Effect of Bead Type

Secondly, different types of beads were the subject of investigation (DC Bead LUMI*M1*™ (70-150 µm), DC Bead LUMI™ 103 (100-300 µm), Tandem™ 107 (60-90 µm) and Tandem™ 110 (75-125 µm)). The sizes of bead evaluated were comparable to the previously tested DC Bead*M1*™ (70-150 µm) and 103 DC Bead™ (100-300 µm), represented in Figure 6.3.

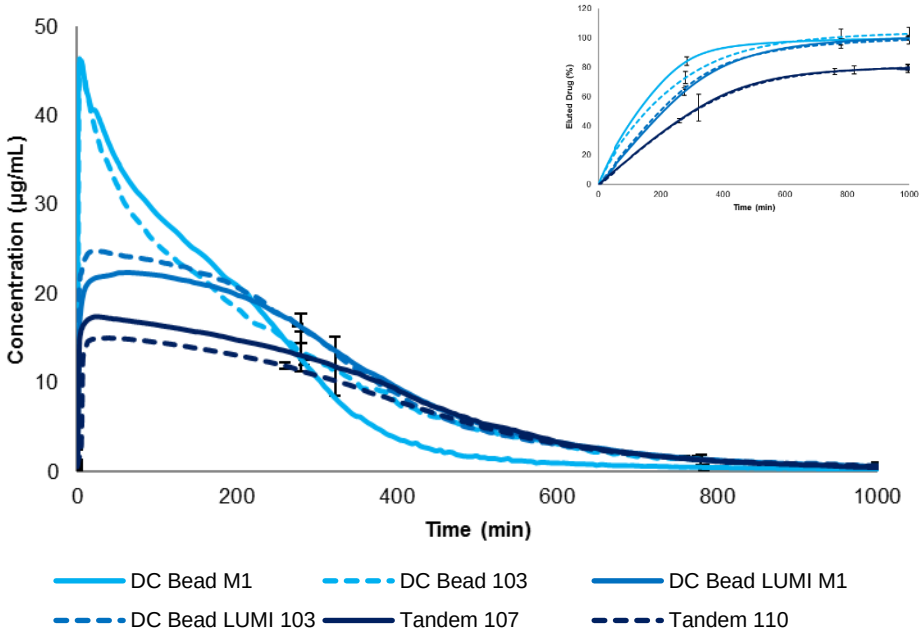

Figure 6.3: Effect of bead type on Dox elution. The experiment was conducted using 0.5 mL of 70-150 and 100-300 µm DC Bead™, 0.5 mL of 70-150 and 100-300 µm DC Bead LUMI™, 0.4 mL 75 and 100 µm Tandem™, loaded with 37.5 mg/mL Dox for DC Bead™ and DC Bead LUMI™ but 50 mg/mL for Tandem™, mixed with 2.5 mL glass beads, in PBS (154 mM) and a flow rate of 2 mL/min. Inset is the data presented as the percent of Dox eluted. *Repeat experiment of DC Bead*M1*™ (sample number = 3, error bars = standard deviation every 100 data points).

Each bead was loaded with the same concentration of Dox, however both sizes of Tandem™ only achieved an 80 % elution. Each size of Tandem™ held onto 20 % of loaded Dox and this could not be extracted using the traditional method of forced extraction. DC Bead™ and DC Bead LUMI™ are composed of a similar bead chemistry and both completely eluted, although it should be noted that a larger concentration of Dox was initially released from DC Bead™ compared with DC Bead LUMI™, which had a longer slower release of drug. These results can be considered clinically relevant, for example it is possible that in some circumstances a condition would benefit from an initial high concentrated of drug [4], whilst others would benefit from a slower more controlled sustained release [5].

Each size range in this study overlaps with the smaller or larger section of beads. The smaller beads did not necessarily elute faster in the case of DC Bead LUMI™, yet it must be taken into consideration that error bars and size range overlapped in this bead type.

The next product considered in this work was HepaSphere™. This device was found to gel and block the filter membrane, this stopped the flow of PBS, and it was not possible to produce elution data. Pressure built up in the elution cell and forced small fragments of the embolic to pass through the membrane, these travelled to the UV detector, which distorted the UV readings (data not shown). Smaller pore sized filter membrane did not prevent the fragments passing through, therefore HepaSphere™ was eliminated from further analysis with this type of elution.

Overall, it would appear that bead type can be an influential factor. It should be noted that Tandem™ was loaded with a different concentration of drug compared with the amount of bead, this is because the manufacturer guidelines are to load 1 mL of bead with 50 mg/mL of Dox [6], slightly greater than DC Bead™ and DC Bead LUMI™ loading of 37.5 mg/mL Dox per 1 mL of beads [7]. In order to compare the different types of bead the experiment would require the same concentration of drug, therefore the mass of Tandem™ bead was reduced to 0.4 mL in contrast to 0.5 mL of DC Bead™ and DC Bead LUMI™. This allowed loading of the same concentration of Dox across all bead types.

According to Boston Scientific Inc., Tandem™ can load 98 ± 2 % of 50 mg Dox or Iri per mL of microspheres, and that Tandem™ releases Iri 5 – 8 times slower than DC Bead*M1*™ (70-150 µm) and DC Bead™ (100-300 µm) [8]. Yet in this elution method Tandem™, DC Bead™ and DC Bead LUMI™ eluted at similar rates, although this comparison was with Dox and not Iri, it is difficult to conceive this level of difference between these bead types. It is stated that the elution of Iri is a slower more controlled and more sustained from DC Bead LUMI™ than DC Bead™, but the curves are clinically proven to fall within specification of each other [9]. It would be of particular interest to further test these statements because the mechanism of elution may well be very different for Iri.

6.2.3. Effect of Drug Concentration

The third investigation evaluated the effects of drug loading concentration on elution. Various sizes of DC Bead™, DC Bead LUMI™ and Tandem™ that had already been tested during the bead size or bead

type study, were dosed with different concentrations of Dox, illustrated in Figure 6.4 (DC Bead™ M1, 103, 305 and 507 – 25, 37.5 and 45 mg/mL), Figure 6.5 (DC Bead LUMI™ M1 and 103 – 25, 37.5 and 45 mg/mL) and Figure 6.6 (Tandem™ 107 and 110 – 25, 50 and 75 mg/mL).

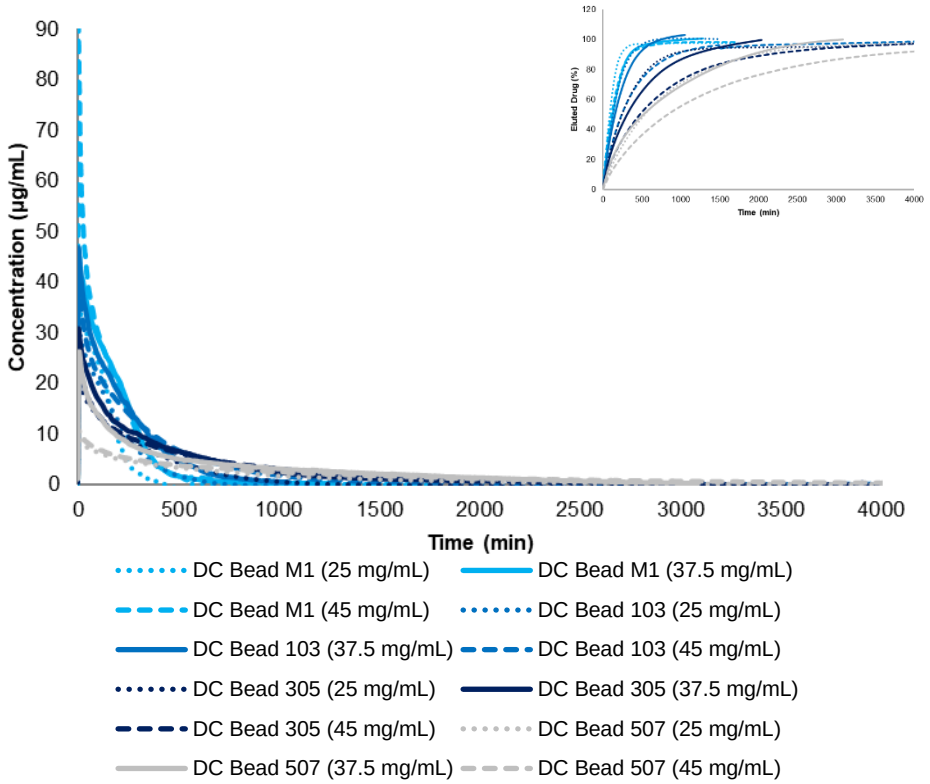

Figure 6.4: Effect of Dox concentration on elution. The experiment was conducted using 0.5 mL of 70-150 µm, 100-300 µm, 300-500 and 500-700 µm DC Bead™, loaded with 25, 37.5 and 45 mg/mL Dox, mixed with 2.5 mL glass beads, in PBS (154 mM) and a flow rate of 2 mL/min. Inset is the data presented as the percent of Dox eluted (sample number = 1 and 2).

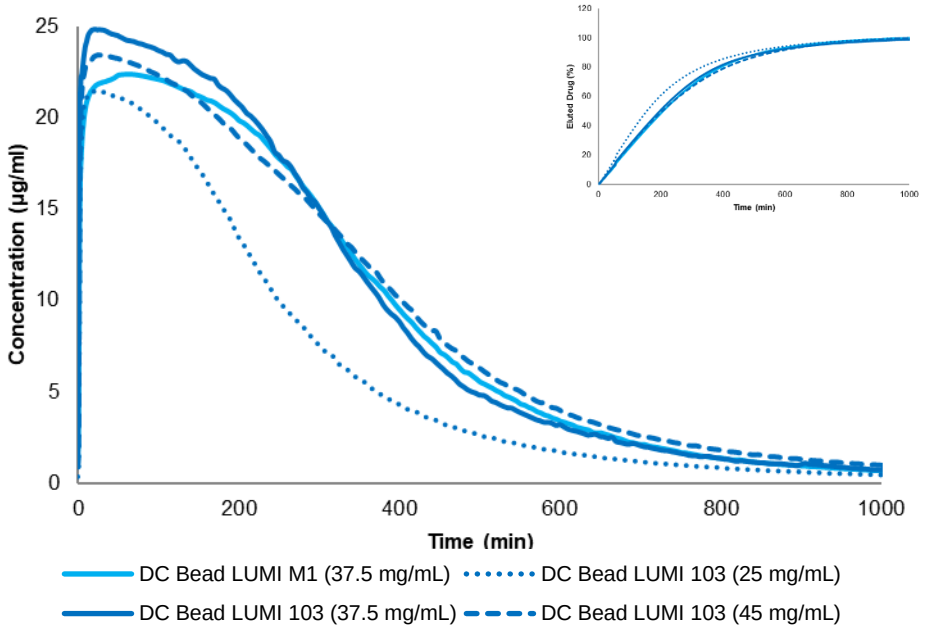

Figure 6.5: Effect of Dox concentration on elution. The experiment was conducted using 0.5 mL of 100-300 µm DC Bead LUMI™, loaded with 25, 37.5 and 45 mg/mL Dox, mixed with 2.5 mL glass beads, in PBS (154 mM) and a flow rate of 2 mL/min. Inset is the data presented as the percent of Dox eluted (sample number = 1 and 2).

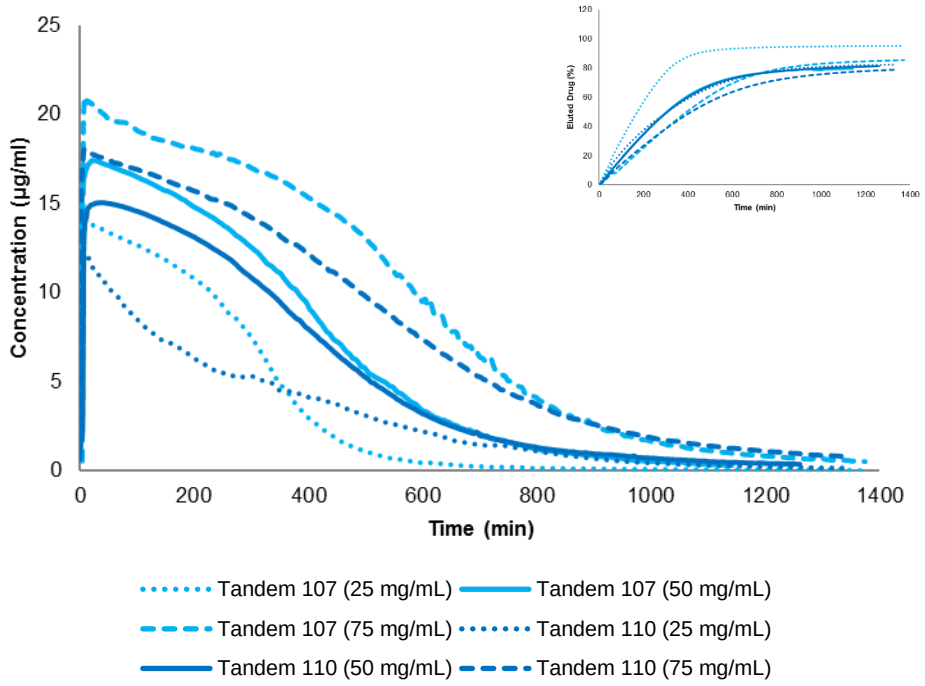

Figure 6.6: Effect of Dox concentration on elution. The experiment was conducted using 0.4 mL of 75 and 100 µm Tandem™, loaded with 25, 50 and 75 mg/mL Dox, mixed with 2.5 mL glass beads, in PBS (154 mM) and a flow rate of 2 mL/min. Inset is the data presented as the percent of Dox eluted (sample number = 1 and 2).

An increase in drug concentration increases the time required for elution of drug in all bead types. Tandem™ was loaded with different concentrations because the loading instructions differed. 75 µm Tandem™ loaded at 25 mg/mL came the closest to complete elution, this sample was the smallest investigated bead size, loaded with the lowest evaluated drug concentration, however there were no replicates of this experiment due to a lack of sample, and so it could have been an anomalous result.

Since the other curves eluted only 79 – 86 %, all sample from all beads types were tested for drug loading by removing the residual solution from loaded beads and analysing the concentration of drug unbound to the beads. The results were that all bead sizes, bead types and later drug types bound to more than 99 % of the drug. After each elution experiment beads were collected and the drug extracted from the beads using solutions of 1% sodium chloride (NaCl)/dimethyl sulfoxide (DMSO), 15 % NaCl, 0.1 M hydrochloric acid (HCl) or 10 % KCl/ethanol (for preparation of extraction solutions see Chapter 2). The small concentrations of drug remaining in DC Bead™ and DC Bead LUMI™ were extracted, confirming that these beads can completely elute but that a small percentage remained in the beads because the experiments were stopped prematurely. The Tandem™ extractions did not contain any drug which leads to the belief that Tandem™ is not capable of completely eluting the remaining loaded drug. The structure of Tandem™ was later found to a have different surface and core, Dox could be held inside this structure and will be discussed in more detail in Chapter 7.

6.2.4. Effect of Drug Type

Embolic beads are indicated for use with a wide range of drugs. It was of particular interest to compare Dox and Iri elutions for the fourth investigation, as they are both indicated for use with DC Bead™, DC Bead LUMI™, Tandem™ and HepaSphere™. The ITC determined that Iri has much weaker drug-polymer interactions than Dox, as Dox-Dox interactions are another contribution for the strong binding observed in Dox loading, and the maximum capacity of Iri is also greater than that of Dox. As Iri will elute much faster than some other drugs, it is a good indication that open-loop flow-through elution will be suitable under the same conditions for drugs with different physical properties. Because of the high concentration readings and subsequently high absorbance of Iri, a cuvette with a smaller path length of 0.5 cm was employed, rather than the 1 cm cuvette for Dox experiments. Iri was loaded at 50 mg/mL, where Dox was loaded at 37.5 mg/mL because of the manufacturer's instructions for use of loaded Iri

into DC Bead™. Iri was measured at an absorbance of 369 nm, whereas Dox was measured at 483 nm, based on the observed values of λ_{max}. Figure 6.7 illustrates the Iri elution with DC Bead™, and Figure 6.8 demonstrates a comparison of the two drugs Dox and Iri.

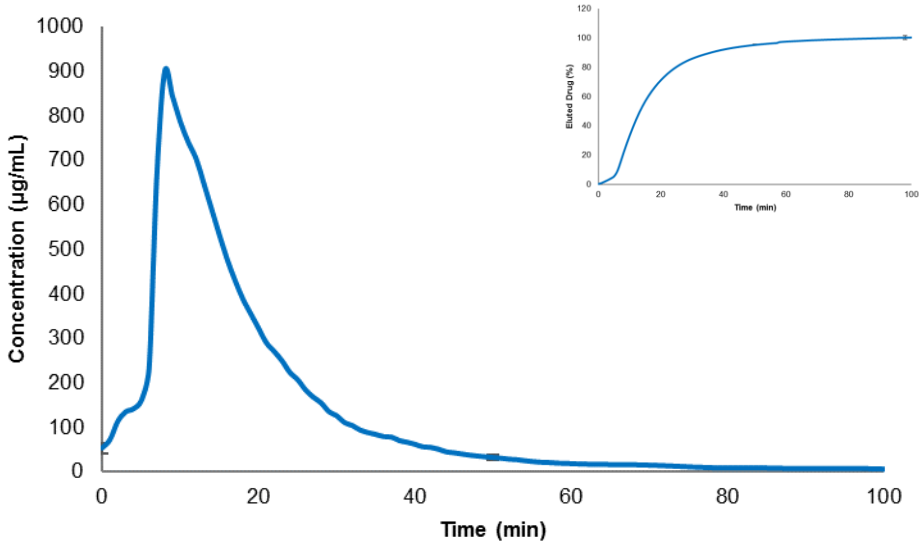

Figure 6.7: Iri elution. The experiment was conducted using 0.5 mL of 100-300 µm DC Bead™, loaded with 50 mg/mL Iri, mixed with 2.5 mL glass beads, in PBS (154 mM) and a flow rate of 2 mL/min. Inset is the data presented as the percent of Iri eluted (sample number = 3, error bars = standard deviation every 50 data points).

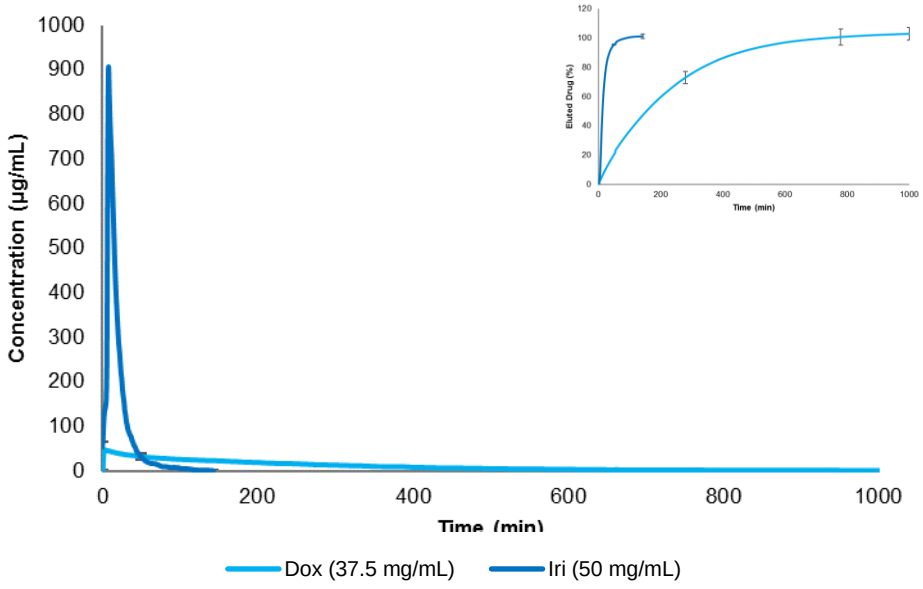

Figure 6.8: Comparison of Dox and Iri elutions. The experiment was conducted using 0.5 mL of 100-300 µm DC Bead™, loaded with either 37.5 mg/mL Dox or 50 mg/mL Iri, mixed with 2.5 mL glass beads, in PBS (154 mM) and a flow rate of 2 mL/min. Inset is the data presented as the percent of drug eluted (sample number = 3, error bars = standard deviation every 100 data points for Dox and every 50 data points for Iri as the elution was much quicker).

The elution of Iri was, as expected, much quicker than Dox, and the results prove that two very different drugs can be evaluated using this method showing two distinctive elution patterns. The Iri profile increased rapidly in the first 2 mins which slowed for the same amount of time and then increased again. This could have occurred from residual drug unbound to the beads and immediately detected upon beginning the experiment. Both drugs fully eluted showing a robust and reproducible method.

6.2.5. Effect of Slow Flow

Flow rate was reduced in the final investigation, to create a mimic closer to that of an embolised vessel. The majority of experiments prior to this study were conducted at a flow rate of 2 mL/min, as this was deemed the most suitable test parameter. However, in this portion of the work experiments were conducted at 0.1 mL/min, only 10 times fasters than a reported occluded vessel [1].

Originally slow flow experiments seemed to display some unusual characteristics, demonstrated in Figure 6.9. At particular timepoints there were dips in the elution curve, these coincided with sunrise until sunset on particularly clear forecasts. It was known that Dox is degraded by light, but the extent was unknown, and this had never before interfered with the results. This led to a degradation experiment of Dox, which tested the stability of the drug in direct light, whereby Dox standards left on a windowsill were analysed before and after 8 hours, one was in direct sunlight and other wrapped in foil. UV analysis showed the Dox standard unprotected by sunlight decreased significantly in concentration from an average of 50.17 mg/mL to an average of 42.28 mg/mL, which was a reduction of 15.73 %. It was thought that previous results had not illustrated a dip in concentration because they were conducted at faster flow rates, which meant that experiments, usually prepared during the day and initiated in the late afternoon/evening, were not exposed to light. At 2 mL/min the majority of the drug eluted in hours, so any decrease would have been less noticeable and have had a much smaller effect than at 0.1 mL/min.

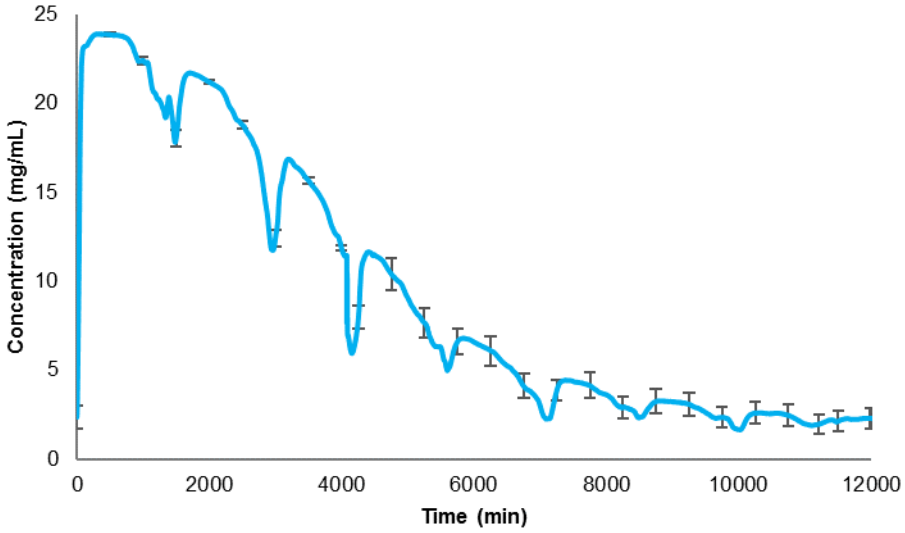

Figure 6.9: Degradation of Dox with exposure to sunlight. The experiment was conducted using 0.5 mL of 100-300 µm DC Bead LUMI™, loaded with 37.5 mg/mL Dox, mixed with 2.5 mL glass beads, in PBS (154 mM) and a flow rate of 0.1 mL/min (sample number = 3, error bars = standard deviation every 100 data points for Dox).

To rectify this situation the water bath, which was a Perspex box and contained the beads in a transparent plastic tube, was covered in tin foil to minimise exposure to light. The silicone tubing, which carried the drug into the UV detector, also had a layer of foil to block out the light. The cover of the UV machine could not be closed to allow the cells to receive and discard the elution medium, this should not interfere with measurement readings according to the manufacturer, therefore a piece of foil was placed over the compartment to shade the flow-through extraction cell. The cell contained the drug for the shortest amount of time, so the effects were not as important in this position as in the occluded tube.

As can be seen in Figure 6.10, with a flow rate of 0.1 mL/min the maximum length of experiment was just over 7 days with DC Bead LUMI™ 103 (100-300 µm) loaded at 37.5 mg/mL Dox, where test had been stopped early and the amount of Dox eluted from that sample was slightly more than 81 %. The products DC Bead*M1*™ (70-150 µm) and LifePearl™ 100 (75-125 µm) had particularly similar elution profiles, and this resemblance was also expressed in the ITC binding data between these two bead types. As expected, Tandem™ eluted much less than the other beads.

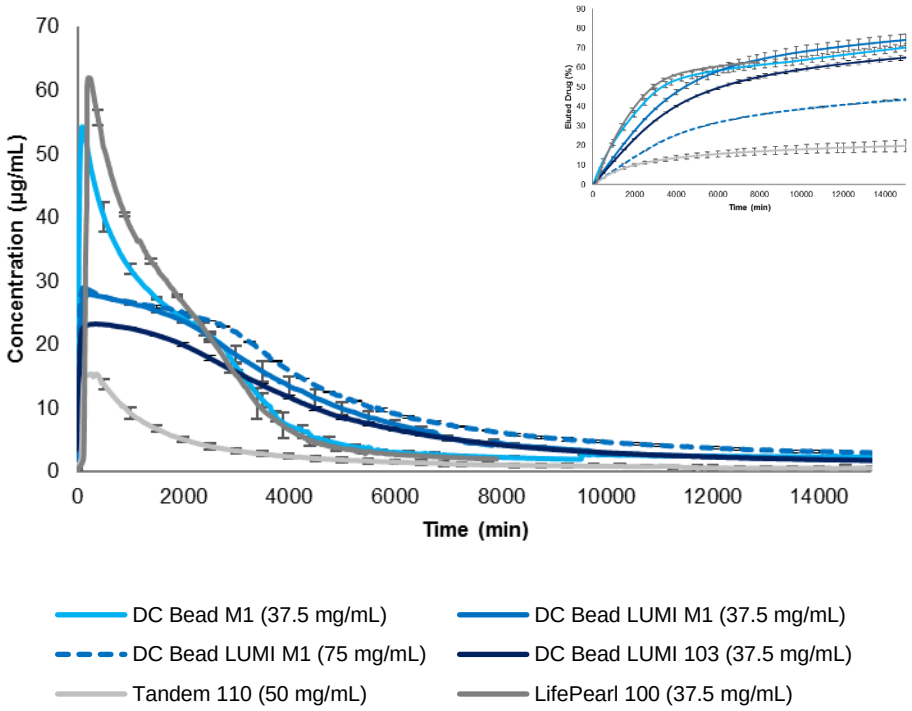

Figure 6.10: Slow flow elutions. The experiments were conducted using 0.5 mL of 70-150 µm DC Bead™, 70-150 µm DC Bead LUMI™, 100-300 µm DC Bead LUMI™ and 100 µm LifePearl, and 0.4 mL of 100 µm Tandem™, loaded with either 37.5, 50 or 75 mg/mL Dox, mixed with 2.5 mL glass beads, in PBS (154 mM) and a flow rate of 0.1 mL/min. Inset is the data presented as the percent of drug eluted (sample number = 3, error bars = standard deviation every 100 data points for Dox).

It is proposed in Figure 6.11 that the entire elution of drug would take 14 – 16 days, if the elution path stayed on the same trajectory. It would be of interest to reduce the flow rate further, perhaps by removing the pump and allowing the eluent to pass to and from the beads using gravity. At a flow rate 0.1 mL/min an extrapolation completes the elution in 5 – 6 months, close to that of *in vivo* studies which identified residual drug (89 % eluted) in a porcine hepatic artery, 90 days after implantation of 100-300 and 700-900 µm DC Bead™ loaded at 37.5 mg/mL. It is worth mentioning that this model was generated with a slightly different bead, which is known to have faster release kinetics [4].

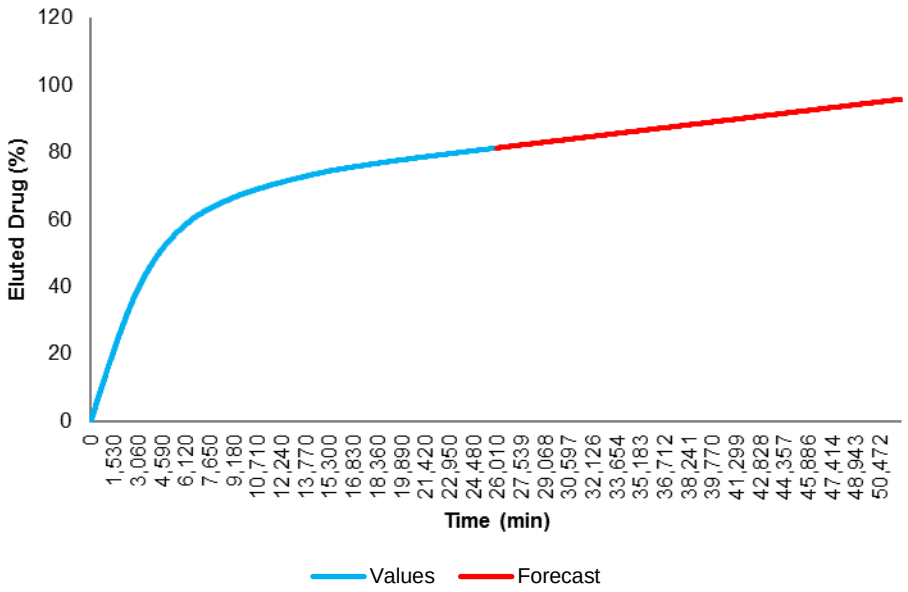

Figure 6.11: Forecast of slow flow elution. Data is from Figure 6.10, the experiment was conducted using 0.5 mL of 100-300 µm DC Bead LUMI™, loaded with 37.5 mg/mL Dox, mixed with 2.5 mL glass beads, in PBS (154 mM) and a flow rate of 0.1 mL/min (sample number = 3).

6.2.6. Difference and Similarity Factors

Difference factor (f_1) and similarity factor (f_2) were calculated for dissolution comparisons [10]. f_1 and f_2 values were not collected for the drug concentration data in section 6.2.3, as most curves had only one or two replicates. The Tandem™ 107 (60-90 µm) sample in the effect of bead type data has an f_1 value >15, and the DC Bead LUMI*M1*™ (70-150 µm) 37.5 mg/mL Dox loaded slow flow experiment has an f_2 value of <50, which shows the elution curves are comparatively different. During these experiments a kink occurred in the tubing of one of the samples, this altered the flow rate and affected the results. It was immediately amended and only affected a small portion of the data, but the difference affected the f_1 and f_2 values. There was no significant difference between any other replicate curves, as the average f_1 values were >15 and the average f_2 values were <50 for all other samples. This shows that all other work had a degree of similarity between each sample of the same experiment.

Table 6.1: Difference and similarity calculations between elution curves. Highlighted red are f_1 values greater than 15 and f_2 values less than 50 (sample number = 3, error = standard deviation).

Figure Number	Figure Name	Data Label	f_1 Value	f_2 Value
Figure 6.1	Effect of bead size on Dox elution	DC Bead M1	7.78 ± 3.39	87.00 ± 6.42
		DC Bead M1*	4.58 ± 2.91	92.11 ± 5.50
		DC Bead 103	5.47 ± 3.92	85.11 ± 12.57
		DC Bead 305	9.73 ± 6.33	70.90 ± 18.43
		DC Bead 507	2.87 ± 1.34	85.72 ± 6.75
Figure 6.3	Effect of bead type on Dox elution	DC Bead M1	7.78 ± 3.39	87.00 ± 6.42
		DC Bead 103	5.47 ± 3.92	85.11 ± 12.57
		DC Bead LUMI M1	5.01 ± 3.17	88.88 ± 8.72
		DC Bead LUMI 103	1.84 ± 1.25	93.91 ± 3.41
		Tandem 107	19.00 ± 15.30	52.36 ± 25.97
		Tandem 110	3.64 ± 0.84	82.00 ± 4.94
Figure 6.8	Comparison for Dox and Iri elutions	Dox (37.5 mg/mL)	5.47 ± 3.92	85.11 ± 12.57
		Iri (50 mg/mL)	2.29 ± 1.66	97.63 ± 1.11
Figure 6.10	Slow flow elutions	DC Bead M1 (37.5 mg/mL)	3.06 ± 2.53	58.03 ± 10.86
		DC Bead LUMI M1 (37.5 mg/mL)	3.47 ± 3.33	49.34 ± 18.09
		DC Bead LUMI M1 (75 mg/mL)	1.00 ± 0.94	82.52 ± 12.37
		DC Bead LUMI 103 (37.5 mg/mL)	1.78 ± 1.46	71.90 ± 8.44
		Tandem 110 (37.5 mg/mL)	12.70 ± 11.47	52.71 ± 9.75
		LifePearl 100 (37.5 mg/mL)	0.58 ± 0.48	80.84 ± 7.49

6.3. Conclusion

The study confirmed that each bead size of DC Bead™ is capable of loading the same amount of drug and achieving complete elution, however binding and elution patterns differ. Larger beads take a proportionally longer time to elute Dox, as smaller beads have a larger surface area to volume ratio. DC Bead*M1*™ demonstrated a particular elution profile shape comparable to the inverted ITC binding data. When evaluating the different sizes of DC Bead™, 70-150 µm reaches a plateau displaying complete elution earliest, with 100-300 µm next, followed by 300-500 µm and finally 500-700 µm. Each bead size demonstrated a slightly different elution profile, but with the same total amount of Dox eluted. DC Bead™ 70-150 and 100-300 µm displayed a similar elution profile as their bead diameters overlap, but 70-150 µm beads do show a higher accumulated elution profile over the first 500 minutes compared with the larger sized 100-300 µm beads. A larger surface area will have more contact with sodium ions and so a faster elution. Both sizes of Tandem™ bead (75 ± 25 and 100 ± 25 µm) and DC Bead LUMI™ (70-150 and 100-300 µm) have similar elution profiles as again there is an overlap in bead size.

The comparative bead study identified that each type of beads behaved in very different ways within this test. Each bead showed a capability to elute the full concentration of loaded drug, except for Tandem™. It seemed that a considerable proportion of Dox did not elute from Tandem™ beads, but was held within the structure. Whilst DC Bead™ and DC Bead LUMI™ eluted ~100 % of the loaded drug, Tandem™ under the same conditions eluted only ~80 %, which could not then be extracted from the beads using a variety of solutions that had worked well on DC Bead™ and DC Bead LUMI™. The inability of Tandem™ to freely elute all the drug across two separate testing methods suggests, that some permanent attachment to the bead polymer matrix had occurred. Tandem™ contains carboxylic acid (found in the bead), and this along with amines (from the drug) are well-known to react to form stable amides under appropriate conditions. Binding of high drug concentrations within the bead matrix brings these functional groups within close proximity of one another, potentially facilitating a templating reaction, as proposed in the mechanism presented in Figure 6.12.

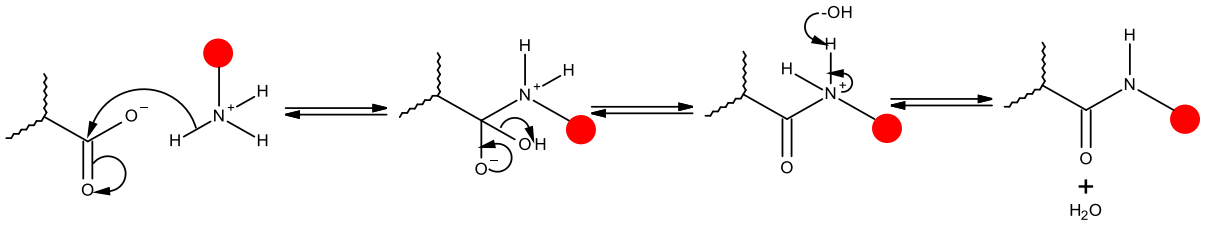

Figure 6.12: Proposed reaction of Tandem™ binding to Dox.

Tandem™ is indicated for loading with 50 mg/mL of Dox, where DC Bead™ and DC Bead LUMI™ is 37.5 mg/mL. To make comparisons between DC Bead™, DC Bead LUMI™ and Tandem™, the same loading concentration of 37.5 mg/mL Dox was used, however for Tandem™ the volume of beads was decreased to 0.4 mL to give a 50 mg/mL load. Although Tandem™ beads are in general loaded with more drug, 150 mg/mL is the maximum concentration of Dox which can be delivered to a patient. Therefore a person may receive 3 mL of Tandem™ or 4 mL of DC Bead™, but in both circumstances would be receiving 150 mg Dox. The report indicates that a patient treated with drug loaded DC Bead™ would receive 100 % of the chemotherapeutic drug, whereas another patient administered drug loaded Tandem™ would receive 80 % of the drug. This could ultimately not only effect recovery but survival rates. Dox release occurred over a similar time frame with the different bead types, however DC Bead™ had a significantly higher burst of drug release than DC Bead LUMI™ and Tandem™ over the first 200 minutes. It is possible that different modalities of the disease state could benefit from different release profiles, such as an initial high impact of drug to the tumour which dissipates over time as the disease reverts or a more constant release of drug with a steadier control of drug release over time. One type of patient may be able to withstand side effects of the initial higher dose and a decrease in side effects thereafter, whilst another person may be more tolerant to the same effects over the course of the treatment, but at this point it is difficult to endorse what implications any of this has in a clinical setting. HepaSphere™ was not compatible with this method, as the bead gelled and blocked flow of eluent.

Beads were loaded with the clinical concentration of Dox, along with a lower and higher concentration. It was observed that drug loading dose is proportional to elution rate, a higher dose showed a higher release of Dox and required a proportionally longer time to elute. The investigation confirmed that 100 % of the drug (25, 37.5 and 45 mg/mL Dox) loaded into DC Bead™ could be eluted from all sizes. It appeared that 20 % of each concentration of drug (25, 50, 75 mg/mL Dox) loaded in Tandem™ beads was irreversibly bound to the structure. This representative method of elution

introduced fresh media to the beads, the elutant was not recirculated and therefore it is reasonable to suggest that there were plenty of sodium ions to extract the Dox from the drug delivery system. Further work is required to fully understand these findings.

Iri eluted at a much greater rate than Dox as expected since Iri had shown much weaker interactions than Dox through the ITC, the work presented confirms the new elution method was capable of generating a reproducible elution profile with the same experimental conditions as Dox.

Slow flow rates of 0.1 mL/min were achieved with the open-loop flow-through elution method. The experiments were terminated before the beads had fully eluted, however the results expressed similar profiles to the experiments conducted at 2 mL/min. This confirms that the method developed was suitably performed at faster flow rates that can represent elution from an embolised vessel.

The f_1 and f_2 values confirmed that there was similarity between the majority of the elution curves. In summary, the development of a novel elution method led to better comparison with beads of different sizes, different types of bead, different drug loading concentrations, different types of drug and flow rates more comparable with embolised blood vessels.

References

1 T. Swaine, Y. Tang, P. Garcia, J. John, L. J. Waters and A. L. Lewis, Evaluation of ion exchange processes in drug-eluting embolization beads by use of an improved flow-through elution method, *Eur. J. Pharm. Sci.*, 2016, **93**, 351–359.

2 R. R. Taylor, Y. Tang, M. V. Gonzalez, P. W. Stratford and A. L. Lewis, Irinotecan drug eluting beads for use in chemoembolization: In vitro and in vivo evaluation of drug release properties, *Eur. J. Pharm. Sci.*, 2007, **30**, 7–14.

3 A. L. Lewis, M. V. Gonzalez, S. W. Leppard, J. E. Brown, P. W. Stratford, G. J. Phillips and A. W. Lloyd, Doxorubicin eluting beads − 1: Effects of drug loading on bead characteristics and drug distribution, *J. Mater. Sci. Mater. Med.*, 2007, **18**, 1691–1699.

4 J. Namur, M. Wassef, J.-M. Millot, A. L. Lewis, M. Manfait and A. Laurent, Drug-eluting Beads for Liver Embolization: Concentration of Doxorubicin in Tissue and in Beads in a Pig Model, *J. Vasc. Interv. Radiol.*, 2010, **21**, 259–267.

5 K. Hong, A. Khwaja, E. Liapi, M. S Torbenson, C. S Georgiades and J.-F. H Geschwind, New Intra-arterial Drug Delivery System for the Treatment of Liver Cancer: Preclinical Assessment in a Rabbit Model of Liver Cancer, *Clin. Cancer Res.*, 2006, **12**, 2563–2567.

6 CeloNova, Embozene Tandem™ (Microspheres for Embolization), http://tecnicasintervencionistas.com/presentacion_cursos/PRESENTACION TANDEM.pdf, (accessed 1 October 2017).

7 BTG, DC Bead™ and DC BeadM1™ loading instructions, http://bead.btg-im.com/uploads/document_r/Loading Instructions Folder v4 web DEBDOX.pdf, (accessed 1 October 2017).

8 J. Blümmel, S. Reinhardt, M. Schäfer, C. Gilbert, L. Sun and J. Ren, Drug-eluting Beads in the Treatment of Hepatocellular Carcinoma and Colorectal Cancer Metastases to the Liver, *Eur. Oncol. Haematol.*, 2012, **8**, 162–166.

9 K. Ashrafi, Y. Tang, H. Britton, O. Domenge, D. Blino, A. J. Bushby, K. Shuturminska, M. den Hartog, A. Radaelli, A. H. Negussie, A. S. Mikhail, D. L. Woods, V. Krishnasamy, E. B. Levy, B.

J. Wood, S. L. Willis, M. R. Dreher and A. L. Lewis, Characterization of a novel intrinsically radiopaque Drug-eluting Bead for image-guided therapy: DC Bead LUMI, *J. Control. Release*, 2017, **250**, 36–47.

10 U.S. Department of Health and Human Services Food and Drug Administration Center for Drug Evaluation and Research (CDER), Guidance for Industry Dissolution Testing of Immediate Release Solid Oral Dosage Forms, https://www.fda.gov/downloads/drugs/guidances/ucm070237.pdf, (accessed 1 June 2014).

Chapter 7 : Microscopic Analysis of Drug Eluting Beads (DEBs) and Related Techniques

7.1. Introduction

Some of the beads used in this study are known to swell, shrink or rearrange under certain conditions and it was therefore hypothesised that these phenomena may have affected drug elution, such as the studies presented in Chapters 5 and 6. For example, Figure 7.1 illustrates the possibility that the change in the elution profile observed without glass beads was a result of bead swelling and bead rearrangement within the cell. During preparation of the experiment a 6 – 7 mm space was left in the flow-through cells for the beads to expand into during each elution without the presence of packing material. It is a well-established concept that as drug is released from drug eluting beads (DEBs) they increase in size. It is thought that once the beads became tightly packed the flow rate slowed, eventually the beads increased in size by such an extent that they moved into the space provided and the flow rate returned to 'normal'. To confirm whether swelling had affected elution, three-dimensional microscopy (3DM) was employed to visualise the swelling process during this method of elution.

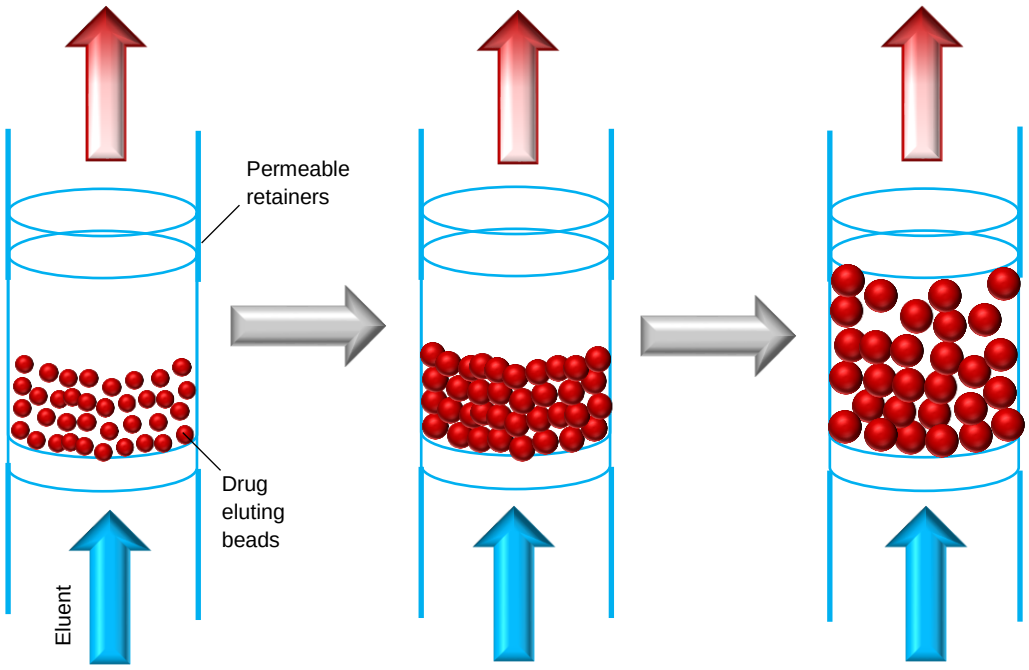

Figure 7.1: Bead size change in an open-loop flow-through cell without packaging material.

Secondly, 3DM was also used to create static images of the different bead types successfully studied in Chapters 4 and 6 (DC Bead™, DC Bead LUMI™, LifePearl™ and Tandem™), under different conditions of unloaded, loaded and eluted drug from the beads, with the most commonly used drug (doxorubicin (Dox)) and at the most appropriate concentration (37.5 mg/mL).

Thirdly, hot stage microscopy (HSM) was employed to investigate bead behaviour at room and body temperatures. HSM is a technique which combines microscopy and thermal analysis of samples, recording visual changes as images at a set temperature or over a range of temperatures with time. The importance in this study is the fact that the equipment can also record changes in colour and light intensity over time. It was theorised that at extremely elevated temperatures the bead structure could become deformed, resulting in less drug binding to the bead. Therefore, the controlled heating capability of the equipment was not necessary in this study, other than to maintain samples at one of two specified temperatures: room temperature to replicate bead loading in a clinic and body temperature to mimic drug release within a patient. Morphology, particle size, and colour intensity are of particular interest, as the instrument can capture these events during loading by the addition of drug to the beads under the lens, or during elution by the addition of salt solution to drug loaded beads. Experiments were conducted with DC Bead*M1*™, Dox and phosphate buffer saline (PBS).

7.2. Results and Discussion

7.2.1. Effects of Bead Swelling Properties

Images were taken at set intervals over the course of drug elution and bespoke software converted the images into a video. A typical open-loop flow-through elution was conducted at a flow rate of 2 mL/min as this ensured the full elution could be capture over ~16 hours. DC Bead™ 100-300 µm loaded at 37.5 mg/mL Dox was selected for microscopic analysis as this was a bead type well known to swell by ~20 % of the loaded diameter and had been well evaluated during elution [1,2]. The points where there was a change in bead size were noted and Figure 7.2 displays the images at these timepoints.

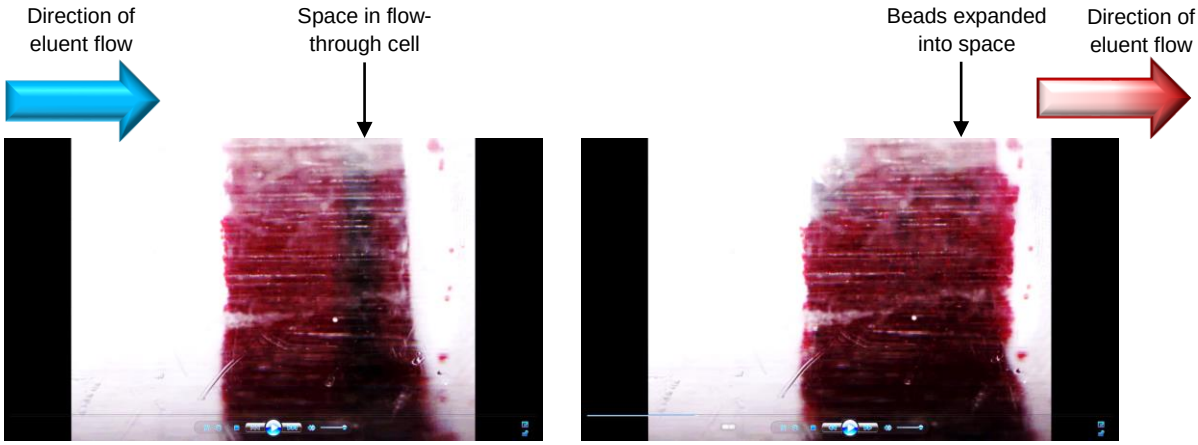

Figure 7.2: Bead changes captured using 3DM at a magnification of x20. The experiment was conducted using 0.5 mL of 100-300 µm DC Bead™, loaded with 37.5 mg/mL Dox and in PBS.

A change in bead size started at 101.16 minutes and ended at 221.05 minutes. The information was compared with changes perceived in a similar experiment demonstrated in Figure 7.3, of drug elution using the open-loop flow-through method with ultra-violet (UV) spectroscopic analysis.

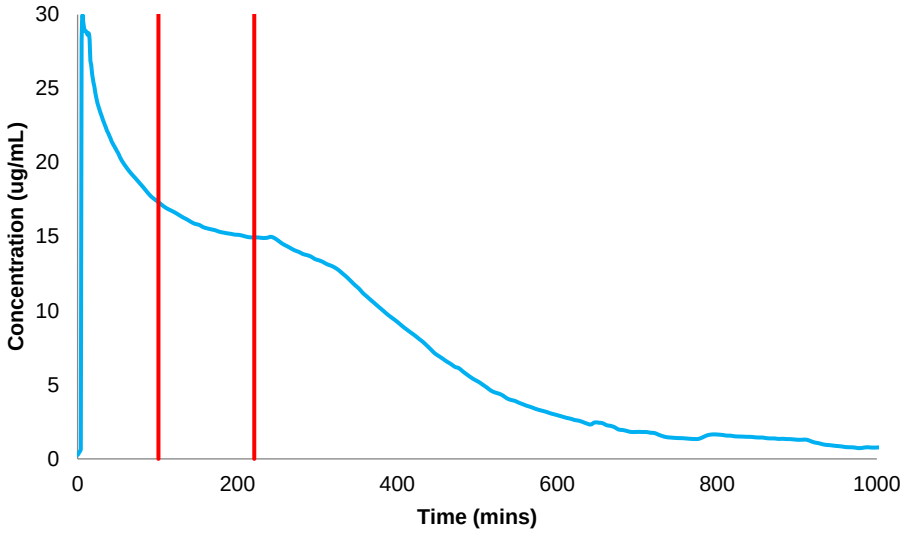

Figure 7.3: The experiment was conducted using 0.5 mL of 100-300 µm DC Bead™, loaded with 37.5 mg/mL Dox, with no packing material, in PBS (154 mM) and a flow rate of 2 mL/min. The red lines indicate the start and end of volume change identified using 3DM data.

Through analysing the data presented in Figure 7.3, it can be seen that 3DM analysis identified a change in bead size during the elution. These changes occurred at a similar time in which changes arose in the UV elution profile. When beads began to swell the flow rate reduced, as the beads packed more tightly against each other and this temporarily decreased the rate of elution. Once the beads had fully expanded they moved into the space provided, settling back to the original flow rate and increasing the rate of elution. It can be concluded that beads with swelling properties, such as those used in this work, will have an altered elution profile due to a change in bead packing, and so it is for this reason that DEBs are rightly packed with glass beads to avoid this issue.

7.2.2. Microscopy of Unloaded, Drug Loaded and Eluted Beads

Beads were analysed using microscopy before loading, after loading (which is also before elution) and after elution, to indicate homogeneous or heterogenous drug loading, and to ascertain the extent of any aggregation and/or fragmentation of the bead. Table 7.1 displays images of a similar bead size for DC Bead*M1*™ (100-300 µm), DC Bead LUMI*M1*™ (100-300 µm), Tandem™ (100 ± 25 µm) and LifePearl™ (100 ± 25 µm) in each of the three scenarios with a 3DM.

Table 7.1: Beads before loading (bland bead), after loading/before elution (loaded bead) and after elution (eluted bead). DC Bead™, DC Bead LUMI™ and LifePearl™ images at a magnification of x250, Tandem™ at a magnification of x500. Beads were loaded with the clinically recommended loading concentrations, i.e. 37.5 mg/mL Dox for DC Bead™, DC Bead LUMI™ and LifePearl™, but 50 mg/mL Dox for Tandem™. Note that the LifePearl™ eluted sample was not continued till complete drug release.

Bead Type and Bead Size (µm)	**Bland Bead**	**Dox Loaded Bead**	**Dox Eluted Bead**
DC Bead™ 103	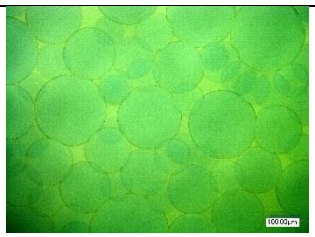	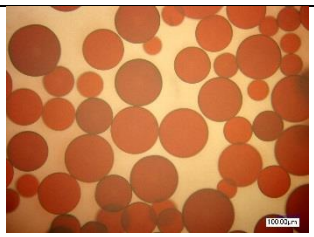	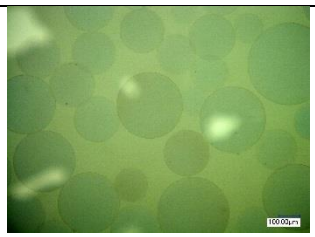
DC Bead LUMI™ 103	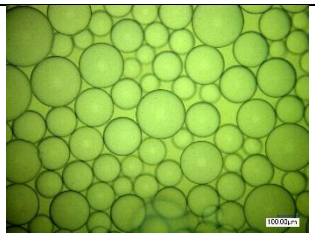	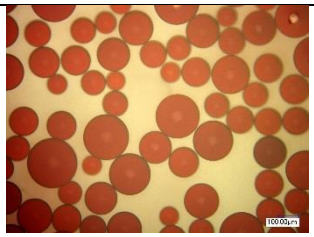	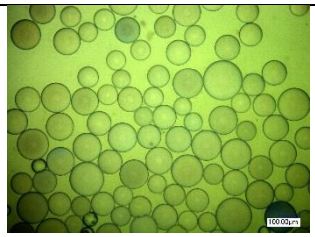
LifePearl™ 100	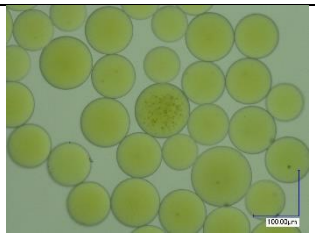	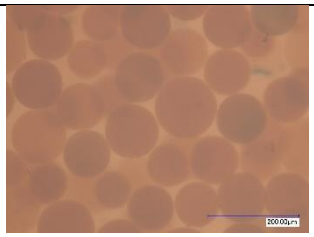	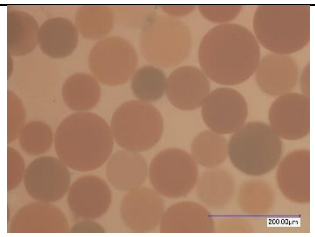
Tandem™ 110	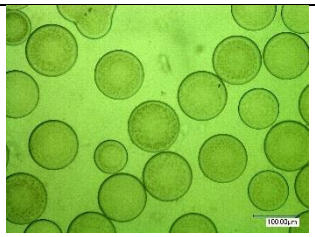	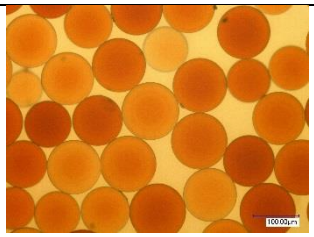	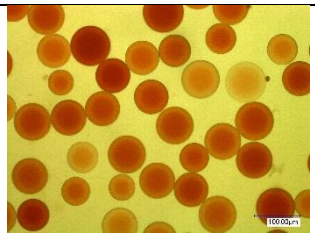

When DEBs are loaded with drug, they commonly transform from the original bead colour to the colour of the loaded drug, in the case of Dox loaded beads they become red. The drug was uniformly dispersed across loaded DC Bead™, DC Bead LUMI™ and LifePearl™, evident from the even colour, however the same cannot be said for Tandem™. There was a range of colour across Tandem™ beads, which could only suggest a range of highly concentrated and less concentrated beads within the sample.

After elution of the drug, the beads should revert to the original bead colour. DC Bead™ and DC Bead LUMI™ released the majority of the drug and so lost most of the red colour. Tandem™ seemed to retain some of the drug and a substantial portion of the beads remained red. In addition to this, a substantial number of beads were highly concentrated with Dox whilst others had eluted a considerable portion, indicating possible further drug loading in addition to drug elution. The uneven loading and elution supports the theory that Tandem™ is a heterogenous bead, whilst the uniform nature of DC Bead™, DC Bead LUMI™ and LifePearl™ supports a homogenous bead across the vial or syringe sample. The LifePearl™ sample was not completely eluted as the experiment was stopped prematurely, therefore the beads have not lost a considerable amount of the red colour. Since some LifePearl™ beads have completely eluted by the loss of red, and as drug was entirely extracted from the beads, it is suggested that this bead is capable of returning to the original bead colour.

Furthermore, LifePearl™ and Tandem™ do have tighter calibrated bead sizes and although this is only a small snapshot of the samples it is noticeable in the images. Bland DC Bead™ was blue, DC Bead LUMI™ yellow, LifePearl™ green and Tandem white, though the pictures show a green tinge this is because of the filter and light mode selected on the microscope. It was not possible to create three-dimensional (3D) images on the instrument because the samples were contained within water but interestingly, certain structures were observed that hadn't been seen on a standard optical microscope. Table 7.2 presents further images of bland beads to identify the key structure of the different products.

Table 7.2: Different magnifications of bland DC Bead™, DC Bead LUMI™, LifePearl™ and Tandem™.

Bead Type and Bead Size (µm)	Magnification		
	x500	x1000	x2500
DC Bead™ 103	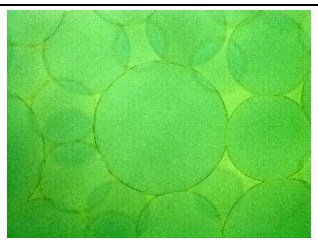	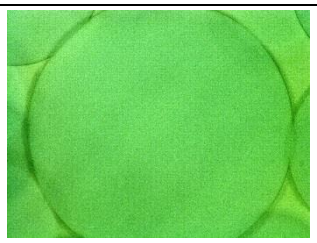	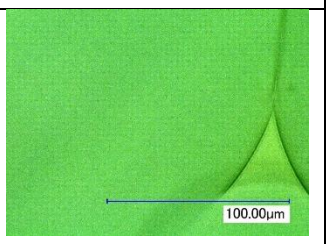
DC Bead LUMI™ 103	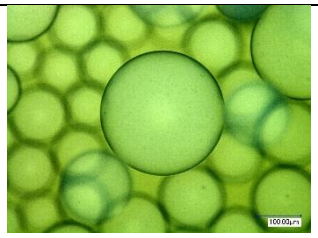	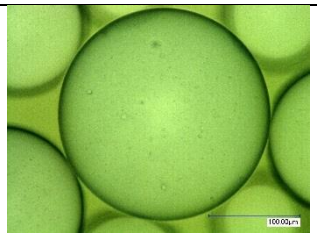	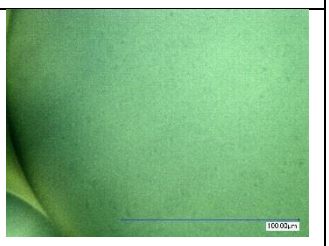
LifePearl™ 100	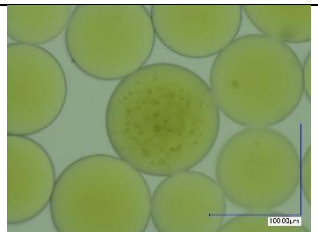	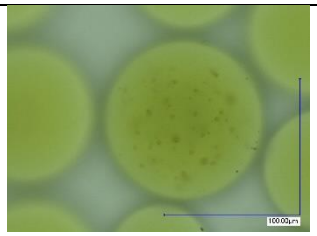	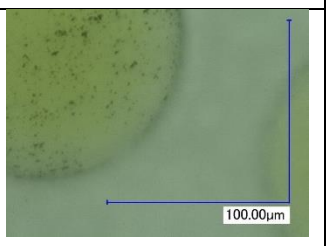
Tandem™ 110	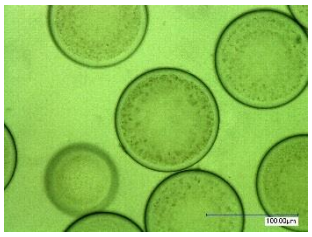	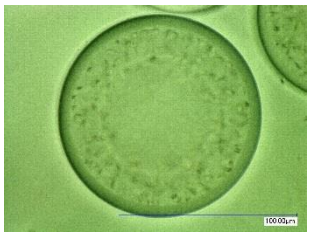	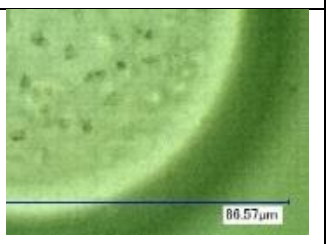

Different magnifications were applied to beads to ascertain particular internal features of interest. DC Bead™ had an extremely smooth uniform appearance. DC Bead LUMI™ was also quite smooth with very small indentations across the surface. Most LifePearl™ beads had a smooth exterior, but some were covered with dark marks. It was unclear from the images whether these were foreign objects or a part of the beads themselves. Tandem™ has an unusual appearance with three distinctive segments. These consist of an outer ring, a dense middle section and separate core. This is a structure inside the beads and not on the surface, as the focus plane is in the middle of the beads and not the external layer.

On close inspection of Tandem™, the surface comprised of small irregular shaped structures. It would be of interest to see how the drug concentration varies across the segments of Tandem™ bead.

7.2.3. Size and Colour Change During Bead Loading

Images obtained using the HSM were taken over time and converted into videos. The images in Figure 7.4 indicate Dox absorbing into the DC Bead*M1*™ at room temperature over 30 minutes. It can be seen that the intense red solution was depleted and became transparent. It is visually possible to see that the beads have changed size, although the equipment was unable to quantify this change, this particular bead is known to decrease in size with drug binding [1,2].

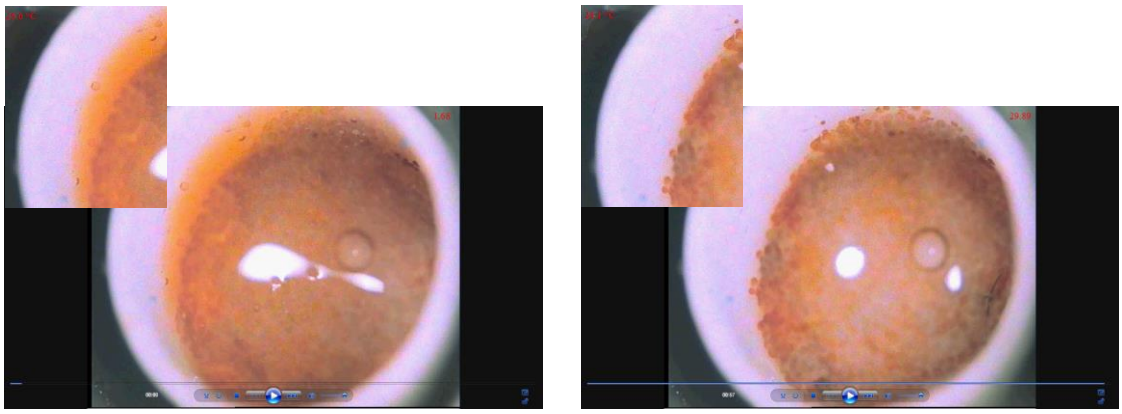

Figure 7.4: Images of 1 mM Dox into 10 mg DC Bead*M1*™ with insert of zoomed image, at 1 minute and 30 minutes after the addition of 10 µL of the drug.

An additional experiment was conducted at 37 °C to mimic body temperature, whereby salt solution was added to Dox loaded beads to observe the release of drug over 30 minutes, in the reverse of the previous test. Just as salts from blood in the body would facilitate an ion-exchange process, the red drug was removed from the beads, the solution turned from transparent back to red and the beads transformed back to blue, as shown in Figure 7.5. It may be difficult to see the blue beads under the red solution, but a darker colour can be seen at 30 minutes in comparison to the earlier image. Supporting earlier findings, beads seemed to increase in size with the elution of drug as water was drawn into the bead structure.

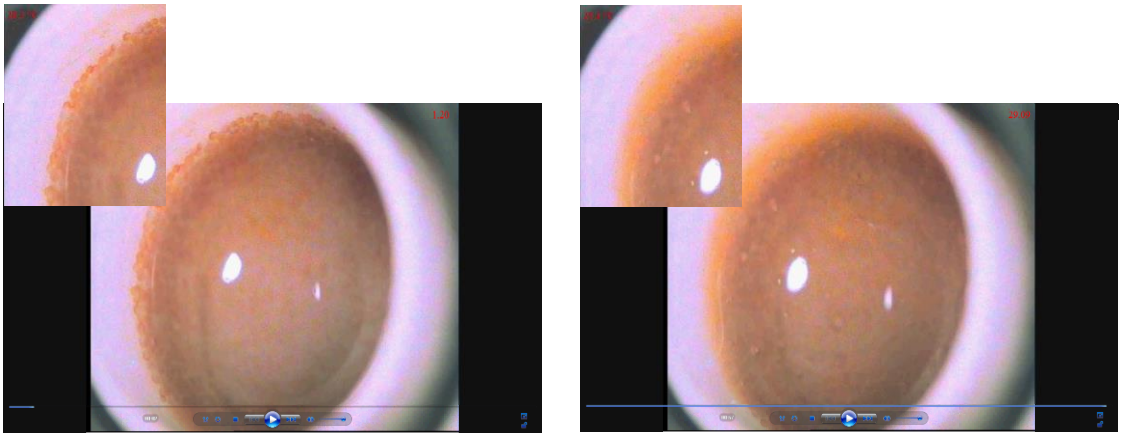

Figure 7.5: Images of 10 mg DC Bead*M1*™ loaded with 1 mM Dox with insert of zoomed image, at 1 minute and 30 minutes after adding 10 µL 15 mM PBS.

HSM can detect the change in colour of a sample, but since the solution and bead interchange colour this was problematic. The instrument uses a small window which can be placed within the microscopic image by the user, during the experiment the pixels within the area are detected for changes in red, green and blue (RGB). The RGB and light intensity data could be plotted in a graph, and compared to different beads or different drugs indicating the extent of drug bound or eluted from the beads. Because the solution covered the beads, it would have been difficult to identify a colour change. This is because the window of colour detection must be placed where there was solution with no beads, as this would readily change depending from red (in the case of Dox) to transparent. The problem occurred in foreseeing where the solution will lay and where beads will not before the addition of drug or salt, as the window must be set before the experiment was initiated. This could be thought-provoking further work.

7.3. Conclusion

Elution viewed under the 3DM showed a clear volume change which matched the profile artifacts seen with UV spectrophotometric data. This confirms that the swelling effect of certain beads altered the elution profile and justifies the used of glass beads to eliminate these effects.

Microscopic images displayed DC Bead™, DC Bead LUMI™ and LifePearl™ to homogenously load the drug and was capable of achieving complete elution. Images indicate a large portion of Dox was present in Tandem™ after elution. It also demonstrated that Tandem™ had heterogenous loading, the red colour of Dox indicating significant variability, it is as yet unknown what potential implications this may have on a patient. HepaSphere™ had extensive evidence of aggregation and fragmentation, as it was unsuitable for the elution method it was excluded from further microscopic analysis.

HSM has thereby confirmed its suitability for bead-drug analysis under controlled temperature conditions. The method developed could be used for further bead type and drug type comparison.

References

1 K. Hong, A. Khwaja, E. Liapi, M. S Torbenson, C. S Georgiades and J.-F. H Geschwind, New Intra-arterial Drug Delivery System for the Treatment of Liver Cancer: Preclinical Assessment in a Rabbit Model of Liver Cancer, *Clin. Cancer Res.*, 2006, **12**, 2563–2567.

2 A. Lewis, M. González, A. Lloyd, B. Hall, Y. Tang, S. Willis, S. Leppard, L. C Wolfenden, R. R Palmer and P. Stratford, DC Bead: In Vitro Characterization of a Drug-delivery Device for Transarterial Chemoembolization, *J. Vasc. Interv. Radiol.*, 2006, **17**, 335–342.

Chapter 8 : Conclusion and Future Work

8.1. Conclusions

A novel set of *in vitro* methods have been developed to standardise and characterise the binding and release of selected drugs from different types of drug eluting bead (DEB), as described in the objectives of the thesis and stated in Chapter 1. These methods were created to overcome the limitations experienced with existing techniques by mimicking the *in vivo* environment and providing reproducible and *in vivo* correlated data. *In vitro* test methods with strong correlation to *in vivo* behavior are key in the development of a DEB, including material choice and drug selection to offer efficacious and predictable clinical solutions. In order to effectively characterise DEB products it was important to understand the rate and extent of drug binding and release *in vivo*. Comparative analysis between different DEB is challenging because of their variable physicochemical properties, such as bead size, bead density, drug dose, drug type and swelling. As the methods reported in literature were inadequate to generate comparative data, new methods were investigated.

The achievements of each objective are as follows:

8.1.1. Chapter 3

1. The application of isothermal titration calorimetry (ITC) to investigate drug-bead binding interactions.

The first portion of this objective was the development of an ITC method capable of identifying the number of binding sites occupied by the drug on the bead. This was achieved as the binding ratio was initially found to be 0.43:1 [1], which later increased to 0.90:1 2-acrylamido-2-methylpropane sulfonate sodium salt (AMPS):doxorubicin (Dox) upon acid washed the beads. It was deemed necessary to wash the beads in acid to increase the initial binding due to the nature of the method. Temperature had no effect on the binding ratio but did increase the rate of binding. The change in pH caused by acid washing the beads was not the reason for the drug-bead interaction. An increase in the bead mass increased

the moles of drug bound to the beads possibly as result of a decline in experimental error. An increase in the drug concentration had no effect on the binding ratio. A dramatic increase or decrease in the recommended number of injections proved to reduce the accuracy of the experiments. The thermodynamic system of the selected experimental parameters included hydrogen bonding, electrostatic, van der Waals and hydrophobic interactions resulting in conformational changes, consequently the reactions were both enthalpically and entropically driven, and spontaneous regardless of the systems temperature. Using a method of drug extraction and quantifying residual drug, the saturation point was determined to be the position whereby enthalpy decreased. In addition, Dox was found to aggregate under the experimental concentrations used in this study.

8.1.2. Chapter 4

The second portion of the first objective was to compare different sized beads, different bead types, and different drugs. It was difficult to determine the binding interaction of larger beads in the DC Bead™ type than 70-150 µm, although with small additions of drug the rate of binding was comparable. LifePearl™ bound to less drug than DC Bead™, 0.74:1 compared with 0.92:1. DC Bead LUMI™, Tandem™ and HepaSphere™ were not compatible for the developed calorimetric method. In addition to Dox, Mitoxantrone (Mit), Irinotecan (Iri) and Topotecan (Top) were well-suited drugs which bound with DC Bead™ through the titration technique. Dox bound to one AMPS site per drug molecule, whereas Mit bound to two sites per drug molecule with a ratio 0.42:1 or 0.84:1 if individual drug binding site are considered. Iri and Top both bound to one site per drug molecule corresponding to 0.78:1 and 0.92:1, but possibly to two different sites in the first and second portion of the experiment. In the case of Iri this was attributable to two ionised sites at the pH of the acid washed beads and drug mixture, but naturally occurred in Top because of the ordinarily two ionised sites at the acidic pH of the drug.

8.1.3. Chapter 5

2. The development of a novel method to determine the release of drug from DEBs.

The second objective was accomplished through an elution method which mimicked an embolised vessel and addressed the limitations of the previous methods. For the new method of elution tested

parameters were: DEB packing configuration, geometry and volume, eluent flow rate, drug loading and eluent concentration. A single pass eluent flow through system was used to mimic *in vivo* depletion, which overcame issues associated with self-aggregation and low extractability of certain drugs. The first set of experiments identified the need to degas the eluent using helium through an aerator. This not only reduced the formation of air bubbles in the sample and prevented them from travelling to the UV detector, but it also improved the reproducibility of the data and minimised elution profile artifacts. Sand was discovered not to be an appropriate packing material, but glass beads improved the reproducibility of the elution curve, eliminating imperfections and the swelling impact. A 1:5 ratio provided a uniform mixture of DEB:glass bead at both flow rates of 1 and 2 mL/min. A flow rate of 2 mL/min worked well for practicality with reliable results. To conserve the bead samples, 0.5 mL was found to be a suitable volume which gave precise and accurate results. Increasing the flow rate and increasing the concentration of sodium chloride (NaCl) was noticed to increase the rate of elution. Elution was proportional to the availability of sodium ions up to a certain concentration (308 mM) and flow (5 mL/min). The composition of medium influenced the release kinetics, sometimes this was dependent upon the concentration of salt such as in simulated body fluid (SBF) which closely matched the results of phosphate buffer saline (PBS) and NaCl. In Ringer's solution complete elution of the drug was not achieved and other factors must have influenced the ion-exchange mechanism.

8.1.4. Chapter 6

Once again, an additional part of the second objective was to use the representative method of elution to compare bead size, bead type, drug concentration, drug type and slow flow rates. An increase in bead size increased the rate of elution, as the surface area to volume ratio decreased. Different types of beads provided different elution profiles, DC Bead LUMI™ had a slower release profile than DC Bead™ as DC Bead™ had a higher initial burst of Dox than DC Bead LUMI™. DC Bead™ and DC Bead LUMI™ fully loaded and eluted each concentration of drug, where Tandem™ held onto ~20 % of the loaded drug. Traditional, as well as innovative methods of forced extraction could not completely remove the drug from Tandem™, suggesting some permanent attachment of the drug to the bead. HepaSphere™ had to be excluded from the test samples as the product gelled, blocking the flow of eluent and an abundance of smaller fragments suspended in solution passed through the cell filters, generating falsely high spectrophotometry measurements. Beads were loaded with various clinical

concentrations of Dox and it was found that an increased drug loading dose decreased the rate of elution. Iri eluted at a much greater rate than Dox, with complete elution of 50 mg/mL Iri in just 100 minutes compared with 37.5 mg/mL Dox in 1000 minutes for DC Bead™. The data from slow flow rates of 0.1 mL/min were representative of the faster flow rates and indicate that the method may be suitable for even slower flow rates of 0.01 mL/min that can represent elution from an embolised vessel. Even though experiments were terminated early and samples had not completely eluted, LifePearl™ showed similar results to that of DC Bead™ which correlates well with the ITC data.

8.1.5. Chapter 7

3. Confirmation of drug loading, drug elution and microscopic analysis.

The final objective identified swelling effects, along with visual characteristics of bland beads, loaded beads and eluted beads. Three-dimensional microscopy (3DM) allowed for visual analysis of changes in the open-loop flow-through elution. These results showed that bead swelling properties may have impacted the elution profile. Microscopic analysis indicated homogenous loading and near complete elution from DC Bead™, DC Bead LUMI™ and Lifepearl™, but heterogenous loading and incomplete elution from Tandem™. The loading and elution of beads under the hot stage microscopy (HSM) had magnified visual advantages that the open-loop flow-through elution method did not have.

In summary, this thesis proposed successful alternative methods of DEB evaluation. They not only address conventional test method limitations, but gather additional knowledge of drug-bead interactions which will undoubtable assist in the development of the best treatment options and paves the way further for research in treatment of inoperable cancers.

8.2. Future work

Further work could be carried out in several areas, these potential research opportunities include:

8.2.1. Isothermal Titration Calorimetry (ITC)

1. Optimisation of the ITC technique for the analysis of dense DEBs such as DC Bead LUMI™ and Tandem™. Discover a suitable cleaning method and removal of samples from the ITC cell, in particular for the analysis of HepaSphere™ which gels when reconstituted in liquid [2].
2. Perfect the method for analysing larger beads, for example DC Bead™ 100-300, 300-500 and 500-700 µm. Identify the distribution of the drug during the titration using a method of either cryostat to distinguish loading characteristics across segments of the beads [3], fluorescence or the green values throughout the distance of the beads [3].
3. Measure beads before, during and after calorimetry to determine shrinking effects [3,4].
4. Additional drug analysis of such chemotherapeutics agents as Daunorubicin, Epirubicin, Idarubicin and Vandetanib [5]. As well as combination drug mixtures potentially loading multiple drugs into one bead or mixing a variety of drug loaded beads. Dox-Rapamycin has shown synergistic activity with equivariant clinical results but reduced toxicity [6], binding and elution profiles could be of interest. Dox-Iri combinations could determine how they compete and interact with one another, as Iri can penetrate deep into the beads [7] and Dox can displace the outer section of drug on the surface of beads [3].
5. Drug binding to DEBs has been evaluated using ITC and drug elution could also investigated using ITC with a method of salt titrated into drug loaded beads, to identify any correlation with the open-loop flow-through elution technique [8].
6. The interaction of an imaging agent during the elution of drug loaded beads could be studied, to ascertain whether this hinders elution and what effect this has on different types of beads [9,10].
7. Use of the MicroCal PEAQ-ITC for greater sensitivity, more reliable results, less instrument preparation, reduced sample size and a shorter experimental time.

8.2.2. Open-Loop Flow-Through Elution

1. Analysis of Tandem™ particularly with Iri, to confirm the manufacturer's statement that this bead elutes 5 – 8 times slower than DC Bead™ [11]. Assessment of the claim that DC Bead™ has a more controlled and sustained released of Iri than DC Bead LUMI™ [12]. Further evaluation of other drugs that have been studied on the ITC, specifically Mit and Top as some drugs are possibly more potent than the currently indicated drug loading compounds [13].
2. Elution rate of individual components of Ringer's solution. To establish any competition for certain ions in comparison with NaCl, such as potassium chloride (KCl), calcium chloride ($CaCl_2$) and sodium bicarbonate ($NaHCO_3$) due to the valency of ions.
3. Reduction in the flow rate from 0.1 to 0.01 mL/min, to mimic the occlusion of an embolised vessel [8]. If possible, experiments could be continued until samples have completely eluted, perhaps without a peristaltic pump and flow maintained by gravity with data collected each day or even each week over the course of a month or several months.

8.2.3. Extraction of Drug

1. Verification of the drug left in Tandem™ after elution, possibly through differential scanning calorimetry (DSC) or thermogravimetric analysis (TGA).

8.2.4. Hot Stage Microscopy (HSM)

1. Use of the red green blue (RGB) detection to correlate drug binding and drug elution data.

8.2.5. Surface Dissolution Imaging (SDI)

Another instrument of interest is the Sirius™ SDi2 for surface dissolution imaging (SDI). This piece of equipment can detect and quantify drug elution through UV absorbance, is temperature controlled, can be operated in an open-loop and generate images of the sample at set intervals. It could be possible to compare SDI to the developed method of elution and confirm the interference of bead swelling effects. Figure 8.1 shows the SDi2 instrument developed by Sirius Analytical Ltd.

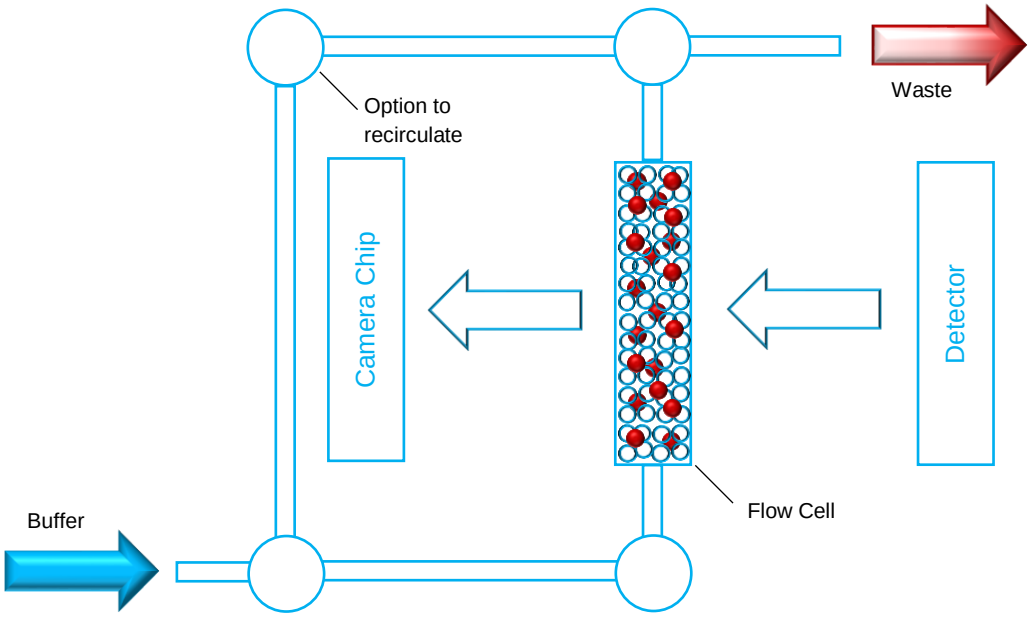

Figure 8.1: Surface dissolution imager [14].

A research group at Biocompatibles Ltd were tasked with the development of a method utilising a gel matrix as a tissue surrogate with a variable cylindrical channel geometry to simulate an embolised arterial vessel. This new assay allowed the evaluation of drug release via convection and diffusion from the DEB into the surrounding environment, illustrated in Figure 8.2. A predetermined extraction was followed by sectioning the arrangement into four equal quarters followed by the quantification of Dox to understand the effect on 'freed' Dox in different DEB formulations [8].

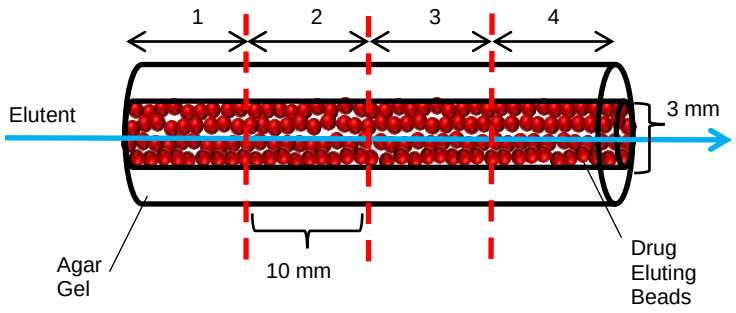

Figure 8.2: Flow-through tissue diffusion model [8].

The cylindrical geometry test has provided evidence of differences in rate of Dox desorption/reabsorption for different DEB formulations. There were Dox concentration changes within the cylindrical column of DC Bead™, whereby the front exposed to a supply of sodium ions was depleted and the distal end accumulated drug exceeding the original loading reaching a maximum load of 45 mg/mL. The diffusion of drug from DEBs into gel could be a method imitated with DSI and could perhaps be a simpler replacement as sectioning and extraction of drug would not be required.

SDI is regularly used for intrinsic dissolution rate (IDR) measurements of the active pharmaceutical ingredient (API), measuring swelling rates for controlled release dosage forms and measuring drug release from compact or whole dosage forms [14]. Figure 8.3 gives an idea of the types of images designed around Nelson and Shah flow cell for dissolution under laminar flow [15] and the USP 4 apparatus cell (flow-through dissolution) [16] that could be produced for DEBs.

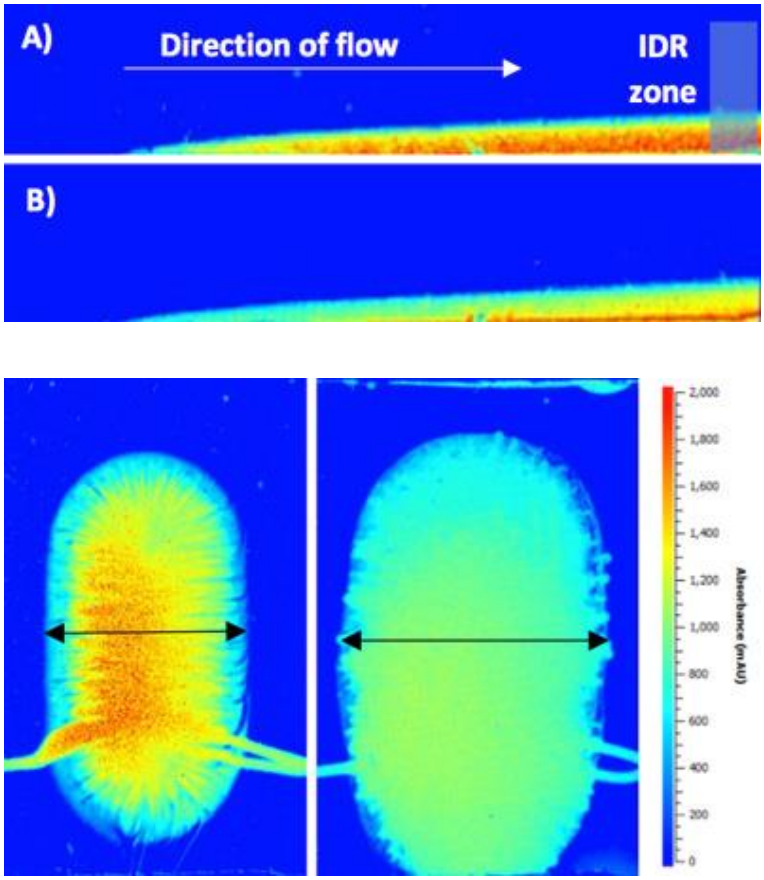

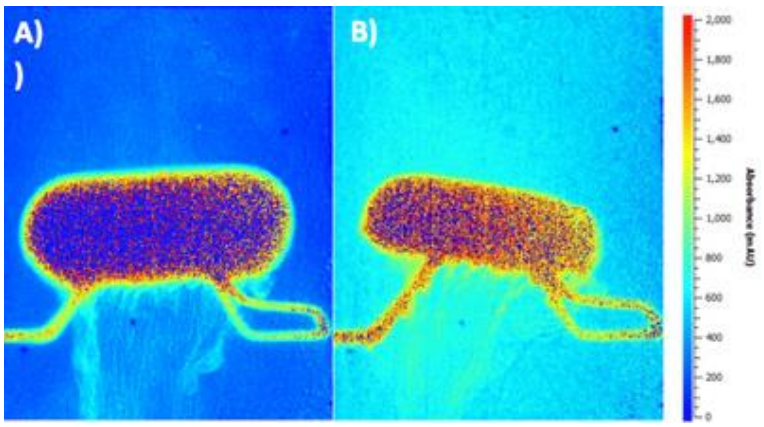

Figure 8.3: Examples of SDI images from Sirius Analytical using the compact or whole dosage flow cell, the top image shows IDR using the compact flow cell, the middle image demonstrates swelling and the bottom image displays drug release from a whole dosage form [14].

1. The study of Sirius™ SDi2 to generate images of the beads during elution with a method similar to that of open-loop flow-through elution. To correlate with elution data, but to identify any key visual difference between this and other methods, such as bead swelling effects [14].
2. Biocompatibles UK Ltd have developed a method for the detection of convection and diffusion of drug from DEBs into gel to simulate convection and diffusion into a blood vessel, a similar method could be developed with imaging instrumentation to compare the two methods [8].

In summary, this thesis has delivered valuable techniques for the evaluation of DEBs, however there were challenges and further work could be conducted to fully explore ten key areas of expansion identified with ITC, elution and microscopic applications for the analysis of drug-bead interactions.

References

1 L. J. Waters, T. S. Swaine and A. L. Lewis, A calorimetric investigation of doxorubicin–polymer bead interactions, *Int. J. Pharm.*, 2015, **493**, 129–133.

2 Merit Medical, HepaSphere™ MicroSphere Instructions for Use, https://www.merit.com/ifu/?i=327962, (accessed 1 October 2017).

3 A. L. Lewis, M. V. Gonzalez, S. W. Leppard, J. E. Brown, P. W. Stratford, G. J. Phillips and A. W. Lloyd, Doxorubicin eluting beads − 1: Effects of drug loading on bead characteristics and drug distribution, *J. Mater. Sci. Mater. Med.*, 2007, **18**, 1691–1699.

4 A. Lewis, M. González, A. Lloyd, B. Hall, Y. Tang, S. Willis, S. Leppard, L. C Wolfenden, R. R Palmer and P. Stratford, DC Bead: In Vitro Characterization of a Drug-delivery Device for Transarterial Chemoembolization, *J. Vasc. Interv. Radiol.*, 2006, **17**, 335–342.

5 A. L. Lewis, DC Bead™: a major development in the toolbox for the interventional oncologist, *Expert Rev. Med. Devices*, 2009, **6**, 389–400.

6 R. E J Forster, Y. Tang, C. Bowyer, A. Lloyd, W. Macfarlane, G. Phillips and A. Lewis, *Development of a combination drug-eluting bead: Towards enhanced efficacy for locoregional tumour therapies*, 2012, vol. 23.

7 R. R. Taylor, Y. Tang, M. V. Gonzalez, P. W. Stratford and A. L. Lewis, Irinotecan drug eluting beads for use in chemoembolization: In vitro and in vivo evaluation of drug release properties, *Eur. J. Pharm. Sci.*, 2007, **30**, 7–14.

8 T. Swaine, Y. Tang, P. Garcia, J. John, L. J. Waters and A. L. Lewis, Evaluation of ion exchange processes in drug-eluting embolization beads by use of an improved flow-through elution method, *Eur. J. Pharm. Sci.*, 2016, **93**, 351–359.

9 E. Liapi and J.-F. H. Geschwind, Transcatheter Arterial Chemoembolization for Liver Cancer: Is It Time to Distinguish Conventional from Drug-Eluting Chemoembolization?, *Cardiovasc. Intervent. Radiol.*, 2011, **34**, 37–49.

10 R. J. Lewandowski, J.-F. Geschwind, E. Liapi and R. Salem, Transcatheter Intraarterial Therapies: Rationale and Overview, *Radiology*, 2011, **259**, 641–657.

11 J. Blümmel, S. Reinhardt, M. Schäfer, C. Gilbert, L. Sun and J. Ren, Drug-eluting Beads in the Treatment of Hepatocellular Carcinoma and Colorectal Cancer Metastases to the Liver, *Eur. Oncol. Haematol.*, 2012, **8**, 162–166.

12 K. Ashrafi, Y. Tang, H. Britton, O. Domenge, D. Blino, A. J. Bushby, K. Shuturminska, M. den Hartog, A. Radaelli, A. H. Negussie, A. S. Mikhail, D. L. Woods, V. Krishnasamy, E. B. Levy, B. J. Wood, S. L. Willis, M. R. Dreher and A. L. Lewis, Characterization of a novel intrinsically radiopaque Drug-eluting Bead for image-guided therapy: DC Bead LUMI, *J. Control. Release*, 2017, **250**, 36–47.

13 R. E. J. Forster, S. A. Small, Y. Tang, C. L. Heaysman, A. W. Lloyd, W. Macfarlane, G. J. Phillips, M. D. Antonijevic and A. L. Lewis, Comparison of DC Bead-irinotecan and DC Bead-topotecan drug eluting beads for use in locoregional drug delivery to treat pancreatic cancer, *J. Mater. Sci. Mater. Med.*, 2010, **21**, 2683–2690.

14 Sirius Analytical, Sirius SDi2, http://www.sirius-analytical.com/products/sdi2, (accessed 1 October 2017).

15 K. G. Nelson and A. C. Shah, Convective Diffusion Model for a Transport-Controlled Dissolution Rate Process, *J. Pharm. Sci.*, 1975, **64**, 610–614.

16 The United States Pharmacopeial Convention, Dissolution, https://www.usp.org/sites/default/files/usp/document/harmonization/gen-method/stage_6_monograph_25_feb_2011.pdf, (accessed 1 October 2017).

Appendix

Isothermal Titration Calorimetry (ITC) Calibrations

Isothermal titration calorimetry (ITC) calibration instructions were obtained from Malvern Instruments Inc, Massachusetts, United States of America (USA).

Noise Test

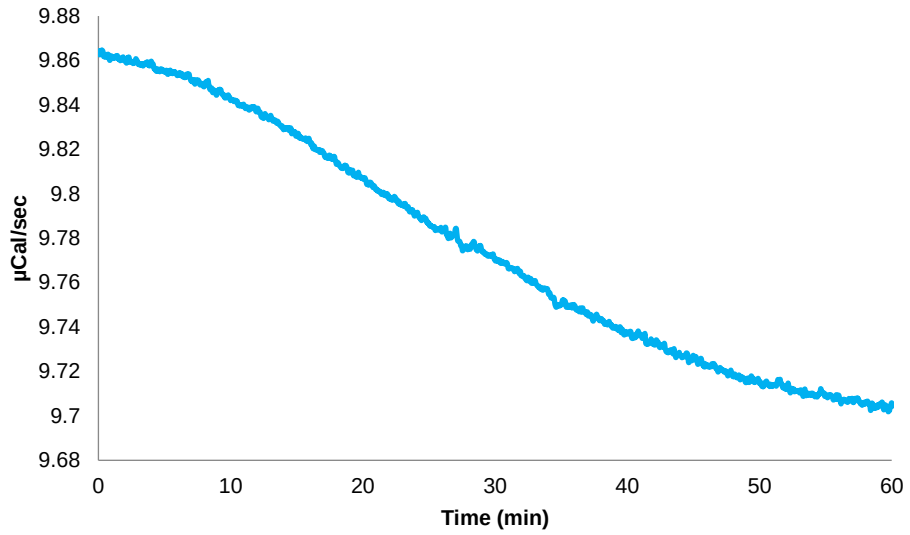

Criteria = Root mean squared (RMS) <0.5 µcal/sec. Water in the reference cell, sample cell and syringe. Injection number = 0. Cell temperature (°C) = 30. Reference power (µCal/sec) = 10. Initial delay (sec) = 3600. Syringe concentration (mM) = 0. Cell concentration (mM) = 0. Stir Speed = 307. Filter period (sec) = 2. Feedback mode/gain = High. ITC equilibration options = Fast equil; auto.

RMS = 0.257.

Water-Water

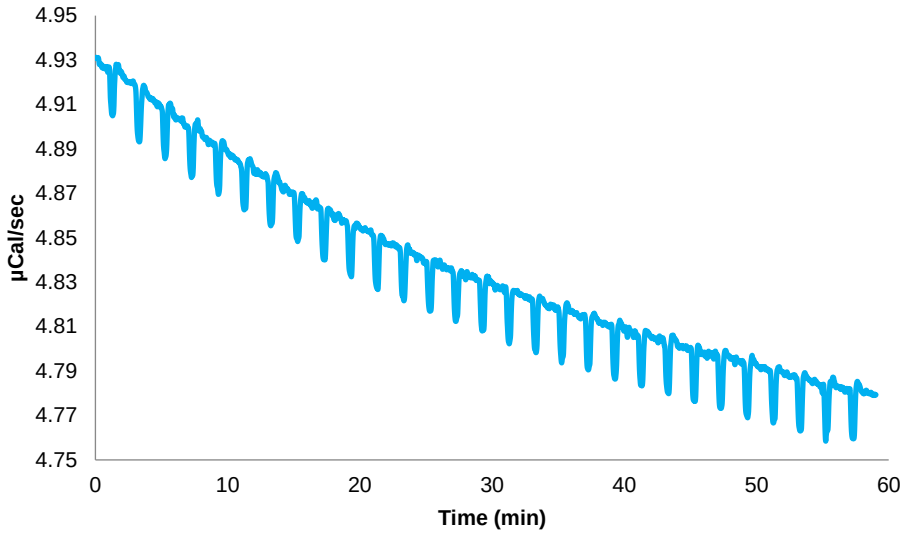

Water in the reference cell, sample cell and syringe. Injection number = 30. Cell temperature (°C) = 30. Reference power (µCal/sec) = 5. Initial delay (sec) = 60. Syringe concentration (mM) = 0. Cell concentration (mM) = 0. Stir Speed = 307. Volume (µL) = 10. Duration (sec) = 20. Spacing (sec) = 120. Filter Period (sec) = 2. Feedback mode/gain = High. ITC equilibration options = Fast equil; auto. Please note the water test can be performed in conjunction with the noise test.

Peaks of similar shape and size.

Differential Power (DP)/Y-Axis Test

Criteria = Error <1 %. Experimental temp = 30. Number of pulses = 6. Reference power = 10. Filter period = 2. Stiring speed = 300. Feedback mode/gain = High. Calibration power (µCal/sec) = 1. Pulse duration (sec) = 300. Pulse spacing (sec) = 600.

Errors = all <1 %, data appeared similar that of the manual.

Calcium Chloride ($CaCl_2$)-Ethylenediaminetetraacetic acid (EDTA)

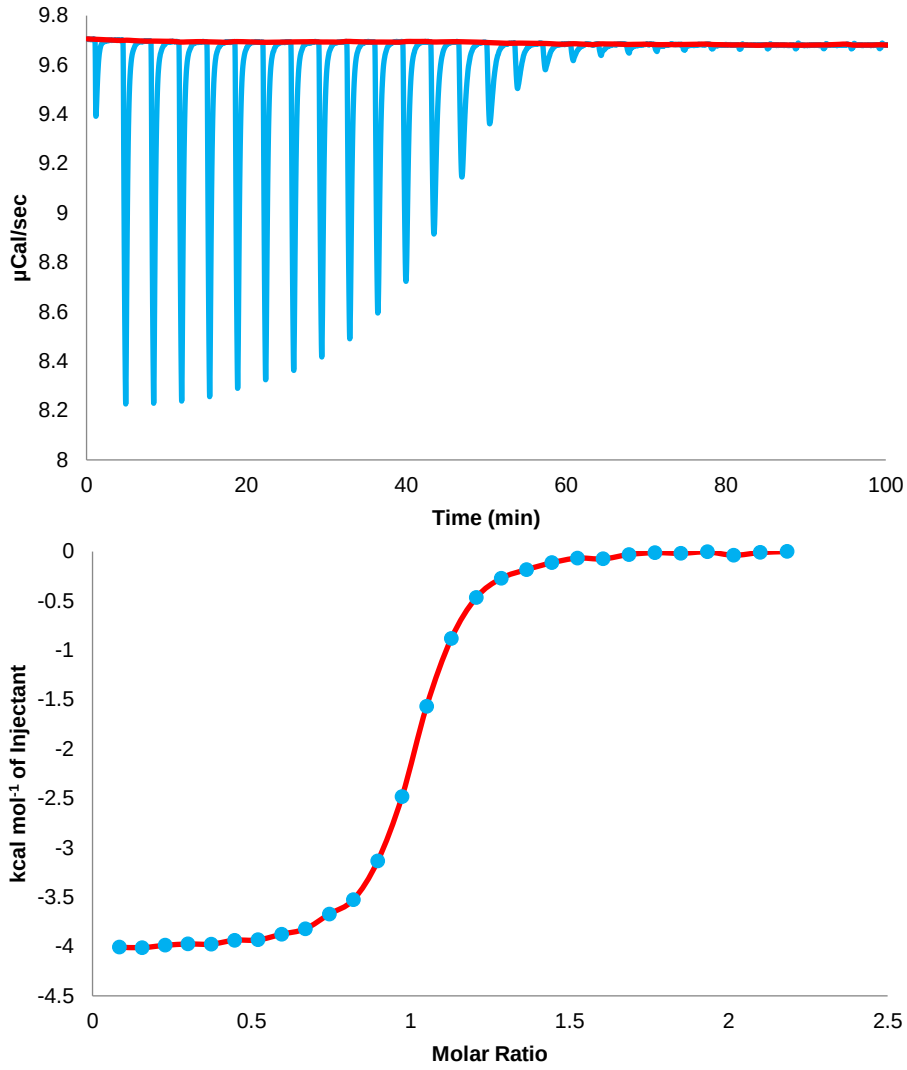

Criteria = *N* (stoichiometry) 0.969 ± 5 % Sites (0.921 ≤ *N* ≥ 1.017), *K* (binding constant) 2.09 x 10^6 ± 20 % M^{-1} (1.67 x 10^6 ≤ *K* ≥ 2.51 x 10^6), Δ*H* (enthalpy) -4259 ± 10 % cal/mol (-4685 ≤ Δ*H* ≥ -3833). 0.1 mM EDTA in the reference cell, sample cell and 1.0 mM $CaCl_2$ in the syringe. Injection number = 29. Cell temperature (°C) = 25. Reference power (µCal/sec) = 10. Initial delay (sec) = 60. Syringe concentration (mM) = 1.0. Cell concentration (mM) = 0.1. Stir Speed = 307. Volume of 1st injection (µL) = 2. Duration of 1st injection (sec) = 4. Volume after 1st injection (µL) = 10. Duration after 1st injection (sec) = 20. Spacing (sec) = 210. Filter Period (sec) = 2. Feedback mode/gain = High. ITC equilibration options = Fast equil; auto. Please note $CaCl_2$-EDTA test kit and instructions were supplied by Malvern Instruments Inc, Massachusetts, USA.

N = 0.982 ± 0.00113 Sites, *K* = 2.17 x 10^6 ± 3.96 x 10^5 M^{-1}, Δ*H* = -4025 ± 7.128 cal/mol, Δ*S* (entropy) = 14.9 cal/mol/deg.

Ultra-Violet Visible (UV-Vis) Spectrophotometry Calibrations

Doxorubicin (Dox) Standards

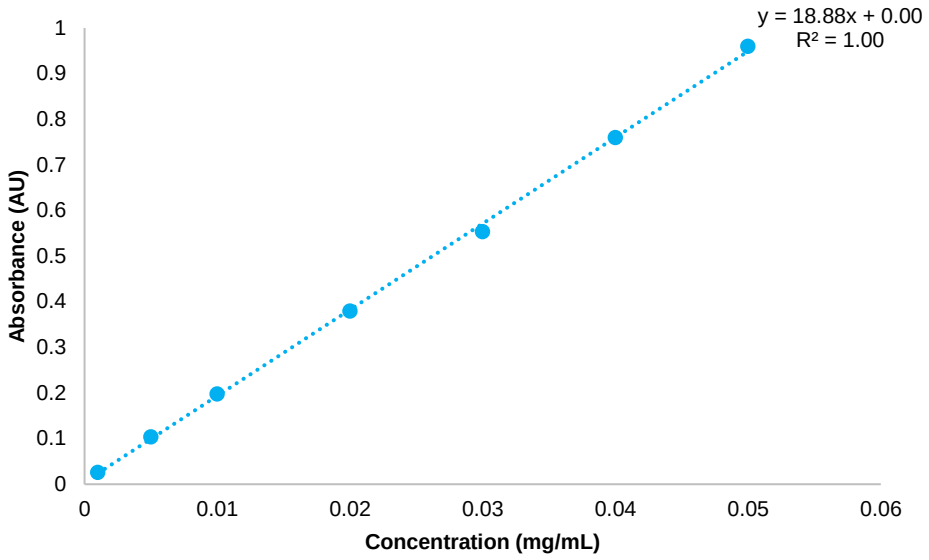

Irinotecan (Iri) Standards

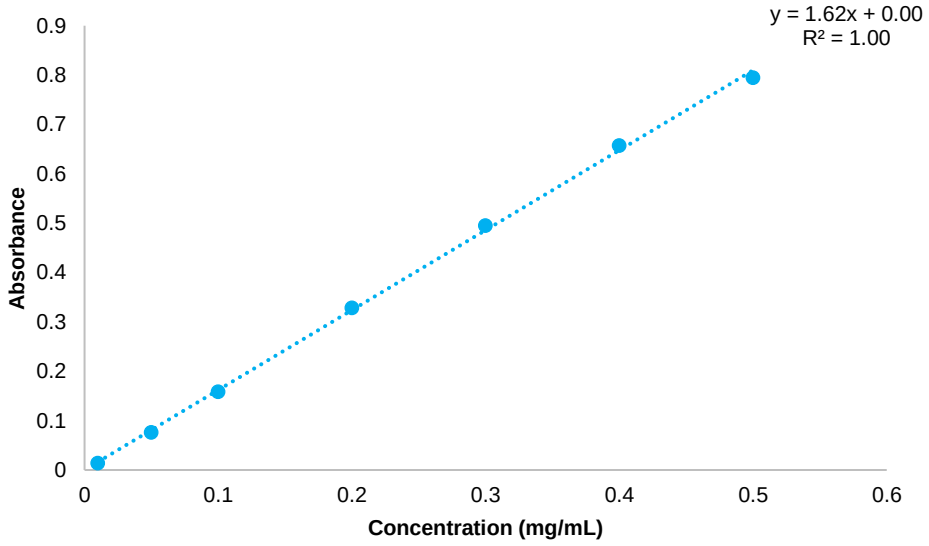

Peer Reviewed Publications

A calorimetric investigation of doxorubicin-polymer bead interactions.

TS Swaine, LJ Waters, AL Lewis.

International Journal of Pharmaceutics, Vol. 493, 129-133, 2015.

Evaluation of ion exchange processes in drug-eluting embolization beads by use of an improved flow-through elution method.

T Swaine, Y Tang, P Garcia, J John, LJ Waters, AL Lewis.

European Journal of Pharmaceutical Sciences, Vol. 93, 351-359, 2016.

Additional Research Outputs

Poster Presentations

Synergy (A Multidisciplinary Approach to Interventional Oncology), Miami, USA, 2014.

42nd Annual Meeting & Exposition of the Controlled Release Society (CRS), Edinburgh, United Kingdom (UK), 2015.

2nd Annual European MicroCal Meeting, Paris, France, 2016.

UK and Ireland Controlled Release Society (UKICRS) Workshop & Symposium, Cardiff, UK, 2016.

Oral Presentations

42nd Annual Meeting & Exposition of the Controlled Release Society (CRS), Edinburgh, UK, 2015.

OMICS Biomaterials Annual Conference and Expo, London, UK, 2016.

Three Minute Thesis (3MT®) Competition – Finalist: Cancer's Magic Bullet, Huddersfield, UK, 2017.

Postgraduate Researcher (PGR) Conference, Huddersfield, UK, 2017.

Professional Affiliations

Royal Society of Chemistry (RSC)

Academy of Pharmaceutical Sciences (APS)